The Synthesis of Fucose and Drug Conjugated Polymer Nanoparticles Capable of Metal Ion Encapsulation

HUNG Sui Lam

Supervised by Dr Paul Thornton

Co-supervised by Prof. Patrick McGowan

Submission date: 29/01/2026

Submitted in accordance with the requirements for the degree of Doctor of Philosophy

School of Chemistry, University of Leeds

The candidate confirms that the work submitted is his own and that appropriate credit has been given within the thesis where reference has been made to the work of others.

1. Acknowledgements

I would like to express my deepest gratitude to my main supervisor, Dr. Paul Thornton, for his invaluable guidance, unwavering support, and dedicated mentorship throughout my thesis writing. I am also thankful to my second supervisor, Prof. Patrick McGowan, for his support.

I extend special thanks to Dr. Jeanine Williams for generously providing access to and training on the HPLC system, to Dr. Alexander Kulak for facilitating the use of SEM-EDX, and to Dr. Mohammed Asaf for making the TGA instrument available to me.

I am profoundly grateful to my family for their steadfast emotional and financial support, which sustained me throughout this challenging journey.

Finally, I wish to thank my friend and labmate, Kunal Bapat, for his companionship, encouragement, and constant support during my time in the laboratory.

2. Abstract

This research presents a dual approach to advancing cancer therapy and sustainable polymer synthesis. To overcome the limitations of chemotherapeutic drugs like camptothecin (CPT), such as poor solubility and off-target effects, a series of polymer-drug conjugates were developed. These conjugates, utilising biodegradable polymers including polysarcosine (PSar) and polyglutamic acid (PGA), were engineered to self-assemble into nanoparticles (NPs), improving CPT's water solubility and enabling targeted delivery to pancreatic cancer cells via fucose modification. The synthesis of camptothecin glycinate initiated polysarcosine (CPT-Gly-PSar) conjugates achieved a high drug content but exhibited instability in NPs formation. This was overcome by PGA conjugation, forming PGA-(PSar-Gly-CPT), which produced stable NPs in PBS solution for four weeks across different concentrations. Also, PSar modification further refined NP uniformity, with PGA-[(CPT-Gly)-*co*-(PSar)] outperforming PGA-(CPT-Gly) in size consistency and stability. The fucose-incorporated conjugate, PGA-[(CPT-Gly)-*co*-(F-PSar)], achieved a high drug content and formed stable NPs. Drug release studies showed a slow, sustained release in pH7.4 PBS solution, but its extremely slow CPT release in pH5.0 acetic buffer solution showing it may be a potential candidate of adjuvant therapeutic for targeting S-phase cancer cells.

Additionally, Cu^{2+} ion complexation using PGA-[(CPT-Gly)-*co*-(F-PSar)] was explored to integrate chemotherapeutic and chemodynamic therapies (CDT) for enhanced efficacy. Cu^{2+} complexation was analysed via thermogravimetric analysis (TGA) revealed an incomplete metal complexation possibly due to acid produced during sample preparation. Energy dispersive X-ray (EDX) analysis identified the residue as copper oxide, and dialysis at acidic solution confirmed the Cu^{2+} release in acidic conditions.

Concurrently, to eliminate the use of toxic phosgene derivatives in polymer production, amino acid diketopiperazines (DKPs) and morpholines (DKMs) were synthesised as the alternatives of NCAs and assessed for ring-opening polymerisation (ROP) to produce biocompatible and biodegradable poly(amino acids) and polydepsipeptides.

This work advances cancer therapy through innovative, targeted drug delivery systems and promotes sustainable polymer chemistry by developing safer synthesis alternatives, laying a foundation for future clinical and environmental applications.

Contents

3. List of Figures

4. List of Tables

5. List of Abbreviations

ABC-	ATP-binding cassette
Ala-	Alanine
Boc-	tert-butoxycarbonyl
CA19-9	Carbohydrate antigen-19-9
$CDCl_{3-}$	Deuterated chloroform-
CDT-	Chemodynamic therapy-
CI-	Combination index
DKP-	Diketopiperazine
Cbz-	Carboxybenzyl
CMC	Critical micellar concentration
CPT-	Camptothecin -
CPT-Gly-	Camptothecin glycinate
CPT-Gly-PSar-	Camptothecin gycinate initiated polysarcosine
MTT-	3-(4,5-dimethylthiazol-2-yl)-2,5-diphenyltetrazolium bromide
DAD-	Diode array detector
DEPT-135-	Distortionless Enhancement by Polarization Transfer
DBU-	1,8-diazabicyclo[5.4.0]- undec-7-ene
DCC-	N,N'-Dicyclohexylcarbodiimide
DCM-	Dichloromethane
DHB-	2,5-Dihydroxybenzoic acid
DI-	Deionised
DIPEA-	N,N-Diisopropylethylamine

DKM-	Diketomorpholine
DLS -	Dynamic light scattering-
DMAP -	Dimethylaminopyridine
DMF-	Dimethylformamide-
DMSO-	Dimethyl sulfoxide-
EDX-	Energy dispersive X-ray
EDC-	1-Ethyl-3-(3-dimethylaminopropyl)carbodiimide
EDC.HCl	1-Ethyl-3-(3-dimethylaminopropyl)carbodiimide hydrochloride
EPR-	Enhanced Permeability and Retention
FDA-	Food and drug administration-
FTIR-	Fourier-transform infrared
F-PSar-	Fucose-polysarcosine or fucosylated polysarcosine
GA-	Glycolic acid
Glu(OBzyl)-	L-Glutamic acid γ-benzyl ester
Glu(OtBu)	L-Glutamic acid 5-tert-butyl ester diketopiperazine
Glu(OBzyl)-GA DKM-	benzyl 3-(2,5-dioxomorpholin-3-yl)propanoate or Glu(OBzyl)-glycolic acid - diketomorpholine
HCl-	Hydrochloric acid
HPLC-	High performance liquid chromatography
LiHMDS-	Lithium bis(trimethylsilyl)amide
Lys(Cbz)-	N6-Carbobenzyloxy-L-lysine
MALDI-TOF -	Matrix-assisted laser desorption/ionisation time-of-flight
MOR-	Metal alkoxide

MSA- Methanesulfonic acid

MWCO- Molecular weight cut-off

NCA- N-carboxyanhydride

NHS- N-Hydroxysuccinimide

Ni(0)Cod_2- Bis(cyclooctadiene)nickel(0)

NMR- Nuclear magnetic resonance

NPs- Nanoparticles

$O_2 \cdot^-$- Superoxide radical

·OH- Hydroxyl radical

PAla- Polyalanine

PBS- Phosphate buffered saline

PDAC- Pancreatic ductal adenocarcinoma

Pgp P-glycoprotein

Phe- Phenylalanine

PDI- Polydispersity Index

PEG- Poly(ethylene glycol)

PGA- Poly(glutamic acid)

PGA(CPT-Gly-PSar)- camptothecin glycinate initiated polysarcosine conjugated poly(Glutamic acid)

PGA-(Gly-CPT)- Camptothecin glycinate conjugated poly(glutamic acid)

PGA-[(Gly-CPT)-*co*-(PSar)]- Random coupling of camptothecin glycinate and polysarcosine with poly(glutamic acid)

PGA-[(Gly-CPT)-*co*-(F-PSar)]- Random coupling of camptothecin glycinate and fucosylated polysarcosine with poly(glutamic acid)

PGlu(OBzyl)- Poly(γ-benzyl-L-glutamate)

P(Glu(OBzyl)-GA)- Poly(γ-benzyl-L-glutamate- glycolic acid) alternating copolymer

P(Glu-GA)- Poly(Glutamic acid- glycolic acid) alternating copolymer

P(Glu-GA)-(CPT-Gly-PSar)- Camptothecin glycinate initiated polysarcosine conjugated poly(Glutamic acid- glycolic acid) alternating copolymer

P(Glu-GA)-[(Gly-CPT)-*co*-(F-PSar)]- Random coupling of camptothecin glycinate and fucosylated polysarcosine with poly(glutamic acid- glycolic acid) alternating copolymer

P(Sar-GA)- Poly(sarcosine-glycolic acid) alternating copolymer

RB flask Round bottom flask

ROS- Reactive oxygen species

PPhe- Polyphenylalanine

PSar- Polysarcosine

r.t.- Room temperature

ROP- Ring-opening polymerisation

Sar- Sarcosine

Sar-GA DKM- 4-methylmorpholine-2,5-dione or sarcosine-glycolic acid diketomorpholine

SEM- Scanning electron microscopy

SIPr-tetrafluoroborate 1,3-Bis(2,6-diisopropylphenyl)-4,5-dihydroimidazolium

SIPr.HCl- 1,3-Bis(2,6-diisopropylphenyl)imidazolinium Chloride

SPPS- Solid-phase peptide synthesis

$Sn(Oct)_2$- Tin (II) 2-ethylhexanoate

TBD-	1,5,7-Triazabicyclo[4.4.0]dec-5-ene
TFA-	Trifluoracetic acid
TGA	Thermogravimetric analysis
THF-	Tetrahydrofuran
TLC-	Thin layer chromatography
TME-	Tumour microenvironment
Top-	Topoisomerase

Chapter 1. Introduction to Research

1.1. Background Introduction

Pancreatic ductal adenocarcinoma (PDAC), commonly referred to as pancreatic cancer throughout this paper, represents the predominant form of pancreatic malignancy, accounting for more than 90% of all diagnoses [1]. Its average five-year survival rate consistently below 10%, stems primarily from late-stage detection with fewer than 20% of patients are identified at a localised, potentially curable phase, owing to the lack of distinct early symptoms and dependable biomarkers [2,3]. Staging follows the tumour-node-metastasis classification, categorising the disease into resectable, locally advanced, or metastatic stages [3]. In the absence of treatment, median survival is 3-5 months for metastatic disease and 6-10 months for locally advanced cases [4]. Even surgical resection extends it only to 11-15 months [4].

Conventional therapies, including chemotherapy, surgery, and radiation, have achieved limited progress in enhancing outcomes [5,6]. Even when surgical resection was performed at the earliest stages, two year survival rates linger around 50%, highlighting the urgent demand for innovative therapeutic approaches [5,6].

Addressing pancreatic cancer effectively stands as a challenge in oncology. A key barrier for many chemotherapeutic agents is their suboptimal bioavailability, often due to poor aqueous solubility in biological fluids like blood [7,8]. Moreover, these potent drugs inadvertently affect healthy tissues, triggering severe adverse effects unless protected by a delivery vehicle [9,10]. Polymeric nanoparticles mitigate these issues by encapsulating hydrophobic drugs, thereby enhancing solubility, facilitating targeted release, and minimising unintended interactions with non-cancerous cell [8,9].

To optimise therapeutic efficacy, an ideal polymeric drug delivery system must exhibit certain essential characteristics. The polymer should be biodegradable, allowing for safe bodily elimination after drug release [11,12]. It also needs to self-assembly into nanostructures in aqueous media, effectively encapsulating and transporting therapeutic payloads [13,14]. Poly(amino acids) fulfil these criteria, as they are inherently biodegradable, biocompatible, and non-toxic [15, 16], while the diverse side chains (R groups) of amino acids enable tailored functionalities to suit specific applications [16].

Amphiphilic block copolymers, consisting of at least one hydrophobic and one hydrophilic segment, are widely employed for such systems. In the context of poly(amino acids), the hydrophobic block is typically formed from amino acids with hydrophobic R groups, whereas the hydrophilic block derives from those with polar or charged R groups. These block copolymers can self-assembly in aqueous solutions to form NPs, with hydrophobic segments clustering into a core to reduce water contact [14]. Meanwhile, hydrophilic segments orient outward stabilising the NPs structure [13,14]. During polymer self-assembly, dissolved hydrophobic anticancer drugs can associate with the core, becoming entrapped and shielded from external degradation or premature release [17]. This encapsulation not only protects surrounding tissues from the drug's toxicity but also preserves the drug's integrity. Nevertheless, these systems face notable limitations, including low drug loading capacity [18] and burst release [19], which can compromise therapeutic precision and outcomes.

To overcome these challenges, the concept of pharmacologically active polymers emerged in 1975 [20]. In which , a polymer chain is divided into three different moieties and carrying different molecules: hydrophilic part for solubility, covalently attached therapeutic agents for controlled release, and targeting groups for site-specific delivery [20]. Covalently bonded highly hydrophobic drug molecule allows polymer to self-assembly and can be released under specific conditions preventing burst release. For pancreatic cancer, where nearly all patients overexpress fucose receptors [21,22], incorporating fucose as a targeting ligand enhances cellular recognition, thereby improving delivery specificity and treatment efficacy [21,23].

Other than chemotherapy, chemodynamic therapy (CDT) represents an emerging cancer treatment that exploits the tumour’s distinctive microenvironment to produce reactive oxygen species (ROS) such as $O_2{\cdot}^-$ and ·OH, via metal ion catalysed Fenton and Fenton-like reactions causing cancer cell death [24,25]. Additionally, CDT synergises with other therapies like chemotherapy, radiotherapy, and photodynamic therapy, where catalytic metal ions sensitise cancer cells and amplify overall effectiveness [26,27]. Thus, integrating metal ions with chemotherapeutic agents holds substantial promise for cancer management, and this report will outline the process made toward this aim.

In addition to exploring polymeric drug conjugate synthesis for targeted pancreatic cancer

therapy, this report also investigates through experimental approaches to seek safer alternatives to conventional poly(amino acids) production methods, with the goal of achieving more sustainable synthesis. Triphosgene is utilised to produce poly(amino acids) [28]. Yet, it decomposes into phosgene, a highly toxic, volatile gas infamous for its use as a chemical weapon in World War I and other warfare [29,30], upon contact with moisture or heat [31]. This hazard intensifies during large-scale production, where phosgene leaks could have catastrophic consequences. Recognising these dangers, there is a compelling imperative to explore safer alternatives for poly(amino acids) production.

1.2. Chapter Guide to This Research Study

In the 2nd chapter, research focuses on using two poly(amino acids), PSar and PGA as the major building blocks to create novel drug conjugates that overcome the solubility and delivery challenges of camptothecin (CPT), a potent chemotherapeutic agent [32, 33]. PSar acts as the hydrophilic moiety of the drug conjugate while PGA may be employed as the polymeric backbone on which covalent functionalisation with drug molecules may be achieved. Pro-drug camptothecin glycinate (CPT-Gly) initiated PSar (CPT-Gly-PSar) and PGA conjugated CPT-Gly-PSar, PGA(CPT-Gly-PSar), were synthesised to assess how PSar impacts CPT's water-solubility and how PGA conjugation improves NPs formation. Two additional conjugates, PGA-(Gly-CPT) and PGA-[(Gly-CPT)-*co*-(PSar)] were synthesised to explore the influence of PSar modified drug conjugate on NPs properties.

In the 3rd chapter, to achieve targeted delivery for pancreatic cancer, fucose should be presented on the NPs exterior to allow nanoparticle-pancreatic cell binding. Consequently, modified fucose was used to initiate the polymerisation of Sar-NCA, yielding fucose-terminated PSar (F-PSar). This was then used to create PGA-[(Gly-CPT)-*co*-(F-PSar)], capitalising on fucose's affinity for pancreatic cancer cells. This conjugate was further complexed with Cu^{2+} ions to introduce CDT which will be discussed in chapter 5.

Chapter 4 aims to advance polymer synthesis by developing alternatives to amino acid N-carboxyanhydrides (NCAs), whose production relies on toxic phosgene derivatives. New monomers, including amino acid diketopiperazines (DKPs) such as sarcosine DKP (Sar-DKP), alanine DKP (Ala-DKP), amide activated N-Boc-Ala-DKP, glutamic acid γ-benzyl ester DKP (Glu(OBzyl)-DKP), and lysine(Cbz)-DKP (Lys(Cbz)-DKP), along with amino acid morpholines

(DKMs) such as sarcosine-glycolic acid DKM (Sar-GA DKM) and glutamic acid(OBzyl)-glycolic acid DKM (Glu(OBzyl)-GA DKM), were synthesised. Their capability and effectiveness for ROP is evaluated to explore a safer, more sustainable approach to poly(amino acid) or polyester-amide production. Then poly(Glutamic acid- glycolic acid) (P(Glu-GA)) produced from ROP of Glu(OBzyl)-GA DKM was used to synthesise two drug conjugates, P(Glu-GA)-(CPT-Gly-PSar) and P(Glu-GA)-[(Gly-CPT)-*co*-(F-PSar)], to study the physical impacts of replacing PGA with P(Glu-GA) in the nanoparticle's formation.

Chapter 5 aims to incorporate Cu^{2+} ion into the drug conjugate for the co-delivery of chemotherapeutic and chemodynamic therapeutic agents. The Cu^{2+} complexed drug conjugate slowly release CPT and affecting S-phase cancer cells, while Cu^{2+} catalysing formation of reactive oxygen species (ROS) inducing cell death. The metal loading was estimated by thermogravimetric analysis (TGA).

In summary, this research aims to develop a fucose-targeted drug conjugate capable of Cu^{2+} ion loading, for pancreatic cancer treatment, combining chemotherapeutic and CDT for enhanced efficacy. Simultaneously, it explores novel DKP and DKM monomers to replace NCAs, reducing the use of hazardous reagents in poly(amino acids) synthesis. These efforts aim to contribute to the advancement of targeted drug delivery and sustainable polymer chemistry.

1.3. Research Novelty

This study presents several innovative contributions to the field of polymer-drug conjugates and nanomedicine for cancer therapy.

The work introduces F-PSar as a hydrophilic stealth component in combination with CPT-Gly conjugated onto a PGA backbone. To the best of my knowledge, this is the first report of a PGA- based conjugate simultaneously incorporating both fucose for active targeting and PSar for enhanced biocompatibility and stealth properties. The fucose moiety plays a significant role in fucose-mediated endocytosis for pancreatic cancer targeting. Furthermore, the resulting drug conjugate demonstrates the ability to self-assemble into stable nanoparticles concentration of 1.0 mg/mL while exhibiting the capability to carry metal ions, opening

potential applications in combination therapies.

Moreover, the exploration of alternating P(Glu-GA)as substitutes for PGA. This modification yielded two entirely novel drug conjugates, expanding the structural diversity of PGA-based delivery systems

In parallel, an attempt was made to synthesise Sar-NCA alternatives through the preparation of Sar-GA DKM, a novel cyclic monomer. Although its ROP was unsuccessful, its synthesis represents a new chemical route worthy of documentation. Additionally, extensive investigations into the ROP of amino acid DKPs using a wide range of catalysts were conducted. These systematic studies contribute new insights into the challenging ROP of DKPs and represent an original effort toward more sustainable or cost-effective routes for poly (amino acids) synthesis.

Collectively, these innovations distinguish this work from existing CPT-polymer conjugates and provide a versatile platform for the development of targeted nanomedicines against pancreatic cancer.

1.4. General Experimental

1.4.1. Synthesis of Monomers

1.4.1.1. Synthesis of Amino Acid NCAs

Amino acid (1.0 eqv) was placed in a three-necked RB flask fitted with a condenser and a dropping funnel. The system was purged with nitrogen for 15 minutes, three times. Anhydrous THF and α-pinene (2.0 eqv) were then added to the flask. Triphosgene (0.67 eqv), dissolved in anhydrous THF, was added dropwise via the dropping funnel once the reaction mixture was heated to reflux. The reaction was monitored, and completion was indicated when the solid dissolved, signifying the formation of NCA. The solution was filtered and evaporated using rotary evaporation, yielding a crude product which was dissolved in minimal amount of THF and precipitated into hexane (in an 8:1 hexane ratio). The mixture was stored overnight in a freezer to facilitate precipitation. The product was collected by vacuum filtration and washed with cold THF to remove unreacted triphosgene and α-pinene.

Recrystallisation was repeated three times, and the final product was dried under vacuum overnight.

1.4.1.2. Synthesis of Amino Acid DKPs Via Thermal Condensation Reaction

Amino Acid was added into an RB flask equipped with an air condenser. Ethylene glycol was added into the reaction flask followed by heating at 170 °C overnight under strong nitrogen flow into the system. The nitrogen flow can reduce the oxidisation of amino acid and side reactions and drive the reaction to completion by removing the water steam generated during reaction. The solution was turned into clear yellow solution after the reaction. The crude product was collected by suction filtration or liquid-liquid extraction. The crude product was purified by hot recrystallisation in methanol then dried in vacuum overnight.

1.4.2. ROP Amino Acid Monomers

1.4.2.1. ROP of Amino Acid NCAs

NCA was added to a Schlenk tube, which was purged with nitrogen three times, 15 minutes each. Amine initiator was dissolved in anhydrous DMF and added to the reaction flask at 0°C in an ice bath. The reaction mixture was allowed to warm slowly to room temperature over two days under a constant nitrogen bubbling through the reaction solution.

After the polymerisation, the crude product was precipitated by adding diethyl ether, followed by centrifugation. The product was washed with diethyl ether three times and dried under vacuum to yield the final polymer.

1.4.2.2. ROP of Amino Acid DKPs

Amino acid DKPs were placed in a Schlenk tube and purged with nitrogen three times for 15 minutes each. Amine initiator was then added to the reaction flask, either alone or in combination with various solvents and catalysts. The reaction mixture was heated to different temperatures under nitrogen and maintained for two weeks. ^{1}H-NMR analysis was

performed daily to monitor the reaction progress. After two weeks, regardless of the extent of the reaction, the mixture was subjected to dialysis before further processing.

1.4.3. Drug Conjugation

Carboxylate acid (1.0 eqv), EDC.HCl (3.0 eqv) and NHS (3.0 eqv) were placed in an RB flask and purged with nitrogen three times for 15 minutes each. Anhydrous DMF was then added, and the mixture was stirred for 1 hour in ice bath to activate the carboxylate groups. Subsequently, CPT-Gly and PSar or F-PSar in anhydrous DMF was added. The reaction mixture was allowed to warm to room temperature while kept stirring for two days. The crude product was dialysed against methanol overnight then in DI water for two days then freeze dried.

1.5. Instrumentations, General Methods and Materials

1.5.1. Instruments

1.5.1.1. Nuclear Magnetic Resonance (NMR) Spectroscopy

NMR spectroscopy was utilised to analyse both polymers and small molecules using two distinct instruments. For polymers, ^{1}H-NMR spectra were recorded on a Bruker AV-NEO 500 MHz spectrometer equipped with a 5 mm DCH cryoprobe and housed in WILMAD 528-PP NMR tubes. For small molecules, the spectra were obtained using a Bruker AV3HD 400 MHz spectrometer fitted with a 5 mm BBO Probe and contained in Norell® XR-55 NMR tubes. In all experiments, chemical shifts were calibrated to a trimethylsilane reference standard set at 0 ppm. The resulting spectra were processed and evaluated using MestreNova® Research Lab software.

1.5.1.2. Fourier-Transform Infrared (FTIR) Spectroscopy

FTIR spectra were recorded for solid samples using a Perkin Elmer Spectrum One equipped with Bruker OPUS 7.0 software and a Specac Golden Gate Attenuated Total Reflection

diamond top plate, accumulating 100 scans. Vibrational frequencies are expressed in cm^{-1}.

1.5.1.3. Matrix-Assisted Laser Desorption/Ionisation -Time of Flight Mass Spectrometry (MALDI-TOF MS)

Matrix-Assisted Laser Desorption/Ionisation Time-Of-Flight (MALDI-TOF) Spectroscopy Mass Spectrometry was carried out using a MALDI-TOF spectrometer (Shimadzu AXIMA performance) in positive mode. 2,5-Dihydroxybenzoic acid (DHB) was used as the matrix and the samples were dissolved in DMF.

1.5.1.4. Dynamic Light Scattering (DLS)

Dynamic Light Scattering (DLS) experiments were performed using a Malvern Zetasizer Nano ZSP instrument. This system features a 4 mW He-Ne laser with a wavelength of 633 nm and an avalanche photodiode (APD) detector, configured with a non-invasive back-scatter-optic setup to detect light scattered at a 173° angle. Samples were prepared in disposable 12 mm poly(styrene) cuvettes, equilibrated for two minutes, and measured at a stable temperature of 25°C. The collected data underwent cumulative analysis of the experimental correlation function, with particle diameters calculated from diffusion coefficients using the Stokes-Einstein equation. To ensure accuracy, each measurement was repeated three times. The results were then evaluated using the Malvern Zetasizer Software.

1.5.1.5. High Performance Liquid Chromatography (HPLC)

HPLC analysis was performed using an Agilent 1290 Infinity II HPLC system (Agilent, Santa Clara, CA, United States), with a diode array detector (DAD). The DAD was set to record the chromatogram at a wavelength of 254 nm. Chromatographic separations were performed using an InfinityLab Poroshell 120 EC-C18 (2.1×50 mm i.d., 1.9 µm; Agilent, Santa Clara, CA, United States) at a column temperature of 40ºC. The mobile phase used was 0.1 % TFA in water (95 %) and 0.1 % TFA in acetonitrile (5%) and the gradient running to 5 % water over 5 minutes at a flow rate of 0.5 mL/min. Injection volume was 1 µL. Retention time for

camptothecin is 2.47 minutes. The correlation coefficient for camptothecin in drug release study was 0.999478.

1.5.1.6. Scanning Electron Microscopy (SEM)

Scanning Electron Microscopy (SEM) samples were loaded on conductive carbon adhesive taps and sputter-coated with a thin layer of iridium (4 nm thickness) in a Quorum Q150RS sputter-coater. The samples were analysed with Nova NanoSEM 450 (FEI) instrument.

1.5.1.7. Thermogravimetric Analysis (TGA)

Thermogravimetric Analysis (TGA) was performed with PerkinElmer TGA 4000. The weight change of samples was analysed in a ceramic bowl at a heating rate of 10 ^{o}C per minute until 900 ^{o}C.

1.5.1.8. Energy Dispersive X-ray (EDX)

Samples were loaded on silicon wafer then were analysed with Nova NanoSEM 450 (FEI) instrument equipped with an Energy-Dispersive X-ray Spectroscopy (EDX) system.

1.5.2. General Methods

1.5.2.1. Preparation of Phosphate Buffered Saline (PBS) and Sodium Acetate Buffer Solutions

One PBS tablet was dissolved in DI water (200.0 mL) under stirring to obtain a PBS buffer solution (pH 7.4). A sodium acetate buffer solution was prepared by dissolving 3.69 mL glacial acetic acid in 1.0 L of DI water before 1.42 g of NaOH was slowly added. The pH of the solution formed was then adjusted using NaOH and HCl solution.

1.5.2.2. Preparation of Nanoparticles for DLS analysis

The drug conjugate to undertake self-assembly was dissolved in DMF at a concentration of 100.0 mg/mL. This drug conjugate solution was added slowly to the aqueous medium via autopipette, under vigorous stirring at 1200 rpm to produce NPs with different concentrations. This stirring was maintained for 30 minutes as NPs creation took place. Then NPs sample was taken for DLS analysis and then stored in at room temperature for reanalysis over a period of time.

1.5.2.3. Preparation of Nanoparticles for SEM Analysis

The drug conjugate was first dissolved in DMF, yielding a solution with a concentration of 100.0 mg/mL. This solution was then gradually added to DI water using an autopipette under vigorously stirred at 1200 rpm to create NPs with different concentrations. This stirring was continued for 30 minutes as nanoprecipitation took place. Following this, the resulting solution was subjected to dialysis (MWCO: 2000) against DI water for two days to remove DMF. Then the NPs was freeze dried. Then the NPs was gently spread on conductive carbon adhesive taps and sputter-coated with a thin layer of iridium (4 nm thickness) before SEM analysis.

1.5.2.4. Drug Release Studies

The drug conjugate was first dissolved in DMF, yielding a solution with a concentration of 100.0 mg/mL. This solution was then slowly transferred into an aqueous medium using an autopipette, while being vigorously stirred at 1200 rpm for 30 minutes to ensure NPs formation. Next, the resulting mixture was subjected to dialysis (MWCO: 6000) in the same aqueous medium at a temperature of 37°C, with continuous stirring to maintain consistency. During dialysis, 1.0 mL samples were periodically removed from the aqueous medium, and an equal volume of fresh aqueous medium was added back to maintain the volume. Finally, the collected samples were stored in a freezer to preserve them until analysis could be performed.

1.5.2.5. MALDI-TOF Analysis Calculations

Number average molecular weight (M_n) of polymer was calculated through below equation:

$$Mn = \frac{\sum Ni * Mi}{\sum Ni}$$

Where *Ni* is the number of molecules with molecular weight *Mi*.

While weight average molecular weight (M_w) of polymer was calculated through below equation:

$$Mw = \frac{\sum Ni * Mi^2}{\sum Ni * Mi}$$

1.5.2.6. CPT content (w/w%) Estimation Via H^1 NMR Spectrometry Analysis

Drug content of drug conjugates was estimated through the integrated proton ratio of the 500 MHz ^{1}H NMR Spectra.

Component of Drug Conjugates	Molecular Weight
Repeating unit of PSar	71
CPT in drug conjugate	347.3
CPT-Gly in Drug conjugate	404.4
PGA repeating unit	129
CPT-Gly in Durg conjugate	404.4-17 (to compensate the -OH loss in PGA after conjugation)
Repeating unit of P(Glu-GA)	187.2

2.7-3.0 ppm: 3H from PSar (-N(C**H$_3$**)-)

3.8-4.4 ppm: 1H from PGA (-NH-C**H**-C=O-) , 2H from CPT-Gly (-NH-C**H$_2$**-C=O-), 2H form PSar (-N(CH_3)-C**H$_2$**-)

5.1-5.6 ppm: 4H from CPT-Gly (-N-C**H₂**-, -O-C**H₂**-)

$$Drug\ Content\ \left(\frac{w}{w}\%\right) for\ (CPT-Gly-PSar) = \frac{347.3}{404.4 + (\frac{2.7-3.0ppm}{3} * 71)}$$

$$Drug\ Content\ \left(\frac{w}{w}\%\right) for\ PGA(CPT-Gly)$$
$$= \frac{(5.1-5.6\ ppm)/4 * 347.3}{\left((3.8-4.4\ ppm) - \frac{5.1-5.6\ ppm}{2}\right) * 129 + (\frac{5.1-5.6\ ppm}{4} * (404.4-17))}$$

For simplicity, the molecular weight of fucose was neglected, and the drug content (w/w%) of PGA-(PSar-Gly-CPT) was estimated through the same equation of below

$$Drug\ Content\ \left(\frac{w}{w}\%\right) for\ PGA-[(CPT-Gly)-co-(PSar\ or\ F-PSar)]$$
$$= \frac{(5.1-5.6\ ppm)/4 * 347.3}{\left((3.8-4.4\ ppm) - \frac{5.1-5.6\ ppm}{2} - \left(\frac{2.7-3.0\ ppm}{3} * 2\right)\right) * 129 + \left(\frac{2.7-3.0\ ppm}{3} * 71\right) + (\frac{5.1-5.6\ ppm}{4} * (404.4-17))}$$

1.5.2.7. CPT content (w/w%) Estimation for P(Glu-GA)-[(CPT-Gly)-co-(F-PSar)] And P(Glu-GA)-(PSar-Gly-CPT)

Drug content of drug conjugates was calculated from the integrated proton ratio of the 500 MHz ^{1}H NMR Spectra.

2.7-3.0 ppm: 3H from PSar (-N(C**H₃**)-)

3.7-5.3 ppm: 3H from P(Glu-GA) (-NH-C**H**-C=O-, -C=O-C**H₂**-O-), 4H from CPT-Gly (-NH-C**H₂**-C=O, -O-C**H₂**-), 2H form PSar (-N(CH_3)-C**H₂**-)

5.4-5.6 ppm: 2 H from CPT-Gly (-N-C**H₂**-)

$$Drug\ Content\ \left(\frac{w}{w}\%\right)\ for\ P(Glu-GA)-[(CPT-Gly)-co-(F-PSar)]$$

$$\&\ PGlu-GA(PSar-Gly-CPT)$$

$$=\frac{(5.4-5.6ppm)/2*347.3}{\left((3.7-5.3ppm)-(5.4-5.6ppm*2)-\left(\frac{2.7-3.0ppm}{3}*2\right)\right)*187.2+\left(\frac{2.7-3.0ppm}{3}*71\right)+(\frac{5.4-5.6ppm}{2}*(404.4-17))}$$

1.5.2.8. Metal Ion Release Study

The Cu^{2+} complexed drug conjugate was first dissolved in DMF, yielding a solution with a concentration of 100.0 mg/mL. This solution was then slowly transferred into an aqueous medium using an autopipette, while being vigorously stirred at 1200 rpm for 30 minutes to allow nanoprecipitation. Next, the resulting mixture was subjected to dialysis (MWCO: 6000) in the same aqueous medium at a temperature of 37°C, with continuous stirring to maintain consistency. During dialysis, 1.0 mL samples were periodically removed from the aqueous medium, and an equal volume of fresh aqueous medium was added back to maintain the volume. Finally, the collected samples were stored in a freezer to preserve them until analysis could be performed.

1.5.3. Materials

1.5.3.1. Solvents

All solvents used if not specified were purchased from either Sigma Aldrich or Fisher.

1.5.3.2. Amino Acids

Chemical	Supplier	Chemical	Supplier
H-Glu(OBzl)-OH	Fluorochem	Boc-Gly-OH	Fluorochem
Sarcosine	Fluorochem	N-Boc-Glu(OBzl)-OH	Fluorochem
L- Alanine	Fluorochem	Boc-Lys(Z)-OH	Fluorochem
H-Glu(OBzl)-OH	Fluorochem	Boc-Sar-OH	Fluorochem
H-Glu(OtBu)-OH	Fluorochem	Boc-Gly-OH	Fluorochem

1.5.3.3. Polymer Initiator

Chemical	Supplier	Chemical	Supplier
Benzylamine	Sigma Aldrich	Hexylamine	Fluorochem
Benzylalcohol	Fluorochem	Poly(ethylene glycol) methyl ether	Sigma Aldrich
Poly(ethylene glycol) diamine	Thermo Scientific	Methoxypolyethylene glycol amine	Thermo Scientific

1.5.3.4. Other Chemicals

Chemical separate the Chemicals from chapter to chapter	Supplier	Chemical	Supplier
Triphosgene	Fluorochem	Hydrobromic acid, 33% in Acetic Acid	Sigma Aldrich
trifluoracetic acid	Fluorochem	α-pinene	Sigma Aldrich
Sodium hydroxide	Fisher	sodium bicarbonate	Fisher
L(-)-Fucose	Acros	Acetic anhydride	Sigma Aldrich
K_2CO_3	Fluorochem	3-(Boc-amino)propyl bromide	Fluorochem
N,N-Diisopropylethylamine (DIPEA)	Fluorochem	Camptothecin (CPT)	Fluorochem
N,N'-Dicyclohexylcarbodiimide (DCC)	Fluka	N-Hydroxysuccinimide (NHS)	Apollo Scientific
4-Dimethylaminopyridine (DMAP)	Acros Organics	1-(3-Dimethylaminopropyl)-3-ethylcarbodiimide hydrochloride (EDC.HCl)	Fluorochem
Alanine-DKP	Thermo Scientific	Sarcosine-DKP	Thermo Scientific
Bis(1,5-cyclooctadiene)nickel(0) ($Ni(0)Cod_2$)	Thermo Scientific	Glycolic acid	Thermo Scientific
tert-Butyl 2-hydroxyacetate	Thermo	2-Chloro-1-	Thermo

	Scientific	methylpyridinium iodide	Scientific
1,3-Bis-(2,6-diisopropylphenyl)imidazolinium chloride (SIPr.HCl)	Thermo Scientific	chloroacetyl chloride	Thermo Scientific
Di-tert-butyl dicarbonate	Fluorochem	pyridine	Thermo Scientific
ethylenediamine	Thermo Scientific	Lithium bis(trimethylsilyl)amide (LiHMDS) (1M in Toluene)	Sigma Aldrich
Tin(II) 2-ethylhexanoate ($Sn(Oct)_2$)	Sigma Aldrich	Methanesulfonic acid (MSA)	Thermo Scientific
1,5,7-Triazabicyclo[4.4.0]dec-5-ene (TBD)	Fluorochem	1,8-Diazabicyclo[5.4.0]undec-7-ene (DBU)	Sigma Aldrich
Schreinen' s Thiourea Catalyst	Fluorochem	Copper (II) Chloride, anhydrous	Thermo Scientific

1.6. References

1. Sarantis, P., Koustas, E., Papadimitropoulou, A., Papavassiliou, A. G., & Karamouzis, M. V. (2020). Pancreatic ductal adenocarcinoma: treatment hurdles, tumor microenvironment and immunotherapy. World Journal of Gastrointestinal Oncology, 12(2), 173-181. https://doi.org/10.4251/wjgo.v12.i2.173

2. Tao, X., Xiang, H., Pan, Y., Shang, D., Guo, J., Gao, G., … & Xiao, G. G. (2021). Pancreatitis initiated pancreatic ductal adenocarcinoma: pathophysiology explaining clinical evidence. Pharmacological Research, 168, 105595. https://doi.org/10.1016/j.phrs.2021.105595

3. Hidalgo, M. (2010). Pancreatic cancer. New England Journal of Medicine, 362(17), 1605-1617. https://doi.org/10.1056/nejmra0901557

4. Pancreatric Section, British Society of Gastroenterology, Pancreatic Society of Great Britain and Ireland, Association of Upper Gastrointestinal Surgeons of Great Britain and Ireland, Royal College of Pathologists, & Special Interest Group for Gastro-Intestinal Radiology (2005). Guidelines for the management of patients with pancreatic cancer periampullary and ampullary carcinomas. Gut, 54 Suppl 5(Suppl 5), v1–v16. https://doi.org/10.1136/gut.2004.057059

5. Lemmens, V., Bosscha, K., Schelling, G. v. d., Brenninkmeijer, S., Coebergh, J., & Hingh, I. H. J. T. d. (2011). Improving outcome for patients with pancreatic cancer through centralization. British Journal of Surgery, 98(10), 1455-1462. https://doi.org/10.1002/bjs.7581

6. Adamska, A., Domenichini, A., & Falasca, M. (2017). Pancreatic ductal adenocarcinoma: current and evolving therapies. International Journal of Molecular Sciences, 18(7), 1338. https://doi.org/10.3390/ijms18071338

7. Gupta, K., Dakhole, M., Jinnawar, K., & Umekar, M. (2023). Strategies for improving hydrophobic drugs solubility and bioavailability. International Journal of Pharmaceutical Chemistry and Analysis, 10(3), 164-174. https://doi.org/10.18231/j.ijpca.2023.029

8. Narvekar, M., Xue, H., Eoh, J. Y., & Wong, H. L. (2014). Nanocarrier for poorly water-soluble anticancer drugs—barriers of translation and solutions. AAPS PharmSciTech, 15(4), 822-833. https://doi.org/10.1208/s12249-014-0107-x

9. Sawant, S. and Shegokar, R. (2014). Cancer research and therapy: where are we today?. International Journal of Cancer Therapy and Oncology, 2(4), 020408. https://doi.org/10.14319/ijcto.0204.8

10. Stortecky, S. and Suter, T. M. (2010). Insights into cardiovascular side-effects of modern anticancer therapeutics. Current Opinion in Oncology, 22(4), 312-317. https://doi.org/10.1097/cco.0b013e32833ab6f1

11. Hong, S., Koo, K., Lee, S., Park, H., Yoo, H., Kim, J., … & Cho, D. (2010). Biodegradable polymer droplet for efficient drug delivery using flagellated bacteria. 10th IEEE International Conference on Nanotechnology. https://doi.org/10.1109/nano.2010.5698031

12. Noorsal, K., Ghani, S. M., Yunos, D. M., Mohamed, M. S., Yahya, A., Rusop, M., … & Wui, W. T. (2010). Evaluation of degradation properties of polyglycolide and its potential as delivery vehicle for anticancer agents. AIP Conference Proceedings. https://doi.org/10.1063/1.3377819

13. Khan, W., Saravanan, M., Farah, S., Kumar, N., & Domb, A. J. (2011). Biodegradable polymers derived from amino acids. Macromolecular Bioscience, 11(12), 1625-1636. https://doi.org/10.1002/mabi.201100324

14. Avsar, S. Y., Kyropoulou, M., Leone, S., Schoenenberger, C., Meier, W., & Palivan, C. G. (2019). Biomolecules turn self-assembling amphiphilic block co-polymer platforms into biomimetic interfaces. Frontiers in Chemistry, 6. https://doi.org/10.3389/fchem.2018.00645

15. Lehninger, A. L., Nelson, D. L., & Cox, M. M. (2005). Lehninger principles of biochemistry (4th ed., pp. 75–110). W.H. Freeman. chrome-extension://efaidnbmnnnibpcajpcglclefindmkaj/https://librarymohsin.wordpress.com/wp-content/uploads/2018/07/lehninger-principles-of-biochemistry-fourth-edition-david-l-nelson-michael-m-cox1.pdf

16. Sangamesh Kumbar, Cato Laurencin, & Meng Deng. (2014). Natural and synthetic biomedical polymers (pp. 43–53, Chapter 3: Proteins and Poly (Amino Acids); p. 333-346, Chapter 20: Polymeric Materials in Drug Delivery). Elsevier.

17. Hartgerink, J. D., Beniash, E., & Stupp, S. I. (2001). Self-assembly and mineralization of peptide-amphiphile nanofibers. Science, 294(5547), 1684-1688. https://doi.org/10.1126/science.1063187

18. Nicolas, J. (2016). Drug-initiated synthesis of polymer prodrugs: combining simplicity and efficacy in drug delivery. Chemistry of Materials, 28(6), 1591-1606. https://doi.org/10.1021/acs.chemmater.5b04281

19. Avgoustakis, K. (2002). Plga–mpeg nanoparticles of cisplatin: in vitro nanoparticle degradation, in vitro drug release and in vivo drug residence in blood properties. Journal of Controlled Release, 79(1-3), 123-135. https://doi.org/10.1016/s0168-3659(01)00530-2

20. Ringsdorf, H. (1975). Structure and properties of pharmacologically active polymers. Journal of Polymer Science: Polymer Symposia, 51(1), 135-153. https://doi.org/10.1002/polc.5070510111

21. Yoshida, M., Takimoto, R., Murase, K., Sato, Y., Hirakawa, M., Tamura, F., … & Kato, J. (2012). Targeting anticancer drug delivery to pancreatic cancer cells using a fucose-bound nanoparticle approach. PLoS ONE, 7(7), e39545. https://doi.org/10.1371/journal.pone.0039545

22. Munkley, J. (2019). The glycosylation landscape of pancreatic cancer (review). Oncology Letters. https://doi.org/10.3892/ol.2019.9885

23. Yu, H., Rowley, J. V., Green, D. C., & Thornton, P. D. (2020). Fucose-modified thermoresponsive poly(2-hydroxypropyl methacrylate) nanoparticles for controlled doxorubicin release from an injectable depot. Materials Advances, 1(5), 1293-1300. https://doi.org/10.1039/d0ma00280a

24. Tang, Z., Liu, Y., He, M., & Bu, W. (2018). Chemodynamic therapy: tumour microenvironment-mediated fenton and fenton-like reactions. Angewandte Chemie International Edition, 58(4), 946-956. https://doi.org/10.1002/anie.201805664

25. Hassannia, B., Vandenabeele, P., & Berghe, T. V. (2019). Targeting ferroptosis to iron out cancer. Cancer Cell, 35(6), 830-849. https://doi.org/10.1016/j.ccell.2019.04.002

26. Ren, Z., Sun, S., Sun, R., Cui, G., Hong, L., Rao, B., … & Mao, Z. (2019). A metal–polyphenol-coordinated nanomedicine for synergistic cascade cancer chemotherapy and chemodynamic therapy. Advanced Materials, 32(6). https://doi.org/10.1002/adma.201906024

27. Xue, T., Xu, C., Wang, Y., Wang, Y., Tian, H., & Zhang, Y. (2019). Doxorubicin-loaded

nanoscale metal–organic framework for tumor-targeting combined chemotherapy and chemodynamic therapy. Biomaterials Science, 7(11), 4615-4623. https://doi.org/10.1039/c9bm01044k

28. Otake, Y., Nakamura, H., & Fuse, S. (2018). Rapid and Mild Synthesis of Amino Acid N-Carboxy Anhydrides: Basic-to-Acidic Flash Switching in a Microflow Reactor. Angewandte Chemie International Edition, 57(35), 11389-11393. https://doi.org/10.1002/anie.201803549

29. Eckert, H. and Forster, B. (1987). Triphosgene, a crystalline phosgene substitute. Angewandte Chemie International Edition in English, 26(9), 894-895. https://doi.org/10.1002/anie.198708941

30. cruzvinchristopher. (2008, September 9). Chemical Warfare Left Its Legacy. Scribd. https://www.scribd.com/document/896681928/Chemical-Warfare-Left-Its-Legacy

31. Material Safety Data Sheet - University of Nevada, Reno,ehslegacy.unr.edu/msdsfiles/26588.pdf. Accessed 05 Aug. 2023.

32. Hatefi, A. and Amsden, B. G. (2002). Camptothecin delivery methods. Pharmaceutical Research, 19(10), 1389-1399. https://doi.org/10.1023/a:1020427227285

33. Okuno, S., Harada, M., Yano, T., Yano, S., Kiuchi, S., Tsuda, N., Sakamura, Y., Imai, J., Kawaguchi, T., & Tsujihara, K. (2000). Complete regression of xenografted human carcinomas by camptothecin analogue-carboxymethyl dextran conjugate (T-0128). Cancer research, 60(11), 2988–2995.

Chapter 2. Synthesis of Poly(Amino Acids) and their corresponding Drug Conjugates

2.1. Introduction

Poly(amino acids) are excellent candidates for use as drug delivery systems. They are biodegradable, biocompatible, and originate from a bio-renewable source. Controlled synthesis of such polymers typically involves the conversion of an amino acid to a cyclic structure that can undergo ROP. This chapter will disclose the synthesis of two poly(amino acids), PSar and PGA, which may be included in a drug delivery vehicle to provide hydrophilicity and sites for drug/polymer conjugation.

2.1.1. Amino Acids

Amino acids are fundamental building blocks of proteins are essential components found in all living organisms. Each amino acid is characterised by a consistent structure that includes an amino group, a carboxylic group, and a unique side chain (R group), which differentiates one amino acid from another (Figure 2.1-1)[1]. These R groups vary in structure, size, and electric charge, thereby determining the chemical properties of both the individual amino acid and the protein they form. For example, the nature of the R group influences key properties such as solubility in water, the pH of the solution, and protein polarity [1].

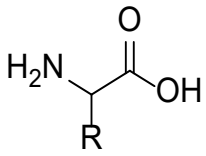

Figure 2.1-1. Molecular structure of amino acids

More than 300 amino acids have been identified in cells, but only 21 directly take part in polypeptide or protein synthesis during mRNA translation [2]. The remaining amino acids typically serve other roles, often acting as intermediates in biosynthesis pathways or the product of post-translational modification of proteins [3]. Among these, some play significant roles in metabolic processes. For instance, sarcosine a N-methylated derivative of glycine functions as both the intermediate and by-product in the synthesis and degradation

of glycine, and it is commonly found in muscles and other bodily tissues [4].

2.1.2. Poly(Amino Acids)

A linear polypeptide chain is formed when amino acids are covalently joint together through a peptide bond by removal of water molecules [1]. The biologically occurring polypeptides are of a wide range of molecular weights and can include 2,000 amino acid repeat units in the chain with specific amino acid sequence [1]. Unlike polypeptides, poly(amino acids) are artificially synthesised polymers that often consist of one type of amino acid as the repeat unit. Random, block and graft copolymers can also be created but polymers of specific amino acid order analogous to polypeptides can only viably be done by solid-phase peptide synthesis (SPPS)[5]. Polypeptides, including artificial ones, can be hydrolysed under physiological conditions or by enzymatic catalysis yielding a mixture of their constituent amino acids, which are then absorbed and metabolised by cells [6,7]. Despite its biodegradability, the half-life of polypeptides can be as long as seven years under most intracellular conditions, which shows that poly(amino acids) can be created to be chemically robust, but they may also be biodegradable and are biocompatible and non-toxic to cells[1,7].

The chemical and physical properties of polypeptides are determined by the sequence and the nature of constituent amino acids' R groups that are presented along the polypeptide chain. While poly(amino acids) lacks the specific amino acid sequence that polypeptides and proteins possess, they can possess the diverse functionalities that are afforded by the amino acid R group. Therefore, polymers can be created that are cationic/ anionic or hydrophilic/ hydrophobic based on the amino acids polymerised for different applications [7]. Crucially, because of their biodegradability and biocompatibility, poly(amino acids) is widely used as drug carriers [7].

2.1.2.1. Solid-phase peptide synthesis (SPPS)

The creation of poly(amino acids) with precise amino acid sequences, like polypeptides, can only be done by SPPS (Scheme 2.1-1)[5]. The general process for synthesising peptides starts

by attaching the first amino acid (AA_1) to a resin support through its C-terminal carboxyl group. Then the peptide chain is constructed step-by-step, extending toward the N-terminal end. Each new amino acid is linked to the growing chain via its α-amino group, while temporary protecting groups (P) prevent any reactive side chains. Once the amino acid is attached, the resin is filtered and washed to eliminate excess reagents and byproducts. The N-protecting group (R) on the amino acid is then removed, followed by another wash of the resin before coupling of the subsequent amino acid. This sequence of coupling, washing, deprotection, and washing is repeated for each subsequent amino acid coupling, until the entire desired peptide sequence is assembled. Once complete, all protecting groups are deprotected, the resin is washed again, and the finished peptide is cleaved from the resin. (Scheme 2.1-1)[8].

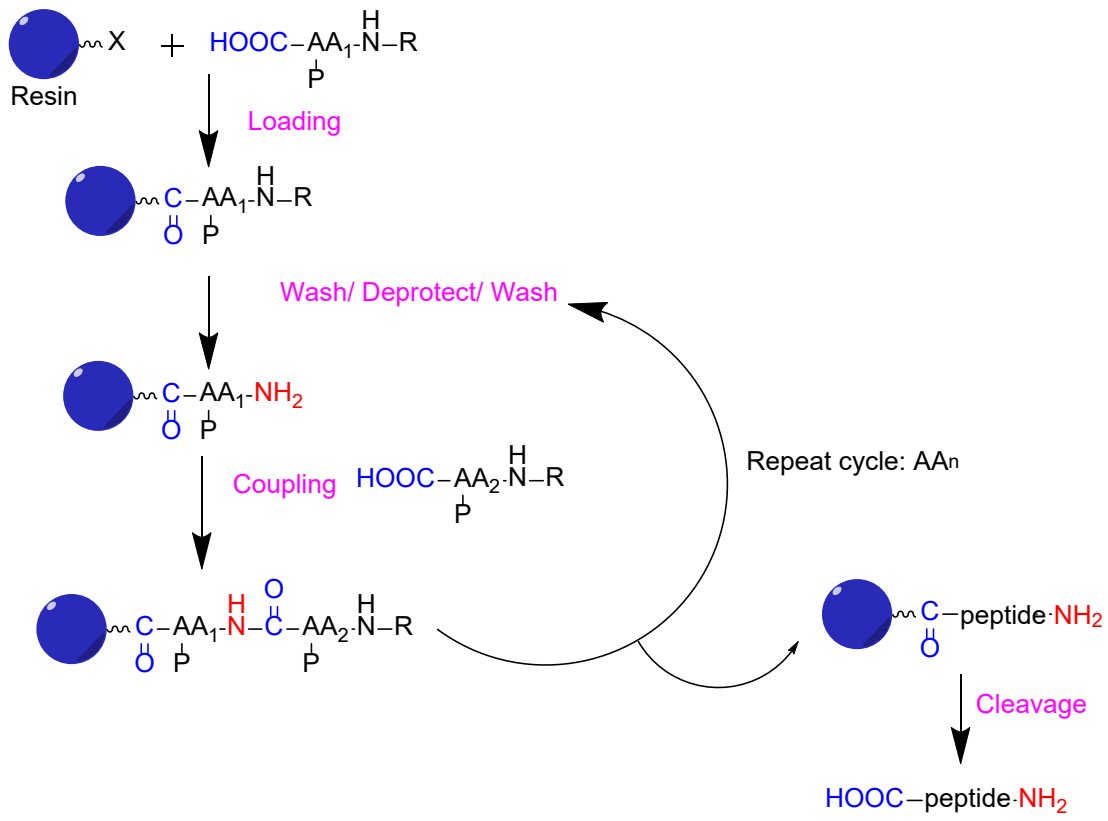

Scheme 2.1-1. General procedure of solid-phase peptide synthesis (SPPS) [8]

However, SPPS faces significant challenges as peptide length increases. The crude yield and purity of synthesised peptides drop sharply due to steric hindrance and chain aggregation as the peptide length increases. These issues impair the efficiency of coupling and deprotection

steps by hindering interactions between the growing peptide, coupling reagents, and the solid support [9,10,11]. As a result, the repetitive cycles become less effective and time consuming with amplifying yield losses with each additional amino acid [9,10,11]. Consequently, SPPS is constrained in the length of peptides it can produce, which limits its scalability and sustainability for large scale or environmentally conscious applications and was not employed in this research study.

2.1.2.2. Ring Opening polymerisation of Amino Acid N-carboxyanhydrides (NCAs)

The polymerisation of amino acid NCAs offers the most economical and efficient approach for synthesising long chains of poly(amino acids) [11]. Amino acid NCAs are cyclic monomers commonly made from refluxing amino acids with phosgene derivatives (Scheme 2.1-2).

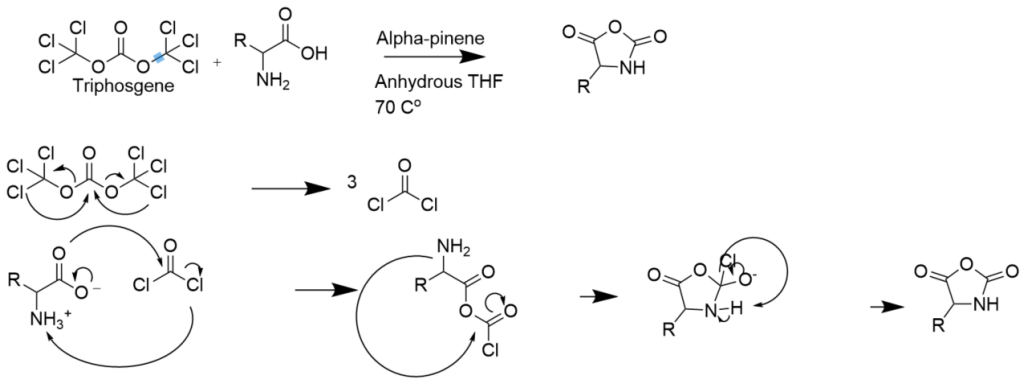

Scheme 2.1-2. Reaction mechanism of amino acid-NCA synthesis with triphosgene

Polymerisation commences when a nucleophile, usually a primary amine, attacks the anhydrous carbon in the NCA ring prompting ring opening, carbon dioxide release, and the formation of a new amine terminus that propagates the chain by targeting additional NCA units [11]. This reaction is termed as ring opening polymerisation (ROP) (Scheme 2.1-3). This process allows the control of polymer chain length by adjusting the monomer to initiator ratio where the polymer could grow linearly if side reactions were absent, providing a significant advantage in polymer synthesis [11,12].

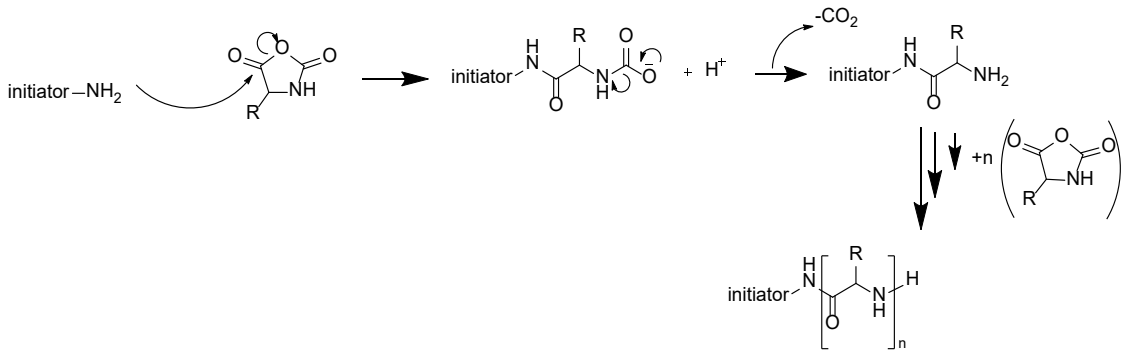

Scheme 2.1-3. Reaction mechanism of the amine- initiated ROP of amino acid NCAs

However, NCAs can be initiated by a deprotonated NCA where the resulting anion acts as a nucleophile that initiates chain growth and both amine initiation and monomer initiation mechanism take place simultaneously during the polymerisation (Scheme 2.1-4) [11]. The loss of reactivity control over the growing polymer chain-end results in amine, carbamate or NCA anion end groups that are free to undergo a variety of unwanted side reactions [11]. Moreover, crystalline NCAs often harbour minute traces of acid, acid chlorides, or isocyanates that can terminate growing chains [11]. Consequently, polymers prepared by NCA ROP using amine initiators often deviate from expected molecular weights based on feed ratios [11]. While transition metal complexes can suppress these side reactions increasing both reaction selectivity and efficiency [13], for the production of biomaterials intended for in vivo use, such as drug delivery vehicles, the use of toxic organometallic catalyst should be avoided. This research opted against them in favour of a simpler, greener alternative by conducting ROP at 0°C to minimise side reactions effectively [11,14]. Furthermore, only Sar-NCA and Glu(OBzyl)-NCA were used to produce PSar and PGA in this research, Sar-NCA lacks an acidic proton to enable monomer initiation, and dialysis ensures PGA achieves a minimum molecular weight threshold.

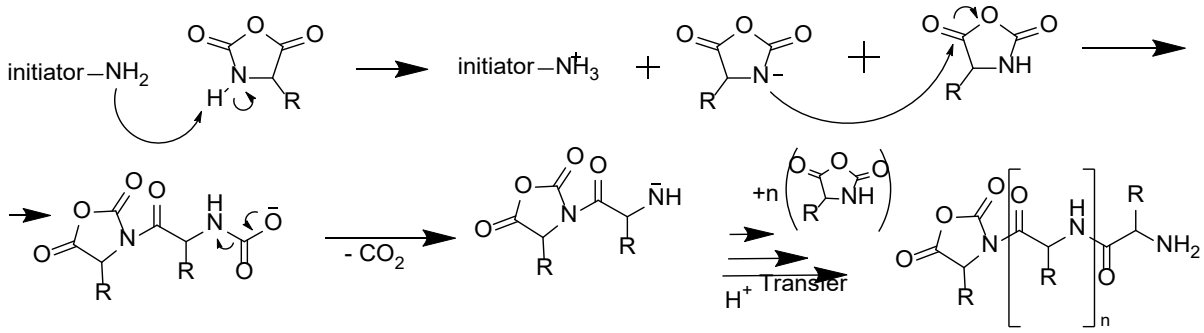

Scheme 2.1-4. Reaction mechanism of monomer-initiated ROP of amino acid-NCAs

In contrast to SPPS, NCA ROP has far superior efficiency in both time and cost for the production of poly(amino acids) [9,10,11,12]. It is straightforward, requiring only the NCA, an initiator, and a solvent without catalysts [11]. This straightforward approach yields high molecular weight polymers in large quantities, while maintaining the integrity of chiral centres with no detectable racemisation [15]. Additionally, ROP enables good control over the molecular weights of the resulting poly(amino acids) [12,15,16]. The versatility of this method is further enhanced by the wide range of available NCAs with over hundred distinct types have been synthesised, allowing for the production of poly(amino acids) with diverse properties tailored to various applications [16]. Furthermore, the living nature of poly(amino acids) produced by ROP of NCAs allows for facile synthesis of block-*co*-polymers or end-group functionalisation via the terminal amine [11].

2.1.3. Polymer Nanoparticles

Amphiphilic block copolymers are polymers composed of at least one hydrophobic block and one hydrophilic block. In the context of poly(amino acids), the hydrophobic block is typically formed from amino acids with hydrophobic R groups, such as phenylalanine or valine, while the hydrophilic block consists of amino acids with polar or charged R groups, like lysine or glutamic acid. These copolymers can self-assemble in aqueous solutions to form NPs, driven by the tendency of the hydrophobic blocks to aggregate forming a core to minimise their interfacial tension in water [17]. Meanwhile, the hydrophilic blocks remain exposed to the aqueous environment, stabilising the NPs structure [18,19,20].

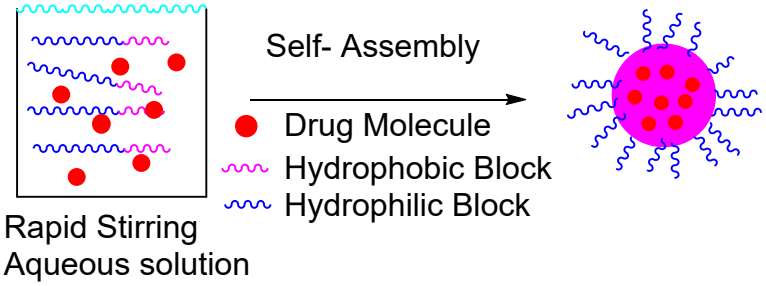

Figure 2.1-2. When the amphiphilic polymer is dissolved in a polar solvent that is miscible with water (e.g. DMF) is dropped into rapidly stirred water, it self-assembles into a NPs by hiding the hydrophobic blocks in the core while the hydrophilic blocks are exposed to the external aqueous environment.

During polymer self-assembly, other dissolved hydrophobic materials such as anti-cancer drugs may interact with the hydrophobic block and become entrapped in the hydrophobic core [21,22] (Figure 2.1-2). This encapsulation serves multiple purposes; it shields the external environment from the cytotoxic effects of the drug, protects the drug from premature degradation or reaction with external factors and allowing sustained and controlled release [20,23]. Furthermore, the hydrophilic outer layer prevents the NPs from interacting with proteins or other blood components, reducing the risk of aggregation through steric repulsion [19,24,25]. Consequently, amphiphilic block copolymer NPs have been extensively explored for use in drug delivery due to their versatility, stability, and ability to be tailored for specific treatments [18]. For instance, these polymers can be engineered to target particular cancer cells by incorporating cell-targeting groups, while remaining stable in non-target environments or during storage [7,14].

2.1.4. Drug Delivery Mechanisms

In cancer therapy, NPs carry anticancer drug to the target site through two main pathways to increase their access and accumulations in cancer cells [18,20]. The prolonged circulation times causing the NPs to preferentially accumulate in the cancer site by the enhanced permeability and retention (EPR) effect (passive targeting) [18,20]. While active targeting is achieved if the NPs are designed to be stimulus responsive such as pH change caused drug

release [18,20,26,27], or modification of NPs surface with ligands that specifically target receptors that are overexpressed on targeted cancer cells [18,20,27]. This active targeting aims to enhance cancer cells specific accumulation and cellular uptake, further improving therapeutic precision [20].

2.1.5. Enhanced Permeability and Retention (EPR) Effect

Many unique pathophysiological traits are observed in blood vessels of most solid tumours, such as extensive angiogenesis and hence high hypervasculture [28,29,30], defective vascular architecture, hypoplastic in arterioles within and around the tumour [28,29,30], impaired lymphatic drainage or recovery system around the interstitial space of tumour tissues [30,31], and intensive vascular permeability induced by significant raise in synthesis of various permeability mediators [28,29,30,31,32]. Such enhancements play a vital factor in tumour growth which facilitate the provision of nutrients and oxygen to meet the huge need for rapid tumour growth [28]. And this phenomenon is termed as the EPR effect. Not only EPR important for tumour growth, but also in delivery of macromolecular anti-cancer drug which makes the development of highly cancer cell selective drug delivery becomes feasible [28,31,32]. Owing to these unique tumour microenvironment (TME), macro-drug molecules exceeding certain molecular wight threshold tents to accumulate at higher concentration in the tumour interstitial space than in normal tissues [28,29,30,32]. Therefore, EPR effect is being widely accepted and regarded as the most fundamental concept and standard in designing tumour targeting macromolecular anti-cancer drug [28,32]. Therefore, the longer the drug circulates in the blood vessels, more the drug accumulate and higher the drug concentration in tumour tissue. However, in case of pancreatic tumour, which lacks sufficient vascularity and hence, macro-drug molecules cannot be delivered to the tumour tissue effectively by relying only on EPR effect [33,34,35,36]. Therefore, active targeted drug delivery is needed for pancreatic cancer treatment. And an emerging strategy for this task is targeting drug delivery mediated by fucose.

2.1.6. Limitations of Physical Drug Encapsulation

Freely loaded amphiphilic NPs in which the drug molecules are not covalently bound to the polymer is a frequently employed drug delivery system, yet it has many drawbacks. Drug encapsulation typically occurs during self-assembly of amphiphilic polymer in aqueous solution. However, due to the potentially poor solubility of many drug molecules in the polymer matrix, low drug loading may occur [37]. Secondly, burst release occurs when a fraction of the drug is adsorbed onto or located near the surface of the NPs, which rapidly diffuses into the surrounding medium [38]. Thirdly, premature leakage is often observed such as caused by interaction with abundant blood components, such as albumin [39]. As a result, these drug molecules are released in the initial minutes or hours at the injection site after administered, which may result in high local or system toxicity [40]. Moreover, since NPs are mainly prepared in aqueous medium, which cause hydrolysis or oxidisation of some of the components of the NPs during storage, affecting their stabilities and efficacy [41]. Attempts to address this issue through freeze-drying the polymer NPs, this process can rupture NPs leading to drug leakage upon administration [41]. Consequently, this project focus on the creation of drug delivery systems in which drug molecules are covalently bound to the polymer chains that form NPs, hence the drug releasing rate is limited by the drug-polymer linkage hydrolysis, setting the stage for more advanced drug delivery approaches in an attempt to tackle these issues.

2.1.7. Polymer-Drug Conjugates

The modification of hydrophobic chemotherapeutic agents through the covalent incorporation of hydrophilic polymers is another well-established and extensively studied approach aimed at improving their solubility in aqueous environments, which in turn enhances their bioavailability and therapeutic effectiveness in clinical applications [42,43]. For example, PEGylation of camptothecin (CPT) has been successfully utilised to increase its water solubility [42]. To achieve optimal drug loading capacities while ensuring adequate therapeutic effects, these drugs are commonly conjugated with hydrophilic oligomers that function as solubility enhancers [44,45].

However, a significant challenge arises from the tendency of self-assembly NPs to

disintegrate prematurely after administration due to *in vivo* dilution [39,46,47,48,49]. This disintegration is often attributed to the high critical micellar concentrations (CMC) of small-molecular-weight drug conjugates, which can lead to the unintended release of the drug prior to reaching its intended target site [39,46,47,48,49]. This premature release diminishes the drug's therapeutic effectiveness and increases the risk of side effect due to systemic distribution of the toxic drug.

To mitigate this issue, chemical crosslinking is commonly employed to improve the stability of drug conjugates by creating covalent bonds between polymer chains providing reinforcement to the weak intermolecular interactions that facilitate polymer micelle assembly and existence. This reduces the likelihood of premature disintegration and ensures the drug remains intact until it reaches the target site [39,46,47,48,49].

2.1.8. Pharmacologically Active Polymers

Building on the foundation of polymer-drug conjugates, pharmacologically active polymers offer a more refined and sophisticated solution to the challenges of drug delivery. The concept of the pharmacologically active polymer was first introduced in 1975 by Helmut Ringsdorf [50]. In this model, a polymer chain is divided into three different moieties and carrying different molecules: hydrophilic polymeric chain, therapeutic agent and cell targeting group (Figure 2.1-3). The covalent bonding of the therapeutic agent to the polymer ensures that release occurs preferably under specific environmental conditions, such as the acidic extracellular environment of cancerous tissues (pH 6.0-7.0), dropping to pH 5.0-6.0 in late endosomes [51,52]. This pH-responsive, site-specific release mechanism effectively prevents both premature and burst drug release, overcoming the key limitations of both physical encapsulation and traditional polymer-drug conjugates [39,46,47,48,49].

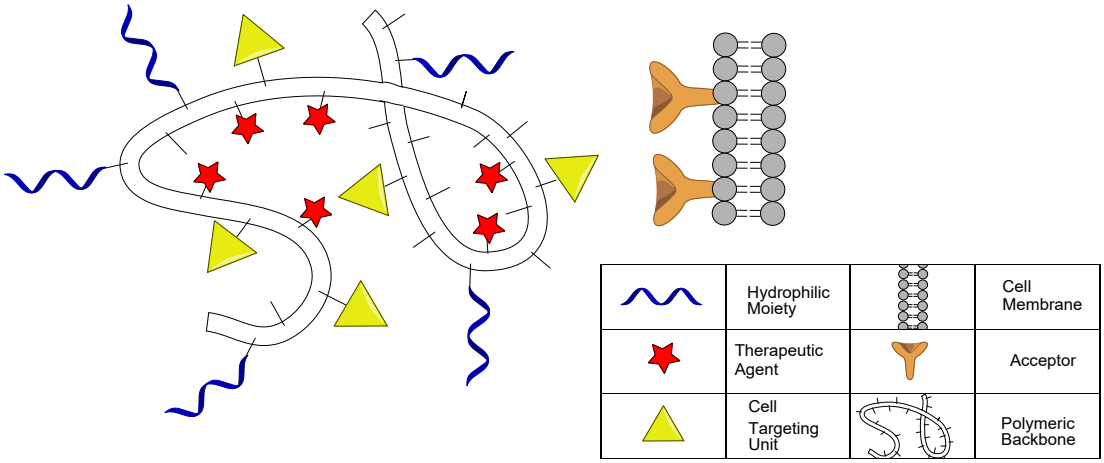

Figure 2.1-3. A model of a pharmacologically active polymer, containing a polymeric backbone carrying chemotherapeutic agent, cell directing group and hydrophilic moiety [50]

By adopting to this concept, my approach centres on a polymeric NPs composed of PGA as the polymeric backbone, to which both fucose-polysarcosine (F-PSar) and the anti-cancer drug camptothecin glycinate (CPT-Gly) were conjugated creating a drug conjugate designed to target pancreatic cell and minimise the burst release effect seen in traditional encapsulation methods. (Figure 2.1-4).

This system leverages the acidic TME to trigger controlled drug release, aiming to enhance therapeutic efficacy while reducing side effects. By integrating fucose-mediated targeting and pH-responsive drug-glycine linker, this approach offers a potential advancement in the treatment of pancreatic cancer.

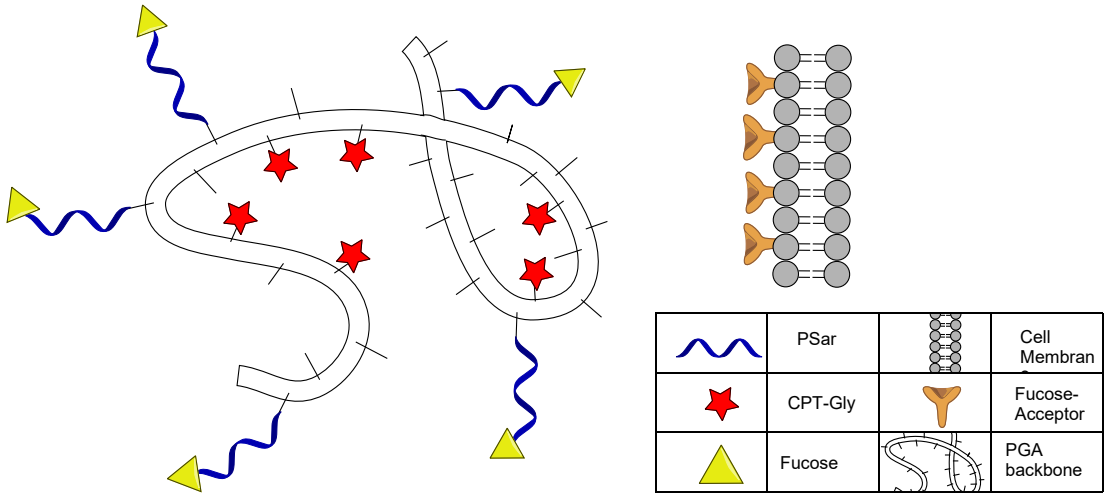

Figure 2.1-4. The model of the target product PGA-[(CPT-Gly)-*co*-(F-PSar)], PGA is the polymeric backbone, CPT-Gly is both the therapeutic agent and the hydrophobic moiety, F-PSar is both the hydrophilic moiety and the cell directing group.

2.1.9. Chemotherapeutic Drugs

Many anticancer drugs that are approved for clinical use suffer from low solubility in aqueous solutions, which limits their efficacy during chemotherapy. This remains a major obstacle in drug development and clinical administration through oral and intravenous or intramuscular injection [40,53,54]. Extensive research has been conducted to counter such problems from different approaches, including using polymeric vesicles [40]. However, many proposed drug delivery systems suffer from the previous mentioned issues, low drug loading, burst release, and non-continuous drug release [40]. Therefore, the effectiveness of drug delivery systems needs to be improved.

2.1.9.1. Camptothecin

CPT is a potent topoisomerase I (top I) poison which stabilise the top I-DNA complex preventing the relegation of the cut DNA strand, which damages the DNA and results in apoptosis of the cell [55,56]. It has been shown by many clinical trials that CPT is the most effective anticancer drug against lung, ovarian, breast, pancreas, and stomach cancers

among all the clinically available anticancer drugs such as 5-fluorouracil, doxorubicin, methotrexate, vincristine, and vinblastine [54,57]. Also, CPT is one of the four main components of FOLFIRINOX which is currently the most effective treatment for advanced state pancreas cancer [58]. Therefore, CPT is chosen as the chemotherapeutic agent in this research.

During DNA replication, top I is attached to DNA strands to release all the torsional strain caused by splitting the DNA double strands by changing the DNA topology through DNA rotation around the breakpoint [54,59]. When CPT attaches and stabilises the top I-DNA complex, which causes the irreversible double stranded breaks of DNA as the result of collision of the stabilised complex with DNA replication fork and transcription bubble, which leads to apoptosis of the affected cell [54,60,61]. Therefore, its cytotoxicity expresses in S-phase when DNA replication is taking place. Compared to G1 and G2 cells, S-phase cells are 100-1000 times more sensitive to CPT [62]. However, less than a quarter of tumour cells are typically in the S-phase, and so slow and continuous release of CPT in tumour cells is favoured to target these cells selectively over time [63,64].

CPT's cytotoxic potential not only selectively targets cells during DNA replication but also possesses unique properties that enable it to bypass specific resistance mechanisms, enhancing its effectiveness compared to other chemotherapeutics. One of the common drug resistances in cancer cells is caused by ATP-binding cassette (ABC) transporters that facilitates the energy-dependent efflux of various hydrophobic drugs [65]. Among these, P-glycoprotein (Pgp) provides the strongest resistance to widest variety of compounds contributing the most in drug resistance across many cancer cell lines [65,66]. Yet, CPT is not a substrate of Pgp and not affected by the overexpressed Pgp in cancer cells. Hence, CPT can be used to treat cancers with or without Pgp mediated multidrug resistance [54,67,68].

CPT was found from the extracts of a trees grown in south-eastern provinces of China of, Camptotheca acuminata, Nyssaceae, which is an indole alkaloid with an unsaturated pentacyclic ring which is rapidly hydrolysed to the ineffective water-soluble carboxylate form under normal physiological pH environment (Figure 2.1-5) while inducing more severe side-effects, such as cumulative haematological toxicity, diarrhoea and chemical or haemorrhagic cystitis, [54,68,69,70]. Therefore, to maintain its cytotoxicity while avoid un-necessitate side-

effects, CPT must be fixed in the lactone form during and after administration.

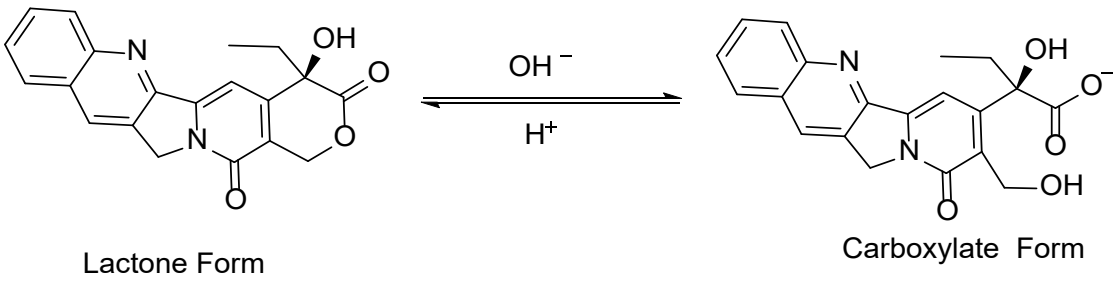

Figure 2.1-5. the conversion of between lactone and carboxylate form of camptothecin.

A facile strategy for CPT modification is to couple one or more amino acids to the C-20 OH group which shields and slow down the hydrolysis of the lactone ring [63,71,72]. Glycine is used to couple to the C-20 OH group because of its structural simplicity through an ester bond forming camptothecin glycinate (CPT-Gly) to stabilise the lactone ring from opening during circulation under physiological conditions prior to entering the cancer cells to maximise its therapeutic effect while reducing toxicity as the CPT-Gly ester bond is slowly hydrolysed releasing CPT [63,71,72]. Moreover, a glycine linker able to reduce the steric hindrance during conjugation therefore enhancing its coupling efficacy [73].

2.1.9.2. Metallic Chemotherapeutics

Metallic chemotherapeutics are metal-based compounds that show potent tumour growth inhibition and tumour toxicity [74]. Metal ions that can form complexes with various ligands at different coordination numbers, geometries, and redox states. Their physical and chemical properties can be tailored specifically with different ligands. For instance, ligands that can be replaced by biomolecules containing nitrogen, sulphur or selenium in proteins causing enzyme inhibition and cell death [75]. While some complexes can even mimic inhibitors of a specific protein or enzyme to prohibit the vital cell activities leading to cell death [75]. Therefore, metallic chemotherapeutics offer great potential in the development of original and highly potent cancer treatments.

However, the use of metallic chemotherapeutic agents is severely limited due to their

intense side-effects, including neurotoxicity, hepatotoxicity, and nephrotoxicity [74]. Moreover, its lack of selectivity and the ability of binding to human serum albumin and proteins killing healthy cells [75]. Therefore, to counter these drawbacks, metallic chemotherapeutics must be encapsulated into a polymeric carrier before administration.

2.1.10. Poly(ethylene Glycol) (PEG)

PEG is a highly hydrophilic, biocompatible, non-immunogenic, and non-toxic polymer widely utilised in biomaterials, biotechnology, and medicine (Figure 2.1-6) [24,25,76].

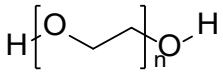

Figure 2.1-6. Poly(ethylene glycol)

Its unique properties, including steric stabilisation, enable PEG to repel other macromolecules and particles in the bloodstream, thereby preventing aggregation and enhancing the stability of drug delivery systems [24,77,78]. As a result, PEG is frequently incorporated as the hydrophilic segment in amphiphilic block copolymers, which are promising candidates for drug delivery vehicles [79]. For instance, PEG-modified poly(amino acid) drug carriers significantly extend drug retention time post-administration, improving therapeutic efficacy [80,81,82]. Moreover, when PEG is synthesised with a molecular weight exceeding 6,000 g/mol, it prolongs the circulation half-life of the drug carrier in the blood, facilitating greater accumulation at tumour sites through the EPR effect [25,79].

2.1.11. Replacement of PEG with Polysarcosine

Amphiphilic block copolymers that generate NPs in aqueous environments frequently incorporate PEG as the hydrophilic segment, primarily due to its favourable properties for *in vivo* applications and approval from the FDA [24,25,76,83]. However, the frequent administration of PEG has been associated with several adverse effects, including hypersensitivity, immunological responses, accumulation in tissues and the accelerated blood clearance effect [84]. The identification of anti-PEG antibodies were first reported in

1984 [85] which enhance the elimination of PEG-conjugated drugs from the bloodstream [86]. Furthermore, there has been a notable increase in both immediate and delayed hypersensitivity reactions to medications containing PEG [87]. Also, PEG's inability to degrade within the body leads to its accumulation in various tissues particularly within macrophages in the liver, pituitary gland, spleen, and eye, as well as in the epithelial cells of the choroid plexus and kidneys in animal tests [88,89,90,91,92,93]. This accumulation manifests as vacuolation, which occurs at all dosage levels and exhibits a dose-dependent severity, with no signs of clearance observed even two months post-administration [93]. Furthermore, it has been tested in monkeys that vacuolation in different organ tissues may adversely affect their functionality and architecture when dosed beyond a certain threshold, with the potential for progressive accumulation of PEG [93]. In addition to these concerning effects, PEG has been documented to interact with various proteins and positively charged amino acids, further complicating its use in drug delivery systems [48,94,95,96].

Given the growing apprehensions regarding the negative impacts of PEG on human health and the destabilisation of NPs caused by its interaction with proteins *in vivo* [48, 88-96]. There is an urgent need to explore alternative polymers for the formulation of NPs intended for drug delivery. Among the array of hydrophilic polymers available, such as polyglycerols, polyoxazolines, polypeptides, and polypeptoids, PSar (Figure 2.1-7), (also known as poly(N-methylated glycine)) has garnered considerable attention as a promising substitute for PEG in recent years [97].

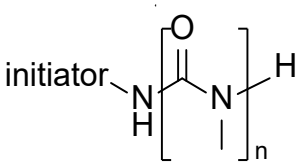

Figure 2.1-7 Polysarcosine

PSar is a non-ionic, hydrophilic stealth polymer that offers several advantages over PEG for biomedical applications [98,99,100]. It exhibits superior biocompatibility and reduced immunogenicity while its structure suggests similar hydrogen bonding capabilities with water and conformational flexibility as PEG [98,99,101,102]. These properties contribute to PSar's excellent hydrophilicity, which is comparable to or even exceeds that of PEG, making it

an attractive candidate for drug delivery applications [98,99,101,102]. More importantly, PSar is a stealth polymer that can provide shielding to NPs prevent the undesired interactions with biomolecules and aggregation thus to enhance blood circulation time [103,104]. Moreover, stealth properties could be achieved for NPs grafted with relatively short PSar with as low as 19 repeating units (1400 Da) of PSar which is lower than that of PEG to achieve stealth properties (2000 to 5000 Da) proving its ability in shielding the NPs from the outer biomolecules and reduce clearance by kidney and liver, expending the circulation time from minutes to hours [103,104,105,106]. Unlike water-insoluble polyalanine (poly isomer of PSar), PSar lacks hydrogen bond donors, preventing the formation of inter-molecular beta-bridges (pairs of hydrogen-bonded peptides in beta conformation) that can lead to aggregation [101]. Notably, PSar has demonstrated the ability to undergo decomposition *in vivo* by liver enzymes, addressing a key limitation of PEG [99]. Given these benefits, this study aims to utilise PSar as the hydrophilic component in the drug delivery systems developed.

2.1.12. Poly(glutamic acid)

PGA is another commonly studied poly(amino acid) [107,108]. It is water-soluble, biodegradable, edible, non-toxic, and anionic polyamide biopolymer, which is synthesised by the nucleophile-initiated ROP of the γ-protected NCA of L- glutamic acid [109]. Owing to its high biocompatibility, over the past decades PGA-containing products such as antimicrobial complexes, vaccine adjuvants, cancer therapy materials, and medical devices including scaffolds for tissue regeneration have been developed [110,111,112].

Each PGA repeat unit contains a carboxylate group for covalent modification. Anticancer drugs including paclitaxel, cisplatin, doxorubicin and camptothecin are suitable for covalent conjugation to PGA [108,113]. Moreover, owing to its anionic nature, PGA will not form aggregates with other negatively charged serum proteins and blood cells, thus overcoming the serum inhibitory effect [109, 114]. While its negative charge could potentially lead to electrostatic repulsion with cell surfaces or complexation with cationic species in the blood, which might reduce cellular uptake [107,115]. Research has consistently shown that these concerns do not compromise the EPR effect and the accumulation and retention of PGA

based drug conjugate [113,116,117,118]. Consequently, PGA serves as an effective polymeric backbone or drug carrier in this study.

2.2. Experimental

2.2.1. Amino Acid N-carboxyanhydrides (NCAs) Synthesis

2.2.1.1. Synthesis of Sar-NCA

Sarcosine (4.45 g, 50.0 mmol, 1.0 eqv) was placed in a three-necked RB flask fitted with a condenser and a dropping funnel. The system was purged with nitrogen for 15 minutes, three times. Anhydrous THF (70.0 mL) and α-pinene (16.0 mL, 100.0 mmol, 2.0 eqv) were then added to the flask. Triphosgene (10.0 g, 33.0 mmol, 0.67eqv), dissolved in 20.0 mL of anhydrous THF, was added dropwise via the dropping funnel once the reaction mixture was heated to reflux. The reaction was monitored, and completion was indicated when the solid sarcosine dissolved, signifying the formation of Sar-NCA. The solution was filtered and evaporated using rotary evaporation, yielding an oily crude product, which was dried under nitrogen stream overnight to allow crystal formation.

The crude solid was dissolved in a minimal amount of THF and precipitated into hexane (in an 8:1 hexane ratio). The mixture was stored overnight in a freezer to facilitate Sar-NCA precipitation. The product was collected by vacuum filtration and washed with cold THF to remove unreacted triphosgene and α-pinene. Recrystallisation was repeated three times, and the final product was dried under vacuum overnight. Yield: 57 %

^{1}H-NMR spectrum (400 MHz, DMSO-d_6) of Sar-NCA: 4.22 ppm (-CH_2-), 2.86 ppm (-CH_3)

2.2.1.2. Synthesis of L-Glutamic acid γ-benzyl ester N-carboxyanhydride (Glu(OBzyl)-NCA)

L-Glutamic acid γ-benzyl ester (1.186 g, 5.0 mmol, 1.0 eqv) was added to a three-necked RB flask equipped with a condenser and a dropping funnel. After purging the system with nitrogen for 15 minutes, three times. Then 50.0 mL of anhydrous THF and α-pinene (1.6 mL, 10.0 mmol, 2.0 eqv) were added to the flask. Triphosgene (1.0 g, 3.3 mmol, 0.67 eqv) dissolved in 20.0 mL of anhydrous THF, was added dropwise through the dropping funnel once the mixture was heated to reflux. The reaction was complete when all solid amino acid

dissolved, indicating the formation of Glu(OBzyl)-NCA.

After completion, the solution was filtered and evaporated using rotary evaporation to yield a solid crude product. The solid was dissolved in a minimal amount of THF and precipitated into hexane (8:1 hexane ratio). The mixture was stored overnight in a freezer to precipitate Glu(OBzyl)-NCA. The product was then collected by vacuum filtration and washed with cold THF to remove any unreacted triphosgene and α-pinene. Recrystallisation was performed three times before drying the final product under vacuum overnight. Yield: 81%

^{1}H-NMR spectrum (400 MHz, DMSO-d_6) of Glu(OBzyl)-NCA: 9.09 ppm (-NH), 7.37 ppm (-OBzyl), 5.10 ppm (-OBzyl), 4.45 ppm (-CH-), 2.54-1.89 ppm (-C**H$_2$**-C**H$_2$**-)

2.2.2. Ring Opening Polymerisation of NCAs

2.2.2.1. Synthesis of PGlu(OBzyl)

Glu(OBzyl)-NCA (2.0 g, 7.6 mmol, 1000.0 eqv) was added into a Schlenk tube and purged with nitrogen for 15 minutes, three times, before hexylamine (0.99 µl, 0.0076 mmol, 1.0 eqv) in 50.0 mL of anhydrous DMF at 0^{o}C was added into the reaction flask. The reaction solution was kept at 0^{o}C in ice bath and was allowed to slowly rise to room temperature for four days under nitrogen bubbling. The completion of polymerisation was confirmed with ^{1}H-NMR, and the crude product was precipitated in diethyl ether and collected by centrifugation and wash with diethyl ether for three times and dried in vacuum. yield: 99%

2.2.2.1.1. Deprotection of OBzyl Group

Poly(γ-benzyl-L-glutamate) (PGlu(OBzyl)) (1.0 g) was dissolved in 20.0 mL of trifluoroacetic acid (TFA), and 6.0 mL of hydrobromic acid in acetic acid (33% HBr/AcOH) was added to the reaction flask dropwise. The reaction mixture was stirred at room temperature for 90 minutes and precipitated in cold diethyl ether and collected by centrifugation, followed by drying under vacuum overnight. The above process was repeated twice to fully deprotect the OBzyl protecting group.

The resulting polymer was dissolved in a saturated solution of Na_2CO_3 and dialysed (MWCO:

12k-14kDa) against DI water for three days. After dialysis, the pH value of the polymer solution was adjusted to pH 1.0 by addition of concentrated HCl to protonate polyglutamic acid sodium salt and precipitate out polyglutamic acid. The precipitated polymer was washed with 0.1M HCl solution twice and later washed with DI water five times and freeze-dried to obtain the final product-PGA. Yield: 60%

^{1}H-NMR spectrum (500 MHz, DMSO-d_6) of PGA: 12.13 ppm (-COOH), 8.23 ppm (-NH), 3.96 ppm (-CH-), 2.28-1.94 ppm (-C**H$_2$**-C**H$_2$**-), 1.24-0.84 ppm (initiator).

2.2.2.2. Synthesis of PSar

Sar-NCA (2.0 g, 17.4 mmol, 70.0 eqv) was added to a Schlenk tube, which was purged with nitrogen three times, 15 minutes each. Hexylamine (32.6 µL, 0.25 mmol, 1.0 eqv) was dissolved in 5.0 mL of DMF and added to the reaction flask at 0°C in an ice bath. The reaction mixture was allowed to warm slowly to room temperature over two days under a constant nitrogen flow.

After the polymerisation, the crude product was precipitated in diethyl ether, followed by centrifugation. The product was washed with diethyl ether three times and dried under vacuum to yield the final PSar polymer. Yield: 99%

^{1}H-NMR spectrum (400 MHz, DMSO-d_6) of PSar: 7.95 ppm (-NH-), 4.33-3.93 ppm (-CH_2-), 2.96-2.75 ppm (-CH_3), 1.37-0.85 ppm (Initiator)

2.2.3. Drug Conjugation Synthesis

2.2.3.1. Synthesis of Boc-Gly-CPT

CPT (50.0 mg, 0.144 mmol, 1.0 eqv), Boc-Gly-OH (75.4 mg, 0.432 mmol, 3.0 eqv) and DMAP (35.2 mg, 0.288 mmol, 2.0 eqv) were added into a 100.0 mL two necked flask. Purged with nitrogen for three times before addition of DCM (40.0 mL). The reaction mixture was cooled in ice bath to 0^{o}C, then DCC (89.0 mg, 0.432 mmol, 3.0 eqv) in DCM was added into the reaction mixture slowly through a needle. The reaction mixture was allowed to warm to room temperature and left for 24 hours.

After the reaction, the solution was filtered and solvent evaporated under reduced pressure

to yield a crude product. The crude product was purified by column chromatography (eluent: DCM: acetone, 8:2). Yield: 99%

2.2.3.2. Deprotection of Boc Group to Yield CPT-Gly

Boc-Gly-CPT (0.5 g) was dissolved in DCM (10.0 mL) and trifluoracetic acid (5.0 mL) was added into the solution, which was stirred for 15 minutes at room temperature. The end point of reaction was determined by thin layer chromatography (TLC). The reaction solution was evaporated under nitrogen flow, and the product was recrystallised in methanol/ diethyl ether three times to obtain the TFA salt of CPT- Gly. The TFA salt was removed by dissolving the product in DMF then added 0.5 mL of triethylamine. The CPT-Gly was then precipitated out in diethyl ether/ hexane 1:1 and washed with diethyl ether three times and dried in vacuum overnight. Yield: 82%.

^{1}H-NMR spectrum (400 MHz, DMSO-d_6) of CPT-Gly: 8.72 ppm (=CH-), 8.17 ppm (=CH-), 7.88-7.74 ppm (=CH-), 7.23 ppm (=CH-), 6.68 ppm (-NH_2), 5.54- 5.33 ppm (-N-CH_2-, -O-CH_2-), 4.12-3.87 ppm (-CH_2-C=O-), 2.17 ppm (CH_3-C**H**$_2$-), 0.94 ppm (-CH_3)

2.2.3.3. Synthesis of CPT-Gly-PSar Drug Conjugate

CPT-Gly (50.0 mg, 0.12 mmol, 1.0 eqv) and Sar-NCA(58.3 mg, 0.51 mmol, 4.1 eqv) were added to an RB flask, which was purged with nitrogen for three times (15 minutes each). 5.0 mL of anhydrous DMF was then added to the reaction flask. The reaction mixture was stirred continuously at 0°C in an ice bath for two days with a steady flow of nitrogen bubbling through the solution. The resulting polymer-drug conjugate was precipitated in diethyl ether, washed three times with diethyl ether, and dried under vacuum overnight. Yield: 99%

^{1}H-NMR spectroscopy (400 MHz, DMSO-d_6) of PSar-Gly-CPT: 8.71 ppm (=CH-), 8.44 ppm (-NH-), 8.17 ppm (=CH-), 7.86- 7.74 ppm (=CH-), 7.17 ppm (=CH-), 5.50- 5.31 ppm (-N-CH_2-, -O-CH_2-), 4.36-3.99 ppm (-C=O-CH_2-N- (PSar)), 2.95-2.73 ppm (-N-CH_3), 2.17 ppm (CH_3-C**H**$_2$-), 0.92 ppm (CH_3) (*Figure 2.3-18*)

2.2.3.4. Synthesis of PGA-(PSar-Gly-CPT) Conjugate

PGA (3.2 mg, 0.025 mmol, 1.0 eqv), EDC.HCl (14.4 mg, 0.075 mmol, 3.0 eqv) and NHS (8.7

mg, 0.075 mmol, 3.0 eqv) were added to a Schlenk tube, which was purged with nitrogen three times (15 minutes each) before addition of 1.0 mL of anhydrous DMF. The reaction mixture was allowed to stir for an hour in ice bath to activate the carboxylate group. Then, PSar-Gly-CPT (20.0 mg) in 1.0 mL of anhydrous DMF was added into the reaction mixture. The reaction mixture was allowed to warm to room temperature and stirred for two days. The crude product was dialysed against DI water three days before being freeze dried. Yield: 78%

^{1}H-NMR spectrum (500 MHz, DMSO-d_6) of PGA-(PSar-Gly-CPT): 8.68 ppm(=CH-), 8.45 ppm (-NH-), 8.17 ppm (=CH-), 7.86-7.71 ppm (=CH-), 7.16 ppm (=CH-), 5.50-5.28 ppm (-N-CH_2-, -O-CH_2-), 4.28-3.96 ppm (-NH-C**H**-C=O-,-NH-C**H$_2$**-C=O-, -N(CH_3)-C**H$_2$**-), 2.89-2.71 ppm (-N-CH_3), 2.43-1.78 ppm (-C**H$_2$**-C**H$_2$**-)

2.2.3.5. Synthesis of PGA-(Gly-CPT) Conjugate

PGA (10.0 mg, 0.078 mmol, 1.0 eqv), EDC.HCl (45.0 mg, 0.23 mmol, 3.0 eqv) and NHS (27.0 mg, 1.45 mmol, 3.0 eqv) were added to a Schlenk tube. Purged with nitrogen for three times (15 minutes each) before addition of 1.0 mL of anhydrous DMF. The reaction mixture was allowed to stir for an hour in ice bath to activate the carboxylate group, then CPT-Gly (14.0 mg, 0.034 mmol, 0.44 eqv) in 1.0 mL of anhydrous DMF was added into the reaction mixture. The reaction mixture was allowed to warm to room temperature while kept stirring for two days. The crude product was dialysed against methanol overnight then in DI water for two days then freeze dried. Yield: 73%

^{1}H-NMR spectrum (400 MHz, DMSO-d_6) of PGA-(CPT-Gly) drug conjugate: 8.66- 7.16 ppm (=CH-, -NH-), 5.51-4.97 ppm (-N-CH_2-, -O-CH_2-), 4.21-3.95 ppm (-NH-C**H**-C=O-,-NH-C**H$_2$**-C=O-), 2.39- 1.84 ppm (-C**H$_2$**-C**H$_2$**-, CH_3-C**H**$_2$-), 1.23-0.91 ppm (initiator)

2.2.3.6. Synthesis of PGA-[(CPT-Gly)-co-(PSar)] Conjugate

PGA (10.0 mg, 0.078 mmol, 1.0 eqv), EDC.HCl (45.0 mg, 0.23 mmol, 3.0 eqv) and NHS (27.0 mg, 1.45 mmol, 3.0 eqv) were added into Schlenk tube. Purged with nitrogen for three times (15 minutes each) before addition of 2.0 mL of anhydrous DMF. The reaction mixture was allowed to stir for an hour in ice bath to activate the carboxylate group, then PSar (7.5 mg, 0.0015 mmol, 0.02 eqv), CPT-Gly (11.2 mg, 0.028 mmol, 0.36 eqv) in 1.0 mL of anhydrous

DMF were added into the reaction mixture. The reaction mixture was allowed to warm to room temperature while kept stirring for two days. The crude product was dialysed against methanol overnight then in DI water for two days then freeze dried. Yield: 60%

^{1}H-NMR spectrum (400 MHz, DMSO-d_6) of PGA-[(CPT-Gly)-*co*-(PSar)]: 8.69 ppm (=CH-),8.29 ppm (-NH), 8.17 ppm (=CH-), 7.89-7.*73* ppm (=CH-), 7.19 ppm (=CH-), 5.*49*-5.*29* ppm (-N-CH_2-, -O-CH_2-), 4.*34*-3.9*1* ppm (-NH-C**H**-C=O-,-NH-C$\mathbf{H_2}$-C=O, -N(CH_3)-C$\mathbf{H_2}$-), 2.94-2.7*2* ppm (-N(C$\mathbf{H_3}$)-), 2.42-1.86 ppm (-C$\mathbf{H_2}$-C$\mathbf{H_2}$-, CH_3-C$\mathbf{H}_2$-), 1.23- 0.90 ppm (initiator)

2.3. Result & Discussion

The overarching aim of this research is to create a polymer-drug conjugate that can complex with metal ion as a potentially highly effective drug delivery system. The polymer-drug conjugate should form NPs in aqueous solution and so the designed macromolecule consists of different polymeric components. Initially the synthesis of the poly(amino acid) components PSar and PGA were created, followed by the creation of their corresponding drug conjugates CPT-Gly-PSar, PGA-(PSar-Gly-CPT), PGA-(Gly-CPT) and PGA-[(CPT-Gly)-*co*-(PSar)]. Their differences in physical behaviour in aqueous solution were analysed and discussed in terms of chemical structural design for the creation of fucose incorporation drug conjugate that synthesised later.

2.3.1. Synthesis of Amino Acid NCAs

In this study, poly(amino acids) was produced through the ROP of amino acid NCAs. This method of poly(amino acid) creation provides greater control and a more straightforward route to polymer in the absence of catalysts compared to polycondensations and is much more efficient/less labour intensive compared to SPPS [9,10,11,12]. Therefore, synthesis of Sar-NCA and Glu(OBzyl)-NCA were the very first step to the final drug conjugate synthesis. Through reacting with triphosgene, amino acids form a penta-cyclic structure that is susceptible towards nucleophilic attack(Scheme 2.1-2) and eventually forming the final polymer, PSar (Figure 2.3-1) and PGA (Figure 2.3-2).

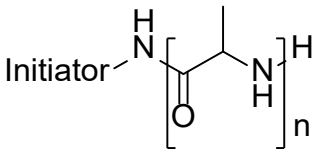

Figure 2.3-1. PSar

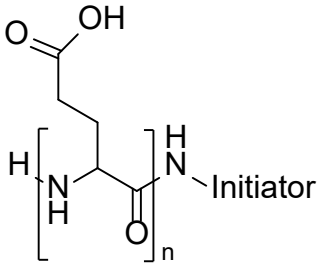

Figure 2.3-2. PGA

2.3.1.1. Synthesis of Sar-NCA

Sar-NCA (Figure 2.3-3) was synthesised using triphosgene as a precursor monomer of PSar. It was obtained as a white powder, yield 57% and confirmed through ^{1}H-NMR spectroscopy.

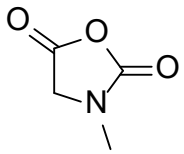

Figure 2.3-3. Sar-NCA

The ^{1}H-NMR spectrum displayed characteristic peaks at 2.86 ppm, corresponding to the methyl group, and at 4.22 ppm, representing the two protons of the sarcosine backbone (Figure 2.3-4) consistent to that of literature [119]. The remaining peaks in the spectrum are assigned to DMSO-d_6 and water that is associated with highly hygroscopic DMSO. The lack of further peaks confirmed that a highly pure product was formed, which is essential for successful ROP

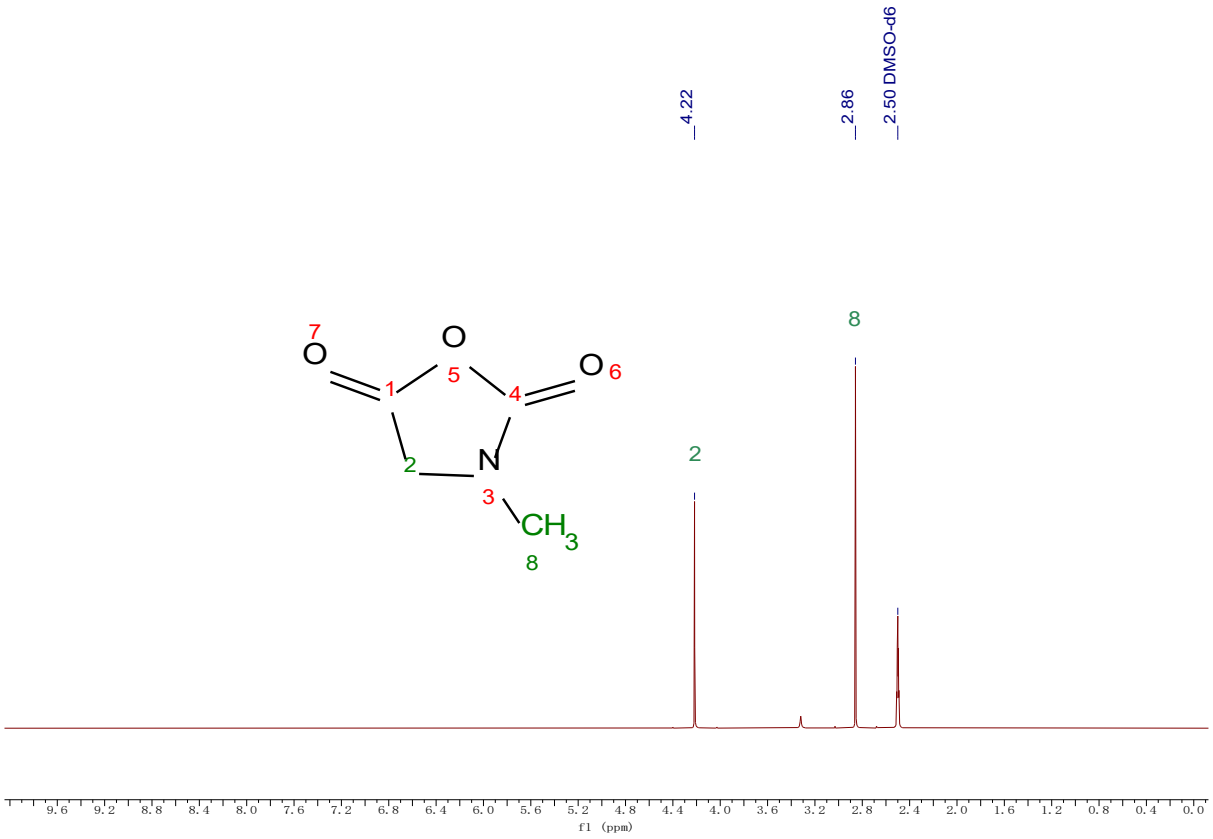

Figure 2.3-4. ^{1}H-NMR spectrum (400 MHz, DMSO-d_6) of Sar-NCA: 4.22 ppm (-CH_2-), 2.86 ppm (-CH_3) [119].

FTIR spectroscopy further validated the successful synthesis of Sar-NCA, with a sharp peak observed at 1851 cm^{-1} which corresponds to the anhydride stretch of the NCA monomer (Figure 2.3-5). The presence or absence of this peak is extremely useful to confirm NCA creation. While peak at 1757 cm^{-1} were correspond to the C=O bonds stretch.

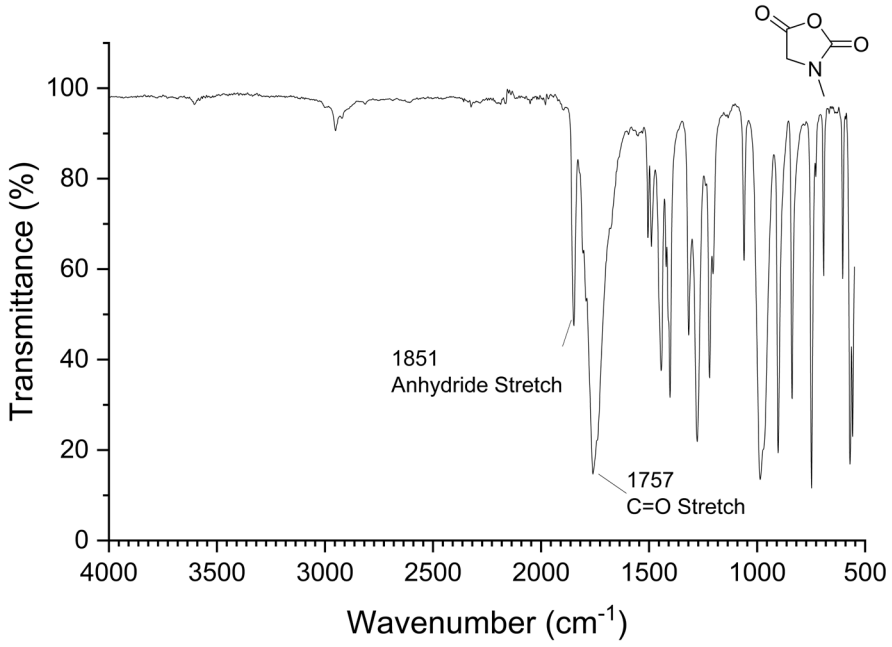

Figure 2.3-5. FTIR spectrum of Sar-NCA

2.3.1.2. Synthesis of Glu(OBzyl)-NCA

Glu(OBzyl)-NCA (Figure 2.3-6) was obtained as a white powder, yield 81% and its chemical structure was confirmed by ^{1}H-NMR spectroscopy (Figure 2.3-7). Glu(OBzyl)-NCA was produced as a monomer of PGlu(OBzyl) and subsequently PGA.

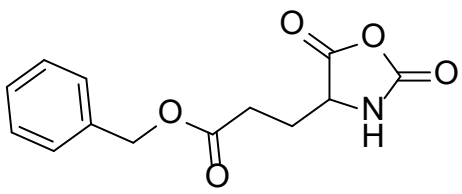

Figure 2.3-6. Glu(OBzyl)-NCA

The ^{1}H-NMR spectrum shows distinct peaks, including 9.09 ppm for the amide proton, 7.37 ppm for the five aromatic protons of the OBzyl protecting group, 5.10 ppm for the two non-aromatic protons of the protecting group, 4.45 ppm for the proton present on the carbon atom that is connected to the amino group, and a range of peaks (2.54 to 1.89 ppm) for the

four protons of the side chain (Figure 2.3-7) consistent to that in literature[120].

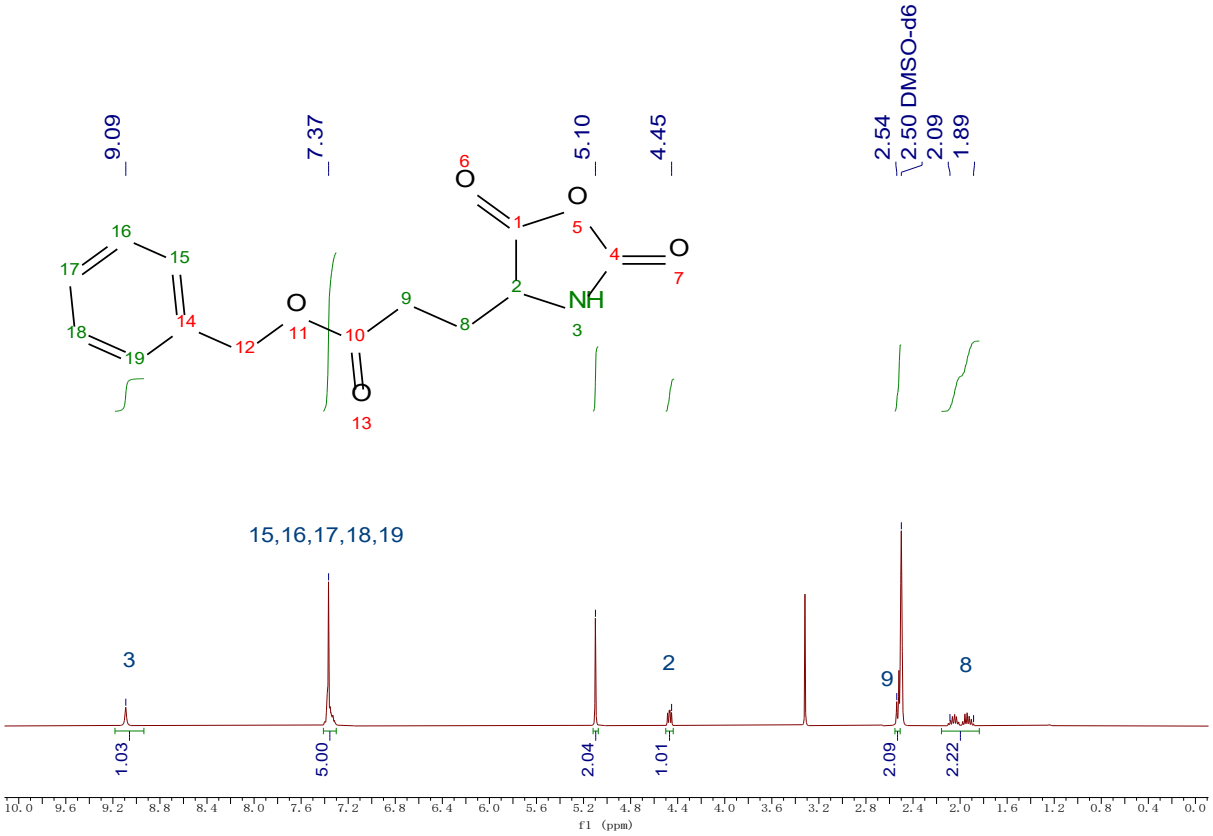

Figure 2.3-7. ^{1}H-NMR spectrum (400 MHz, DMSO-d_6) of benzyl ester glutamic acid-NCA: 9.09 ppm (-NH), 7.37 ppm (-OBzyl), 5.10 ppm (-OBzyl), 4.45 ppm (-CH-), 2.54-1.89 ppm (-C**H**$_2$-C**H**$_2$-) [120].

FTIR spectroscopy further confirmed the structure of Glu(OBzyl)-NCA by revealing peaks characteristic of its functional groups: an amide stretch at 3248 cm^{-1}, an anhydride stretch at 1863 cm^{-1}, and a C=O stretch at 1771 cm^{-1} (Figure 2.3-8).

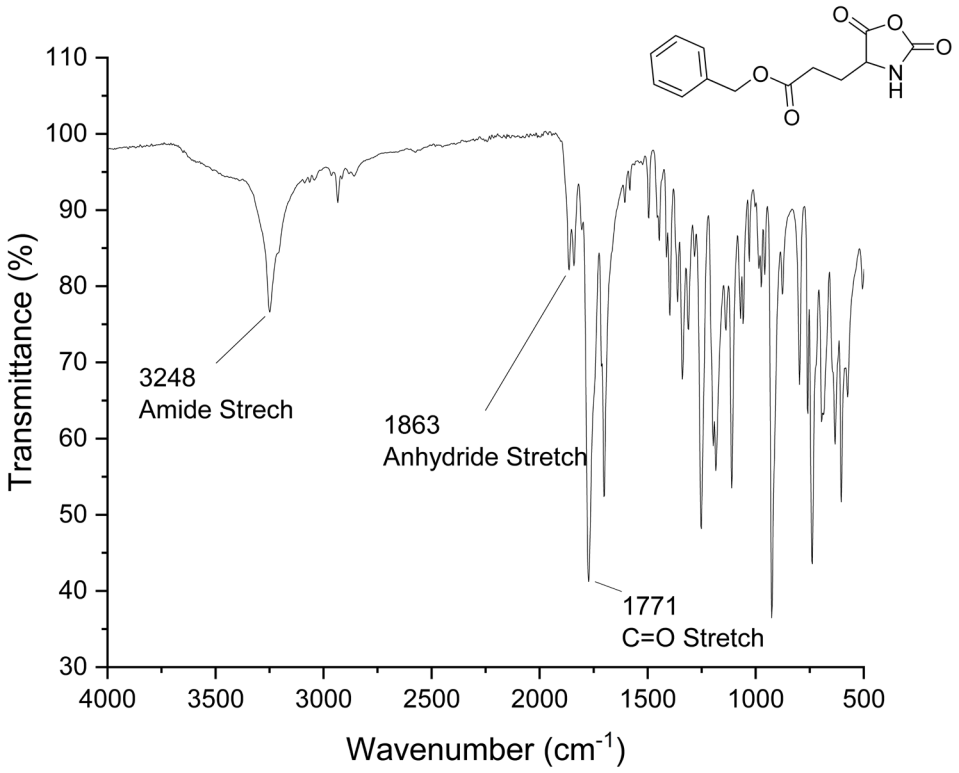

Figure 2.3-8. FTIR spectrum of Glu(OBzyl)-NCA

2.3.2. Synthesis of PSar

PSar was then synthesised via Sar-NCA ROP through hexylamine initiation (Figure 2.3-9). PSar is synthesised as a potential replacement for PEG owing to its comparable hydrophilicity and was produced for inclusion as the hydrophilic moiety of the drug conjugate [121,122,123]. Also, owing to its stealth properties, it prevents the undesired interactions of NPs with biomolecules and aggregation enabling the NPs to diffuse in physiological environments, such as the bloodstream, allowing the NPs to potentially reach their target site *in vivo,* with potentially harmful and wasteful polymer aggregation prevented [103,104]. This PSar was synthesised with a specific purpose: to demonstrate that PSar modification can enhance the water solubility and stability of NPs in drug conjugates. For simplicity, hexylamine was used as the initiator as the alkyl chain provides clear NMR peaks, and fucose was not included at this stage.

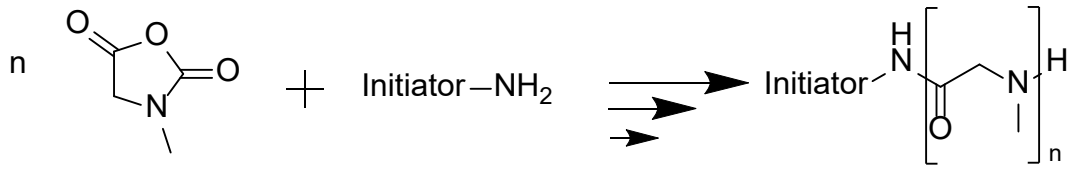

Figure 2.3-9. Ring opening polymerisation of Sar-NCA.

The synthesised polymer was analysed by ^{1}H-NMR spectroscopy to confirm its structure. The peak at 7.95 ppm corresponds to the two nitrogen protons, while peaks within the range of 4.33-3.93 ppm represent the two protons in the backbone of the PSar repeating unit. Additionally, peaks within the range of 2.96-2.75 ppm correspond to the methyl group of the PSar repeat unit, and a broader range of 1.37-0.85 ppm accounts for the 13 protons provided by from the initiator (Figure 2.3-10) consistent to the literature [119]. By integrating the ^{1}H-NMR spectrum, it was determined that the polymer consists of approximately 60 repeating units.

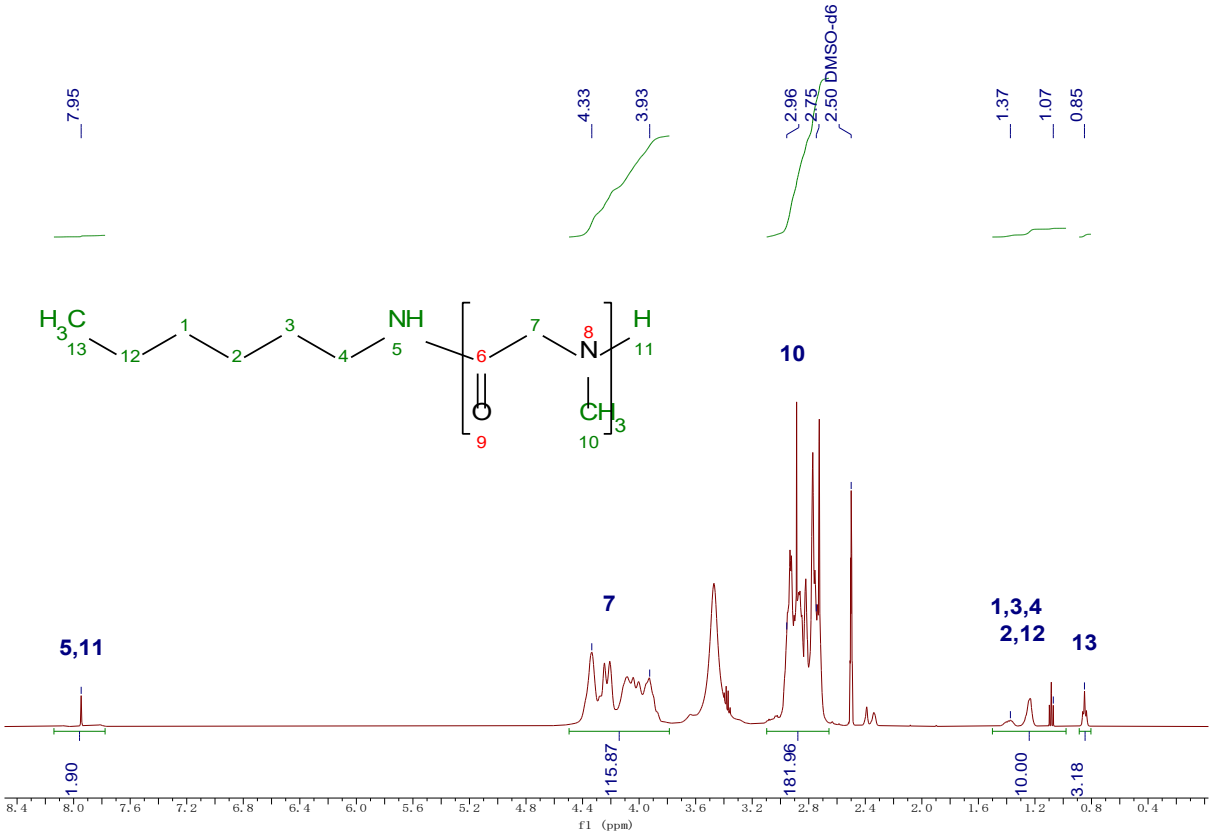

Figure 2.3-10. ^{1}H-NMR spectrum (400 MHz, DMSO-d_6) of PSar: 7.95 ppm (-NH-), 4.33-3.93 ppm (-CH_2-), 2.96-2.75 ppm (-CH_3), 1.37-0.85 ppm (Initiator)

MALDI-TOF mass spectrometry analysis was carried out to further determine the degree of polymerisation achieved for the PSar synthesised. Its M_n and M_w were calculated through the below equations

$$Mn = \frac{\sum Ni*Mi}{\sum Ni} = \; Mn = \frac{90*4862.918+82*4933.998+\cdots+18*3938.035+18*3866.955}{90+82+\cdots+18+.18} = 4842.00$$

Where *Ni* is the number of molecules or the intensity of percentage with molecular weight *Mi*.

$$Mw = \frac{\sum Ni*Mi^2}{\sum Ni*Mi} = \; Mw = \frac{90*4862.918^2+82*4933.998^2+\cdots+18*3938.035^2+18*3866.955^2}{90*4862.918+82*4933.998+\cdots+18*3938.035+18*3866.955} = 4880.10$$

The MALDI spectrum shows the PSar has a number average molecular weight (M_n) of 4842.00 g/mol, a weight average molecular weight (M_w) of 4880.10 g/mol, and a very narrow dispersity of a 1.008$Đ_M$. (Figure 2.3-11). The repeat unit of the PSar synthesised was calculated to be 66, showing good correlation with the NMR data.

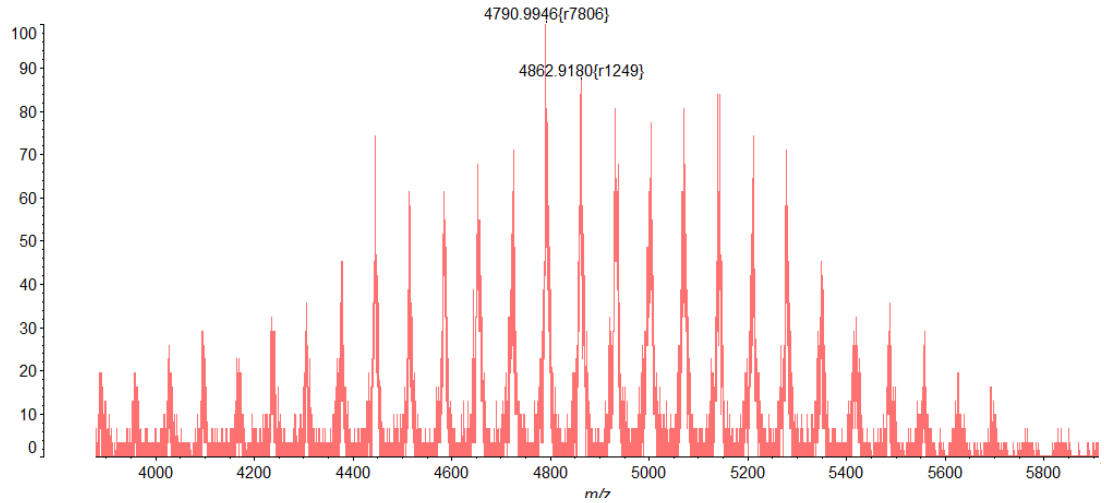

Figure 2.3-11. MALDI-TOF mass spectroscopy analysis of PSar synthesised. M_n = 4842.00, M_w = 4880.10, dispersity= 1.008$Đ_M$, Repeat unit: 66.

However, because of the different of ionisation efficiency of different molecular weight polymer chains, higher molecular weight polymer chains generally exhibit lower ionizability compared to lower molecular weight species [124, 125]. This occurs because larger macromolecules require higher laser fluence for effective desorption and ionisation, and

they tend to form fewer charged species per molecule. As a result, the mass spectra are often biased toward the lower molecular weight population, leading to an under-representation of high-mass polymers. Also, detector saturation resulting from strong signals of matrix-related and low-mass oligomer ions can further potentiating this problem [126]. These discrimination effects shift the observed molecular weight distribution toward lower values, potentially underestimating the true average molecular weight (M_w and M_n) of the polymer.

2.3.3. Synthesis of PGA

The carboxylate group of PGA may be covalently coupled CPT-Gly, PSar, and cell targeting groups by EDC/NHS coupling, providing further function to the polymeric component [108,113,127,128].

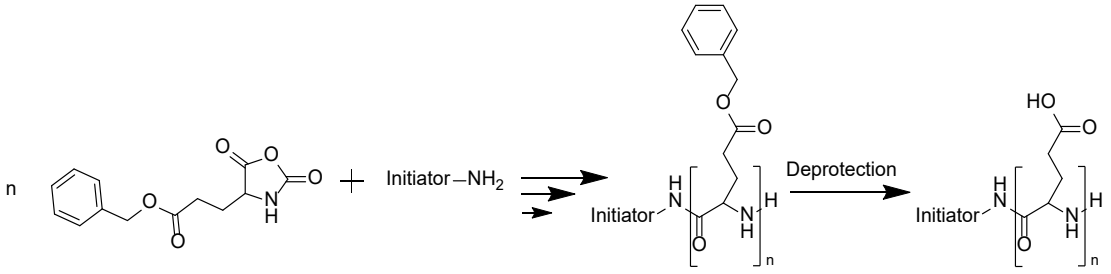

Figure 2.3-12. Ring opening polymerisation of Glu(OBzyl)-NCA to produce PGA

PGA was successfully synthesised via ROP of Glu(OBzyl)-NCA through hexylamine initiation, followed by acid-mediated cleavage of the benzyl protecting groups to yield the final polymer (Figure 2.3-12). Dialysis bag with high MWCO (12k-14k Da) was used to ensure the removal of oligomer and the minimal repeating unit is no less than 78.

The structure of PGA was confirmed using ^{1}H-NMR spectroscopy (Figure 2.3-13) which shows only trace of protecting group proton peak at 5.32 ppm remain, indicating the successful deprotection and the PGA was used as it is. A broad peak at 12.13 ppm corresponding to the carboxylic acid proton, peaks from 8.23 ppm representing the amine and amide protons, a peak at 3.96 ppm for the backbone proton, peaks from 2.28 to 1.94 ppm for the four protons of the side chain, and peaks from 1.23 to 0.84 ppm for the initiator protons consistent to the literature [129]. After deprotection and dialysis, the overall yield

was less than expectation with only 60%. This moderate yield may be attributed to factors such as formation of oligomer during the ROP reaction like initiation by impurities (e.g., moisture) or undesired initiation by amine of NCA, backbiting reactions, or chain cleavage during the acid-mediated deprotection of the benzyl groups [11].

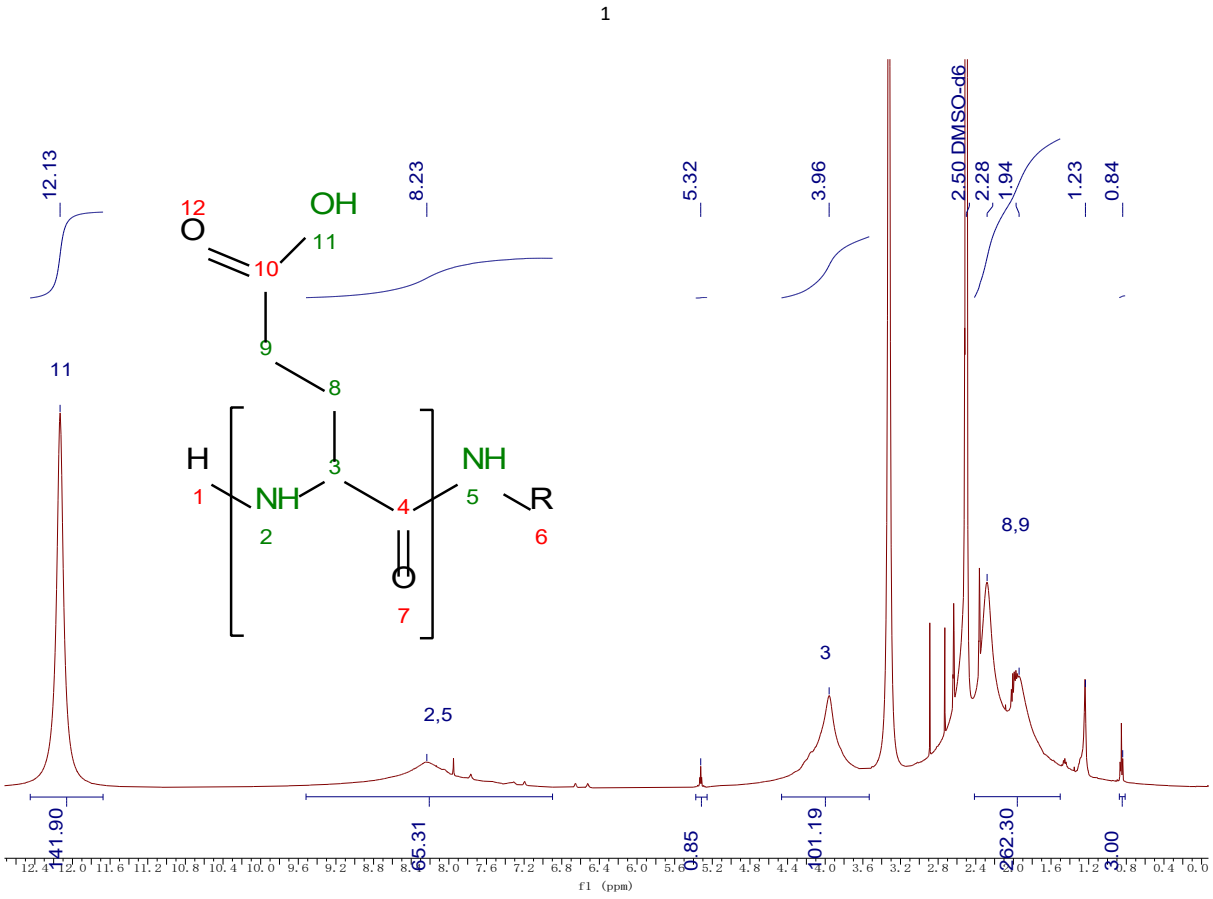

Figure 2.3-13. ^{1}H-NMR spectrum (500 MHz, DMSO-d_6) of PGA: 12.13 ppm (-COOH), 8.23 ppm (-NH), 3.96 ppm (-CH-), 2.28-1.94 ppm (-C**H**$_2$-C**H**$_2$-), 1.24-0.84 ppm (initiator) [129].

2.3.4. Synthesis of CPT-Gly Conjugate

To enable the efficient conjugation of CPT to PGA, the tertiary hydroxy group of CPT was chemically modified through DCC/DMAP conjugation with Boc-Gly-OH. This modification fulfils several critical objectives: it mitigates steric hindrance between adjacent CPT molecules attached to PGA by increasing their spatial separation, thereby improving coupling efficiency [107]; it enhances the water solubility of CPT owing to the hydrophilic

properties of glycine [63]; it introduces a primary amino group, which functions as a nucleophile, facilitating a direct and efficient coupling reaction with the carboxylate groups of PGA[107,113]; also, its ester bond linkage between glycine and CPT can be hydrolysed in acidic conditions allowing the release of free CPT in the cancer cells [63,71].

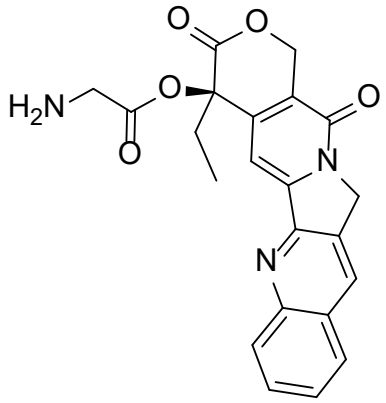

Figure 2.3-14. CPT-Gly

The successful synthesis of the CPT-Gly was confirmed through ^{1}H-NMR and FTIR spectroscopy. The disappearance of the hydroxy group proton signal at 6.5 ppm in ^{1}H-NMR, confirming the esterification of CPT's hydroxy group with glycine(Figure 2.3-14).

Subsequent deprotection conducted in a 1:1 mixture of DCM: TFA, hydroxy or carboxylic acid proton signals were not observed in ^{1}H-NMR spectrum, verifying that the CPT lactone ring remained intact under these conditions (Figure 2.3-15) consistent to the literature [63].

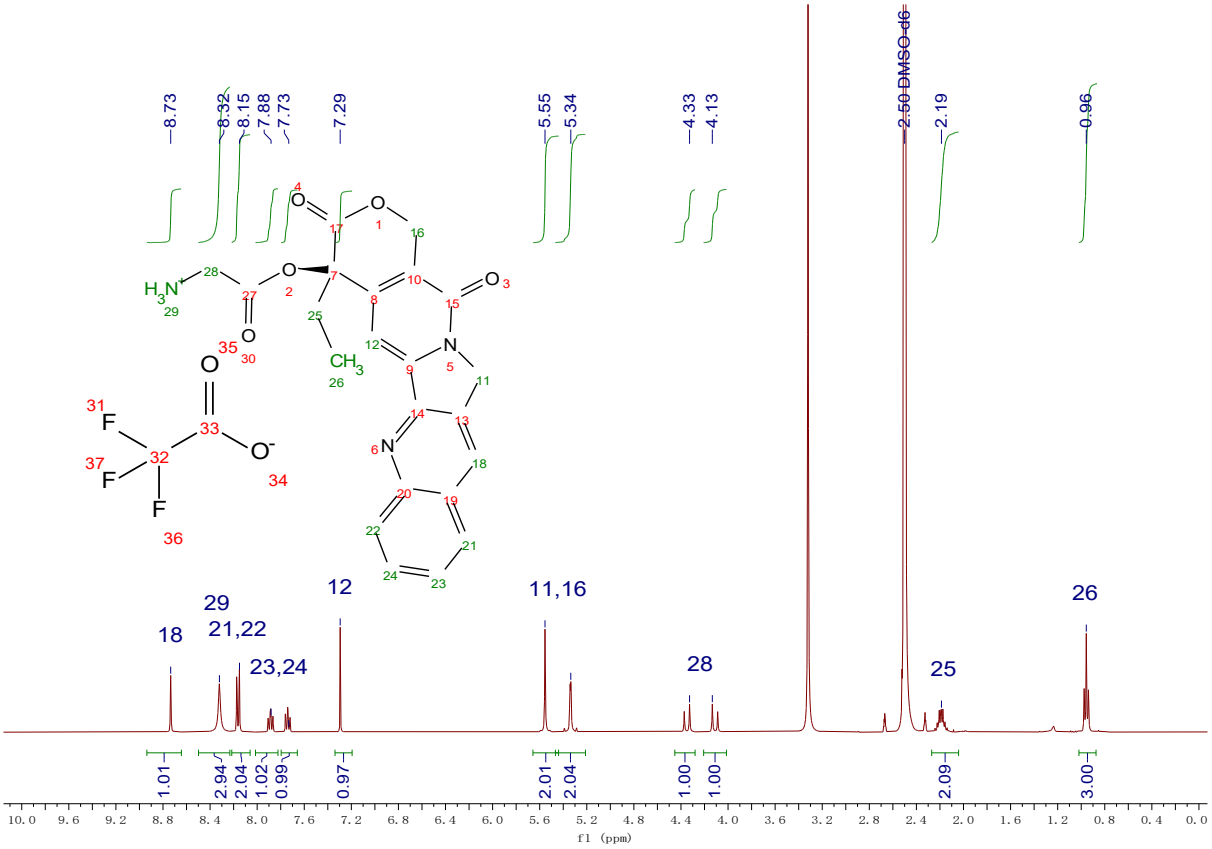

Figure 2.3-15. ^{1}H-NMR spectrum (400 MHz, DMSO-d_6) of CPT-Gly. TFA salt: 8.73 ppm (=CH-), 8.32 ppm (-NH_3^+), 8.15- 7.73 ppm (=CH-), 7.29 ppm (=CH-), 5.55- 5.34 ppm (-N-CH_2-, -O-CH_2-), 4.33-4.13 ppm (-CH_2-C=O-), 2.19 ppm (CH_3-C**H**$_2$-), 0.96 ppm (-CH_3) [63].

Furthermore, the removal of the TFA salt and neutralisation of the amine cation were evidenced by the elimination of a peak at 8.32 ppm which correspond to the primary ammonium salt and the emergence of a new peak at 6.68 ppm representing the primary amine in the ^{1}H-NMR spectrum (Figure 2.3-16).

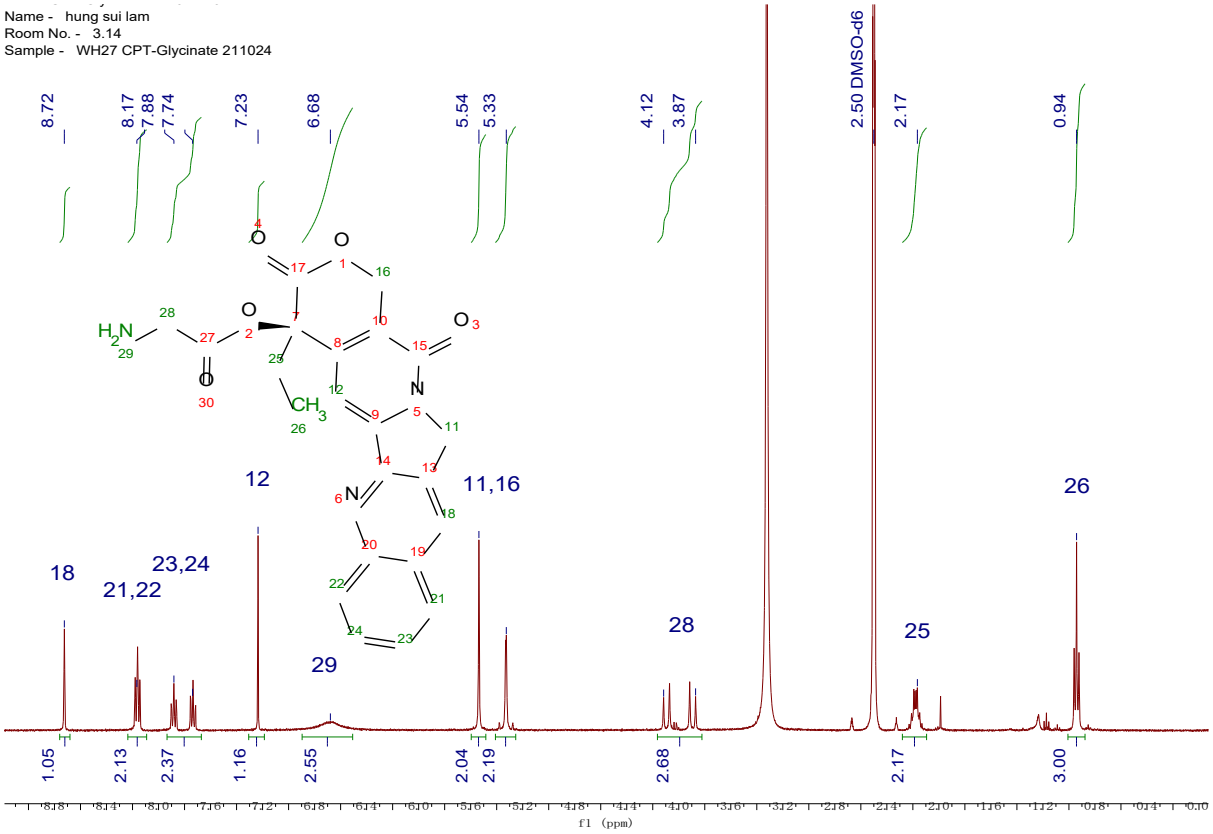

Figure 2.3-16. ^{1}H-NMR spectrum (400 MHz, DMSO-d_6) of CPT-Gly: 8.72 ppm (=CH-), 8.17 ppm (=CH-), 7.88- 7.74 ppm (=CH-), 7.23 ppm (=CH-), 6.68 ppm ($-NH_2$), 5.54- 5.33 ppm ($-N-CH_2-$, $-O-CH_2-$), 4.12- 3.87 ppm ($-CH_2-C=O-$), 2.17 ppm (CH_3-CH_2-), 0.94 ppm ($-CH_3$)

FTIR spectroscopy provided additional confirmation of the structural modifications, revealing characteristic absorption bands at 3402 cm^{-1} (broad, indicative of a primary amine stretch) and 1752 cm^{-1} (sharp, corresponding to an ester carbonyl stretch) in the CPT-Gly conjugate (Figure 2.3-17).

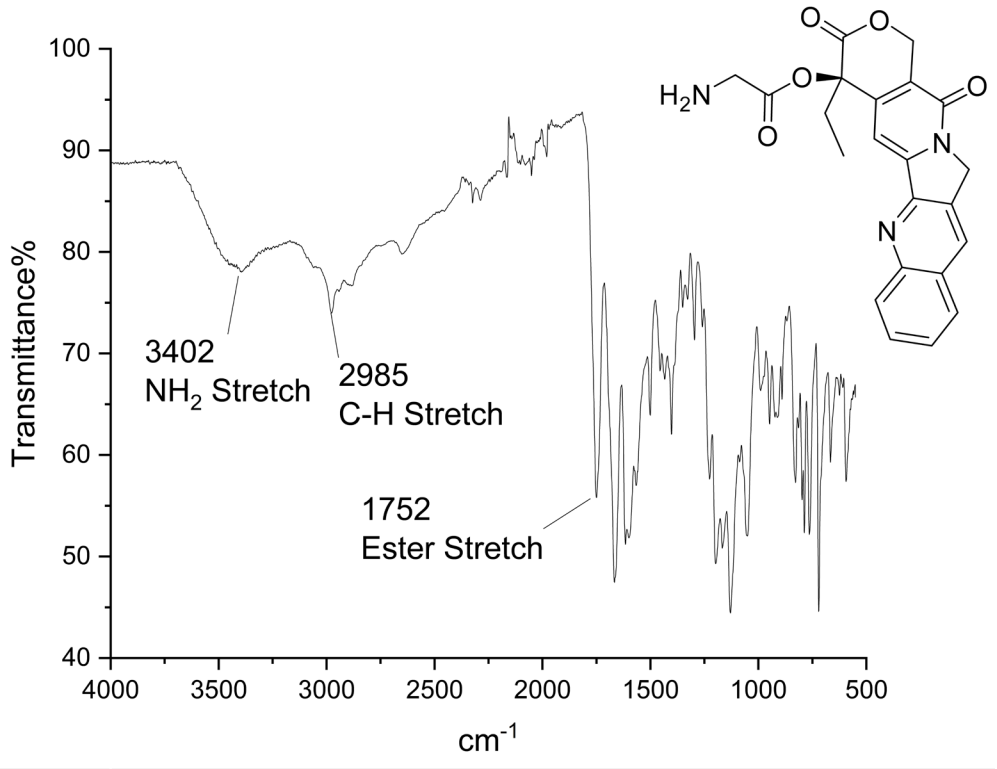

Figure 2.3-17. FTIR Spectra of CPT-Gly, amine stretch at 3402 cm^{-1}, ester carbonyl stretch at 1752 cm^{-1}.

2.3.5. Synthesis of CPT-Gly-PSar

CPT-Gly initiated ROP of Sar-NCA (Scheme 2.3-1) provided a straightforward and efficient approach to enhance the water solubility of the highly hydrophobic CPT. Due to its structural and synthetic simplicity, the CPT-Gly-PSar drug conjugate was designed as a straightforward model to assess the necessity of conjugation with PGA.

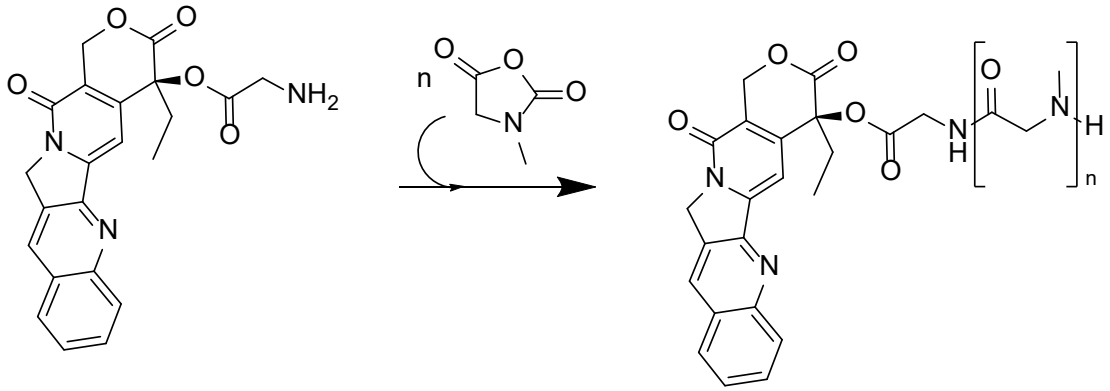

Scheme 2.3-1. Synthesis of CPT-Gly-PSar through CPT-Gly initiated ROP of Sar-NCA

CPT-Gly-PSar with three different extents of CPT conjugation were synthesised, with their respective weight ratios determined by ^{1}H-NMR spectrum peak integration using formular:

$$\frac{CPT.MW}{CPT-Gly.MW+Sar\ repeating\ unit.MW*Sar\ repeating\ unit\ number} = \frac{347.3}{404.4+71*repeating\ unit\ number}.$$

By the above formular 3 different trials of CPT-Gly-PSar were estimated: trial 1, 28%(*Figure 2.3-18*), trial 2, 35% (Appendix 0-1) and trial 3, 44% (Appendix 0-2). Their drug content was estimated purely depends on the ^{1}H-NMR integration; therefore, its resolution and the integration greatly influence the result, and other technique should be used to further verify the drug content. In the ^{1}H-NMR spectra, the range of 8.71 to 7.17 ppm corresponds to six protons from CPT and one amide proton, 5.50 to 5.31 ppm relates to four CPT protons, 4.36 to 3.99 ppm reflects protons on the PSar backbone, and 2.95 to 2.73 ppm indicates the methyl group protons of the PSar side chain. In the ^{1}H-NMR spectra of drug conjugate (28% w/w), the CPT-Gly is linked to PSar chain with 12-13 peat units (Figure 2.3-18). These signals are consistent with the expected structure and indicate successful formation of CPT-Gly-PSar.

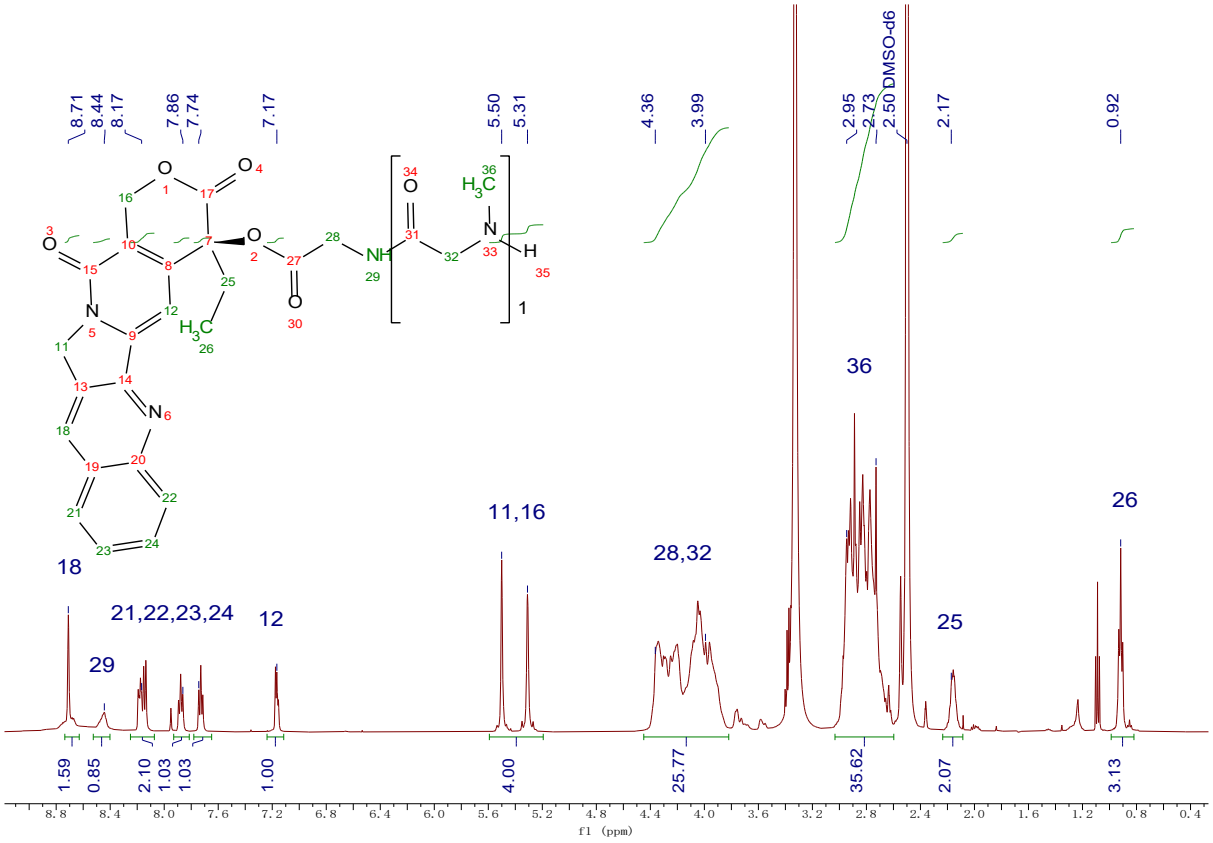

Figure 2.3-18. ^{1}H-NMR spectroscopy (400 MHz, DMSO-d_6) of PSar-Gly-CPT (28% drug content): 8.71 ppm (=CH-), 8.44 ppm (-NH-), 8.17 ppm (=CH-), 7.86- 7.74 ppm (=CH-), 7.17 ppm (=CH-), 5.50- 5.31 ppm (-N-CH_2-, -O-CH_2-), 4.36-3.99 ppm (-C=O-CH_2-N- (PSar)), 2.95-2.73 ppm (-N-CH_3), 2.17 ppm (CH_3-C**H**$_2$-), 0.92 ppm (CH_3)

Subsequently, drug conjugate with higher drug content were produced as confirmed in the ^{1}H-NMR spectra of drug conjugate (35% w/w), the CPT-Gly is linked to PSar chain with 8-9 peat units (Appendix 0-1), and the ^{1}H-NMR spectra of drug conjugate (44% w/w), the CPT-Gly is linked to PSar chain with 4-6 peat units (Appendix 0-2).

The polymers produced contain a hydrophobic drug head group and a hydrophilic PSar tail, ensuring amphiphilicity, which may enable NP formation. All samples did not produce stable and consistent NPs, suggesting that this amphiphilic drug conjugate requires further structural optimisation to achieve stable NP formation.

2.3.6. Synthesis of PGA-(PSar-Gly-CPT)

To enhance the stability of NPs derived from the conjugation of CPT-Gly-PSar, it was conjugated onto PGA not only to increase the hydrophilicity of the polymer-drug conjugates, but also facilitates the nano-precipitation by formation of a hydrophobic core by tying the hydrophobic segment- CPT together via conjugation (Figure 2.3-19) [39,48,49].

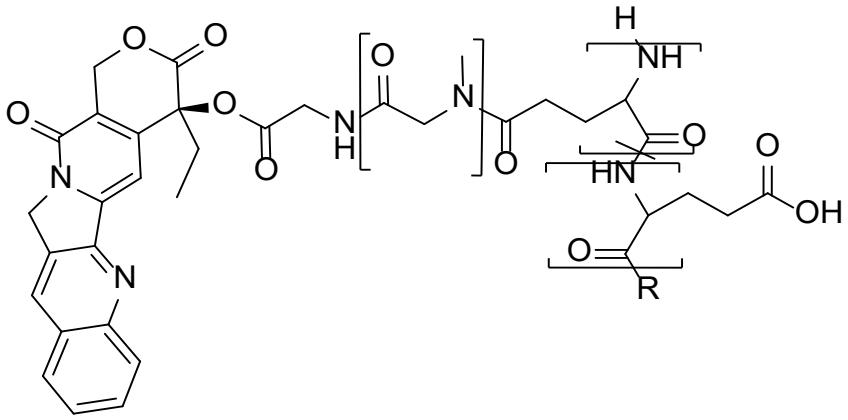

Figure 2.3-19. PGA-(PSar-Gly-CPT). /: indication of the random position of carboxylate side chain and CPT-Gly-PSar in PGA backbone.

PGA-(PSar-Gly-CPT) was synthesised through EDC/NHS coupling reaction with PGA and CPT-Gly-PSar with drug weight ratio quantified by ^{1}H-NMR integration using formular:

$$\frac{(5.31-5.50ppm)/4*347.3}{\left((3.96-4.26ppm)-\frac{5.31-5.50ppm}{2}-\left(\frac{2.75-2.93ppm}{3}*2\right)\right)*129+\left(\frac{2.75-2.93ppm}{3}*71\right)+\left(\frac{5.31-5.50ppm}{4}*(404.4-17)\right)}$$

$$= \frac{\frac{0.24}{4}*347.3}{\left(0.92-\frac{0.24}{2}-\frac{1.0}{3}*2\right)*129+\left(\frac{1.0}{3}*71\right)+\frac{0.24}{4}*387.4} = 0.33$$ (Figure *2.3-20*)

Given drug weight ratio of 33.0% (Trial 1) and 41.9% (Trial 2). Where 5.31-5.50 ppm correspond to the four protons of CPT, 3.96- 4.26 ppm contains a proton from PGA, two protons from CPT-Gly and two protons from PSar, 2.75-2.93 ppm represent the three protons from methyl group; 347.3 is the MW of CPT, 129 is the MW of PGA repeating unit, 71 is the MW of PSar repeating unit, 387.4 represent the MW of CPT-Gly after losing a -OH group during conjugation. The drug content was calculated exclusively from ^{1}H NMR integration, making the results sensitive to spectral resolution and integration accuracy. Therefore, orthogonal techniques should be used to further validate the drug content in the

future. Peaks from 8.71 to 7.68 ppm correspond to the CPT protons and the amide protons of the polymer. A broad peak from 4.26 to 3.96 ppm represents two protons of PSar backbone, two protons of the glycine linker, and one proton from the PGA backbone. A peak from 2.93 to 2.75 ppm corresponds to the three protons of the PSar methyl group. A peak from 2.32 to 1.84 ppm accounts for the four protons of the PGA side chain (Figure 2.3-20). Characteristic peaks in the spectra confirmed the presence of CPT, PSar, and PGA backbone structures (Figure 2.3-20).

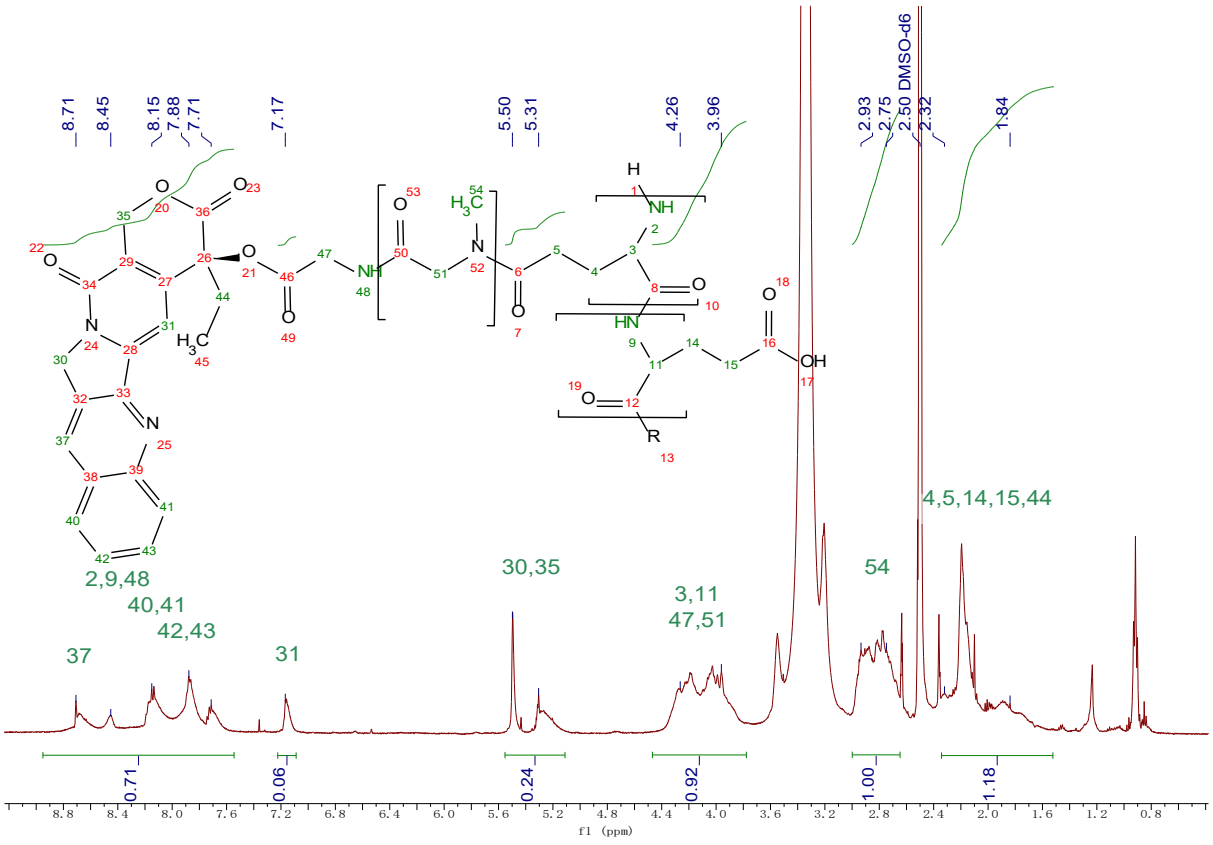

Figure 2.3-20. ^{1}H-NMR spectrum (500 MHz, DMSO-d_6) of PGA-(PSar-Gly-CPT) (33.0% drug load): 8.71 ppm(*=CH-*), 8.45 ppm (*-NH-*), 8.15 ppm (=CH-), 7.88-7.71 ppm (=CH-), 7.17 ppm (=CH-), 5.50-5.31 ppm (-N-CH_2-, -O-CH_2-), 4.26-3.96 ppm (-NH-C**H**-C=O-,-NH-C**H$_2$**-C=O-, -N(CH_3)-C**H$_2$**-), 2.93-2.75 ppm (-N-CH_3), 2.32-1.84 ppm (-C**H$_2$**-C**H$_2$**-)

2.3.6.1. Analysis of PGA-(PSar-Gly-CPT) Nanoparticles

PGA-(PSar-Gly-CPT) with the two different drug conjugation amounts were converted to NPs

by the ‘dropping-in’ method in pH 7.4 PBS solution simulating the physiological conditions, which were assessed by DLS analysis three times each for precision. The formation of NPs indicates the conjugation to PGA does increase the dispersibility because the additional hydrophilicity. But the similarity in drug content of both drug conjugate may suggest the increased hydrophobic interactions between CPT molecules may also facilitate the formation of stable NPs [48,130,131]. NPs close to 200 nm in diameter were produced when PGA-(PSar-Gly-CPT) with 33.0% drug content (w/w) was converted to NPs. Furthermore, DLS results indicated that the conjugates have a low CMC, enabling NP formation at reduced concentrations as low as 100 μg/mL, which is advantageous for drug delivery applications preventing NPs disintegration due to the in vivo dilution (Table 2.3-1) [39,48,49]. And ten times increase in NP concentration to 1.0mL/mL represents a more practical concentration in real therapeutic applications [132] while higher concentration may risk of data distortion due to the particle-particle interactions [133,134]. There is only a 11% increase in particle size at concentration 1.0 mg/mL (Table 2.3-1). The PDI values of these NPs are also less than 0.3, revealing moderate dispersity. A tiny fraction of few thousands nm observed in both DLS results, pointing only minute trace assembles into large aggregates. This is likely overestimated due to the intensity-weighted nature of DLS measurements, which disproportionately emphasises larger particles [106]. This large fraction may arise from the unconjugated CPT-Gly-PSar persisted in the system.

Trial 1	Z-Average (d.nm)	PDI
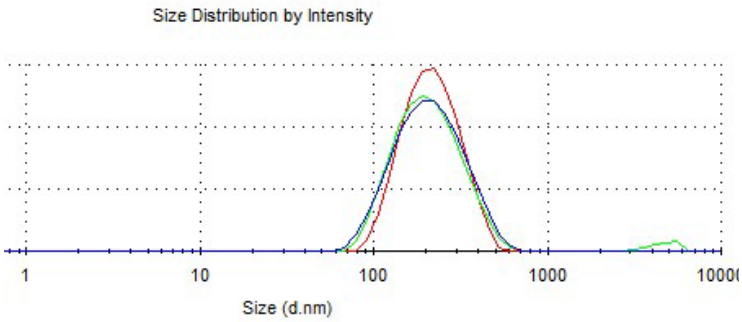 100 µg/mL	188.1 (±1.778)	0.256 (±0.015)
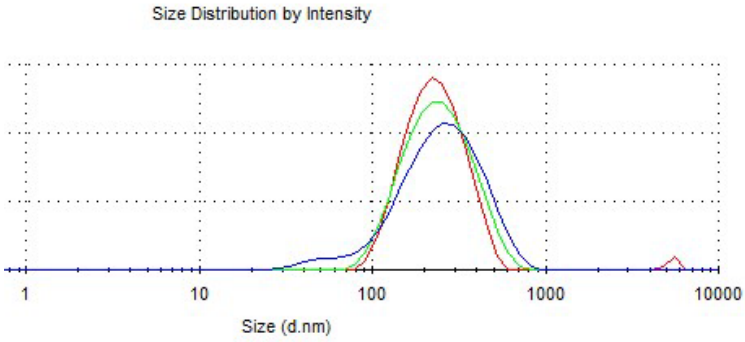 1.0 mg/mL	209.4 (±3.751)	0.251 (±0.009)

Table 2.3-1. The mean of three DLS size distribution by intensity analyses report for PGA-(PSar-Gly-CPT) (Trial 1) at two concentrations in pH 7.4 PBS solution.

However, both the NP size and PDI value increases over time, signifying some particle aggregation and rendering the particles unsuitable for long-term storage in aqueous solution (Table 2.3-2).

Trial 1 (after 4 weeks)	Z-Average (d.nm)	Pdi
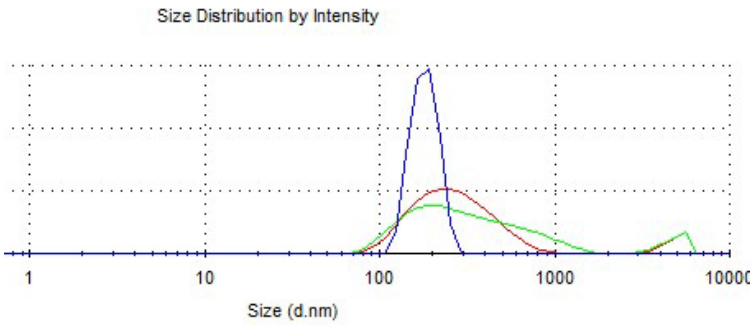 100 µg/mL	353.8 (±146.0)	0.486 (±0.042)
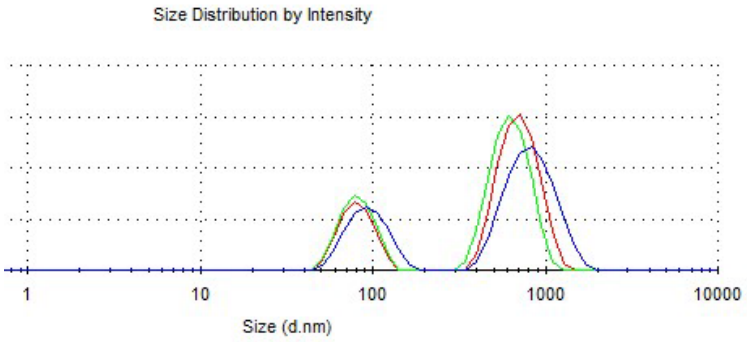 1.0 mg/mL	332.1 (±29.98)	0.636 (±0.05)

Table 2.3-2. The mean result of three DLS size distribution by intensity analyses for PGA-(PSar-Gly-CPT) (Trial 1) at two concentration after 4 weeks in pH 7.4 PBS solution.

NPs created from PGA-(PSar-Gly-CPT) with 41.9% (w/w) drug content possessed even smaller Z-average sizes of 125.7 nm at very low concentration of 100 µg/mL and slightly higher PDI values of 0.338, further increase the concentration to 1.0 mg/mL result in a reduction in both size and PDI value of 110.9 nm and 0.303 respectively (Table 2.3-3). Drug-carrying NPs of such dimensions may be suitable for the cancer treatment [69]. While a tiny fraction of few thousands nm observed in both DLS results, indicating the presence of minute trace of large aggregates. This is likely overestimated by intensity-weighted DLS analysis, which disproportionately emphasises larger particles [126]. This large fraction may arise from the unconjugated CPT-Gly-PSar persisted in the system.

Trial 2	Z-Average (d.nm)	Pdi
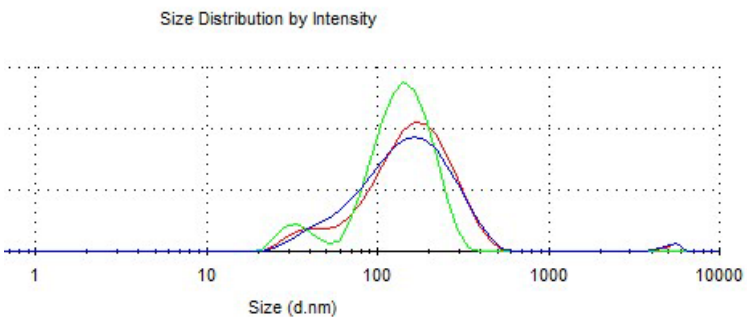 100 µg/mL	125.7 (±4.869)	0.338 (±0.042)
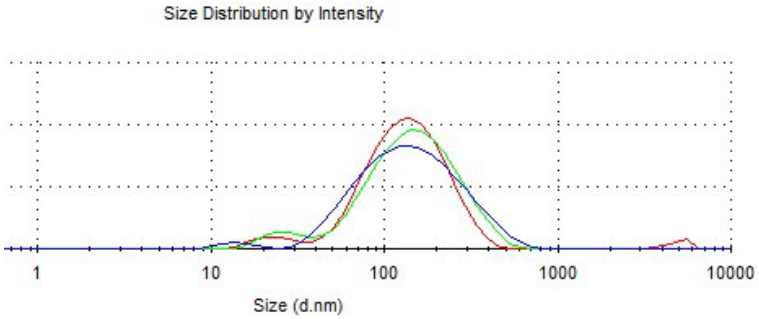 1.0 mg/mL	110.9 (±1.419)	0.303 (±0.027)

Table 2.3-3. The mean result of three DLS size distribution by intensity analyses for PGA-(PSar-Gly-CPT) (Trial 2) at various concentration in pH 7.4 PBS solution.

Four-week storage resulted in particle aggregation, suggesting again that the long-term storage of PGA-(PSar-Gly-CPT) in aqueous solution may not be viable (Table 2.3-4). Because from the date of manufacture and packaging till shipment and to be administered may takes longer than four weeks.

Trial 2 (after 4 weeks)	Z-Average (d.nm)	Pdi
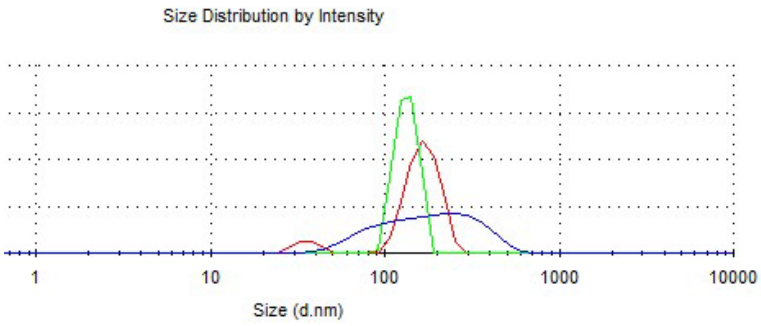 100 µg/mL	308.6	0.422
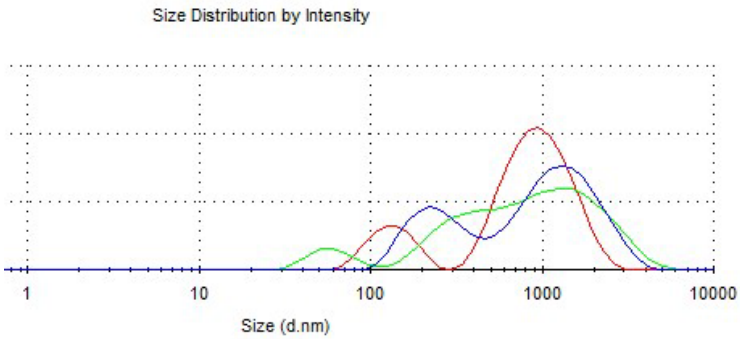 1.0 mg/mL	442.1 (±16.79)	0.520 (±0.06)

Table 2.3-4. The mean result of three DLS size distribution by intensity analyses for PGA-(PSar-Gly-CPT) (Trial 6) at various concentration after 4 weeks in pH 7.4 PBS solution.

The morphology of the NPs was assessed using SEM, revealing spherical shapes for the PGA-(PSar-Gly-CPT) NPs validating the spherical assumption used in the DLS analysis(Table 2.3-5). In SEM images, the particles observed approximately 400 nm in trial 1 and 200 nm in trial 2. These values were larger than the DLS results, which is unexpected because DLS typically reports larger particle sizes owing to the hydration shell surrounding the particles [135,136,137], while SEM measures the dry core diameter of individual particles under vacuum and is therefore expected to yield smaller sizes [138]. This discrepancy can be attributed to the external forces applied during SEM sample preparation, which induced partial deformation or spreading of the NPs. Furthermore, SEM only captures a tiny fraction

of the NPs present in the sample, whereas DLS provides an ensemble-averaged size distribution of particles in suspension. Also, the differences in the sizes of the particles are represented as PDI value reported in the DLS data. Particle aggregation may have occurred between the DLS and SEM measurements which could be attributed to physical stress put on the NPs during freeze drying process causing aggregation or fusion of the NPs [139,140]. Additionally, variations in NP size may be caused by uneven conjugation of the drug conjugate during synthesis. This inconsistency may influence the NPs' physical behaviour in aqueous environments [141]. Finally, some NPs appeared ruptured in SEM images, a phenomenon possibly attributed to rapid water sublimation during the freeze-drying process [41].

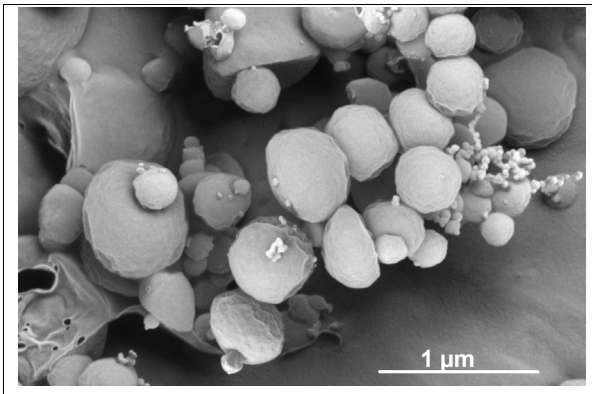	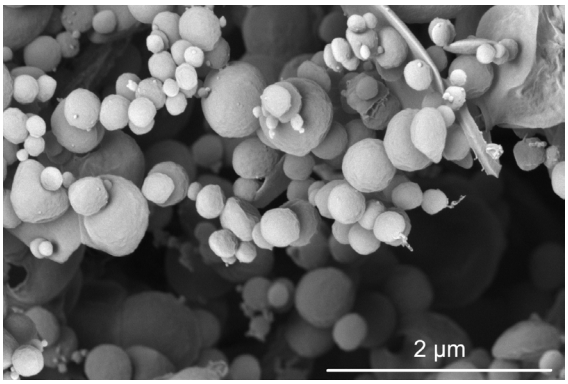
Trial 1	Trial 2

Table 2.3-5. SEM images on two Trials of PGA-(PSar-Gly-CPT)

However, this scheme was not used for metal ion complexation in this study. To effectively deliver metal ions to cancer cells, the metal ion-PGA complex needs to be shielded from the outer physiological environment to prevent the unwanted ion exchange. Based on the chemical structure of the PGA-(PSar-Gly-CPT), the NPs formed may feasibly position PGA on the outer most point, forming a hydrophilic shell that preferably interacts with aqueous solution. Such placement could lead to direct interaction with the external environment, resulting in ion exchange and premature release of metal ions following administration (Figure 2.3-21).

To mitigate this risk, the metal ion- PGA complex should be shielded by the stealth polymer PSar. In this manner, PSar acts in a comparable way to PEG in PEGylated drug delivery systems [103,104,105]. Therefore, modification to the polymer design was done in which

PSar and CPT-Gly are conjugated to PGA independently, rather than with PSar-Gly-CPT. In this strategic placement, the hydrophobic interaction of CPT may help to pull the ion-PGA complex towards inner position of the NPs, while the long chain of PSar shields the ion-PGA complex from external interactions, ensuring controlled release and enhancing the NPs' suitability for drug delivery applications involving metal ions (Figure 2.3-21).

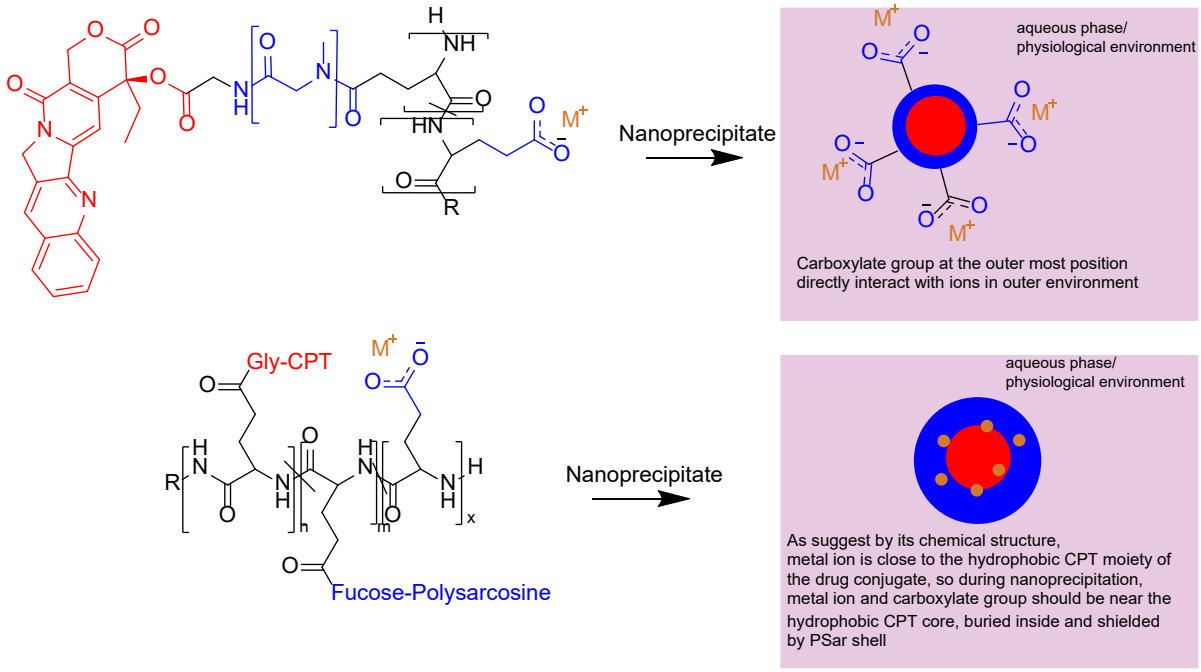

Figure 2.3-21. Illustration of NPs formed from PGA-(PSar-Gly-CPT)-ion complex (top) where the metal ions (M^+) locate at the outer most of the NPs; illustration of NPs formed from PGA-[(CPT-Gly)-*co*-(F-PSar)]- ion complex (bottom) where metal ions are shielded by PSar. \: indication of the random position of carboxylate side chain, CPT-Gly, Fucose-polysarcosine (F-PSar) and CPT-Gly-PSar in PGA backbone.

2.3.7. PSar Conjugation to Achieve a Stable Drug Delivery System

Stable NPs that do not aggregate in aqueous solution are essential if they are to be used as a drug delivery system. Consequently, polymer redesign was done to create a polymer-drug conjugate with incorporation of PSar .

To achieve this, drug conjugate made by the random conjugation of PGA with CPT-Gly only (Scheme 2.3-2) and in combination with PSar (Scheme 2.3-3) were created. In this way, drug

conjugates with and without hydrophilic PSar chains were produced and comparison of the effects of PSar to enhance NP stability in aqueous solution could be made.

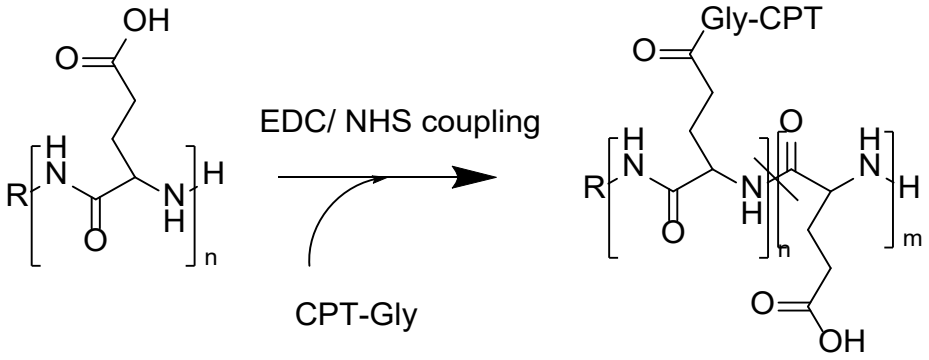

Scheme 2.3-2. Random conjugation of PGA with CPT-Gly for the synthesis of PGA-(CPT-Gly). \: indication of the random position of carboxylate side chain and CPT-Gly in PGA backbone.

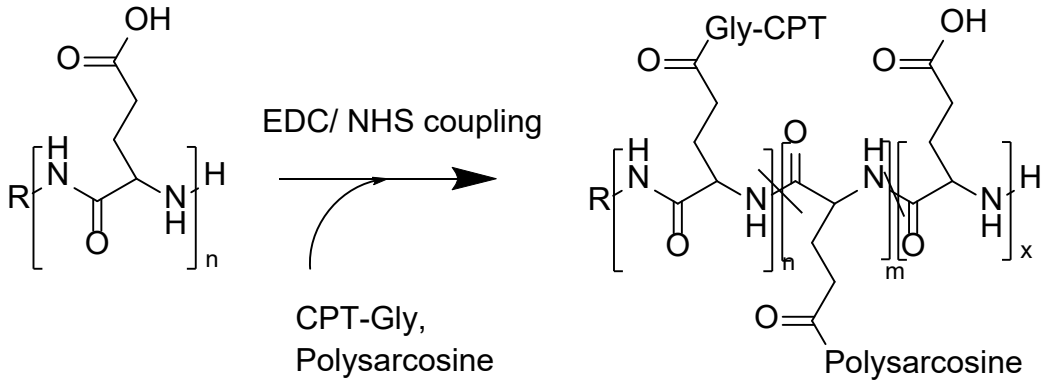

Scheme 2.3-3 random conjugation of PGA with CPT-Gly and PSar or F-PSar for the synthesis of PGA-[(CPT-Gly)-*co*-(PSar or F-PSar). \: indication of the random position of carboxylate side chain, CPT-Gly and PSar or F-PSar PGA backbone.

It should be remembered that the final goal of this research is also to create polymeric drug conjugate that can self-assemble to form NPs containing metal ions. As discussed above (2.3.6.1), compared to PGA-(PSar-Gly-CPT), the aggregation of CPT moiety in PGA-[(CPT-Gly)-*co*-(PSar)] may drag the ion-PGA complex inward, while the long chain of PSar provides shielding to the ion-PGA complex from external interactions, prevent the premature release of metal ions (Figure 2.3-21).

Polymeric drug conjugates were created because freely loaded drug encapsulation has many limitations, including burst release and premature drug leakage [37,38,40,41]. Polymeric

drug conjugates may ensure that the drug will not be released until certain criteria are met to cleave the drug from the polymer, such as the acidic TME catalysing hydrolysis of the labile bond that links the drug and polymer [42,43,63,71,72,107]. The conjugation of PGA with Gly-CPT had been reported previously (Scheme 2.3-2)[107]. However, reduced polymer-drug conjugated solubility and dispersibility in water with increasing CPT content limits its application. In chemotherapy, it is essential that a high concentration of chemotherapeutic reaches the cancer site to kill the cancerous cells. To circumvent aggregations, and to improve the performance of PGA-(Gly-CPT) drug conjugates, hydrophilic PSar is included to enhance solubility, and fucose is incorporated to enable cell binding to pancreatic cancer cells. A polymeric drug conjugate that includes these features is entirely novel but also has great potential for effective pancreatic cancer treatment. Before that, drug conjugate PGA-(Gly-CPT) was first synthesised as a control sample for comparison of the PSar-enhanced drug conjugate (Figure 2.3-22).

2.3.7.1. Synthesis of the Control PGA-(Gly-CPT) Drug Conjugate

To investigate the impact of PSar modification on NP formation and stability, drug conjugate PGA-(Gly-CPT) was synthesised (Figure 2.3-22). This conjugate served as a control sample, allowing for a comparative analysis of the stability and structural advantages introduced by PSar modification [113].

Achieving 100% coupling efficiency of CPT-Gly onto PGA is not feasible due to steric hindrance between adjacent CPT-Gly molecules [113]. As a result, the unmodified carboxylate groups on PGA are serving as the hydrophilic component, while CPT-Gly functions as the hydrophobic segment within the drug conjugate. This amphiphilic nature may enable the conjugate to self-assembly in aqueous environments, forming NPs.

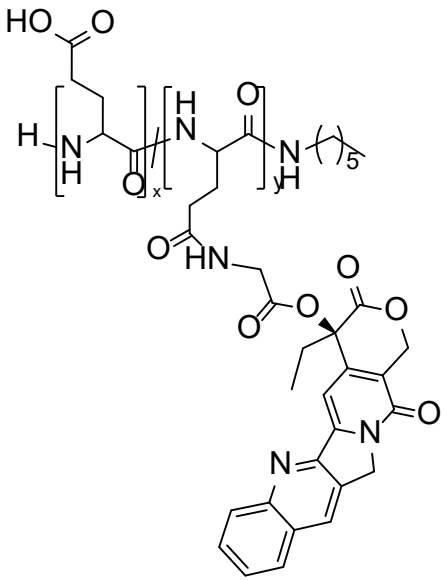

Figure 2.3-22. The chemical structure of PGA-(Gly-CPT). /: indication of the random position of carboxylate side chain and CPT-Gly in PGA backbone.

The structure of the synthesised drug conjugate was verified by ^{1}H-NMR spectroscopy. The ^{1}H-NMR spectrum revealed distinct peaks confirming the presence of PGA and CPT-Gly, with peaks from 8.66 to 7.16 ppm corresponding to the amide proton of the PGA backbone and the protons of CPT, while peaks from 5.51 to 4.97 ppm represented the four protons from CPT. Additionally, peaks from 4.21 to 3.95 ppm were assigned to one proton of the PGA backbone and two protons from the glycine linker, and peaks from 2.13 to 1.84 ppm accounted for the four protons of the PGA side chain and two protons of CPT. (Figure 2.3-23). The drug content was estimated via the following equation:

$$\frac{(4.97-5.51\,ppm)/4*347.3}{\left((3.95-4.21\,ppm)-\frac{4.97-5.51\,ppm}{2}\right)*129+\left(\frac{4.97-5.51\,ppm}{4}*(404.4-17)\right)}$$

$$=\frac{\frac{62.55}{4}*347.3}{\left(61.88-\frac{62.55}{2}\right)*129+\frac{62.55}{4}*387.4}=0.54$$

The drug content was estimated to be 54.0% (w/w). Where 4.97 to 5.51 ppm correspond to the four protons of CPT, 3.95 to 4.21 ppm contains a proton from PGA, two protons from CPT-Gly; 347.3 is the MW of CPT, 129 is the MW of PGA repeating unit, (404.4-17) represent the MW of CPT-Gly after losing a -OH group during conjugation. This drug content was estimated exclusively from ^{1}H NMR integration, making the result sensitive to spectral

resolution and integration accuracy. Therefore, other techniques should be used to further validate the drug content in the future.

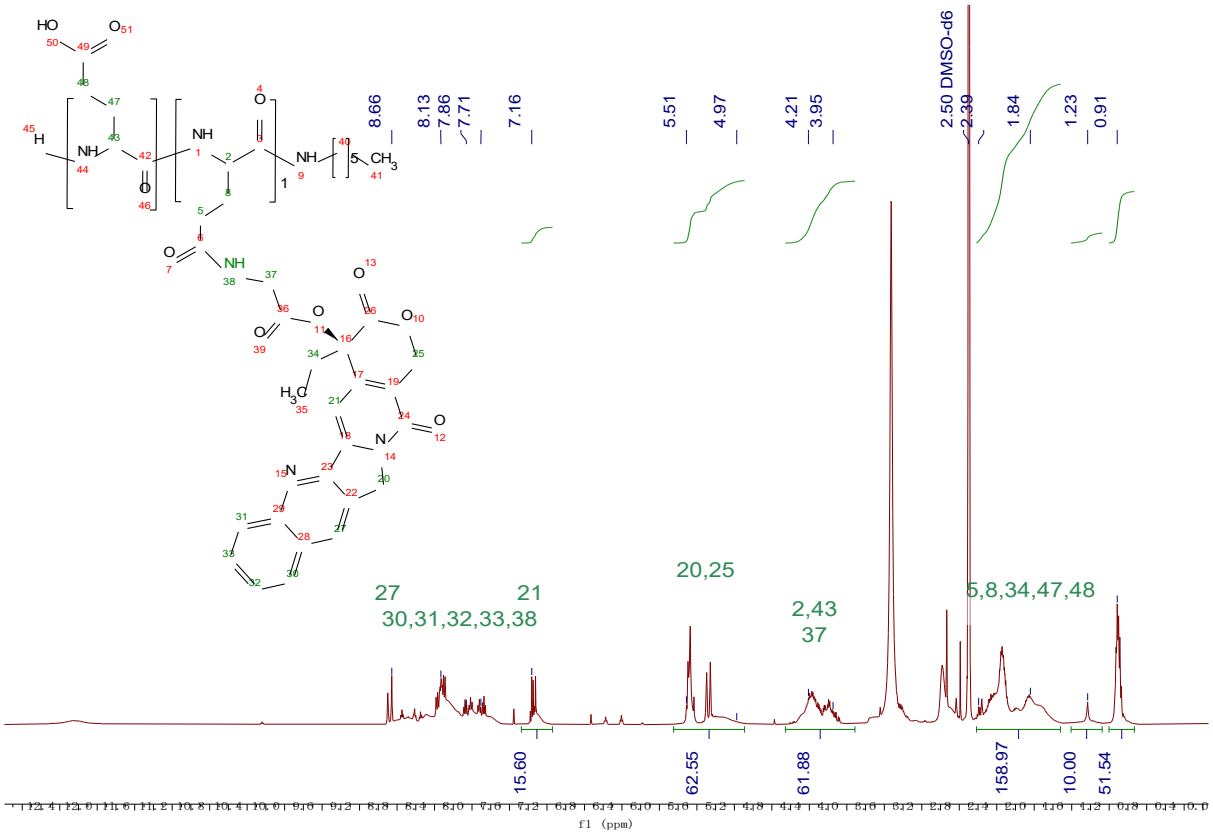

Figure 2.3-23. ^{1}H-NMR spectrum (400 MHz, DMSO-d_6) of PGA-(CPT-Gly) drug conjugate: 8.66- 7.16 ppm (=CH-, -NH-), 5.51-4.97 ppm (-N-CH_2-, -O-CH_2-), 4.21-3.95 ppm (-NH-C**H**-C=O-,-NH-C**H_2**-C=O-), 2.39- 1.84 ppm (-C**H_2**-C**H_2**-, CH_3-C**H_2**-), 1.23-0.91 ppm (initiator)

2.3.7.1.1. DLS Analysis of PGA-(CPT-Gly) Drug Conjugate in pH 7.4 PBS Solution

NPs were prepared by the 'dropping-in' method in pH 7.4 PBS solution to mimic physiological conditions, which were assessed by DLS analysis three times each for precision. DLS analysis showed that the drug conjugate, with approximately 54% (w/w) drug content, was only capable of self-assembling into NPs with a Z- average of 246 d.nm and a PDI value of 0.442 at a concentration as low as 100 µg/mL (Figure 2.3-24). This indicates that while the polymer-drug conjugate can form NPs, the PDI value suggests a considerable size variation that is not ideal for drug carriers [105,142,143].

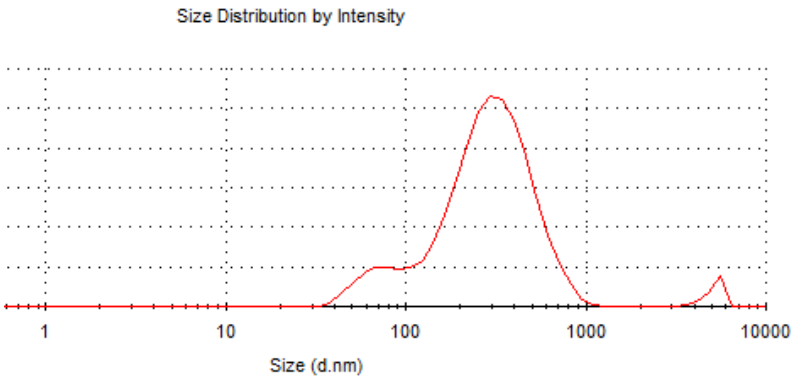

Figure 2.3-24. The mean average of triplicate DLS size distribution by intensity analyses report for PGA(CPT-Gly) (54% drug content) in pH 7.4 PBS solution at concentration 100µg/mL.

To improve solubility and enhance NP formation/stability, PGA-(CPT-Gly) with a lower drug content of approximately 31% (w/w) was synthesised and subjected to DLS analysis under the same conditions. The drug conjugate was able to form NPs at concentration of 600 µg/mL with average size of 133.7 d.nm and PDI value of 0.525 with large aggregate observed, again showing high polydispersity. Furthermore, the size increases significantly to 228.2 d.nm after storage at room temperature for 10 days (Table 2.3-6). Therefore, NPs prepared from PGA(CPT-Gly) are not ideal for use as drug delivery vehicles. The inconsistent NP size distribution and relatively large PDI values highlight the need for modification in polymer design.

PGA(CPT-Gly) (31%) 600 µg/mL in pH 7.4 PBS Solution	Z-Average (d.nm)	PDI value
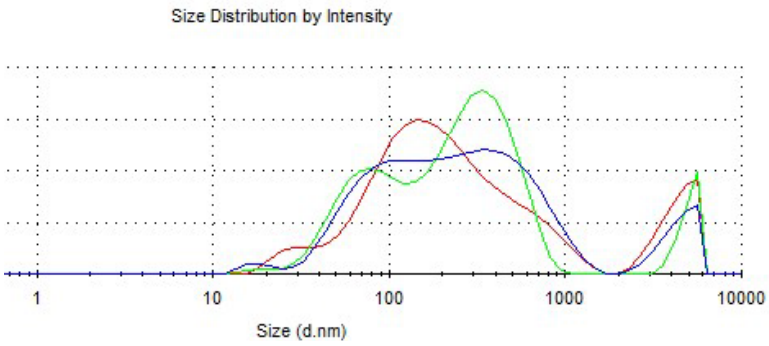	133.7 (±7.605)	0.525 (±0.057)
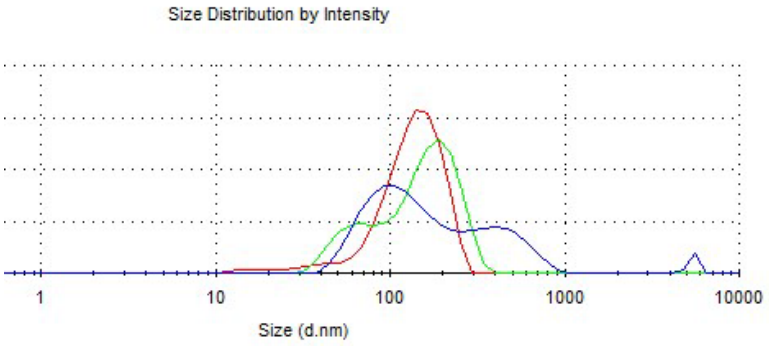 10 Days After	228.2 (±23.01)	0.344 (±0.004)

Table 2.3-6. Three DLS size distribution by intensity analysis result of PGA(CPT-Gly) (31%) 600 µg/mL in pH 7.4 PBS Solution on first day and 10 days after

2.3.7.2. PGA-[(CPT-Gly)-*co*-(PSar)] Drug Conjugate

The feasibility of coupling PSar onto the PGA backbone to increase polymer hydrophilicity and NP stability was then assessed. PGA-[(CPT-Gly)-*co*-(PSar)] (Figure 2.3-25) drug conjugate was successfully synthesised via random coupling of CPT-Gly and PSar with PGA to investigate both the structural integrity of the conjugate and the stability of the resulting NPs in physiological conditions.

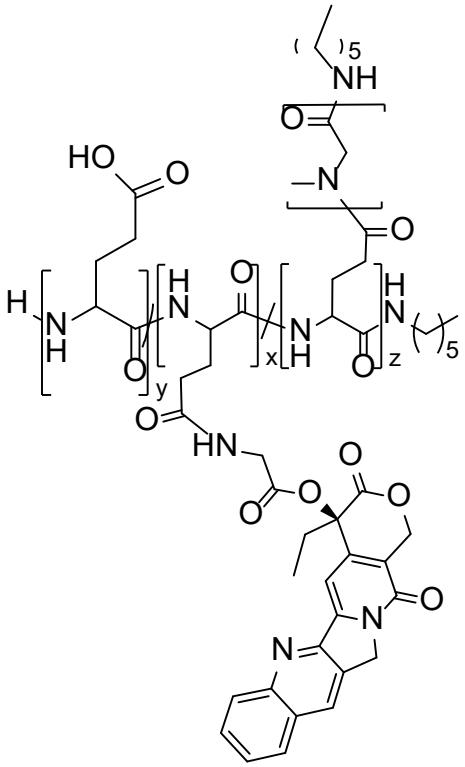

Figure 2.3-25. PGA-[(CPT-Gly)-*co*-(PSar)] drug conjugate. /: indication of the random position of carboxylate side chain, CPT-Gly and PSar in the PGA backbone.

The structure of the synthesised drug conjugate was verified using ^{1}H-NMR spectroscopy. The ^{1}H-NMR spectrum revealed distinct peaks confirming the presence of PGA, CPT-Gly and PSar. Peaks from 8.69 to 7.19 ppm corresponded to the amide proton of the PGA backbone and the protons of CPT, while peaks from 5.49 to 5.29 ppm were attributed to the four protons of CPT. Peaks from 4.34 to 3.91 ppm represented one proton from the PGA backbone, two protons from the PSar backbone, and two protons from the glycine linker. Additionally, peaks from 2.94 to 2.72 ppm indicated the three protons of the PSar methyl group, and peaks from 2.42 to 1.86 ppm accounted for the four protons of the PGA side chain and two protons of CPT (Figure 2.3-26). Characteristic peaks in the spectra confirmed the presence of CPT, PSar, and PGA backbone structures in the system.

The drug content was determined through proton integration in the ^{1}H-NMR spectrum through equation: $$\frac{(5.29-5.49\,ppm)/4*347.3}{\left((3.91-4.34\,ppm)-\frac{5.29-5.49\,ppm}{2}-\left(\frac{2.72-2.94\,ppm}{3}*2\right)\right)*129+\left(\frac{2.72-2.94\,ppm}{3}*71\right)+\left(\frac{5.29-5.49\,ppm}{4}*(404.4-17)\right)}$$

$$= \frac{\frac{0.19}{4} * 347.3}{\left(0.89 - \frac{0.189}{2} - \frac{1.0}{3} * 2\right) * 129 + \frac{1.0}{3} * 71 + \frac{0.19}{4} * 387.4} = 0.279$$

Revealing a drug content of 27.9% (w/w)(Figure 2.3-26). Where 5.29 to 5.49 ppm correspond to the four protons of CPT, 3.91 to 4.34 ppm contains a proton from PGA, two protons from CPT-Gly and two protons from PSar, 2.72 to 2.94 ppm represent the three protons from methyl group; 347.3 is the MW of CPT, 129 is the MW of PGA repeating unit, 71 is the MW of PSar repeating unit, 387.4 represent the MW of CPT-Gly after losing a -OH group during conjugation. The drug content was estimated purely by integration of characteristic signals in the ^{1}H NMR spectra, making the result sensitive to spectral resolution and integration accuracy. Therefore, orthogonal techniques should be used to further validate its drug content in the future.

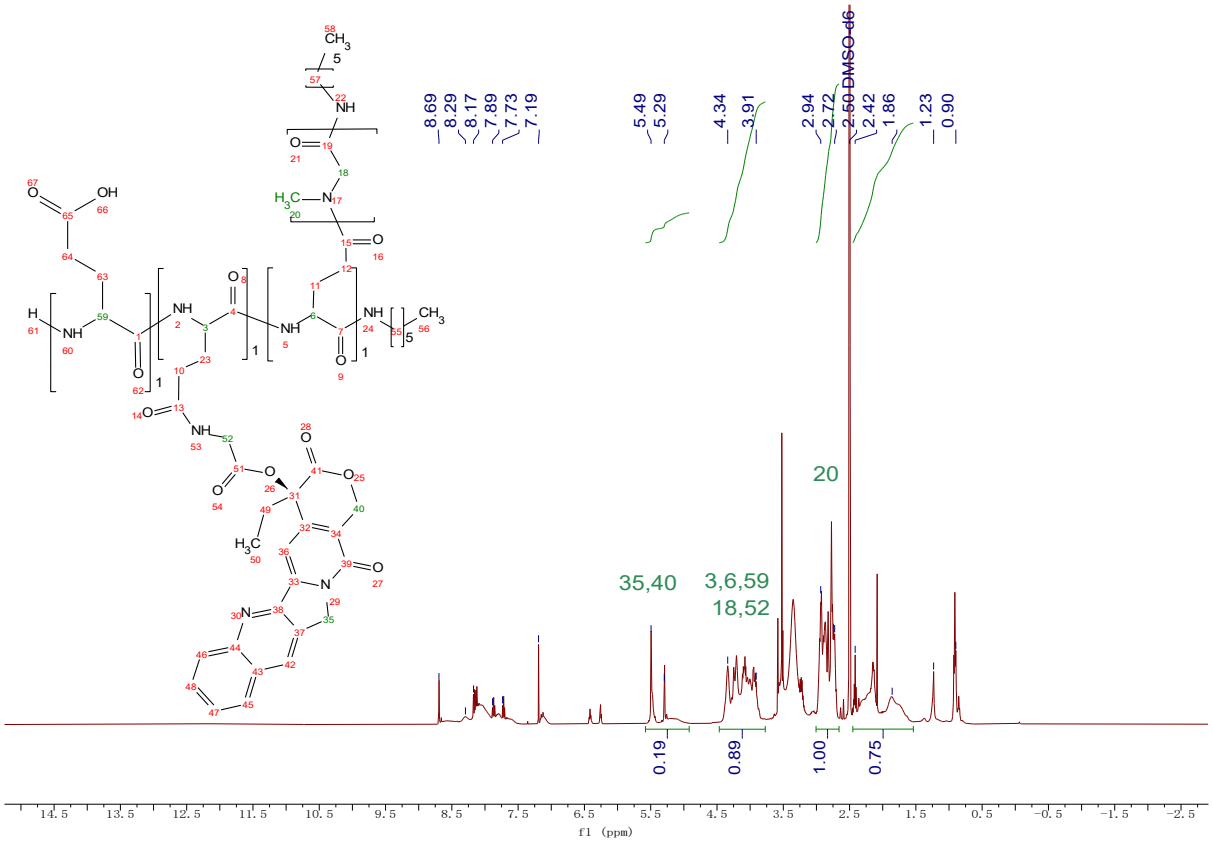

Figure 2.3-26. ^{1}H-NMR spectrum (400 MHz, DMSO-d_6) of PGA-[(CPT-Gly)-*co*-(PSar)]: 8.69 ppm (=CH-),8.29 ppm (-NH), 8.17 ppm (=CH-), 7.89-7.73 ppm (=CH-), 7.19 ppm (=CH-), 5.49-5.29 ppm (-N-CH_2-, -O-CH_2-), 4.34-3.91 ppm (-NH-C**H**-C=O-,-NH-C**H$_2$**-C=O, -N(CH_3)-C**H$_2$**-), 2.94-2.72 ppm (-N(C**H$_3$**)-), 2.42-1.86 ppm (-C**H$_2$**-C**H$_2$**-, CH_3-C**H$_2$**-), 1.23- 0.90 ppm (initiator)

In the polymer produced, PSar acts as the hydrophilic component promoting water solubility and NPs stability [98,99,100]. While CPT-Gly forms the hydrophobic segment, which is expected to aggregate into the core of the NPs in aqueous environments. Since this drug conjugate is mainly composed of amino acid-based components, it can be hydrolysed into its respective amino acids- sarcosine, glycine, and glutamic acid under appropriate conditions [1,6,7]. Moreover, CPT is designed for pH-responsive release, as the ester bond between CPT and glycine is hydrolysed in acidic TME, enabling controlled drug release in response to pH variations [63,71,72].

Additionally, given the potential NP forming capability of the PGA-[(CPT-Gly)-*co*-(PSar)] drug conjugate, it presents an opportunity for co-encapsulation of metal-based chemotherapeutic agents during NP formulation or metal ions complexation for CDT. This expands the potential of the proposed drug delivery system as a multifunctional drug delivery system, combining polymeric drug conjugation with metal-assisted cancer treatment approaches.

2.3.7.2.1. DLS Analysis of PGA-[(CPT-Gly)-*co*-(PSar)] Particles formed in pH 7.4 PBS Solution

NPs were prepared through 'dropping- in' method in pH 7.4 PBS solution to simulate physiological conditions and analysed by DLS three times each to ensure precision. The drug conjugate with 27.9%(w/w) drug content self-assembled to form stable NPs with a desirable size distribution with Z- average 89.62 d.nm (±1.576) and PDI value of 0.302 (±0.003) at a concentration of 600 µg/mL (Table 2.3-7) showing great improvement in terms of Z-average and size distribution comparing to non- PSar conjugated in Table 2.3-6. A tiny fraction of few thousands nm observed in the DLS results, pointing only minute trace assembles into large aggregates. This fraction is probably overestimated, as intensity-weighted DLS is highly sensitive to larger particles, amplifying their apparent contribution [106]. This large fraction may be attributable to residual unconjugated CPT-Gly persisted in the system after dialysis. The Z-average of the NPs gradually increase to 112.4 d.nm on the fifth day then to 204 d.nm with PDI of 0.491 on the thirteen days storage at room temperature, indicating aggregation and its short shelf- life of the NPs after nanoprecipitation (Table 2.3-7). Yet, DLS generally gives a larger particle size due to the presence of a hydration shell [135,136,137] and the

present of minute trace of DMF in the solution from the NPs preparation may affect the stability of NPs during storage.

First Day, 600µg/mL	Z-Average (d.nm)	PDI
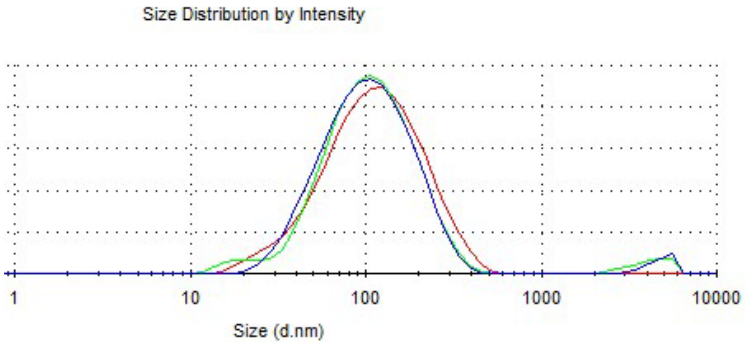	89.62 (±1.576)	0.302 (±0.003)
5 Days After, 600µg/mL	112.4 (±1.735)	0.254 (±0.002)
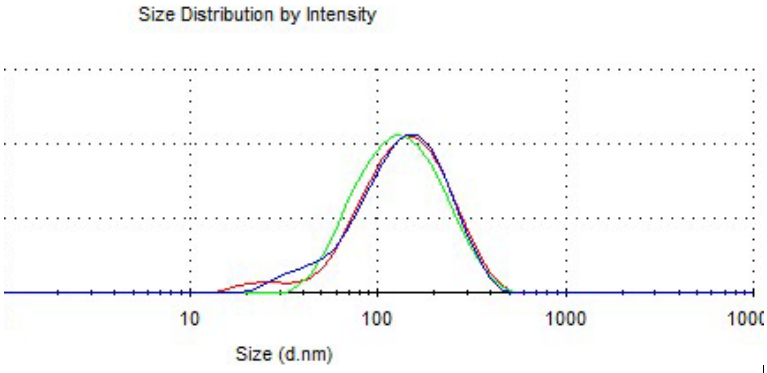		
13 Days After, 600µg/mL	204.0 (±2.919)	0.491 (±0.004)
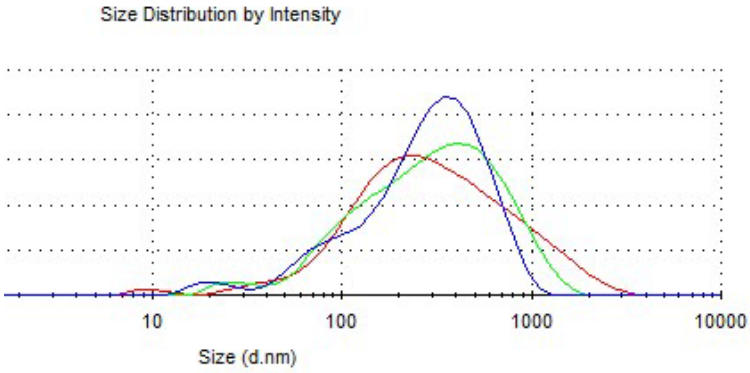		

Table 2.3-7. DLS size distribution by intensity analysis of three trials analysis of PGA-[(CPT-Gly)-*co*-(PSar)] with 27.9% drug content (w/w) pH7.4 PBS at concentration of 600µg/mL.

A drug conjugate with a higher drug conjugation content (34.0% w/w) was then synthesised and analysed by DLS. The results showed that the conjugate successfully formed stable NPs at 1.0 mg/mL with an optimal size of 102 d.nm (±1.375) and a low PDI value of 0.236 (±0.014) in pH 7.4 PBS solution (Table 2.3-8). It represents a more practical concentration in real therapeutic applications [132] while higher concentration may risk of data distortion due to the particle-particle interactions [133,134]. Also, the NPs sizes are suitable for drug delivery where require NPs size smaller than 200nm for efficient endocytosis [143]. And again, large aggregate was detected in one of the triplicate analyses pointing out the overestimation by intensity weighted DLS measurements [106].

1.0 mg/mL	Z-Average (d.nm)	PDI
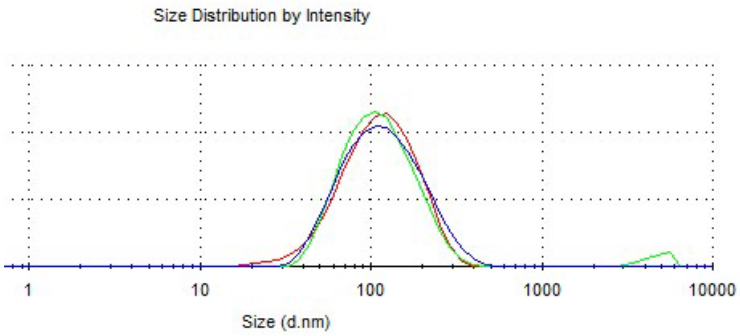	102nm (±1.375)	0.236 (±0.014)

Table 2.3-8. Average DLS size distribution by intensity analysis of three trials analysis of PGA-[(CPT-Gly)-*co*-(PSar)] drug conjugate with 34.0% drug content (w/w) in pH7.4 PBS at concentration of 1.0 mg/mL.

These results strongly suggest that PSar greatly improves the uniformity of the NPs with higher drug content and higher concentration compared to that of PGA-(CPT-Gly) (Table 2.3-6), yielding NPs of appropriate size for use as drug delivery vehicles. But the NPs of this drug conjugate only able to remain desirable deviation in size at physiological condition for less than two weeks in room temperature, such short shelf-life pointing it only to be best administered short after NPs' preparation [105,142,143].

2.3.7.2.2. DLS Result in Different pH

To allow NPs to be delivered effectively into the cancer cells via endocytosis, the NPs need to

remain stable with size smaller than 200 nm in the slight acidic cancer extracellular environment (pH 6.0 -7.0) [51,52,143]. Also to have a probe in to how NPs behave after endocytosis, NPs were prepared in acetate buffer solutions at pH 6.0 and pH 5.5 not only to mimic the endosomes or lysosomes pH of cancer cells, also proving NPs remain stable in the slight acidic cancer extracellular environment [51,52]. At pH 6.0 drug conjugate was able form highly uniform (PDI: 0.277(±0.009)) and small NPs (104nm (±0.2887)) with minute trace aggregate being overestimated by intensity weighted DLS [106] (Table 2.3-9). As the pH decreased to 5.5, the vacant carboxylate groups became protonated, reducing water solubility and the formation of larger NPs (204 d.nm) with an increased PDI of 0.538, indicating a broad size distribution and sign of aggregation (Table 2.3-9). Although the pKa of PGA is 4.45, calculations (data not included) suggest that at pH 5.5, only around 8% of PGA' s carboxylate groups are protonated. These findings indicate that NPs remain stable at slightly acidic pH (≤6.0) ensuring its ability to pass through the acidic extracellular environment (pH 6.0- 7.0) and undergo endocytosis into the cells [51,52,143]. But NPs destabilised and aggregated after entering the more acidic endosomes or lysosomes of cancer cells [51,52], This aggregation within cancer cells may have an unknown impact on the drug release profile; further studies are required to clarify this effect.

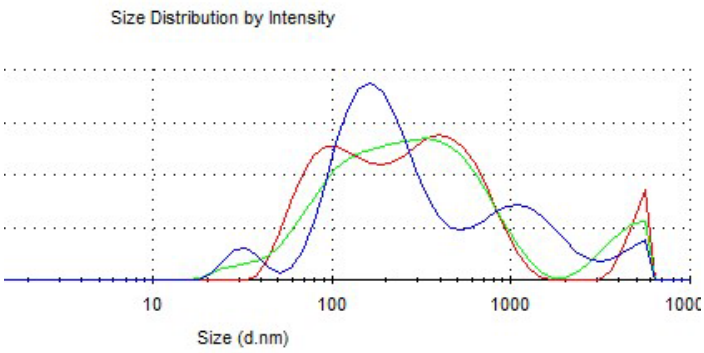 600µg/mL, pH 5.5	Z-Average (d.nm) 204.1 (±7.427)	PDI 0.538(±0.13)
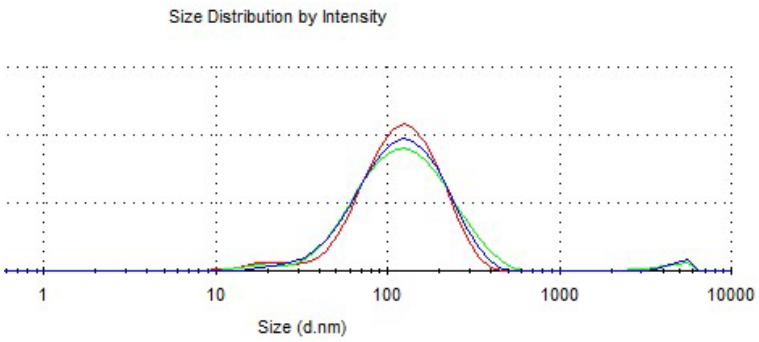 600µg/mL, pH 6.0	104nm (±0.2887)	0.277(±0.009)

Table 2.3-9. Average DLS size distribution by intensity analysis of PGA-[(CPT-Gly)-*co*-(PSar)] with 27.9% drug content (w/w) in pH 5.5 (above) and pH 6.0 (below) Acetate buffer solution at concentration of 600µg/mL.

2.3.7.2.3. Drug Release Study

To assess whether the drug conjugate could prevent the rapid release of toxic CPT in physiological environment during circulation reducing its toxicity towards healthy cells, a proof-of-concept drug release study was conducted in pH 7.4 PBS at 37 ^{o}C to simulate physiological condition over three weeks.

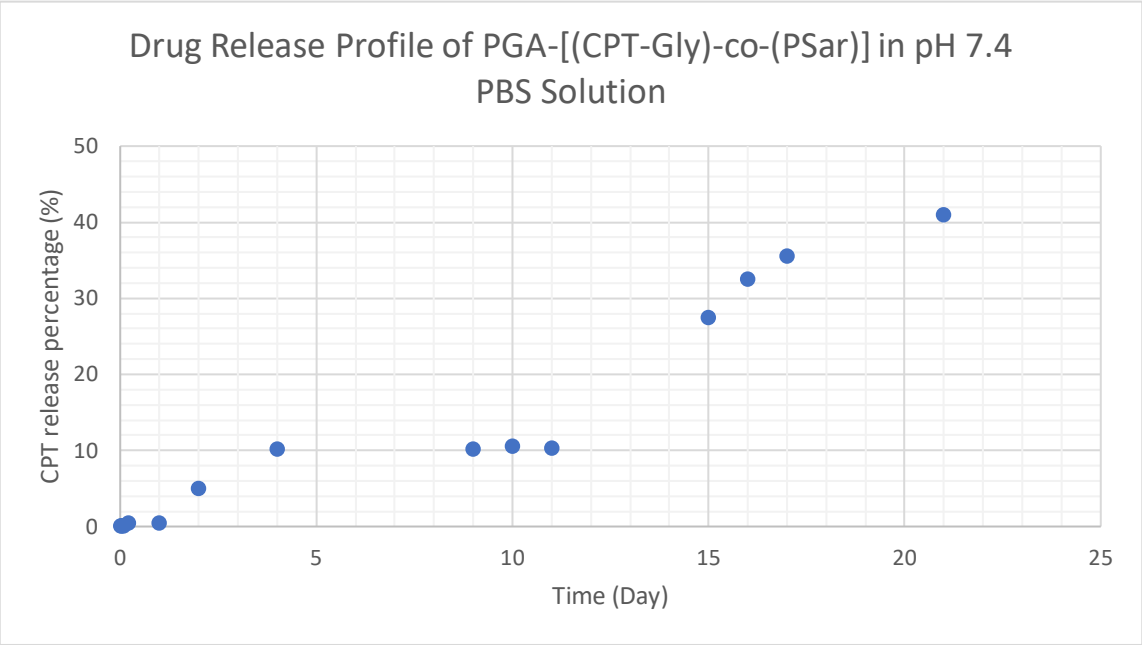

Figure 2.3-27. Drug release study of PGA-[(CPT-Gly)-*co*-(PSar)] with 23% drug content (w/w) in pH7.4 PBS at concentration of 600 µg/mL over three weeks.

The results revealed that approximately 10% of CPT was released during the first week. Following this initial release, a plateau phase occurred with no significant additional release until the third week, when a sudden increase brought the total to about 30%. By the end of the study, approximately 40% of CPT had been released (Figure 2.3-27).

The early release observed primarily attributed to the physically encapsulated CPT during first four days. And the releasing rate slows down suggesting that only the ester bond linking CPT to the conjugate underwent continuous slow hydrolysis, leading a gradual release of CPT over the three-week duration. As this was a proof-of-concept study, analysis was performed only once, experimental error emerged, including an unexpected plateau in the second week. Ideally, the release rate should have decreased after the depletion of physically encapsulated CPT leaving only conjugated CPT slowly hydrolysed and released as observed in Figure 3.3-17. Nevertheless, the findings confirmed that the drug conjugate successfully minimise burst release and extended the drug release timeline, potentially reducing cytotoxicity.

However, biological interactions such as enzymatic and protein effects were excluded from the drug release medium in this study. This represents a limitation that may affect the

reliability of the results compared to *in vivo* behaviour. Nevertheless, this study provides a fundamental understanding of the drug release profile of the conjugate under conditions that mimic physiological pH and ionic strength. More comprehensive studies incorporating relevant biological proteins and enzymes are required in the future to obtain an accurate representation of drug release behaviour.

2.4. Summary

Sar-NCA and Glu(OBzyl)-NCA were synthesised using triphosgene, followed by amine-initiated ROP to generate their respective polymers for drug conjugate preparation. Concurrently, CPT-Gly prodrug was synthesised enhancing its coupling efficiency by alleviating steric hindrance and to introduce a primary amine for effective coupling with PGA's carboxylate groups.

Initially, CPT-Gly was served as an initiator Sar-NCA polymerisation, yielding CPT-Gly-PSar conjugates with different drug content. Incorporation of PSar markedly enhanced solubility but failing to produce stable and consistent NPs. To overcome this issue, PGA coupling was introduced as a solution to produce PGA-(PSar-Gly-CPT). This approach effectively stabilised the NPs by enhancing the structural integrity of the conjugates, allowing them to self-assembly reliably. PGA-(PSar-Gly-CPT) conjugates with 33.0% and 41.9% drug content (w/w) were produced and self-assembly into NPs of 188 d.nm and 125 d.nm, respectively. The improved NPs stability capable of forming NPs at concentration as low as 100 µg/mL and 1.0 mg/mL. SEM imaging confirmed the spherical NP morphology. However, increases in particle size and PDI over time pointed to aggregation, restricting long-term aqueous storage. These results highlight the critical role of PGA coupling, as it not only enables stable NP formation but also able to supports integration of both the therapeutic agents and other functional moieties onto the PGA backbone, improving the overall functionality and stability of the drug delivery system. This approach was later adopted in the synthesis of conjugates such as PGA-[(CPT-Gly)-*co*-(PSar)] and PGA-[(CPT-Gly)-*co*-(F-PSar)].

To enable effective metal ion delivery, a redesigned drug conjugate- PGA-[(CPT-Gly)-*co*-(PSar)] conjugate was synthesised. Rather than conjugating PGA with CPT-Gly-PSar, PSar and CPT-Gly are conjugated to PGA independently, positioning hydrophobic CPT to draw the ion-

PGA complex inward while PSar provided an outer shield against premature ion release. As a benchmark, PGA-(CPT-Gly) conjugates at 54% and 31% drug contents struggled to produce NPs with uniform size distributions at 600 µg/mL, whereas PGA-[(CPT-Gly)-*co*-(PSar)] at 27.9% and 34.0% content generated smaller, more uniform particles at 600 µg/mL (89.62 d.nm, PDI 0.302) and 1.0 mg/mL (102 d.nm, PDI 0.236), respectively. Indicating PSar' s role in enhancing hydrophilicity and consistency. NPs maintained stability with only modest Z-average growth after five days at room temperature, but aggregation occurred during second weeks.

A proof-of-concept drug release study of PGA-[(CPT-Gly)-*co*-(PSar)] in pH 7.4 PBS solution showed 40% CPT release over three weeks, with minimal burst release. Indicating the NPs structure and the bonded CPT in achieving controlled release and mitigating potential toxicity.

2.5. References

1. Lehninger, A. L., Nelson, D. L., & Cox, M. M. (2005). Lehninger principles of biochemistry (4th ed., pp. 75–110). W.H. Freeman. chrome-extension://efaidnbmnnnibpcajpcglclefindmkaj/https://librarymohsin.wordpress.com/wp-content/uploads/2018/07/lehninger-principles-of-biochemistry-fourth-edition-david-l-nelson-michael-m-cox1.pdf

2. Ambrogelly, A., Palioura, S., & Söll, D. (2006). Natural expansion of the genetic code. Nature Chemical Biology, 3(1), 29-35. https://doi.org/10.1038/nchembio847

3. Voet, D., Voet, J. G., & Pratt, C. W. (2006a). Fundamentals of Biochemistry (2nd ed., pp. 80–93). John Wiley & Sons.

4. Balu, D. T. (2016). The nmda receptor and schizophrenia. Advances in Pharmacology, 351-382. https://doi.org/10.1016/bs.apha.2016.01.006

5. Merrifield, B. (1986). Solid phase synthesis. Science, 232(4748), 341-347. https://doi.org/10.1126/science.3961484

6. Khan, W., Saravanan, M., Farah, S., Kumar, N., & Domb, A. J. (2011). Biodegradable polymers derived from amino acids. Macromolecular Bioscience, 11(12), 1625-1636. https://doi.org/10.1002/mabi.201100324

7. Sangamesh Kumbar, Cato Laurencin, & Meng Deng. (2014). Natural and synthetic biomedical polymers (pp. 43–53, Chapter 3: Proteins and Poly (Amino Acids); p. 333-346, Chapter 20: Polymeric Materials in Drug Delivery). Elsevier.

8. Palomo, J. M. (2014). Solid-phase peptide synthesis: an overview focused on the preparation of biologically relevant peptides. RSC Adv., 4(62), 32658-32672. https://doi.org/10.1039/c4ra02458c

9. Schmidt, M., Toplak, A., Rozeboom, H., Wijma, H. J., Quaedflieg, P. J. L. M., Maarseveen, J. H. v., … & Nuijens, T. (2018). Design of a substrate-tailored peptiligase variant for the efficient synthesis of thymosin-α1. Organic &Amp; Biomolecular Chemistry, 16(4), 609-618. https://doi.org/10.1039/c7ob02812a

10. Lee, M. A., Brown, J. S., Loas, A., & Pentelute, B. L. (2024). Investigation of commercially available resins for the automated flow synthesis of difficult or long peptide sequences. Peptide Science, 116(3). https://doi.org/10.1002/pep2.24344

11. Cheng, J. and Deming, T. J. (2011). Synthesis of polypeptides by ring-opening polymerization of α-amino acid n-carboxyanhydrides. Topics in Current Chemistry, 1-26.

https://doi.org/10.1007/128_2011_173

12. Kricheldorf, H. R. (2006). Polypeptides and 100 years of chemistry of α-amino acid n-carboxyanhydrides. Angewandte Chemie International Edition, 45(35), 5752-5784. https://doi.org/10.1002/anie.200600693

13. Collman JP, Hegedus LS, Norton JR, Finke RG (1987) Principles and applications of organotransition metal chemistry, 2nd edn. University Science, Mill Valley

14. Odian, G. (2004). Principles of polymerization.. https://doi.org/10.1002/047147875x

15. Deming TJ. Polypeptide Materials: New Synthetic Methods and Applications. Advanced Materials, 9(4), 299-311. https://doi.org/10.1002/adma.19970090404

16. Pelegri-O'Day, Emma M., et al. "Therapeutic Protein–Polymer Conjugates: Advancing beyond Pegylation." Journal of the American Chemical Society, vol. 136, no. 41, 2014, pp. 14323–14332., https://doi.org/10.1021/ja504390x

17. Xi, E. and Patel, A. J. (2016). The hydrophobic effect, and fluctuations: the long and the short of it. Proceedings of the National Academy of Sciences, 113(17), 4549-4551. https://doi.org/10.1073/pnas.1603014113

18. Din, F. u., Aman, W., Ullah, I., Qureshi, O. S., Mustapha, O., Shafique, S., … & Zeb, A. (2017). Effective use of nanocarriers as drug delivery systems for the treatment of selected tumors. International Journal of Nanomedicine, Volume 12, 7291-7309. https://doi.org/10.2147/ijn.s146315

19. Wang, A. Z., Gu, F., Zhang, L., Chan, J. M., Radovic-Moreno, A., Shaikh, M. R., … & Farokhzad, O. C. (2008). Biofunctionalized targeted nanoparticles for therapeutic applications. Expert Opinion on Biological Therapy, 8(8), 1063-1070. https://doi.org/10.1517/14712598.8.8.1063

20. Thongpon, P., Tang, M., & Cong, Z. (2025). Peptide-based nanoparticle for tumor therapy. Biomedicines, 13(6), 1415. https://doi.org/10.3390/biomedicines13061415

21. Luo, Y., Chen, L., Yan, M., & Xu, F. (2013). Novel ab4-type ctbn-b-mpeg pu micelle-like amphiphilic block copolymer micelles for prednisone drug release. Industrial & Engineering Chemistry Research, 52(4), 1571-1580. https://doi.org/10.1021/ie3024164

22. Jaskula-Sztul, R., Chen, G., Dammalapati, A., Harrison, A. D., Tang, W., Gong, S., … & Chen, H. (2017). Ab3-loaded and tumor-targeted unimolecular micelles for medullary thyroid cancer treatment. Journal of Materials Chemistry B, 5(1), 151-159. https://doi.org/10.1039/c6tb02530g

23. Avsar, S. Y., Kyropoulou, M., Leone, S., Schoenenberger, C., Meier, W., & Palivan, C. G. (2019). Biomolecules turn self-assembling amphiphilic block co-polymer platforms into biomimetic interfaces. Frontiers in Chemistry, 6. https://doi.org/10.3389/fchem.2018.00645

24. Zalipsky, S. and Harris, J. M. (1997). Introduction to chemistry and biological applications of poly(ethylene glycol). ACS Symposium Series, 1-13. https://doi.org/10.1021/bk-1997-0680.ch001

25. Working, P. K., Newman, M. S., Johnson, J. A., & Cornacoff, J. B. (1997). Safety of poly(ethylene glycol) and poly(ethylene glycol) derivatives. ACS Symposium Series, 45-57. https://doi.org/10.1021/bk-1997-0680.ch004

26. Liu, Y., Wang, W., Yang, J., Zhou, C., & Sun, J. (2013). Ph-sensitive polymeric micelles triggered drug release for extracellular and intracellular drug targeting delivery. Asian Journal of Pharmaceutical Sciences, 8(3), 159-167. https://doi.org/10.1016/j.ajps.2013.07.021

27. Rapoport, N. (2007). Physical stimuli-responsive polymeric micelles for anti-cancer drug delivery. Progress in Polymer Science, 32(8-9), 962-990. https://doi.org/10.1016/j.progpolymsci.2007.05.009

28. Maeda, H., Wu, J., Sawa, T., Matsumura, Y., & Hori, K. (2000). Tumor vascular permeability and the epr effect in macromolecular therapeutics: a review. Journal of Controlled Release, 65(1-2), 271-284. https://doi.org/10.1016/s0168-3659(99)00248-5

29. Sherwood, L. M., Parris, E. E., & Folkman, J. (1971). Tumor angiogenesis: therapeutic implications. New England Journal of Medicine, 285(21), 1182-1186. https://doi.org/10.1056/nejm197111182852108

30. Maeda, H., & Matsumura, Y. (1989). Tumoritropic and lymphotropic principles of macromolecular drugs. Critical reviews in therapeutic drug carrier systems, 6(3), 193–210.

31. Matsumura, Y., & Maeda, H. (1986). A new concept for macromolecular therapeutics in cancer chemotherapy: mechanism of tumoritropic accumulation of proteins and the

antitumor agent smancs. Cancer research, 46 12 Pt 1, 6387-92 .

32. Maeda, H. (2001). Smancs and polymer-conjugated macromolecular drugs: advantages in cancer chemotherapy. Advanced Drug Delivery Reviews, 46(1-3), 169-185. https://doi.org/10.1016/s0169-409x(00)00134-4

33. Yoshida, M., Takimoto, R., Murase, K., Sato, Y., Hirakawa, M., Tamura, F., … & Kato, J. (2012). Targeting anticancer drug delivery to pancreatic cancer cells using a fucose-bound nanoparticle approach. PLoS ONE, 7(7), e39545. https://doi.org/10.1371/journal.pone.0039545

34. Peer, D., Karp, J. M., Hong, S., Farokhzad, O. C., Margalit, R., & Langer, R. (2007). Nanocarriers as an emerging platform for cancer therapy. Nature Nanotechnology, 2(12), 751-760. https://doi.org/10.1038/nnano.2007.387

35. Uzunparmak, B. and Şahin, İ. H. (2019). Pancreatic cancer microenvironment: a current dilemma. Clinical and Translational Medicine, 8(1). https://doi.org/10.1186/s40169-019-0221-1

36. Neeße, A., Gress, T. M., Tuveson, D. A., Michl, P., & Krug, S. (2013). Emerging concepts in pancreatic cancer medicine: targeting the tumor stroma. OncoTargets and Therapy, 33. https://doi.org/10.2147/ott.s38111

37. Nicolas, J. (2016). Drug-initiated synthesis of polymer prodrugs: combining simplicity and efficacy in drug delivery. Chemistry of Materials, 28(6), 1591-1606. https://doi.org/10.1021/acs.chemmater.5b04281

38. Avgoustakis, K. (2002). Plga–mpeg nanoparticles of cisplatin: in vitro nanoparticle degradation, in vitro drug release and in vivo drug residence in blood properties. Journal of Controlled Release, 79(1-3), 123-135. https://doi.org/10.1016/s0168-3659(01)00530-2

39. Talelli, M., Rijcken, C. J. F., Hennink, W. E., & Lammers, T. (2012). Polymeric micelles for cancer therapy: 3 C's to enhance efficacy. Current Opinion in Solid State and Materials Science, 16(6), 302–309. https://doi.org/10.1016/j.cossms.2012.10.003

40. Narvekar, M., Xue, H., Eoh, J. Y., & Wong, H. L. (2014). Nanocarrier for poorly water-soluble anticancer drugs—barriers of translation and solutions. AAPS PharmSciTech, 15(4), 822-833. https://doi.org/10.1208/s12249-014-0107-x

41. Maherani, B., Arab-Tehrany, E., Mozafari, M. R., Gaïani, C., & Linder, M. (2011). Liposomes: a review of manufacturing techniques and targeting strategies. Current Nanoscience, 7(3), 436-452. https://doi.org/10.2174/157341311795542453

42. Sun, R., Luo, Q., Li, X., Huang, X., Teng, L., Shen, Z., & Zhu, W. (2021). Supramolecular PEGylation of camptothecin for cancer therapy. Materials Today Nano, 14, 100115–100115. https://doi.org/10.1016/j.mtnano.2021.100115

43. Turecek, P. L., Bossard, M. J., Schoetens, F., & Ivens, I. A. (2016). PEGylation of Biopharmaceuticals: A Review of Chemistry and Nonclinical Safety Information of Approved Drugs. Journal of Pharmaceutical Sciences, 105(2), 460–475. https://doi.org/10.1016/j.xphs.2015.11.015

44. Shen, Y., Jin, E., Zhang, B., Murphy, C. J., Sui, M., Zhao, J., Wang, J., Tang, J., Fan, M., Van

Kirk, E., & Murdoch, W. J. (2010). Prodrugs Forming High Drug Loading Multifunctional Nanocapsules for Intracellular Cancer Drug Delivery. Journal of the American Chemical Society, 132(12), 4259–4265. https://doi.org/10.1021/ja909475m

45. Vicent, M. J., & Duncan, R. (2006). Polymer conjugates: nanosized medicines for treating cancer. Trends in Biotechnology, 24(1), 39–47. https://doi.org/10.1016/j.tibtech.2005.11.006

46. Rösler, A., Vandermeulen, G. W. M., & Klok, H.-A. (2001). Advanced drug delivery devices via self-assembly of amphiphilic block copolymers. Advanced Drug Delivery Reviews, 53(1), 95–108. https://doi.org/10.1016/s0169-409x(01)00222-8

47. Talelli, M., Barz, M., Rijcken, C. J. F., Kiessling, F., Hennink, W. E., & Lammers, T. (2015). Core-crosslinked polymeric micelles: Principles, preparation, biomedical applications and clinical translation. Nano Today, 10(1), 93–117. https://doi.org/10.1016/j.nantod.2015.01.005

48. Kim, S., Shi, Y., Kim, J. Y., Park, K., & Cheng, J.-X. (2009). Overcoming the barriers in micellar drug delivery: loading efficiency,in vivostability, and micelle–cell interaction. Expert Opinion on Drug Delivery, 7(1), 49–62. https://doi.org/10.1517/17425240903380446

49. Sun, R., Luo, Q., Gao, C., & Wang, Y. (2014). Facile fabrication of reduction-responsive nanocarriers for controlled drug release. Polym. Chem., 5(17), 4879–4883. https://doi.org/10.1039/c4py00577e.

50. Ringsdorf, H. (1975). Structure and properties of pharmacologically active polymers.

Journal of Polymer Science: Polymer Symposia, 51(1), 135-153. https://doi.org/10.1002/polc.5070510111

51. Breunig, M., Bauer, S. E., & Goepferich, A. (2008). Polymers and nanoparticles: intelligent tools for intracellular targeting?. European Journal of Pharmaceutics and Biopharmaceutics, 68(1), 112-128. https://doi.org/10.1016/j.ejpb.2007.06.010

52. Liu, X., Chen, Y., Li, H., Huang, N., Jin, Q., Ren, K., … & Ji, J. (2013). Enhanced retention and cellular uptake of nanoparticles in tumors by controlling their aggregation behavior. ACS Nano, 7(7), 6244-6257. https://doi.org/10.1021/nn402201w

53. Ying, V., Haverstick, K., Page, R. L., & Saltzman, W. M. (2007). Efficacy of camptothecin and polymer-conjugated camptothecin in tumor spheroids and solid tumors. Journal of Biomaterials Science, Polymer Edition, 18(10), 1283-1299. https://doi.org/10.1163/156856207782177918

54. Hatefi, A. and Amsden, B. G. (2002). Camptothecin delivery methods. Pharmaceutical Research, 19(10), 1389-1399. https://doi.org/10.1023/a:1020427227285

55. Drwal, M. N., Marinello, J., Manzo, S. G., Wakelin, L. P. G., Capranico, G., & Griffith, R. (2014). Novel dna topoisomerase iiα inhibitors from combined ligand- and structure-based virtual screening. PLoS ONE, 9(12), e114904. https://doi.org/10.1371/journal.pone.0114904

56. Pourquier, P. and Pommier, . (2001). Topoisomerase i-mediated dna damage. Advances in Cancer Research, 189-216. https://doi.org/10.1016/s0065-230x(01)80016-6

57. Okuno, S., Harada, M., Yano, T., Yano, S., Kiuchi, S., Tsuda, N., Sakamura, Y., Imai, J., Kawaguchi, T., & Tsujihara, K. (2000). Complete regression of xenografted human carcinomas by camptothecin analogue-carboxymethyl dextran conjugate (T-0128). Cancer research, 60(11), 2988–2995.

58. Conroy, T., Desseigne, F., Ychou, M., Bouché, O., Guimbaud, R., Bécouarn, Y., … & Ducreux, M. (2011). Folfirinox versus gemcitabine for metastatic pancreatic cancer. New England Journal of Medicine, 364(19), 1817-1825. https://doi.org/10.1056/nejmoa1011923

59. Capranico, G., Marinello, J., & Chillemi, G. (2017). Type i dna topoisomerases. Journal of Medicinal Chemistry, 60(6), 2169-2192. https://doi.org/10.1021/acs.jmedchem.6b00966

60. Pizzolato, J. F. and Saltz, L. B. (2003). The camptothecins. The Lancet, 361(9376), 2235-2242. https://doi.org/10.1016/s0140-6736(03)13780-4

61. Strumberg, D., Pilon, A. A., Smith, M., Hickey, R. J., Malkas, L. H., & Pommier, . (2000). Conversion of topoisomerase i cleavage complexes on the leading strand of ribosomal DNA into 5′-phosphorylated DNA double-strand breaks by replication runoff. Molecular and Cellular Biology, 20(11), 3977-3987. https://doi.org/10.1128/mcb.20.11.3977-3987.2000

62. Li, L. H., Fraser, T. J., Olin, E. J., & Bhuyan, B. K. (1972). Action of camptothecin on mammalian cells in culture. Cancer research, 32(12), 2643–2650.

63. Deshmukh, M., Chao, P., Kutscher, H. L., Gao, D., & Sinko, P. J. (2010). A series of α-amino acid ester prodrugs of camptothecin: in vitro hydrolysis and a549 human lung carcinoma

cell cytotoxicity. Journal of Medicinal Chemistry, 53(3), 1038-1047. https://doi.org/10.1021/jm901029n

64. Li, Y., Lin, B., Agadir, A., Liu, R., Dawson, M. I., Reed, J. C., … & Zhang, X. (1998). Molecular determinants of ahpn (cd437)-induced growth arrest and apoptosis in human lung cancer cell lines. Molecular and Cellular Biology, 18(8), 4719-4731. https://doi.org/10.1128/mcb.18.8.4719

65. Szakács, G., Paterson, J. K., Ludwig, J. A., Booth-Genthe, C., & Gottesman, M. M. (2006). Targeting multidrug resistance in cancer. Nature Reviews Drug Discovery, 5(3), 219-234. https://doi.org/10.1038/nrd1984

66. Ambudkar, S. V., Dey, S., Hrycyna, C. A., Ramachandra, M., Pastan, I., & Gottesman, M. M. (1999). Biochemical, cellular, and pharmacological aspects of the multidrug transporter. Annual Review of Pharmacology and Toxicology, 39(1), 361-398. https://doi.org/10.1146/annurev.pharmtox.39.1.361

67. Beretta, G. L., Gatti, L., Perego, P., & Zaffaroni, N. (2013). Camptothecin resistance in cancer: insights into the molecular mechanisms of a dna-damaging drug. Current Medicinal Chemistry, 20(12), 1541-1565. https://doi.org/10.2174/0929867311320120006

68. Potmesil M. (1994). Camptothecins: from bench research to hospital wards. Cancer research, 54(6), 1431–1439

69. Wall, M. E., Wani, M. C., Cook, C., Palmer, K., McPhail, A., & Sim, G. A. (1966). Plant antitumor agents. i. the isolation and structure of camptothecin, a novel alkaloidal

leukemia and tumor inhibitor from camptotheca acuminata1,2. Journal of the American Chemical Society, 88(16), 3888-3890. https://doi.org/10.1021/ja00968a057.

70. Fassberg, J. and Stella, V. J. (1992). A kinetic and mechanistic study of the hydrolysis of camptothecin and some analogues. Journal of Pharmaceutical Sciences, 81(7), 676-684. https://doi.org/10.1002/jps.2600810718

71. Paranjpe, P. V., Chen, Y., Kholodovych, V., Welsh, W., Stein, S., & Sinko, P. J. (2004). Tumor-targeted bioconjugate based delivery of camptothecin: design, synthesis and in vitro evaluation. Journal of Controlled Release, 100(2), 275–292. https://doi.org/10.1016/j.jconrel.2004.08.030

72. National Center for Biotechnology Information. "PubChem Patent Summary for CN-110577550-A" PubChem, https://pubchem.ncbi.nlm.nih.gov/patent/CN-110577550-A. Accessed 31 August, 2022.

73. Greenwald, R. A. (1998). Camptothecin-20-peg ester transport forms: the effect of spacer groups on antitumor activity. Bioorganic & Medicinal Chemistry, 6(5), 551-562. https://doi.org/10.1016/s0968-0896(98)00005-4

74. Bruijnincx, P. C. A. and Sadler, P. J. (2008). New trends for metal complexes with anticancer activity. Current Opinion in Chemical Biology, 12(2), 197-206. https://doi.org/10.1016/j.cbpa.2007.11.013

75. Che, C. and Siu, F. (2010). Metal complexes in medicine with a focus on enzyme inhibition. Current Opinion in Chemical Biology, 14(2), 255-261. https://doi.org/10.1016/j.cbpa.2009.11.015

76. Zhao, X. and Harris, M. (1997). Novel degradable poly(ethylene glycol) esters for drug delivery. ACS Symposium Series, 458-472. https://doi.org/10.1021/bk-1997-0680.ch028

77. Abuchowski, A.; van Es, T.; Palzuk, N. C.; Davis, F. F. J. Biol. Chem. 1977, 252, 3578-3581.

78. Savoca, K. V.; Abuchowski, A.; van Es, T.; Davis, F. F.; Palczuk, N. C. Biochim. Biophys. Acta 1979, 578, 47

79. La, S. B., Nagasaki, Y., & Kataoka, K. (1997). Poly(ethylene glycol)-based micelles for drug delivery. ACS Symposium Series, 99-116. https://doi.org/10.1021/bk-1997-0680.ch007

80. Lee, E. (2003). Polymeric micelle for tumor ph and folate-mediated targeting. Journal of Controlled Release, 91(1-2), 103-113. https://doi.org/10.1016/s0168-3659(03)00239-6

81. Bae, Y., Nishiyama, N., Fukushima, S., Koyama, H., Matsumura, Y., & Kataoka, K. (2004). Preparation and biological characterization of polymeric micelle drug carriers with intracellular ph-triggered drug release property: tumor permeability, controlled subcellular drug distribution, and enhanced in vivo antitumor efficacy. Bioconjugate Chemistry, 16(1), 122-130. https://doi.org/10.1021/bc0498166

82. Kim, D., Gao, Z. G., Lee, E. S., & Bae, Y. H. (2009). In vivo evaluation of doxorubicin-loaded polymeric micelles targeting folate receptors and early endosomal ph in drug-resistant ovarian cancer. Molecular Pharmaceutics, 6(5), 1353-1362. https://doi.org/10.1021/mp900021q

83. Hu, Y., Hou, Y., Wang, H., & Lu, H. (2018). Polysarcosine as an alternative to peg for therapeutic protein conjugation. Bioconjugate Chemistry, 29(7), 2232-2238. https://doi.org/10.1021/acs.bioconjchem.8b00237

84. Richter, A. W. and Åkerblom, E. (1984). Polyethylene glycol reactive antibodies in man: titer distribution in allergic patients treated with monomethoxy polyethylene glycol modified allergens or placebo, and in healthy blood donors. International Archives of Allergy and Immunology, 74(1), 36-39. https://doi.org/10.1159/000233512

85. Veronese, F. M. (2009). Pegylated protein drugs: basic science and clinical applications.. p.147 https://doi.org/10.1007/978-3-7643-8679-5

86. Alasvand, Neda, et al. “Chapter 13 -Therapeutic Nanoparticles for Targeted Delivery of Anticancer Drugs.” Multifunctional Systems for Combined Delivery, Biosensing and Diagnostics, Elsevier, 12 May 2017,

87. Conover, C., Lejeune, L., Linberg, R., Shum, K., & Shorr, R. (1996). Transitional vacuole formation following a bolus infusion of peg-hemoglobin in the rat. Artificial Cells, Blood Substitutes, and Biotechnology, 24(6), 599-611. https://doi.org/10.3109/10731199609118885

88. Conover, C. D., Linberg, R., Gilbert, C. W., Shum, K., & Shorr, R. (1997). Effect of polyethylene glycol conjugated bovine hemoglobin in both top-load and exchange transfusion rat models. Artificial Organs, 21(10), 1066-1075. https://doi.org/10.1111/j.1525-1594.1997.tb00444.x

89. Conover, C. D., Gilbert, C. W., Shurn, K. L., & Shorr, R. (1997). The impact of polyethylene

glycol conjugation on bovine hemoglobin's circulatory half-life and renal effects in a rabbit top-loaded transfusion model. Artificial Organs, 21(8), 907-915. https://doi.org/10.1111/j.1525-1594.1997.tb00250.x

90. Conover, C. D., Lejeune, L., Shum, K., Gilbert, C. W., & Shorr, R. (1997). Physiological effect of polyethylene glycol conjugation on stroma-free bovine hemoglobin in the conscious dog after partial exchange transfusion. Artificial Organs, 21(5), 369-378. https://doi.org/10.1111/j.1525-1594.1997.tb00733.x

91. Bendele, A. M., Seely, J., Richey, C., Sennello, G., & Shopp, G. M. (1998). Short communication: renal tubular vacuolation in animals treated with polyethylene-glycol-conjugated proteins. Toxicological Sciences, 42(2), 152-157. https://doi.org/10.1093/toxsci/42.2.152

92. Fletcher, A. M., Tellier, P., Douville, J., Mansell, P. W. A., Graziano, M. J., Mangipudy, R. S., … & Achanzar, W. E. (2019). Adverse vacuolation in multiple tissues in cynomolgus monkeys following repeat-dose administration of a pegylated protein. Toxicology Letters, 317, 120-129. https://doi.org/10.1016/j.toxlet.2019.09.023

93. Varlas, S., Georgiou, P. G., Bilalis, P., Jones, J. R., Hadjichristidis, N., & O'Reilly, R. K. (2018). Poly(sarcosine)-based nano-objects with multi-protease resistance by aqueous photoinitiated polymerization-induced self-assembly (photo-pisa). Biomacromolecules, 19(11), 4453-4462. https://doi.org/10.1021/acs.biomac.8b01326

94. C. Ragi, Sedaghat-Herati, M. R., A. Ahmed Ouameur, & Tajmir-Riahi, H. A. (2005). The effects of poly(ethylene glycol) on the solution structure of human serum albumin. Biopolymers, 78(5), 231–236. https://doi.org/10.1002/bip.20281

95. Rixman, M. A., Dean, D., & Ortiz, C. (2003). Nanoscale Intermolecular Interactions between Human Serum Albumin and Low Grafting Density Surfaces of Poly(ethylene oxide). Langmuir, 19(22), 9357–9372. https://doi.org/10.1021/la034057l

96. Hasek, J. (2006). Poly(ethylene glycol) interactions with proteins. Zeitschrift Für Kristallographie Supplements, 2006(suppl_23_2006), 613–618. https://doi.org/10.1524/zksu.2006.suppl_23.613

97. Deng, Y., Zou, T., Tao, X., Semetey, V., Trépout, S., Marco, S., … & Li, M. (2015). Poly(ε-caprolactone)-block-polysarcosine by ring-opening polymerization of sarcosine n-thiocarboxyanhydride: synthesis and thermoresponsive self-assembly. Biomacromolecules, 16(10), 3265-3274. https://doi.org/10.1021/acs.biomac.5b00930

98. Zhang, D., Lahasky, S. H., Guo, L., Lee, C., & Lavan, M. (2012). Polypeptoid materials: current status and future perspectives. Macromolecules, 45(15), 5833-5841. https://doi.org/10.1021/ma202319g

99. Birke, A., Ling, J., & Barz, M. (2018). Polysarcosine-containing copolymers: synthesis, characterization, self-assembly, and applications. Progress in Polymer Science, 81, 163-208. https://doi.org/10.1016/j.progpolymsci.2018.01.002

100. Chen, S., Zhou, P., Yang, W., Hu, D., Chen, P., Sun, P., … & Fan, Q. (2023). Stealth-like polysarcosine-modified nanoparticles with low dye doses and long blood circulation for efficient breast cancer pulmonary metastasis imaging. Biomaterials Science, 11(13), 4644-4651. https://doi.org/10.1039/d3bm00200d

101. Settanni, G., Schäfer, T., Muhl, C., Barz, M., & Schmid, F. (2018). Poly-sarcosine and poly(ethylene-glycol) interactions with proteins investigated using molecular dynamics simulations. Computational and Structural Biotechnology Journal, 16, 543-550. https://doi.org/10.1016/j.csbj.2018.10.012

102. Ramachandran, G. N., Ramakrishnan, C., & Sasisekharan, V. (1963). Stereochemistry of polypeptide chain configurations. Journal of Molecular Biology, 7(1), 95-99. https://doi.org/10.1016/s0022-2836(63)80023-6

103. Klein, P., Klinker, K., Zhang, W., Kern, S., Kessel, E., Wagner, E., … & Barz, M. (2018). Efficient shielding of polyplexes using heterotelechelic polysarcosines. Polymers, 10(6), 689. https://doi.org/10.3390/polym10060689

104. Gupta, T. B., Bui, Q. A., Manirakiza, H., Hajji, L. E., Humbert, N., Mouhamad, A. W., … & Klymchenko, A. S. (2025). Peptide-functionalized fluorescent polymeric nanoparticles: polysarcosine length defines stealth properties.. https://doi.org/10.1101/2025.04.20.649688

105. Di, J., Gao, X., Du, Y., Zhang, H., Gao, J., & Zheng, A. (2021). Size, shape, charge and “stealthy” surface: carrier properties affect the drug circulation time in vivo. Asian Journal of Pharmaceutical Sciences, 16(4), 444-458. https://doi.org/10.1016/j.ajps.2020.07.005

106. Weber, B., Seidl, C., Schwiertz, D., Scherer, M., Bleher, S., Süss, R., … & Barz, M. (2016). Polysarcosine-Based Lipids: From Lipopolypeptoid Micelles to Stealth-Like Lipids in Langmuir Blodgett Monolayers. Polymers, 8(12), 427. https://doi.org/10.3390/polym8120427

107. Li, C. (2002). Poly(l-glutamic acid)–anticancer drug conjugates. Advanced Drug Delivery Reviews, 54(5), 695-713. https://doi.org/10.1016/s0169-409x(02)00045-5

108. Dutta, S., Ray, S., & Nagarajan, K. (2013). Glutamic acid as anticancer agent: an overview. Saudi Pharmaceutical Journal, 21(4), 337-343. https://doi.org/10.1016/j.jsps.2012.12.007

109. Park, C. G., Sung, M., Uyama, H., & Han, D. K. (2021). Poly(glutamic acid): production, composites, and medical applications of the next-generation biopolymer. Progress in Polymer Science, 113, 101341. https://doi.org/10.1016/j.progpolymsci.2020.101341

110. Luo, Z., Guo, Y., Liu, J., Qiu, H., Zhao, M., Zou, W., … & Li, S. (2016). Microbial synthesis of poly-γ-glutamic acid: current progress, challenges, and future perspectives. Biotechnology for Biofuels, 9(1). https://doi.org/10.1186/s13068-016-0537-7

111. Ho, G. H., Ho, T., Hsieh, K. H., Su, Y., Lin, P., Yang, J., … & Yang, S. (2006). Γ-polyglutamic acid produced by bacillus subtilis (natto): structural characteristics, chemical properties and biological functionalities. Journal of the Chinese Chemical Society, 53(6), 1363-1384. https://doi.org/10.1002/jccs.200600182

112. Akagi, T., Matsusaki, M., & Akashi, M. (2010). Pharmaceutical and medical applications of poly-gamma-glutamic acid. Microbiology Monographs, 119-153. https://doi.org/10.1007/978-3-642-12453-2_7

113. Singer, J. W., Bhatt, R., Tulinsky, J., Buhler, K. R., Heasley, E., Klein, P., … & Vries, P. d. (2001). Water-soluble poly-(l-glutamic acid)–gly-camptothecin conjugates enhance

camptothecin stability and efficacy in vivo. Journal of Controlled Release, 74(1-3), 243-247. https://doi.org/10.1016/s0168-3659(01)00323-6

114. Kurosaki, T., Kitahara, T., Fumoto, S., Nishida, K., Nakamura, J., Niidome, T., … & Sasaki, H. (2009). Ternary complexes of pdna, polyethylenimine, and γ-polyglutamic acid for gene delivery systems. Biomaterials, 30(14), 2846-2853. https://doi.org/10.1016/j.biomaterials.2009.01.055

115. Drobník, J. and Rypáček, F. (1984). Soluble synthetic polymers in biological systems. Advances in Polymer Science, 1-50. https://doi.org/10.1007/3-540-12796-8_9

116. Oldham, E., Li, C., Shi, K., Wallace, S., & Huang, P. (2000). Comparison of action of paclitaxel and poly(l-glutamic acid)-paclitaxel conjugate in human breast cancer cells.. International Journal of Oncology. https://doi.org/10.3892/ijo.16.1.125

117. Ye, H., Li, J., Hu, R., Yi, Z., Li, J., Wu, Y., … & Wu, Z. (2006). Poly(γ,l-glutamic acid)–cisplatin conjugate effectively inhibits human breast tumor xenografted in nude mice. Biomaterials, 27(35), 5958-5965. https://doi.org/10.1016/j.biomaterials.2006.08.016

118. Dubey, S. K., Sharma, A. K., Narain, U., Misra, K., & Pati, U. (2008). Design, synthesis and characterization of some bioactive conjugates of curcumin with glycine, glutamic acid, valine and demethylenated piperic acid and study of their antimicrobial and antiproliferative properties. European Journal of Medicinal Chemistry, 43(9), 1837-1846. https://doi.org/10.1016/j.ejmech.2007.11.027

119. Wang, S., Lu, M., Wan, S., Lyu, C.-Y., Tian, Z., Liu, K., & Lu, H. (2024). Precision Synthesis of Polysarcosine via Controlled Ring-Opening Polymerization of N -Carboxyanhydride:

Fast Kinetics, Ultrahigh Molecular Weight, and Mechanistic Insights. Journal of the American Chemical Society, 146(8), 5678–5692. https://doi.org/10.1021/jacs.3c14740

120. Sui, B., Xu, H., Jin, J., Gou, J., Liu, J., Tang, X., Zhang, Y., Xu, J., Zhang, H., & Jin, X. (2014). Self-Assembled Micelles Composed of Doxorubicin Conjugated Y-Shaped PEG-Poly(glutamic acid)2 Copolymers via Hydrazone Linkers. Molecules, 19(8), 11915–11932. https://doi.org/10.3390/molecules190811915

121. Yoo, J., Birke, A., Kim, J., Jang, Y., Song, S. Y., Ryu, S., Kim, B.-S., Kim, B.-G., Barz, M., & Char, K. (2018). Cooperative Catechol-Functionalized Polypept(o)ide Brushes and Ag Nanoparticles for Combination of Protein Resistance and Antimicrobial Activity on Metal Oxide Surfaces. Biomacromolecules, 19(5), 1602–1613. https://doi.org/10.1021/acs.biomac.8b00135

122. Schneider, M., Fetsch, C., Amin, I., Jordan, R., & Luxenhofer, R. (2013). Polypeptoid Brushes by Surface-Initiated Polymerisation of N-Substituted Glycine N-Carboxyanhydrides. Langmuir, 29(23), 6983–6988. https://doi.org/10.1021/la4009174

123. Schneider, M., Tang, Z., Richter, M., Marschelke, C., Förster, P., Wegener, E., Amin, I., Zimmermann, H., Scharnweber, D., Braun, H., Luxenhofer, R., & Jordan, R. (2015). Patterned Polypeptoid Brushes. Macromolecular Bioscience, 16(1), 75–81. https://doi.org/10.1002/mabi.201500314

124. Byrd, H., & McEwen, C. N. (2000). The Limitations of MALDI-TOF Mass Spectrometry in the Analysis of Wide Polydisperse Polymers. Analytical Chemistry, 72(19), 4568–4576. https://doi.org/10.1021/ac0002745

125. Montaudo, G., Montaudo, M. S., Puglisi, C., & Samperi, F. (1995). Characterization of polymers by matrix-assisted laser desorption/ionization time-of-flight mass spectrometry: Molecular weight estimates in samples of varying polydispersity. Rapid Communications in Mass Spectrometry, 9(5), 453–460. https://doi.org/10.1002/rcm.1290090514

126. Rashidzadeh, H., & Guo, B. (1998). Use of MALDI-TOF To Measure Molecular Weight Distributions of Polydisperse Poly(methyl methacrylate). Analytical Chemistry, 70(1), 131–135. https://doi.org/10.1021/ac970568z

127. Yuan, H., Luo, K., Lai, Y., Pu, Y., He, B., Wang, G., Wu, Y., & Gu, Z. (2010). A Novel Poly(l-glutamic acid) Dendrimer Based Drug Delivery System with Both pH-Sensitive and Targeting Functions. Molecular Pharmaceutics, 7(4), 953–962. https://doi.org/10.1021/mp1000923

128. Pu, Y., Chang, S., Yuan, H., Wang, G., He, B., & Gu, Z. (2013). The anti-tumor efficiency of poly(l-glutamic acid) dendrimers with polyhedral oligomeric silsesquioxane cores. Biomaterials, 34(14), 3658-3666. https://doi.org/10.1016/j.biomaterials.2013.01.082

129. Han, J., Ding, J., Wang, Z., Yan, S., Zhuang, X., Chen, X., & Yin, J. (2013). The synthesis, deprotection and properties of poly(γ-benzyl-l-glutamate). Science China Chemistry, 56(6), 729–738. https://doi.org/10.1007/s11426-013-4839-3

130. Wang, Y., Xu, H., & Zhang, X. (2009). Tuning the Amphiphilicity of Building Blocks: Controlled Self-Assembly and Disassembly for Functional Supramolecular Materials. Advanced Materials, 21(28), 2849–2864. https://doi.org/10.1002/adma.200803276

131. Ali, A., Awang, M., Mat, R., Johari, A., Kamaruddin, M. J., & Sulaiman, W. R. W. (2014). Influence of hydrophilic polymer on pure water permeation, permeability coefficient, and porosity of polysulfone blend membranes. Advanced Materials Research, 931-932, 168-172. https://doi.org/10.4028/www.scientific.net/amr.931-932.168

132. pfizer. "DBLTMIRINOTECAN INJECTION CONCENTRATE." Pfizer, pfizer, Aug. 2001, labeling.pfizer.com/ShowLabeling.aspx?id=12202

133. "Choosing the Concentration Range for DLS Size Measurement." Www.horiba.com, www.horiba.com/int/scientific/technologies/dynamic-light-scattering-dls-particle-size-distribution-analysis/concentration-range-for-dls-size-measurement/.

134. Zürich, JKweb, Webdesign Basel &. "LS Instruments | Experimental Guidelines - DLS Sample Preparation." Lsinstruments.ch, lsinstruments.ch/en/theory/dynamic-light-scattering-dls/experimental-guidelines-dls-sample-preparation.

135. Knysh, Alexander, et al. "Dynamic Light Scattering Analysis in Biomedical Research and Applications of Nanoparticles and Polymers." Journal of Biomedical Photonics & Engineering, 30 May 2023, pp. 020203–020203, https://doi.org/10.18287/jbpe23.09.020203.

136. Zürich, JKweb, Webdesign Basel &. "LS Instruments | Experimental Guidelines - DLS Sample Preparation." Lsinstruments.ch, lsinstruments.ch/en/theory/dynamic-light-scattering-dls/experimental-guidelines-dls-sample-preparation.

137. "What Is Dynamic Light Scattering (DLS) and How Does It Work? - Scimed Characterization of Cerium Oxide Nanoparticles Using Vasco Kin." Scimed, 14 Apr. 2026,

www.scimed.co.uk/education/what-is-dynamic-light-scattering-dls-and-how-does-it-work/. Accessed 19 May 2026.

138. Dziendzikowska, K., Czerwińska, M., Grodzicki, W., Oczkowski, M., Królikowski, T., Gromadzka-Ostrowska, J., Męczyńska-Wielgosz, S., Sikorska, K., Kamola, D., Sapierzyński, R., & Kruszewski, M. (2026). Comparative impact of polystyrene, rice bag-derived high-density polyethylene nanoparticles, and polystyrene–silver nanoparticle interactions in a 28-day in vivo study in male and female Wistar rats. Scientific Reports, 16(1). https://doi.org/10.1038/s41598-026-35219-9

139. Niu, L. and Panyam, J. (2017). Freeze concentration-induced plga and polystyrene nanoparticle aggregation: imaging and rational design of lyoprotection. Journal of Controlled Release, 248, 125-132. https://doi.org/10.1016/j.jconrel.2017.01.019

140. Trenkenschuh, E. and Frieß, W. (2021). Freeze-drying of nanoparticles: how to overcome colloidal instability by formulation and process optimization. European Journal of Pharmaceutics and Biopharmaceutics, 165, 345-360. https://doi.org/10.1016/j.ejpb.2021.05.024

141. Ekladious, I., Colson, Y. L., & Grinstaff, M. W. (2018). Polymer–drug conjugate therapeutics: advances, insights and prospects. Nature Reviews Drug Discovery, 18(4), 273-294. https://doi.org/10.1038/s41573-018-0005-0

142. Danaei, M., Dehghankhold, M., Ataei, S., Davarani, F. H., Javanmard, R., Dokhani, A., … & Mozafari, M. R. (2018). Impact of particle size and polydispersity index on the clinical applications of lipidic nanocarrier systems. Pharmaceutics, 10(2), 57. https://doi.org/10.3390/pharmaceutics10020057

143. Foroozandeh, P. and Aziz, A. A. (2018). Insight into cellular uptake and intracellular trafficking of nanoparticles. Nanoscale Research Letters, 13(1). https://doi.org/10.1186/s11671-018-2728-6

Chapter 3. The synthesis of a Fucose-Conjugated Drug Delivery System

3.1. Introduction

The extremely low survival rate of late-stage pancreatic cancer patients highlights the limitations of current treatments and the urgent need for more effective solutions. To address this challenge, a drug conjugate containing fucose cell targeting unit is synthesised in this research with the overarching aim of precisely delivering therapeutic agents to pancreatic cancer cells. The research in this chapter utilises the PGA and CPT-Gly synthesised in chapter 2, incorporating them into a polymer that may act as a drug delivery system for pancreatic cancer treatment.

3.1.1. Introduction of Current Pancreatic Cancer and its Treatment

Pancreatic cancer is the most prevalent form of pancreatic cancer, comprising over 90% of all cases [1]. This highly aggressive and lethal malignancy originates from structural and functional mutations in the exocrine acini and duct cells of the pancreas [2]. Its average five-year survival rate remains below 10%, largely because fewer than 20% of patients are diagnosed at a localised, potentially curable stage due to the absence of clear, distinctive symptoms and reliable biomarkers for early detection [3,4].

Pancreatic cancer is classified using the tumour-node-metastasis system, which divides cases into three stages: resectable, locally advanced, and metastatic disease [3]. The prognosis varies starkly depending on the stage at diagnosis. Without active treatment, median survival is just 3-5 months for metastatic cases and 6-10 months for locally advanced disease [5]. Even with surgical resection, survival extends only to 11-15 months [5]. The tumour's location also influences outcomes. Approximately 65% of PDAC cases occur in the head of the pancreas, where symptoms like obstructive jaundice and pancreatitis may lead to earlier detection [6,7]. In contrast, tumours in the body (15%), tail (10%), or those that are multifocal (2%) tend to present later, correlating with a poorer prognosis [6,7].

Traditional treatment, including chemotherapy, surgery, and radiation, has yielded limited success in improving outcomes [8,9]. Even when surgical resection was performed at the earliest stages, the two-year survival rate is approximately 50% [8,9]. For advanced

pancreatic cancer, gemcitabine has been the standard first-line chemotherapy for more than two decades, though it offers only a modest extension of life expectancy as well as its combinations [9,10]. Combination therapies, such as FOLFIRINOX (a regimen of oxaliplatin, irinotecan, fluorouracil, and leucovorin), have shown slight improvements. In metastatic cases, FOLFIRINOX increases median survival from 6.8 months with gemcitabine alone to 11.1 months, and progression free time from 3.4 to 6.4 months [11]. Despite these advances, the overall impact remains limited, underscoring the critical need for more effective therapeutic strategies.

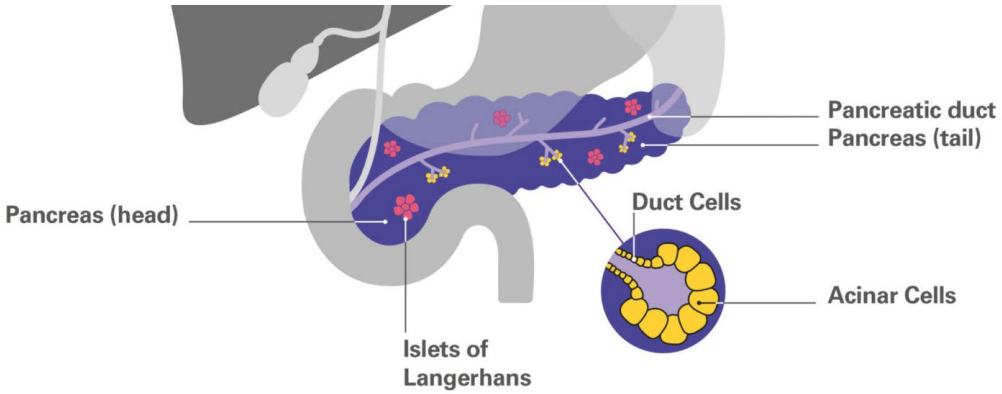

Figure 3.1-1. Anatomy of Pancreas Exocrine pancreas primarily composed of acinar cells and ductal cells. Acinar cells produce digestive enzymes and sodium bicarbonate, which are secreted into ducts and transported to the small intestine for the normal digestion[12]

3.1.2. Difficulties of Current Pancreatic Cancer Treatment

PDAC is a highly aggressive cancer notorious for its poor prognosis, a consequence of its intricate and multifactorial nature. Pancreatic cancer often evades early detection because it lacks simple diagnostic methods and distinctive symptoms in its initial stages [3,4,13]. Typically, symptoms only emerge after cancer has progressed and metastasised to distant sites, leaving fewer than 20% of patients with localised, potentially curable tumours at diagnosis [3,4,13]. This late presentation severely limits opportunities for timely intervention.

The unique TME of pancreatic cancer is marked by dense desmoplasia and extensive

immunosuppression. The TME is shaped by pancreatic stellate cells, fibroblasts, and various proteins that collectively form a formidable physical barrier around the tumour [14]. This barrier not only promotes tumour progression and invasion but also significantly impedes drug delivery [14,15,16,17]. Unlike other cancers with abundant vasculature, pancreatic cancer's desmoplastic stroma reduces stromal vascularisation, undermining conventional drug delivery strategies that rely on the EPR effect to passively target tumour cells [15, 16,17,18].

The difficulty in pancreatic cancer treatment is further heightened by its high genetic heterogeneity, which poses a significant obstacle to effective treatment [1,9]. Cell-targeting drug delivery systems depend on the overexpression of specific receptors for selective uptake, but the variable receptor expression across different tumour regions disrupts this process. For instance, the plasminogen activator receptor may be abundant in invasive tumour areas yet scarce in the tumour's core, leading to inconsistent uptake via receptor-mediated endocytosis and reducing the overall efficacy of targeted therapies [19,20,21].

Furthermore, this heterogeneity are key genetic mutations in genes such as KRAS, CDKN2A/p16, TP53, and SMAD4, each contributing to PDAC's resistance to chemotherapy [1,13,22]. KRAS mutations, found in 75-90% of cases, trigger a cascade of signals that rewire cell metabolism into a growth-promoting state, inhibit apoptosis, which diminishes the cytotoxic impact of chemotherapeutic agents [9,13,23]. The CDKN2A/p16 locus, inactivated in 80-95% of pancreatic cancer, allowing uncontrolled proliferation and enabling cancer cells to bypass DNA damage-induced checkpoints that would otherwise trigger apoptosis or senescence [27,28,29]. TP53, another critical tumour suppressor mutated in 50-74% of cases, its inactivation hinders the recognition of DNA damage and blocks cell cycle arrest, permits cells to proliferate despite genetic damage, driving tumour progression [30]. Similarly, SMAD4, dysregulated in over half of PDAC cases, its disruption associate with various aspects of cancer progression, encompassing autophagy, invasion and metastasis, disrupting DNA damage response and repair further fuelling cancer advancement and resistance [28,31,32]. Overall, around 60 mutations in 12 different signalling pathways accompany the development of aberrant ducts in pancreatic cancer [33]. These mutations are normally responsible for the correct development of the pancreas, are recognised as main contributors in cancer progression influencing its resistance to therapy and correlate

with poor prognosis [9]. Some of these may contribute to the specific resistance to chemotherapy in yet unidentified ways [13].

These mutations do not function independently. Together, they sustain survival signalling, disable apoptotic pathways, and accelerate tumour proliferation, giving rise to diverse subpopulations of cancer cells with varying treatment sensitivities. This genetic and environmental complexity creates a multifaceted barrier, making the development of effective therapeutic strategies for pancreatic cancer exceptionally challenging.

3.1.3. Adjuvant Therapy and Recurrence of Pancreatic Cancer

For patients with resectable pancreatic cancer, surgical resection remains the only potential curative option [34]. However, 60-80% of patients experience recurrence after resection and die of metastatic disease [35,36]. Adjuvant therapy significantly extends median survival to approximately two years [8,9,13,34], far surpassing the 10-15 months observed in those who undergo surgery alone without additional treatment [34,37]. This underscores the critical role of adjuvant therapy in post-operation management. Common chemotherapeutic agents include fluorouracil, gemcitabine, leucovorin, etc, or their combination were commonly used in postsurgical adjuvant treatment [35,36,38,39]. The optimal timing for initiating adjuvant therapy appears to be between 28 and 59 days after surgery showing the highest overall survival median compared to earlier (within 28 days) or later (beyond 59 days) starts [37]. Even in cases of postoperative complications or slow recovery leading to delayed treatment beyond 12 weeks, patients still derive survival benefits over surgery alone [37,40]. Given that resectable pancreatic cancer still accounts for 10-20% of cases [3,4], and surgery alone yields dismal outcomes [34]. Therefore, there is a need for further research into adjuvant therapies to optimise survival rates.

3.1.4. Introduction to Fucose Targeted Drug Delivery

Pancreatic cancer, especially in its advanced stages, poses significant treatment challenges, as evidenced by the limited survival rates associated with current therapies [8,9,10,11]. Approximately 80% of the patients with advanced stage of pancreatic cancer are treated

with gemcitabine, gemcitabine combined with Erlotinib, or FOLFIRINOX, yet these regimens result in median survival times of only 5.7 months, 6.8 months, and 11.1 months, respectively [9,10,11,41,42]. As discussed above, the disappointing outcomes stem in part from the pancreatic cancer's unique TME, which is marked by dense desmoplasia and reduced vascularisation creating a substantial obstacle to drug delivery, particularly for treatments that depend on the EPR effect to passively target tumour cells [14,15,16,17,18].

To overcome this issue, targeted drug delivery methods for anticancer drugs have been explored aiming to enhance the effectiveness of anticancer drugs while reducing side effects by delivering them directly to cancer cells [43]. Such methods capitalise on the differences in receptor expression between tumour and normal cells, enabling selective targeting of diseased cells [43] . Receptors like folate [44], integrins [45], and epidermal growth factor [46] have been widely utilised for this purpose. To achieve this specificity, various molecules—including saccharides [47], antibodies [48], vitamins [44], peptides,[49] etc., are conjugated to nanocarriers, allowing them to bind to receptors overexpressed on cancer cells [43]. This targeted strategy offers a promising alternative to overcome the barriers posed by pancreatic cancer's complex TME.

Among the potential targets, fucose stands out due to its significant role in cancer biology [43]. Fucose receptors are overexpressed in numerous cancers, including pancreatic [15], colon [50], breast [51], lung [52], thyroid [53], ovarian [54] and colorectal [55] cancers etc. In pancreatic cancer, nearly all patients exhibit abnormal secretion of fucosylated antigens such as Sialyl Lewis X-I and carbohydrate antigen-19-9 (CA19-9) which contains another glycan known as Sialyl Lewis A [56], which are detectable in both sera and tumour tissues [57,58,59,60,61]. For instance, CA19-9, in particular, is elevated in about 75% of patients and serves as a widely recognised tumour marker for pancreatic cancer detection [62,63]. This increase in fucosylation, driven by heightened expression of fucosyltransferases, enzymes that responsible for catalysing fucosylation [64], plays a critical role in processes like cell growth, adhesion, and metastasis [64]. This substantial demand for fucose in cancer cells, sourced from enzymatic synthesis from mannose [65] and or extracellular and lysosomal free fucose through pathway like endocytosis [66], further highlights its relevance as a therapeutic target[57,59].

Therefore, the present study developed a fucose-bound drug conjugate to deliver CPT to pancreatic cancer cells through fucose receptor-mediated endocytosis [15]. This approach seeks to improve treatment precision and efficacy, offering a potential solution to overcome the formidable biological barrier of pancreatic cancer TME.

3.1.5. Mechanism of Receptor-Mediated Endocytosis Drug Delivery

NPs can enter cells through various mechanisms, such as simple diffusion driven by concentration gradients and translocation, which are energy-independent processes [67]. However, pancreatic cancer is marked by dense desmoplasia and hypovascularity within the TME [14,16,17], receptor- mediated endocytosis stands out as the preferred method for delivering therapeutic agents [15,43]. This process involves a ligand, which is fucose-bound NPs in this study, binding to a specific receptor on the cell surface triggering a conformational change prompting the plasma membrane to invaginate and form an intracellular compartment called clathrin- coated vesicle [68,69,70]. These clathrin vesicles are limited in size, typically accommodating NPs size up to 150 nm with a maximum of size of 200 nm [71]; larger NPs are mainly internalised through alternative pathways like micropinocytosis or phagocytosis [71].

Later, the clathrin-coated vesicles shed their clathrin coating and merge to create early endosomes then mature into late endosomes, which eventually fuse with lysosomes [72,73]. Within the mildly acidic environment of the late endosome (pH 6.2-6.4), receptors and their bound ligands are sorted, and their subsequent fates define the receptor classification [22,74]. Receptor- mediated endocytosis is classified into four major pathways based for the final destination of both receptor and ligand [75,76,77,78]. Although fucose receptors are less extensively studied [79], their binding behaviour and affinity for sugars like mannose and N-acetylglucosamine suggest they align with class I receptors similar to other sugar-binding receptors [79,80,81]. After endocytosis class I receptors are recycled back to the plasma membrane, while their ligands dissociate and are degraded in the lysosome [22].

3.1.6. Use of Chemotherapeutic Agents in Pancreatic Cancer treatment

3.1.6.1. Gemcitabine

Gemcitabine (difluorodeoxycytidine) is a deoxycytidine analogue having a broad spectrum of antitumor activity [82]. Once inside cells, it undergoes phosphorylation to form diphosphate and triphosphate derivatives, which drives its dual inhibitory mechanisms. difluorodeoxycytidine diphosphate strongly inhibits ribonucleotide reductase, thereby blocking the conversion of ribonucleotides to deoxyribonucleotides [83]. Meanwhile, difluorodeoxycytidine triphosphate competes with deoxycytidine triphosphate for integration into elongating DNA strands, causing DNA polymerase to halt at the incorporation site [83]. Since a 1997 study demonstrated gemcitabine's superiority over fluorouracil in terms of overall survival, performance status, and pain management, it has emerged as the standard therapy for locally advanced and metastatic pancreatic cancer [10,42]. Subsequent trials combining gemcitabine with newer chemotherapeutics such as fluorouracil [84], irinotecan [85], oxaliplatin [86], pemetrexed [87] and exatecan mesylate [88], etc. have yielded only marginal or negligible improvements in survival compared to gemcitabine monotherapy.

For patients with advanced disease, treatment with gemcitabine alone typically results in a median survival of just 5.6 to 6.8 months [10,11]. This limited efficacy not only attributed from the poor drug penetration into the hypo-vascularised, dense tumour stroma as mentioned above [14,15,16,17]. But also, because the rapid development of gemcitabine chemoresistance often within weeks of treatment initiation [89].

Cancer cells develop resistance through three primary pathways. First, reduced expression of transporters impairs the uptake of water-soluble drugs, including nucleoside analogues like gemcitabine [90]; for instance, downregulation of nucleoside transporters directly limits gemcitabine entry [91,92,93]. Second, genetic alterations diminish drug sensitivity by disrupting cell cycle regulation, enhancing DNA repair, or inhibiting apoptosis [1,13,22,90] for example, downregulation of deoxycytidine kinase which is essential for initial activation of gemcitabine [83,94,95] and the upregulation of ribonucleotide reductase which counteract the inhibition effect of gemcitabine [83,96]. Third, upregulation of ABC transporters that facilitates the energy-dependent efflux of various hydrophobic drugs [90].

Among these, Pgp provides the strongest resistance to widest variety of compounds contributing the most in drug resistance across many cancer cell lines [90,97]. Although gemcitabine is not a substrate of ABC transporters, its deaminated metabolite dFdU is effluxed by these transporters enabling continuous deamination of gemcitabine [98]. Inhibition of ABC transporters result in intracellular accumulation of dFdU, thereby blocking deamination boosting gemcitabine levels and cytotoxicity, and improve sensitivity of gemcitabine in gemcitabine-resistant cell [98,99].

3.1.6.2. FOLFIRINOX

FOLFIRINOX, a combination chemotherapy regimen comprising oxaliplatin, irinotecan, fluorouracil, and leucovorin, offers significant improvements over gemcitabine monotherapy for advanced pancreatic cancer. Compared to gemcitabine's median overall survival of 6.8 months and progression-free survival of 3.3 months, FOLFIRINOX extends these to 11.1 months and 6.4 months, respectively [41].

While individual components fluorouracil [84], irinotecan [85] or oxaliplatin [86] fail to enhance survival when used alone or paired with gemcitabine, their combination in FOLFIRINOX produces a synergistic effect through their distinct mechanisms. Irinotecan, an analogue of CPT and a potent top-I inhibitor, arrest cells at S-phase by stabilising top- I- DNA complexes or the DNA double-strand breaks that accumulate as replication forks collide with these complexes [100]. Fluorouracil, which targets DNA synthesis and repair primarily in the S-phase [101], achieves greater cytotoxicity when administered after irinotecan, with leucovorin enhancing its efficacy [100,102,103]. Oxaliplatin further amplifies this effect by potentiating irinotecan-induced S-phase arrest [104], creating conditions that enhance the impact of subsequent S-phase-targeting agents like fluorouracil [100,102,103]. Additionally, oxaliplatin synergises with fluorouracil, improving overall survival compared to either of them [105].

The non-overlapping toxicity profiles among fluorouracil, leucovorin, irinotecan, and oxaliplatin, allow FOLFIRINOX to deliver a broad spectra of antitumor activity, with each component enhancing the others through different mechanisms of action to promote cancer cell apoptosis [41,102,104].

However, better clinical outcomes of FOLFIRINOX also comes with higher toxicity, including a higher incidence of grade 3 or 4 adverse events compared to gemcitabine [41]. As a result, FOLFIRINOX is preferred treatment for patients with metastatic pancreatic cancer who have a good performance status [41].

In this research, only camptothecin, analogue of irinotecan, is incorporated into the polymeric drug conjugate produced. Not only because its highly hydrophobicity which could again be induced as the hydrophobic moiety in the drug conjugate promoting nanoprecipitation and its facile prodrug- CPT-Gly synthesis, but also greatly reduced the difficulties in characterisation in ^{1}H-NMR due to peak overlap from other therapeutics.

3.2. Experimental

3.2.1. Modification of L-fucose

3.2.1.1. Conversion of Fucose to Tetra-O-Acetyl-Fucose

L-Fucose (1.0 g, 6.1 mmol, 1.0 eqv) and acetic anhydride (5.7 mL, 61 mmol, 10.0 eqv) were combined in 10.0 mL of glacial acetic acid. Then, 0.2 mL of concentrated H_2SO_4 was added to the mixture. The reaction was stirred at room temperature for three hours. After completion, 100.0 mL of DCM was added, and the mixture was washed twice with 20.0 mL of water, followed by three washes with saturated Na_2HCO_3 solution (20.0 mL each). The organic layer was dried over anhydrous $MgSO_4$, and the solvent was removed under vacuum. Yield: 74%.

^{1}H-NMR spectrum (400 MHz, $CDCl_3$) of Tetra-O-Acetyl-Fucose: 6.33-3.95 ppm (-O-CH-), 2.17-1.99 ppm (-C=O-CH_3), 1.30-1.14 ppm (-O-CH-C**H$_3$**) (Figure 3.3-2) [106]

3.2.1.2. Regioselective Anomeric Deacetylation of fucose

Tetra-O-Acetyl-fucose (1.0 g, 3.0 mmol, 1.0 eqv, 0.3 M) was dissolved in 10.0 mL of anhydrous THF, and benzylamine (0.493 mL, 4.5 mmol, 1.5 eqv) was added. The reaction was stirred at room temperature overnight. After completion, the solvent was evaporated under vacuum, and the product was purified by column chromatography (DCM: Acetone 9:1).

Yield: 68%.

^{1}H-NMR spectrum (400 MHz, $CDCl_3$) of 3,4,5-Tri-O-acetyl-fucose: 5.48 -4.41 ppm (-O-CH-), 2.17 ppm (-C=O-CH_3), 2.10 ppm (-C=O-CH_3), 2.00 ppm (-C=O-CH_3), 1.31-1.15 ppm (-O-CH-C**H$_3$**) (Figure 3.3-4) [106, 107].

3.2.1.3. Synthesis of 2-(3-((tert-butoxycarbonyl)amino)propoxy)-6-methyltetrahydro-2H-pyran-3,4,5-triyl triacetate

3,4,5-Tri-O-acetyl-fucose (0.5 g, 1.7 mmol, 1.0 eqv, 0.1 M), anhydrous K_2CO_3 (0.95 g, 6.9 mmol, 4.0 eqv), and 3-(Boc-amino)propyl bromide (0.82 g, 3.4 mmol, 2.0 eqv) were added to a RB flask and purged with nitrogen for 15 minutes three times. Next, 17.0 mL of anhydrous DMF was added. The reaction mixture was stirred under nitrogen at room temperature for two days. Afterward, the solvent was evaporated under nitrogen flow at room temperature, and the product was purified by column chromatography (eluent: Ethyl Acetate: Hexane 2:8, then gradually switched to Ethyl Acetate: Hexane 3:7). The purified product was stored in its Boc-protected form to prevent deacetylation by the free amino group. Yield: 47%.

^{1}H-NMR spectrum (400 MHz, $CDCl_3$) of 2-(3-((tert-butoxycarbonyl)amino)propoxy)-6-methyltetrahydro-2H-pyran-3,4,5-triyl triacetate: 5.36-5.03 ppm (-O-CH-), 4.83 ppm (-NH_2-), 4.15 ppm (-O-CH-), 3.81-3.19 ppm (-O-C**H$_2$**-CH_2-, -CH_2-C**H$_2$**-NH-), 2.17- 1.98 ppm (-C=O-CH_3), 1.78 ppm (-CH_2-C**H$_2$**-CH_2-), 1.43 ppm (-O-C-(C**H$_3$**)$_3$), 1.15 ppm (-O-CH-C**H$_3$**) (Figure 3.3-6).

^{13}C-NMR spectrum (100 MHz, $CDCl_3$): 96.28 ppm (-O-CH-O-), 71.05 ppm (-O-CH-), 68.01 ppm (-O-CH-,-O-CH-), 67.05 ppm (-O-C**H$_2$**-CH_2-), 64.39 ppm (-O-CH-), 38.30 ppm (-CH_2-C**H$_2$**-NH-), 29.49 ppm (-CH_2-C**H$_2$**-CH_2-), 28.31 ppm (-O-C-(C**H$_3$**)$_3$), 20.57 ppm (-O-C-(C**H$_3$)$_3$**), 15.81 ppm (-O-CH-C**H$_3$**)

3.2.2. Synthesis of F-PSar$_{35}$

Sar-NCA(2.0 g, 17.4 mmol, 35.0 eqv) was placed in a Schlenk tube and purged with nitrogen three times. Separately, 2-(3-((tert-butoxycarbonyl)amino)propoxy)-6-methyltetrahydro-2H-pyran-3,4,5-triyl triacetate (222.2 mg, 0.50 mmol, 1.0 eqv) was dissolved in a mixture of 1.0

mL DCM and 1.0 mL TFA. This solution was stirred at room temperature in open air for 30 minutes to remove N-Boc protecting group, the end point of deprotection was tracked by TLC, then dried under nitrogen flow.

The deprotected 2-(3-((tert-butoxycarbonyl)amino)propoxy)-6-methyltetrahydro-2H-pyran-3,4,5-triyl triacetate was dissolved in anhydrous DMF along with DIPEA (0.21 mL, 1.2 mmol, 5.0 eqv), and the mixture was added to the Schlenk tube containing Sar-NCA. The reaction was stirred overnight under nitrogen bubbling at 0°C in an ice bath.

The completion of polymerisation was confirmed with ^{1}H-NMR and the crude F-Psar$_{35}$ product was precipitated in diethyl ether, followed by centrifugation. The product was washed with diethyl ether three times and dried under vacuum to yield the final fucosylated PSar. Yield: 99%

^{1}H-NMR spectrum (500 MHz, DMSO-d$_6$) of F-PSar: 5.31-4.87 ppm (-O-CH-), 4.37-3.92 ppm (-C=O-CH$_2$-), 2.98-2.72pm (-N(CH$_3$)-), 2.13- 1.91 ppm (-C=O-CH$_3$) (Figure *3.3-9*)

3.2.3. Synthesis of Fucose incorporated Drug Conjugate - PGA-[(Gly-CPT)-*co*-(F-PSar)] Conjugate

PGA (10.0 mg, 0.078 mmol, 1.0 eqv), EDC.HCl (45 mg, 0.23 mmol, 3.0 eqv) and NHS (27 mg, 1.45 mmol, 3.0 eqv) were added into Schlenk tube. Purged with nitrogen for 15 minutes three times before addition of 1.0 mL of anhydrous DMF. The reaction mixture was allowed to stir for an hour in ice bath to activate the carboxylate group, then F-PSar (18.0 mg, 0.0067 mmol, 0.087 eqv), CPT-Gly (14.0 mg, 0.034 mmol, 0.44 eqv) in 1.0 mL of anhydrous DMF were added into the reaction mixture. The reaction mixture was allowed to warm to room temperature while kept stirring for two days. The crude product was dialysed against methanol overnight then in DI water for two days then freeze dried. Yield: 63%.

^{1}H-NMR spectrum (500 MHz, DMSO-d$_6$) of Acetyl protected PGA-[(CPT-Gly)-*co*-(F-PSar)] drug conjugate: 88.70-7.11 ppm (=C-CH= (CPT),-NH), 5.50-4.92 ppm (-N-CH$_2$-C- (CPT), -O-CH$_2$-C- (CPT), -O-CH- (Fucose)), 4.34- 3.92 ppm(-NH-C**H**-C=O- (PGA), -N(CH$_3$)-C**H$_2$**- (PSar), -O-CH- (Fucose)), 2.92-2.73 ppm (-N(CH$_3$)- (PSar), 2.31-1.66 ppm (-C**H**$_2$-C**H**$_2$- (PGA), -C=O-CH$_3$ (Fucose)) (Figure 3.3-14)

3.2.3.1. Deprotection of O-Acetyl group on PGA-[(Gly-CPT)-co-(F-PSar)] Conjugate

The synthesised drug conjugate was dissolved in 1.0 mL of a DMF/benzylamine mixture (4:1, v/v) and stir in ice bath and allowed to warm to room temperature overnight. The resulting deprotected conjugate was then precipitated using a 1:1 (v/v) diethyl ether/hexane mixture, followed by four successive washes with diethyl ether to ensure purity. Finally, the purified product was dried under vacuum to remove any residual solvents. Yield: 99%

^{1}H-NMR spectrum (500 MHz, DMSO-d_6) of PGA-[(CPT-Gly)-*co*-(F-PSar)] drug conjugate: 8.71-7.13 ppm (=C-CH= (CPT),-NH), 6.66-6.20 ppm (-CH-O**H** (Fucose), 5.47-5.28 ppm (-N-CH_2-C- (CPT), -O-CH_2-C- (CPT), -O-CH- (Fucose))), 4.34- 3.93 ppm(-NH-C**H**-C=O- (PGA), -N(CH_3)-C**H_2**- (PSar), -O-CH- (Fucose)), 2.93-2.72 ppm (-N(CH_3)- (PSar)), 2.26-1.96 ppm (-C**H_2**-C**H_2**- (PGA)), 1.47-1.23 ppm (-CH_2-C**H_3** (CPT), initiator, -O-C-CH_3 (fucose)) (Figure 3.3-16).

3.3. Results and Discussion

Building on the successful synthesis of PGA and PSar in Chapter 2, these polymers were conjugated with CPT-Gly to form two distinct polymeric drug conjugates: PGA-[(CPT-Gly)-*co*-(PSar)] (Figure 2.3-25)and PGA-(CPT-Gly) (Figure 2.3-22). Comparative studies demonstrated that incorporation of PSar significantly enhanced NP size uniformity and colloidal stability, establishing a promising platform for improved CPT delivery.

Leveraging these insights, fucose-modified PSar was produced, leading to the synthesis of PGA-[(CPT-Gly)-*co*-(F-PSar)], a conjugate designed for fucose-mediated cell targeting. The synthesis of F-PSar commenced with full acetylation of fucose's hydroxy groups for protection, followed by selective deprotection of the anomeric position to expose a single hydroxy group. This was then functionalised with a protected primary amine, which served as an initiator for the ROP of Sar-NCA, forming F-PSar. The terminal amine on F-PSar was subsequently conjugated to the PGA backbone alongside CPT-Gly, producing the advanced drug conjugate PGA-[(CPT-Gly)-*co*-(F-PSar)]. This design not only enables fucose-mediated recognition of overexpressed receptors on pancreatic cancer cells but also mitigates the burst release commonly associated with physical drug encapsulation approaches.

The behaviour of the drug conjugates during nanoprecipitation, along with their stability in a

pH 7.4 PBS solution, was assessed using DLS analysis. Then the CPT releasing study of PGA-[(CPT-Gly)-*co*-(F-PSar)] was carried out in both pH 7.4 PBS solution and pH 5.0 acetic buffer solution at 37°C simulating physiological and endosomal/lysosomal environments, respectively.

3.3.1. Synthesis of F-PSar

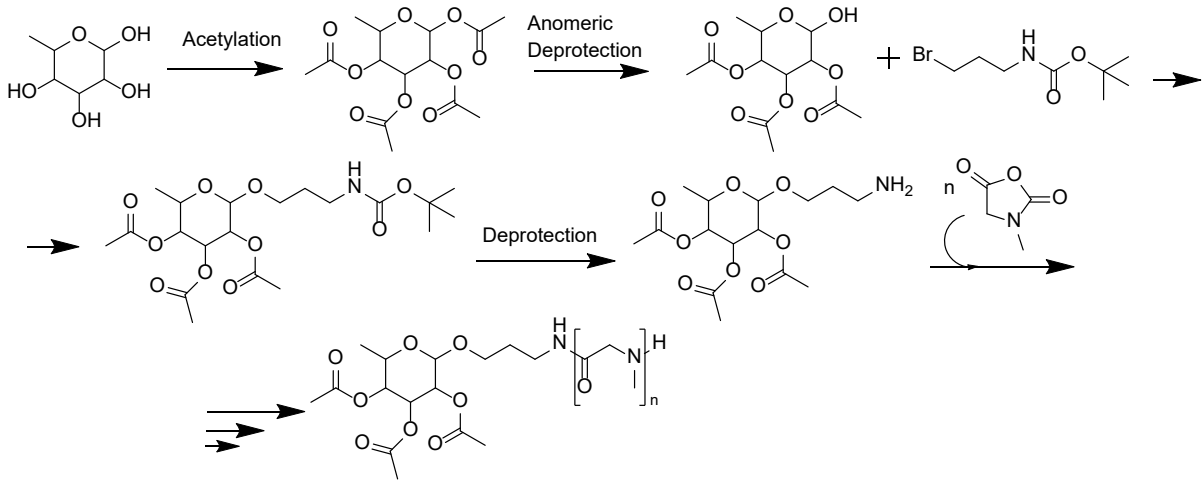

Scheme 3.3-1. Overall reaction scheme F-PSar, from acetyl protection of fucose to the ROP of Sar-NCA

3.3.1.1. Synthesis of Acetylation of Fucose

To synthesise fucose-conjugated PSar (F-PSar) as the hydrophilic block and cell directing group of the drug conjugate. Fucose needs to be the outer most point of the NPs formed to ensure its interaction with the fucose receptor on the pancreatic tumour cells. Therefore, fucose must be linked to a water-soluble moiety of the drug conjugate, namely PGA backbone or PSar. Because the PGA backbone will be conjugated with CPT-Gly, conjugation to PSar was deemed more suitable to ensure that fucose-presenting NPs are formed. This is perhaps emphasised by the fact that in the drug conjugate, PSar is less hindered than PGA, enhancing fucose accessibility to cell receptors.

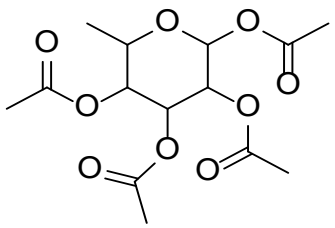

Figure 3.3-1. Tetra-O-Acetyl-Fucose

To ensure that fucose resides at the terminus of PSar, whilst PSar retains secondary amine functionality, fucose was required to be modified to initiate Sar-NCA ROP. To prevent side reactions, the hydroxy groups of fucose were protected via acetylation with acetic anhydride in glacial acetic acid catalysed by H_2SO_4 (Figure 3.3-1). The successful protection is confirmed by ^{1}H-NMR spectroscopy with the distinct acetyl peaks appearing from 2.17-1.99 ppm as 12 protons as indicated by integration, which corresponds to the four acetyl group (Figure 3.3-2) and is consistent the literature [106]. Acetyl acetate was co-eluted with the product which appears to be the main impurity in the reaction as shown in the ^{1}H-NMR spectrum at around 2.20 ppm (Figure 3.3-2).

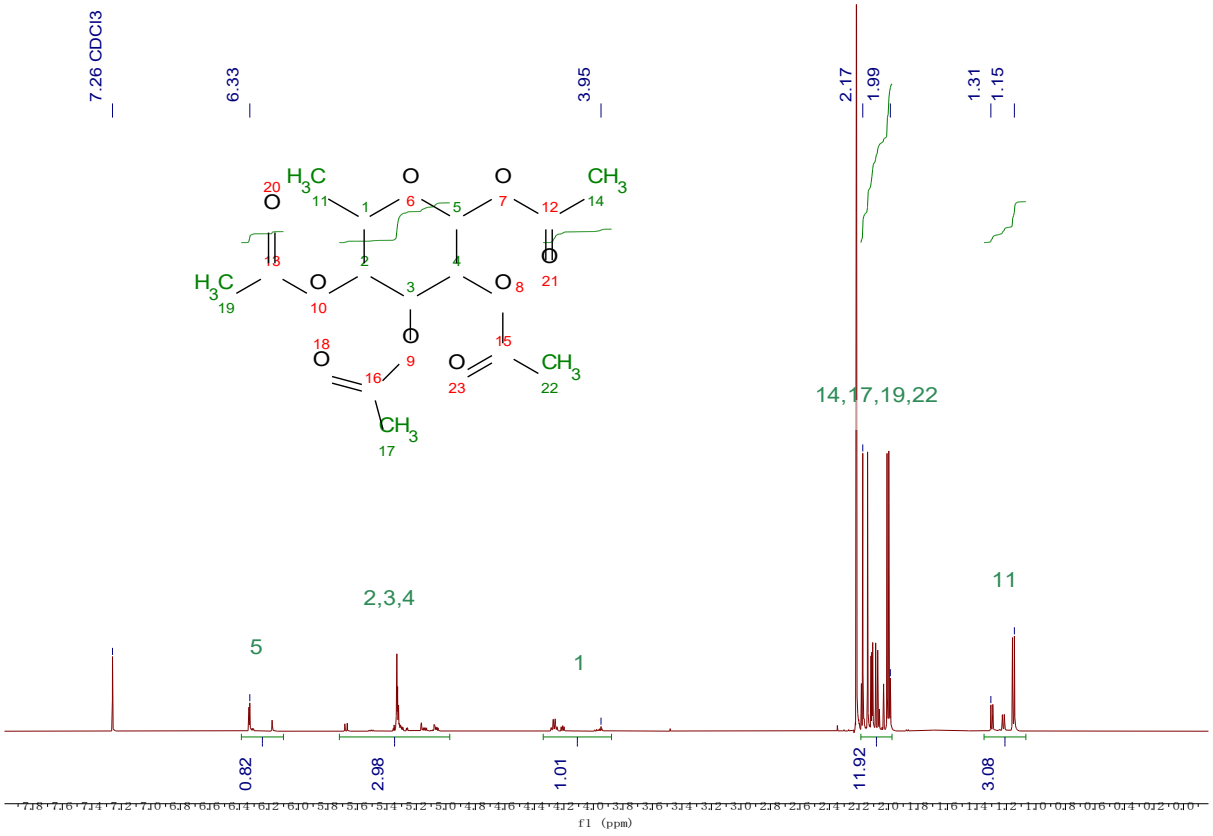

Figure 3.3-2. ^{1}H-NMR spectrum (400 MHz, $CDCl_3$) of Tetra-O-Acetyl-Fucose: 6.33-3.95 ppm (-O-CH-), 2.17-1.99 ppm (-C=O-CH_3), 1.31-1.15 ppm (-O-CH-C**H$_3$**) (Figure 3.3-2) [106]

3.3.1.2. Anomeric O-Acetyl Deprotection

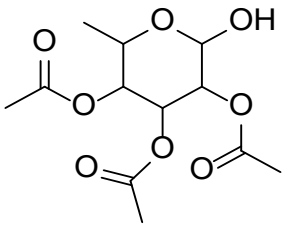

Figure 3.3-3. 3,4,5-Tri-O-acetyl-fucose

The anomeric acetyl group was then selectively removed by addition of 1.5 equivalence of benzylamine in DMF leading to tetra-O-Acetyl-Fucose in DMF which was subsequently purified by column chromatography (Figure 3.3-3). The disappearance of one of the O-acetyl peaks at around 2.0 ppm indicates the deprotection of anomeric acetyl group (Figure 3.3-4)

[106, 107].

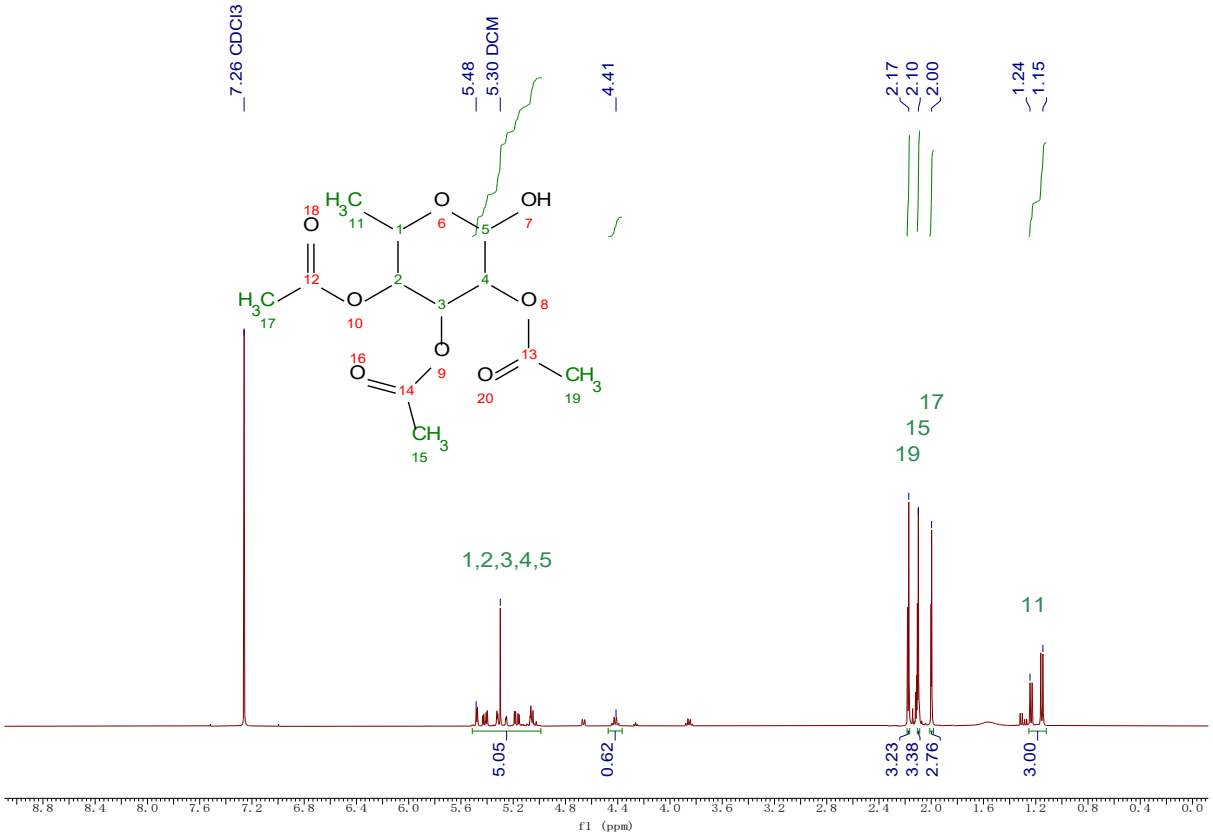

Figure 3.3-4. ^{1}H-NMR spectrum (400 MHz, $CDCl_3$) of 2,3,4-Tri-O-acetyl-fucose: 5.48 -4.41 ppm (-O-CH-), 2.17 ppm (-C=O-CH_3), 2.10 ppm (-C=O-CH_3), 2.00 ppm (-C=O-CH_3), 1.24-1.15 ppm (-O-CH-C**H$_3$**) [106, 107].

3.3.1.3. Synthesis of 2-(3-((tert-butoxycarbonyl)amino)propoxy)-6-methyltetrahydro-2H-pyran-3,4,5-triyl triacetate

After deacetylation of the anomeric hydroxy group, the product was used as a nucleophile to substitute the bromide of 3-(Boc-amino) propyl bromide generating the target compound, with K_2CO_3 to neutralise the acid (Figure 3.3-5). Which can be used to initiate the NCA ROP after Boc group deprotection generating 2-(3-aminopropoxy)-6-methyltetrahydro-2H-pyran-3,4,5-triyl triacetate revealing the amino- group.

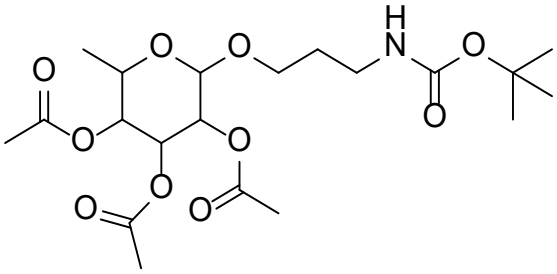

Figure 3.3-5. 2-(3-((tert-butoxycarbonyl)amino)propoxy)-6-methyltetrahydro-2H-pyran-3,4,5-triyl triacetate

The product was characterised by ^{1}H-NMR spectroscopy: the peak at 1.43 ppm represents the 9 protons of N-Boc group. The 3 distinct acetyl peaks appear at 2.17 ppm, 2.09 ppm and 1.98 ppm respectively (Figure 3.3-6).

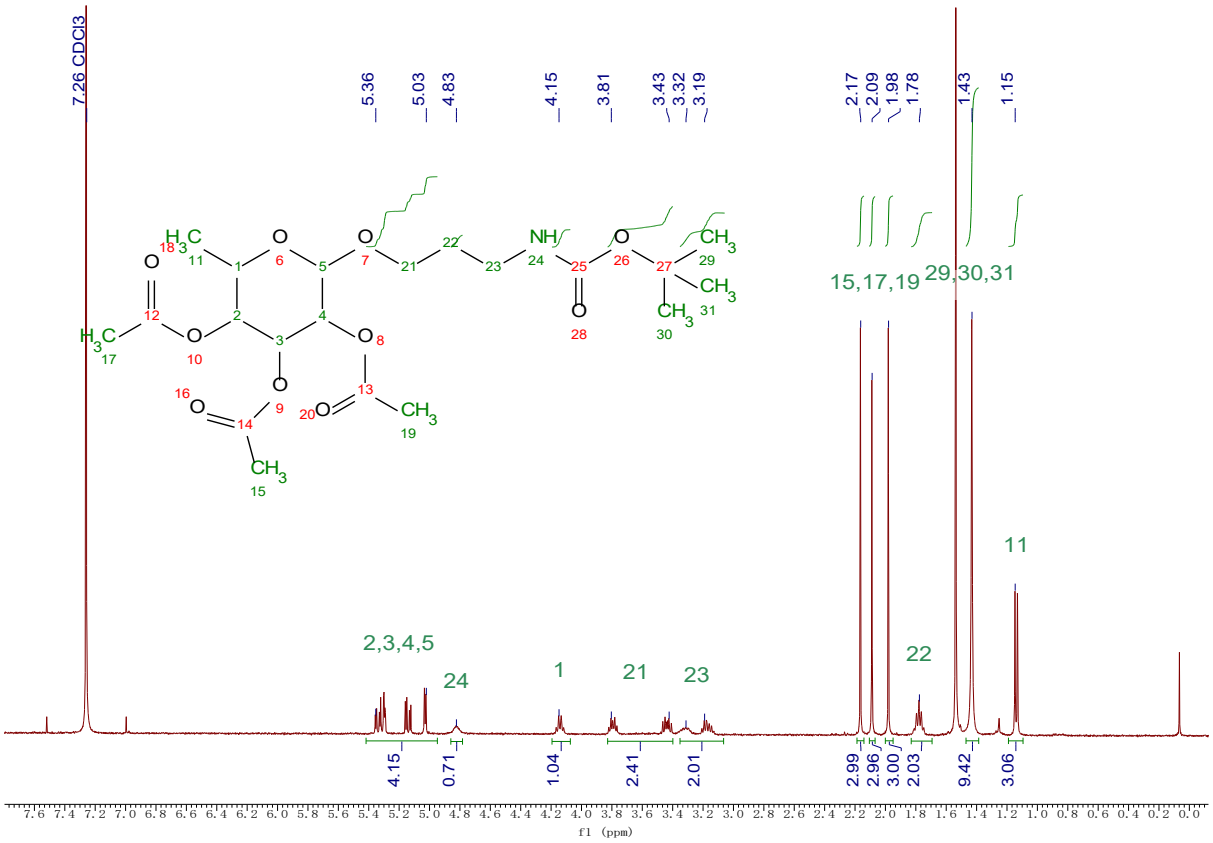

Figure 3.3-6. ^{1}H-NMR spectrum (400 MHz, $CDCl_3$) of 2-(3-((tert-butoxycarbonyl)amino)propoxy)-6-methyltetrahydro-2H-pyran-3,4,5-triyl triacetate: 5.36-5.03 ppm (-O-CH-), 4.83 ppm (-NH_2-), 4.15 ppm (-O-CH-), 3.81-3.19 ppm (-O-C**H$_2$**-CH_2, -CH_2-C**H$_2$**-NH-), 2.17- 1.98 ppm (-C=O-CH_3), 1.78 ppm (-CH_2-C**H$_2$**-CH_2-), 1.43 ppm (-O-C-(C**H$_3$**)$_3$), 1.15 ppm (-O-CH-C**H$_3$**)

The product was further confirmed by Distortionless Enhancement by Polarization Transfer (DEPT-135) to distinguish -**C**H, -**C**H_2, and -**C**H_3 fragments. Peaks at 96.28, 71.05, 68.01 and 64.39 ppm were assigned to the carbons of the six-membered fucose ring, while peaks at 67.05, 38.30 and 29.49 ppm correspond to the propyl carbon chain from 3-(Boc-amino)propyl bromide. The peak at 28.31 ppm is attributed to the three methyl carbons of the Boc protecting group, while the signal at 15.81 ppm corresponds to the methyl carbon of fucose. But due to the nature of DEPT-135, quaternary carbons are not shown in the spectrum which should be addressed with ^{13}C NMR (Figure 3.3-7).

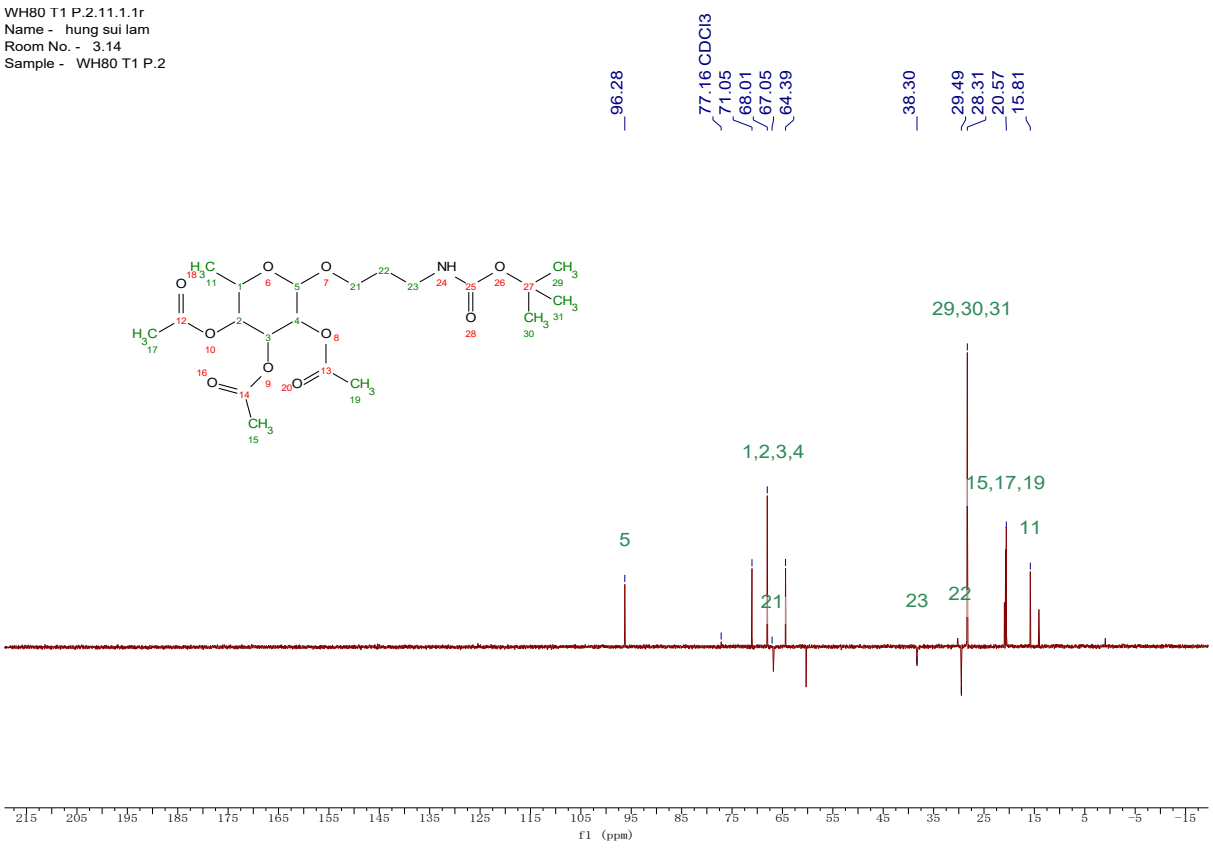

Figure 3.3-7. DEPT135 spectrum (100 MHz, $CDCl_3$): 96.28 ppm (-O-CH-O-), 71.05 ppm (-O-CH-), 68.01 ppm (-O-CH-,-O-CH-), 67.05 ppm (-O-C**H$_2$**-CH_2-), 64.39 ppm (-O-CH-), 38.30 ppm (-CH_2-C**H$_2$**-NH-), 29.49 ppm (-CH_2-C**H$_2$**-CH_2-), 28.31 ppm (-O-C-(C**H$_3$**)$_3$), 20.57 ppm (-O-C-(C**H$_3$**)**$_3$**), 15.81 ppm (-O-CH-C**H$_3$**)

These NMR signals are consistent with the expected structure of the modified fucose, and the absence of additional peaks indicates that a pure product was obtained. This is important for subsequent ROP of Sar- NCA, as impurities can initiate uncontrolled polymerisation.

3.3.1.4. ROP of Sar-NCA Initiated by 2-(3-aminopropoxy)-6-methyltetrahydro-2H-pyran-3,4,5-triyl triacetate

To synthesise fucose-modified polysarcosine (F-PSar) (Figure 3.3-8), careful control of reaction conditions was necessary to prevent unwanted side reactions. The N-Boc protecting group was cleaved immediately prior to the ROP of Sar-NCA with 1:1 TFA: DCM solution, as the O-acetyl group on fucose can be removed by reaction with a primary amine. The end point of the deprotection was determined by TLC. To ensure successful polymerisation, excess DIPEA was added to the reaction mixture to neutralise residual TFA from the deprotection step ensuring the initiation. Till this stage F-PSar is made (Scheme 3.3-1). To prevent the deacetylation by the free secondary amine end group of PSar, the reaction was conducted in an ice bath with nitrogen bubbling through the reaction solution to increase the rate of polymerisation [108].

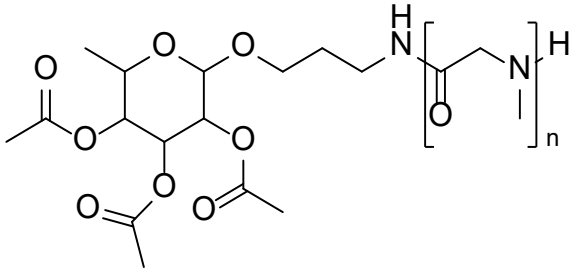

Figure 3.3-8. The chemical structure of *F-PSar*

The resulting F-PSar structure was confirmed using ^{1}H-NMR spectroscopy. The spectrum displayed characteristic peaks at 2.13-1.91 ppm for the acetyl groups of fucose, 2.98-2.73 ppm for the methyl group of PSar, 4.37-3.92 ppm for the two protons of the PSar backbone, and 5.31-4.87 ppm for the five protons of fucose. (Figure 3.3-9). Through integration of the

^{1}H-NMR spectrum, the degree of polymerisation was calculated to be approximately 103 repeating units (Figure 3.3-9).

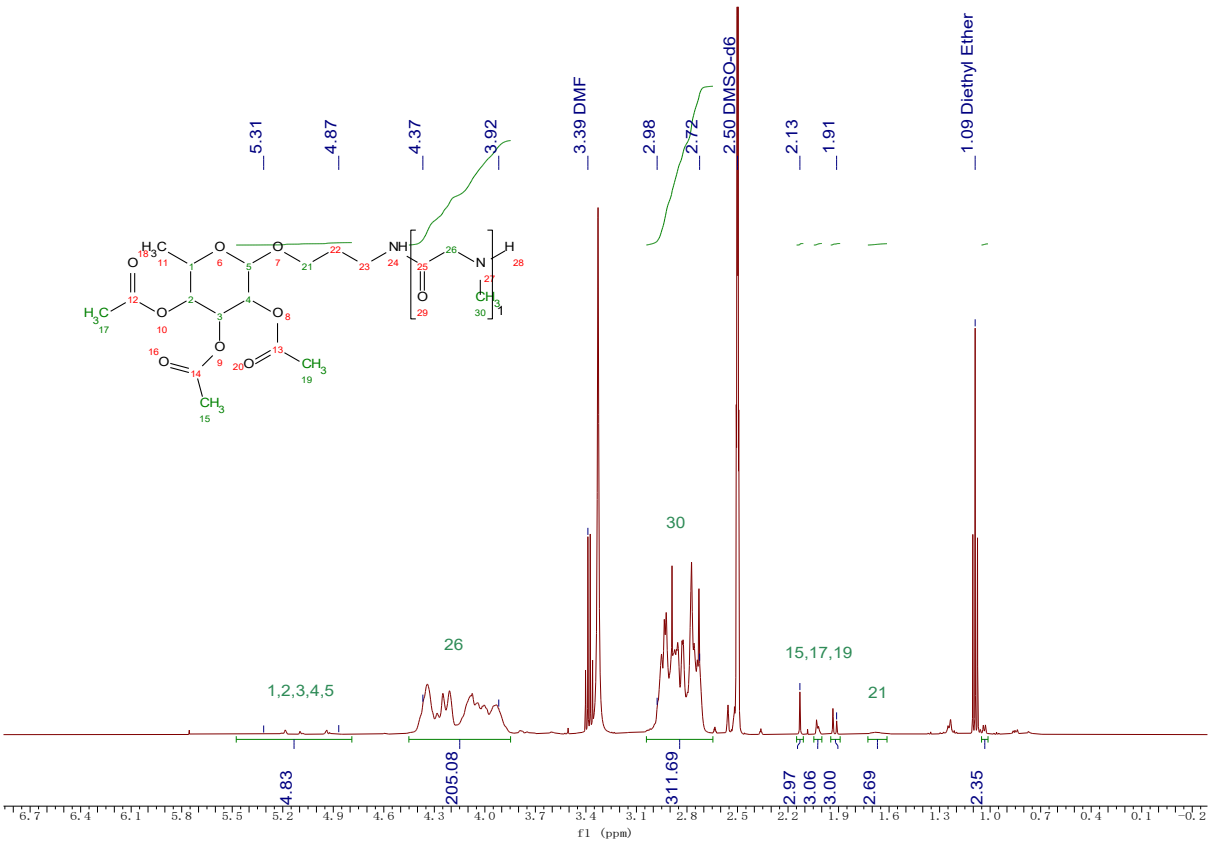

Figure 3.3-9. ^{1}H-NMR spectrum (500 MHz, DMSO-d_6) of F-PSar: 5.31-4.87 ppm (-O-CH-), 4.37-3.92 ppm (-C=O-CH_2-), 2.98-2.72pm (-N(CH_3)-), 2.13- 1.91 ppm (-C=O-CH_3)

3.3.1.5. MALDI-TOF mass spectrometry Analysis of F-PSar

The molecular weight of the synthesised F-PSar was determined by MALDI- TOF mass spectrometry. Its M_n and M_w were calculated through the below equations

$$Mn = \frac{\sum Ni*Mi}{\sum Ni} = \; Mn = \frac{44*1968.61+62*2039.05+\cdots+10*3600.20+5*3671.20}{44+62+\cdots+10+5} = 2697.46$$

Where *Ni* is the number of molecules or the intensity of percentage with molecular weight *Mi*.

$$Mw = \frac{\sum Ni*Mi^2}{\sum Ni*Mi} = \; Mw = \frac{44*1968.61^2+62*2039.05^2+\cdots+10*3600.20^2+5*3671.20^2}{44*1968.61+62*2039.05+\cdots+10*3600.20+5*3671.20} = 2770.51$$

The dispersity of the polymer $=\frac{Mw}{Mn} = \frac{2770.51}{2697.46} = 1.027\ Đ_M$ (Figure 3.3-10). However, the degree of polymerisation, calculated as 33 repeat units based on MALDI data, was only one-third of that estimated from ^{1}H-NMR integration. This discrepancy suggests that some Sar-NCA may have been initiated by impurities, such as moisture, present in the reaction mixture. Or the deprotection of N-Boc group was not completed with some of the fucose initiator successful initiate the Sar-NCA which resulted in the integration error in ^{1}H-NMR spectrum.

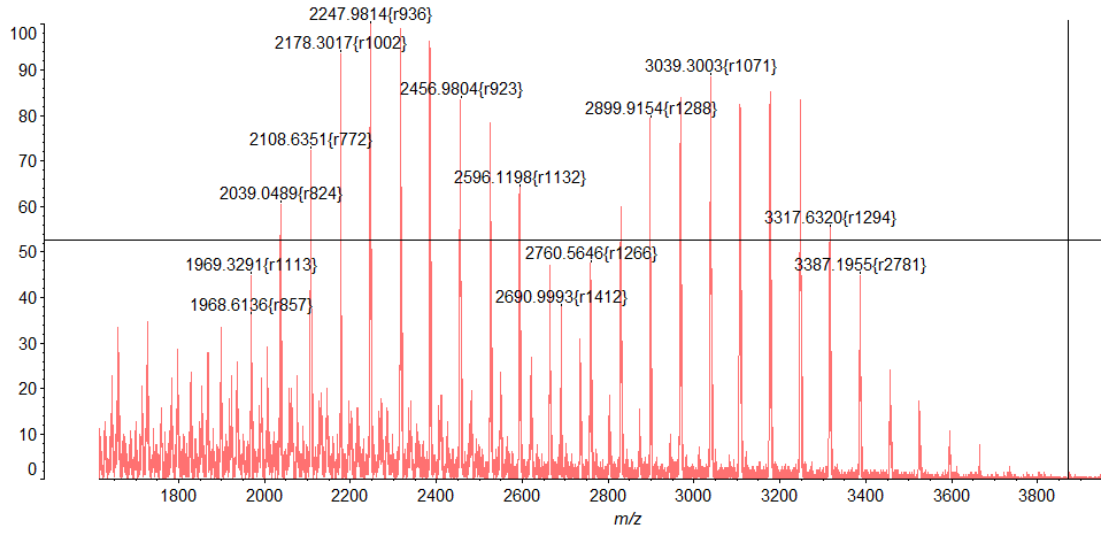

Figure 3.3-10. MALDI-TOF mass spectrometry analysis data of F-PSar: Number-average molecular weight (M_n)=2697.46; Weight-average molecular weight (M_w)= 2770.51. The dispersity of the polymer = 1.027 $Đ_M$.

By subtracting the molecular weight of the detected peaks from that of the PSar repeating units, multiple molecular weights corresponding to fragmented fucose initiators (e.g., 331, 260, and 188) were identified in approximately half of the observed peaks (Table 3.3-1). This result confirms that about half of the PSar chains were started by the fucose initiator, while the remaining chains were initiated by impurities. This mixed initiation led to the bimodal molecular weight distributions observed in the MALDI spectra, spanning 1968–2690 Da and 2760–3387 Da.

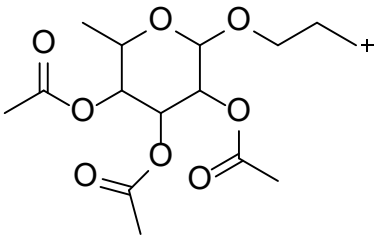	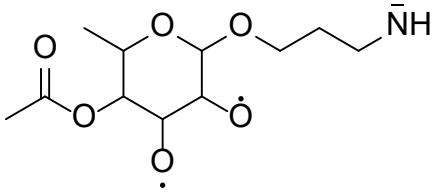	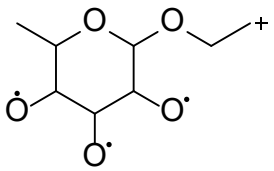
MW: 331	MW: 260	MW: 188

Table 3.3-1. Molecular weight of some of the fragmented fucose initiator.

However, as discussed in previous chapter, because of the lower ionisation efficiency of high-molecular-weight polymer chains, they tend to generate fewer charged ions per molecule and weaker signals [109,110]. Also, detector saturation by intense matrix ions and low-molecular-weight oligomers signals further shift the observed molecular weight distribution toward lower values, potentially resulting in an underestimation of the true average molecular weights (M_w and M_n) of the polymer [111].

3.3.1.6. Deacetylation of F-PSar

To assess whether the terminal secondary amine of F-PSar reacts with the O-acetyl protecting group during ROP, a portion of F-PSar was subjected to O-acetyl group deprotection with excessive benzylamine. As depicted in (Figure 3.3-11), the absence of acetyl peaks around 2.0 ppm following deacetylation indicates the complete removal of acetyl group. This informs that formation of acetamide under the given reaction conditions does not occur, confirming that the terminal secondary amine of PSar did not remove the O-acetyl group during ROP. Consequently, the terminal secondary amine of PSar retains its status as an active nucleophile, suitable for subsequent coupling reactions.

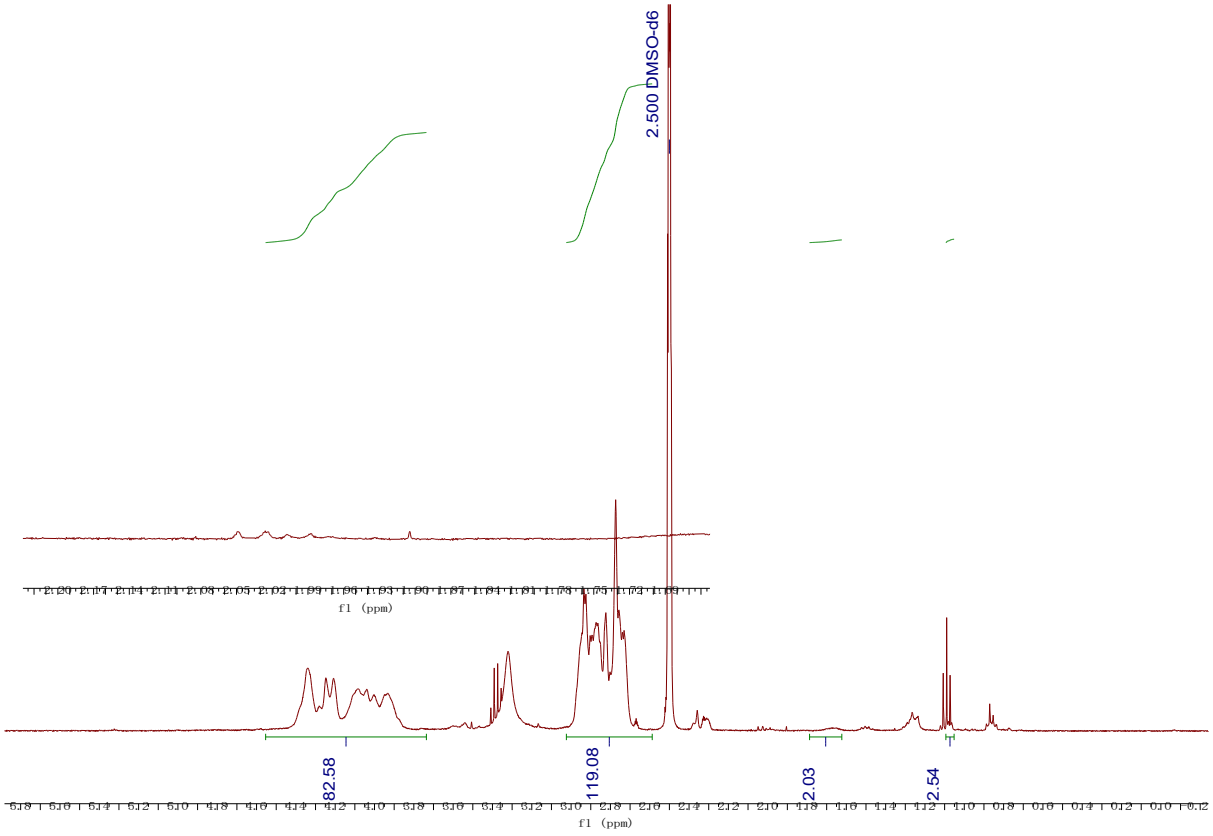

Figure 3.3-11. ^{1}H-NMR spectrum (400 MHz, DMSO-d_6) of F-PSar after deacetylation

3.3.2. Synthesis of Fucose Incorporated Drug Conjugate to Achieve Stable Fucose-Mediated Drug Delivery System

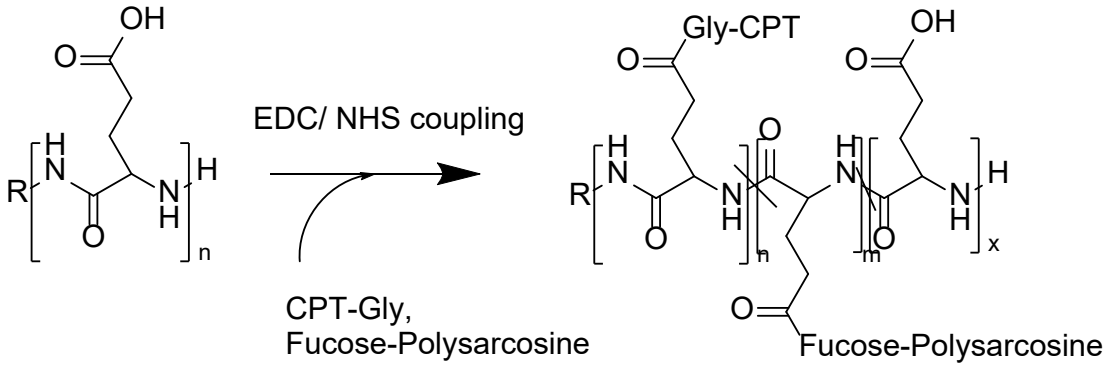

Scheme 3.3-2. Reaction scheme of PGA-[(CPT-Gly)-*co*-(F-PSar)]. \: indication of the random position of carboxylate side chain, CPT-Gly and F-PSar in PGA backbone.

To obtain drug conjugate containing fucose to achieve fucose-mediated drug delivery, PSar

was replaced with F-PSar, and underwent a similar reaction scheme producing PGA-[(CPT-Gly)-*co*-(F-PSar)] (Scheme 3.3-2). With a fucose attached to the end point of hydrophilic polymer chain, allowing the fucose-receptor interactions of the cancer cell inducing endocytosis.

3.3.2.1. PGA-[(CPT-Gly)-co-(F-PSar)] Drug Conjugate

3.3.2.1.1. O-Acetyl Protected PGA-[(CPT-Gly)-*co*-(F-PSar)] Drug Conjugate

The drug conjugate was synthesised via EDC/NHS-mediated coupling in DMF, where F-PSar, PGA, and CPT-Gly were assembled into a single polymeric system (Figure 3.3-12). In this design, fucose attached to the terminus of PSar, the resulting F-PSar serves as the active targeting moiety, facilitating selective drug delivery to fucose receptor-expressing cells. Meanwhile, PSar functions as the hydrophilic segment, enhancing the water solubility and stability of the NPs, while CPT-Gly serves both as the chemotherapeutic agent and the hydrophobic domain, driving self-assembly via nanoprecipitation in aqueous environments.

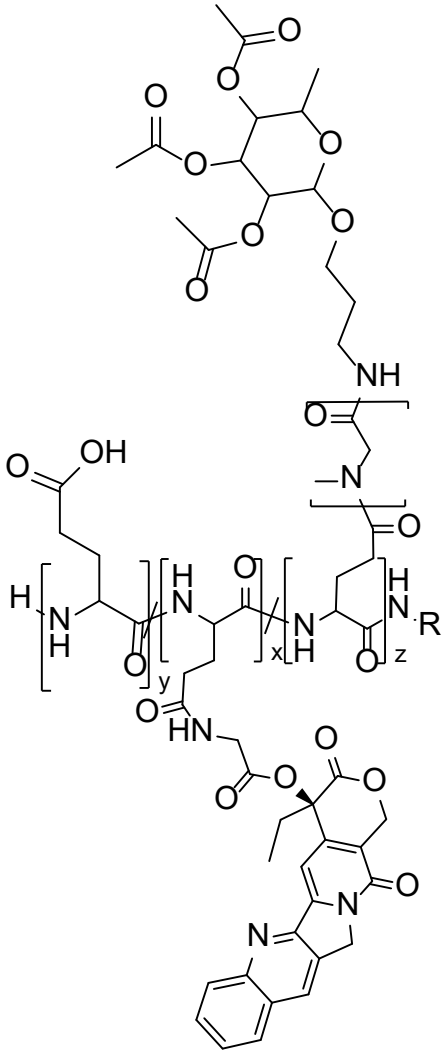

Figure 3.3-12. Acetyl protected PGA-[(CPT-Gly)-*co*-(F-PSar)] Drug Conjugate. /: indication of the random position of carboxylate side chain, CPT-Gly and protected F-PSar in PGA backbone.

The presence of three distinct peaks at ~2.00 ppm in the ^{1}H-NMR spectrum, corresponding to the O-acetyl groups of fucose, indicating the present of F-PSar in the system (Figure 3.3-13).

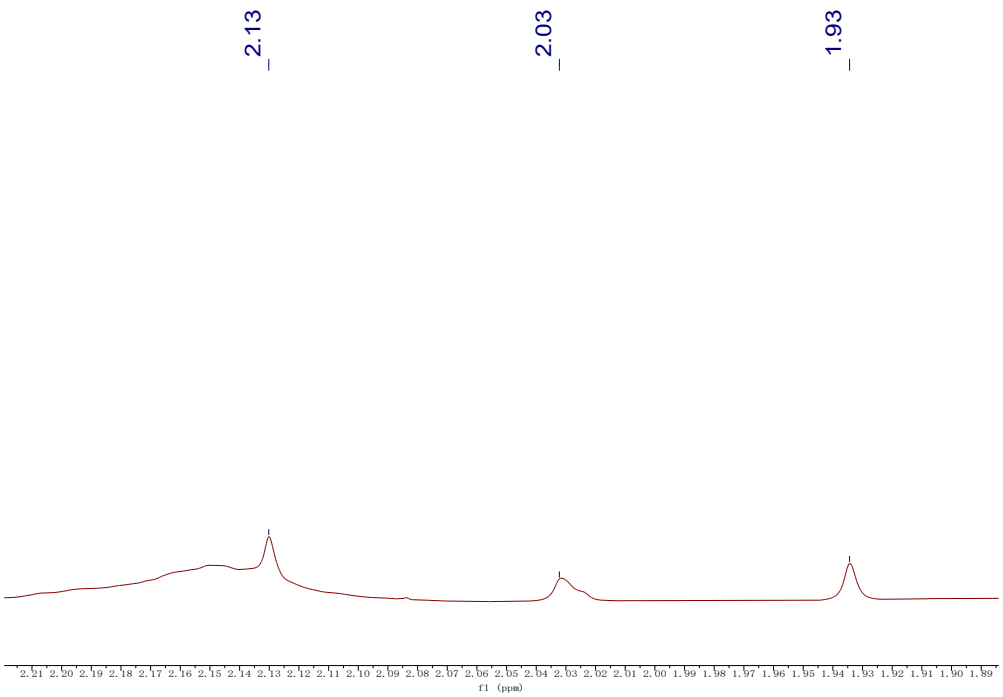

Figure 3.3-13. Zoom in image of ^{1}H-NMR spectrum (500 MHz, DMSO-d_6) of Acetyl protected PGA-[(CPT-Gly)-*co*-(F-PSar)] drug conjugate, 2.13 ppm, 2.03 ppm, 1.93 ppm are the acetyl protecting group of fucose.

Peaks from 8.70 to 7.11 ppm corresponded to the amide proton of the PGA backbone and the protons of CPT, while peaks from 5.50 to 4.92 ppm were attributed to four protons of CPT and 4 protons of fucose. Peaks from 4.34 to 3.92 ppm represented one proton from the PGA backbone, two protons from the PSar backbone, a proton from fucose, and two protons from the glycine linker. Additionally, peaks from 2.92 to 2.73 ppm indicated the three protons of the PSar methyl group, and peaks from 2.31 to 1.66 ppm accounted for the four protons of the PGA side chain, two protons of CPT and protons from the three acetyl groups (Figure 3.3-14). Characteristic peaks in the spectra confirmed the presence of CPT, PSar, O-Acetyl and PGA backbone structures. And the absence of additional peaks confirmed the purity of the product that was used in the subsequent procedures.

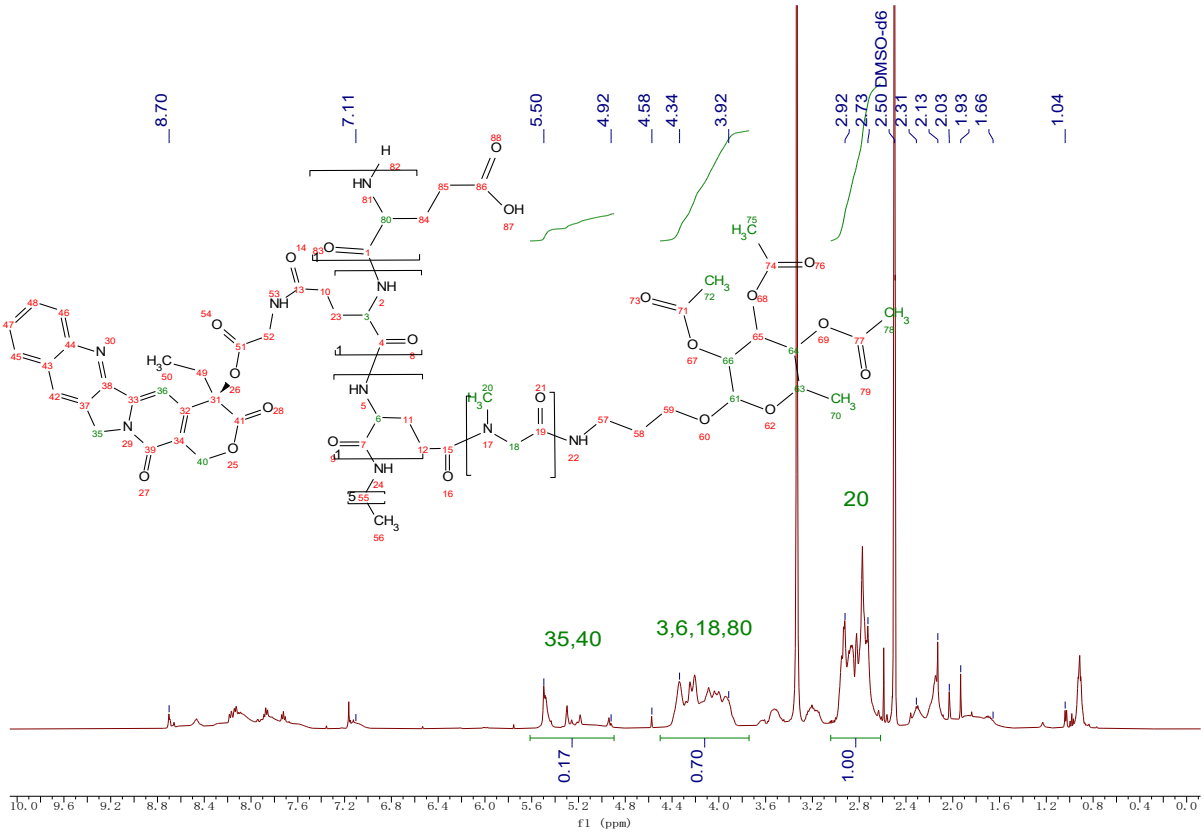

Figure 3.3-14. ^{1}H-NMR spectrum (500 MHz, DMSO-d_6) of Acetyl protected PGA-[(CPT-Gly)-*co*-(F-PSar)] drug conjugate (drug content (w/w): 44.2%): 8.70-7.11 ppm (=C-CH= (CPT),-NH), 5.50-4.92 ppm (-N-CH_2-C- (CPT), -O-CH_2-C- (CPT), -O-CH- (Fucose)), 4.34- 3.92 ppm(-NH-C**H**-C=O- (PGA), -N(CH_3)-C**H_2**- (PSar), -O-CH- (Fucose)), 2.92-2.73 ppm (-N(CH_3)- (PSar), 2.31-1.66 ppm (-C**H_2**-C**H_2**- (PGA), -C=O-CH_3 (Fucose))

3.3.2.1.2. Deprotection of O-Acetyl Protecting Group in PGA-[(CPT-Gly)-*co*-(F-PSar)] Drug Conjugate

A key challenge in the synthesis was the selective deprotection of the O-acetyl groups on fucose without compromising the ester linkage of CPT-Gly. Conventional strong bases such as sodium methoxide could not be used for deacetylation due to the unintended hydrolysis of the CPT-Gly ester bond. To circumvent this issue, benzylamine, a weak base, was employed as the deprotecting agent. The efficacy of benzylamine in selectively removing O-acetyl groups from fucose has been proven in previous experiment [Regioselective Anomeric

Deacetylation of fucose]. Moreover, the bulky structure of benzylamine, compared to other primary amines like hexylamine, further reduces the likelihood of CPT-Gly ester cleavage due to steric hindrance, ensuring the integrity of the drug conjugate during deprotection. However, real challenges arise when in experiment. CPT cleavage was observed when the benzylamine: DMF ratio is larger than 1:4, and uncomplete deprotection was observed when below this ratio. And CPT cleavage occurred when performed at room temperature regardless of the ratio while ice bath greatly reduces this risk. Still uncomplete deprotection or CPT cleavage were observed in some of the reaction trials leading to a need to seek optimisation in the future.

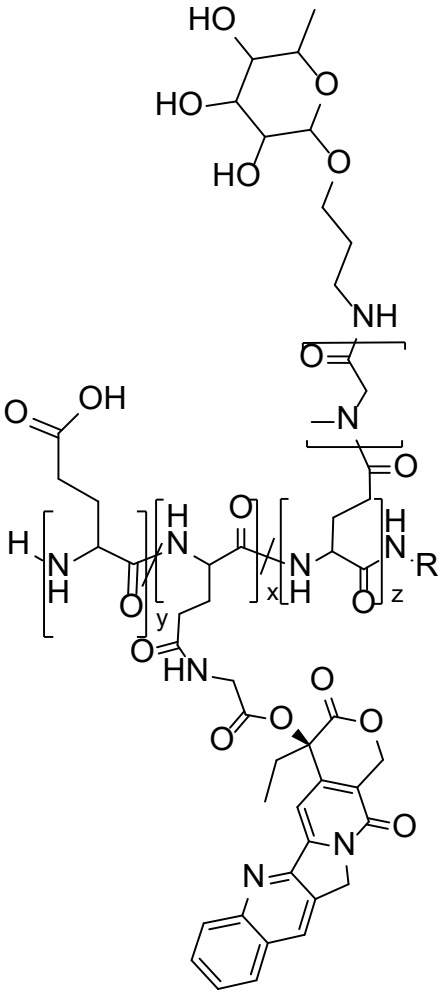

Figure 3.3-15. PGA-[(CPT-Gly)-*co*-(F-PSar)] Drug Conjugate. /: indication of the random position of carboxylate side chain, CPT-Gly and F-PSar in PGA backbone.

The disappearance of peaks at 2.13 ppm, 2.03 ppm, 1.93 ppm in ^{1}H-NMR spectrum indicated the successful deprotection of the acetyl protecting group of fucose (Figure 3.3-16). The drug content was determined through proton integration in the ^{1}H-NMR spectrum through equation:

$$\frac{(5.28-5.47\ ppm)/4*347.3}{\left((3.93-4.34\ ppm)-\frac{5.28-5.47\ ppm}{2}-\left(\frac{2.72-2.93\ ppm}{3}*2\right)\right)*129+\left(\frac{2.72-2.93\ ppm}{3}*71\right)+\left(\frac{5.28-5.47\ ppm}{4}*(404.4-17)\right)}$$

$$=\frac{\frac{0.42}{4}*347.3}{\left(1.05-\frac{0.42}{2}-\frac{1.0}{3}*2\right)*129+\frac{1.0}{3}*71+\frac{0.42}{4}*387.4}=0.414$$

Revealing a drug content of 41.4% (w/w) (Figure 3.3-16). Where 5.28-5.47 ppm correspond to the four protons of CPT, 3.93-4.34 ppm contains a proton from PGA, two protons from CPT-Gly and two protons from PSar, 2.72-2.93 ppm represent the three protons from methyl group; 347.3 is the MW of CPT, 129 is the MW of PGA repeating unit, 71 is the MW of PSar repeating unit, 387.4 represent the MW of CPT-Gly after losing a -OH group during conjugation. Drug content of other four samples were also estimated through ^{1}H NMR integration, yielding an average drug content of 39.8% (±4.4%) (w/w), demonstrating a relatively consistent drug incorporation rate.

The drug content was estimated purely by integration of characteristic signals in the ^{1}H NMR spectra, making the result sensitive to spectral resolution and integration accuracy. Therefore, orthogonal techniques should be used to further validate its drug content in the future.

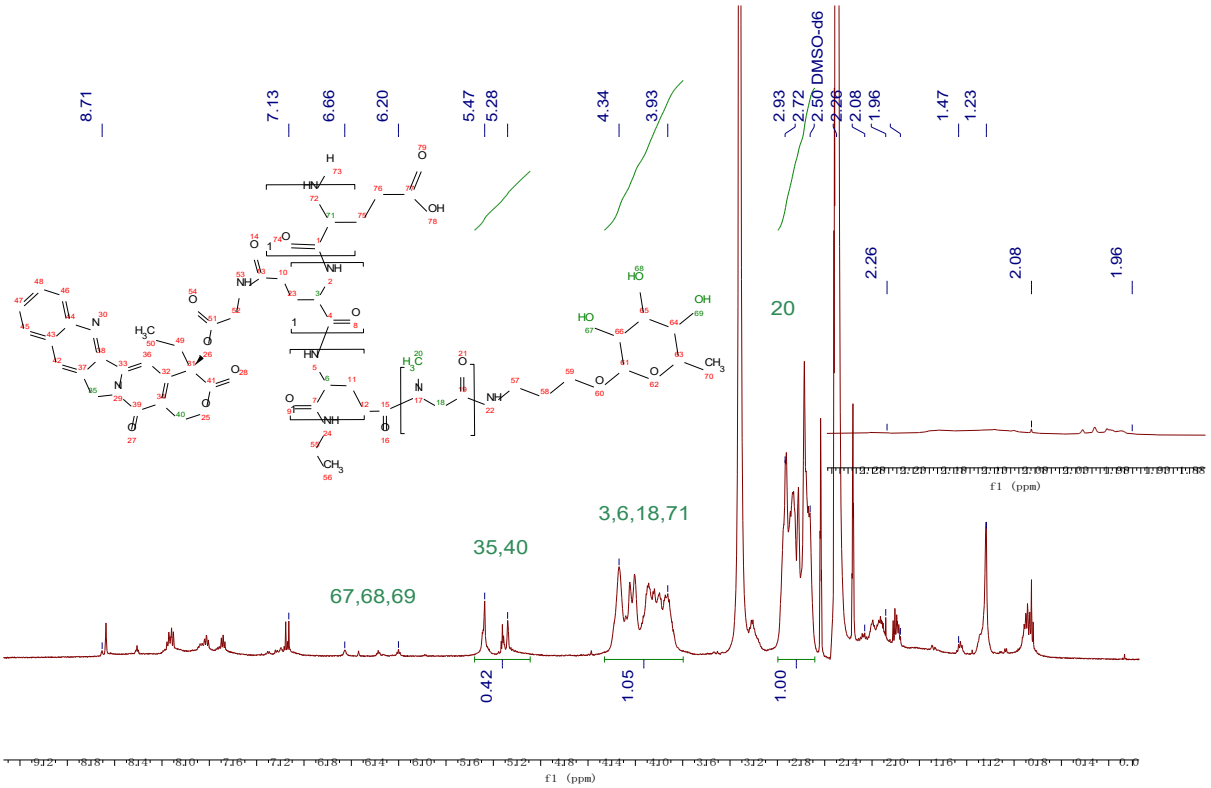

Figure 3.3-16. ^{1}H-NMR spectrum (500 MHz, DMSO-d_6) of PGA-[(CPT-Gly)-*co*-(F-PSar)] drug conjugate (drug content (w/w): 41.4%): 8.71- 7.13 ppm (=C-CH= (CPT),-NH), 6.66-6.20 ppm (-CH-O**H** (Fucose), 5.47-5.28 ppm (-N-CH_2-C- (CPT), -O-CH_2-C- (CPT), -O-CH- (Fucose))), 4.34- 3.93 ppm(-NH-C**H**-C=O- (PGA), -N(CH_3)-C**H_2**- (PSar), -O-CH- (Fucose)), 2.93-2.72 ppm (-N(CH_3)- (PSar)), 2.26-1.96 ppm (-C**H_2**-C**H_2**- (PGA)), 1.47-1.23 ppm (-CH_2-C**H_3** (CPT), initiator, -O-C-CH_3 (fucose)).

3.3.2.1.3. Analysis on Nanoparticles / Nanoprecipitation

NPs were prepared through 'dropping- in' method in pH 7.4 PBS solution to simulate physiological conditions and at concentration of 1.0 mg/mL to simulate the practical concentration in real therapeutic applications [112]. The NPs prepared were analysed by DLS three times each to ensure precision. However, higher concentration was not tested because of the risk of data distortion due to the particle-particle interactions [113,114]. At a drug content of 42.6%, the NPs exhibited a small diameter of 87.19 (±1.117) d.nm and a low PDI of 0.243 (±0.008), indicating high uniformity (Table 3.3-2). Reducing the drug content to 35.4% resulted in a moderate increase in NP size to 113.2 (±2.079) d.nm, with the PDI rising

to 0.322 (±0.012) (Table 3.3-2). Another trial with similar drug content of 34.9% led to a more significant size increase to 156.2 (±3.044) d.nm, with the PDI slightly increasing to 0.331 (±0.021) (Table 3.3-2).

DLS Result	Z-Average (d.nm)	PDI
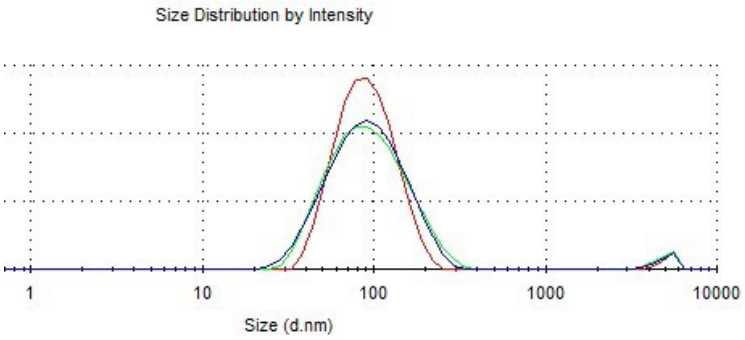 Drug content (w/w): 42.6%	87.19 (±1.117)	0.243 (±0.008)
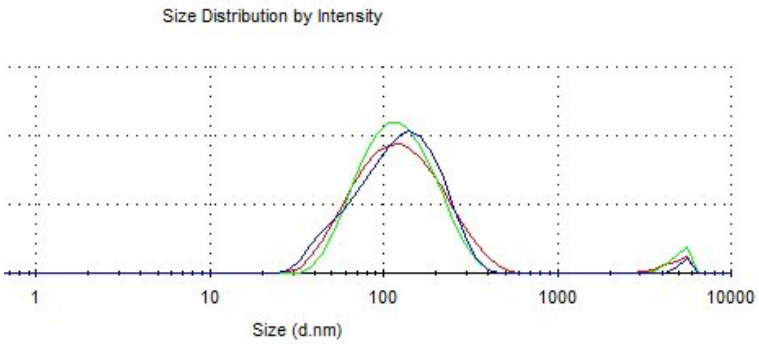 Drug content (w/w): 35.4%	113.2 (±2.079)	0.322 (±0.012)
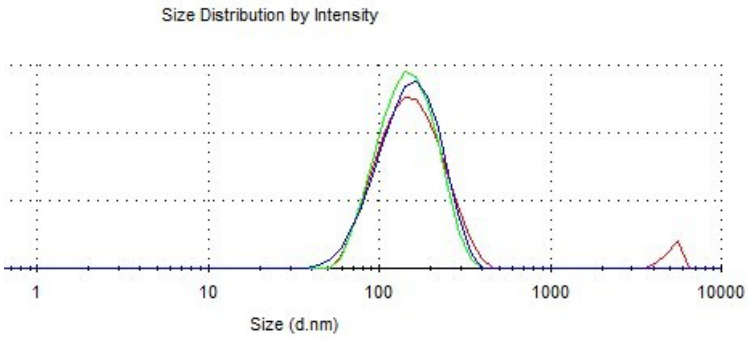 Drug content (w/w): 34.9%	156.2 (±3.044)	0.331 (±0.021)

Table 3.3-2. summary of intensity-weighted diameter distribution of 3 trials DLS analysis, under

concentration of 1.0 mg/mL in pH 7.4 PBS solution

This NP size varied across different trials, likely due to the ambiguous chemical structures formed during the drug conjugation process [115,116,117]. The drug conjugation was conducted in a one-pot reaction via random conjugation between the carboxylate groups of the PGA backbone and the amino groups of CPT-Gly and PSar. The significant differences in molecular size and functional group reactivity between CPT-Gly and PSar led to polydisperse polymer mixtures with varying density of different components along PGA chain [115,116,117]. Additionally, differences in reaction conditions, such as concentration and temperature, further contributed to the differences in the degree and distribution of conjugation, which directly influences the size of the resulting NPs [118]. As a result, NPs ranging from 80-160 nm were produced, which is ideal for pancreatic cancer targeting, where fucose-mediated endocytosis facilitates drug delivery to bypass dense desmoplasia. [14,71].

Additionally, following a two-week storage period at ambient temperature, both the size and PDI of the NPs exhibit only slight increases, highlighting the enduring stability of the NPs formed (Table 3.3-3). And still, minor intensity peak at thousands d.nm was observed in all DLS measurements. Which is likely overestimated due to the intensity-weighted nature of DLS measurements, which disproportionately emphasises larger particles [119]. These aggregates probably result from the unconjugated CPT-Gly remained in the system after dialysis.

DLS Result	Z-Average (d.nm)	PDI
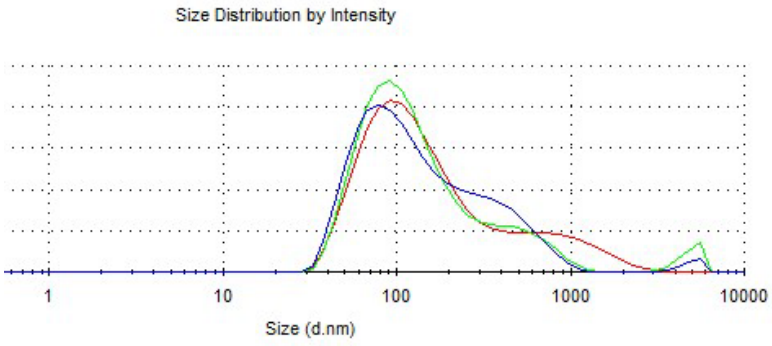 Drug content (w/w): 42.6%	111.9 (±2.669)	0.371 (±0.006)
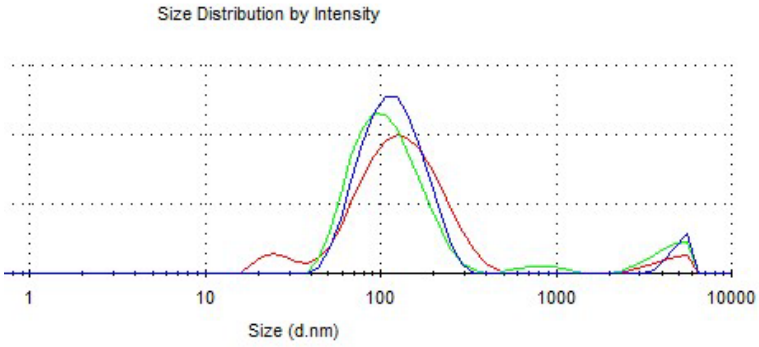 Drug content (w/w): 35.4%	113.6 (±3.736)	0.343 (±0.015)
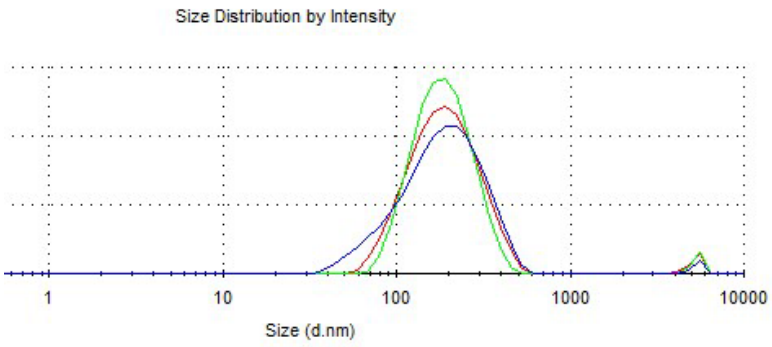 Drug content (w/w): 34.9%	175.6 (±4.596)	0.316 (±0.01)

Table 3.3-3. Summary of intensity-weighted diameter distribution of 3 trials DLS analysis after 2 weeks stored at room temperature, under concentration of 1.0 mg/mL in pH 7.4 PBS solution.

But still, their ability to form stable NPs at concentration as high as 1.0 mg/ml indicates their enhanced drug solubility, potentially prolonged circulation time, and improved

bioavailability, which are crucial factors for effective drug delivery [41,120,121,122]. Furthermore, the presence of the fucose acceptor within the conjugate may facilitate targeted interactions with cancer cells, particularly in pancreatic cancer, where fucose-mediated recognition plays a significant role[15,43,123]. These combined properties highlight the drug conjugate's potential as a promising candidate for pancreatic cancer treatment.

The morphology of the NPs was assessed using SEM, revealing spherical shape for the PGA-[(CPT-Gly)-*co*-(F-PSar)] NPs (Table 3.3-4) justifying the spherical assumption used in the DLS analysis. The particles observed in SEM were generally within 200 nm, showing good agreement with the size populations determined by DLS (80-160 nm). Although DLS typically reports larger particle sizes due to the surrounding hydration shell [124,125], SEM measures the dry core diameter of individual particles under vacuum and is therefore expected to yield smaller values than DLS [126]. In this study, SEM measurements produced slightly larger apparent diameters. This discrepancy is likely caused by the external forces applied during SEM sample preparation, which induced partial deformation or spreading of the NPs. Also, in SEM, only small part of the NPs is observed while DLS provides an ensemble-averaged size distribution of particles in suspension.

Also, the uneven conjugation of the drug conjugate during synthesis that may lead to uneven hydrophobic and hydrophilic density along PGA chain resulting in NP size variations. This heterogeneity may influence the NPs' physical behaviour in aqueous environments [117]. Additionally, some NPs appeared ruptured in SEM images, a phenomenon possibly attributed to rapid water sublimation during the freeze-drying process [127]. Also, large particles were observed in all the SEM images, this could be attributed to physical stress put on the NPs during freeze drying process which causes aggregation or fusion of the NPs [128,129].

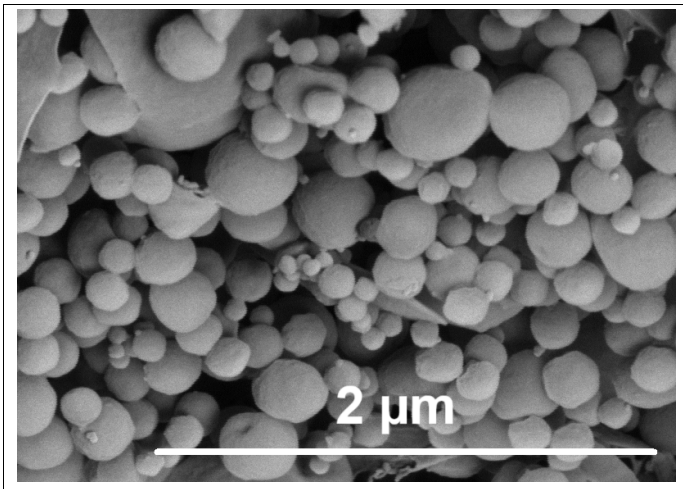 Drug content: 42.6%
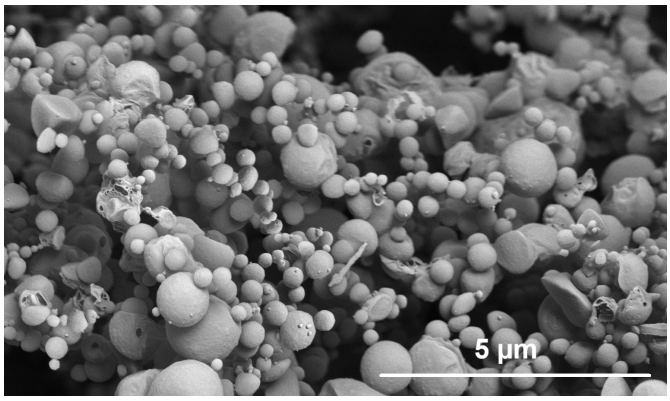 Drug Content: 35.4%
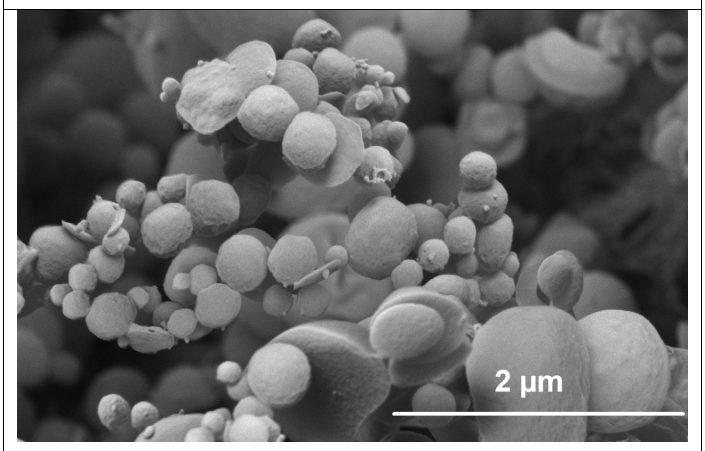 Drug load: 34.9%

Table 3.3-4. SEM images on three trials of PGA-[(CPT-Gly)-*co*-(F-PSar)]

3.3.2.1.4. Analysis of Nanoparticles at Acidic Conditions

To evaluate the impact of pH to the stability of the NPs produced from the drug conjugate, PGA-[(CPT-Gly)-*co*-(F-PSar)], NPs were prepared in acetate buffer solution at two distinct pH levels: 6.0 and 5.5 and analysed with DLS three times each. At pH 6.0 the NPs displayed an average diameter of 164.7 d.nm and a PDI of 0.221 (Table 3.3-5), suggesting a consistent size distribution. In contrast, at pH 5.5, the NPs aggregated, causing their average diameter to increase significantly to 663.5 d.nm, with a PDI of 0.613, indicating a much wider variation in particle sizes (Table 3.3-5). This suggests that the protonation of carboxylate group start at around pH 5.5 and result in dramatic increase in hydrophobicity that leads to aggregation which is similar to the observation in (2.3.7.2.2), reinforcing the reliability of this behaviour for the drug conjugate under acidic conditions.

This finding is particularly meaningful when considering the TME, which typically has a slightly acidic pH ranging from 6.0 to 7.0 [130,131]. Since the NPs remained stable at pH 6.0 but aggregated at pH 5.5, it is reasonable to conclude that they will maintain their integrity within the tumour's slightly acidic environment. This stability is especially critical for pancreatic cancer treatment, which is characterised by hypovascularity and dense desmoplasia [14,15]. As a result, fucose-receptor-mediated endocytosis becomes the primary pathway for NPs to enter tumour cells [15]. However, endocytosis can only efficiently internalise particles up to 150 nm, with a maximum size limit of 200 nm [68,71]. Thus, avoiding aggregation in the TME is vital to keep the NPs within this size range for successful cellular uptake. However, DLS typically yields larger particle sizes due to the presence of a hydration shell [124,125], therefore, the actual size of the NPs could be smaller and easily endocytosed with in pancreatic cancer cells.

pH 6.0 Acetate Buffer Solution	pH 5.5 Acetate Buffer Solution
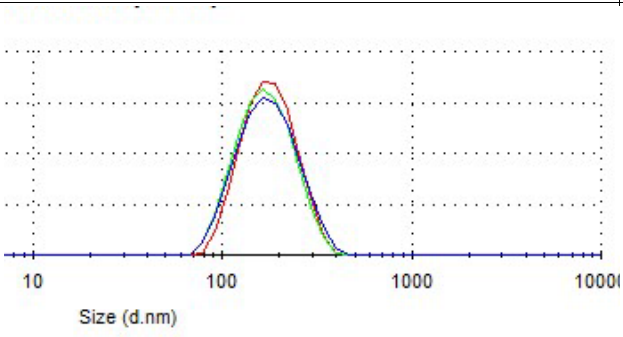	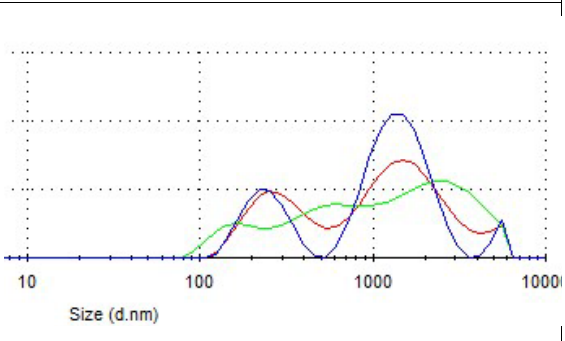
Z-Average: 164.7 d.nm (±4.96) PDI: 0.221 (±0.019)	Z-Average: 663.5 d.nm (±53.22) PDI: 0.613 (±0.015)

Table 3.3-5. Three replicate DLS analysis (size distribution by intensity) of PGA-[(CPT-Gly)-*co*-(F-PSar)] (44.7% drug content) (1.0 mg/mL) in pH 6.0 and pH 5.5 acetate buffer solution.

3.3.2.1.5. Drug Release Study of PGA-[(CPT-Gly)-*co*-(F-PSar)]

Drug release studies were conducted on three individual samples of PGA-[(CPT-Gly)-*co*-(F-PSar)] under two distinct conditions: pH 7.4 PBS, which simulates the physiological environment, and pH 5.0 acetate buffer, designed to mimic the acidic endosomes or lysosomes of cancer cells [130,131]. In both conditions, an initial burst release of approximately 5% of the drug occurred within the first few hours (Figure 3.3-17,Figure 3.3-18), a phenomenon likely attributable to non-conjugated CPT that persisted after purification and presented as the large aggregates in the DLS reports. Indicating the samples require extended duration of dialysis against MeOH. Following the burst release phase, physically encapsulated non conjugated CPT was gradually released over the first three days. After day four, the release rate decreased, with continued drug liberation primarily governed by the slow hydrolysis of the ester linkage between CPT and the polymer conjugate, resulting in sustained CPT release over a period of up to 26 days (Figure 3.3-17).

Under physiological conditions at pH 7.4, a total of approximately 46% of the drug was released after 26 days, aligning closely with previous findings (2.3.7.2.3). This substantial release suggests that the PGA-[(CPT-Gly)-*co*-(F-PSar)] conjugate maintains relative stability in

environments mimicking the physiological condition, potentially minimising the cytotoxicity of CPT during circulation.

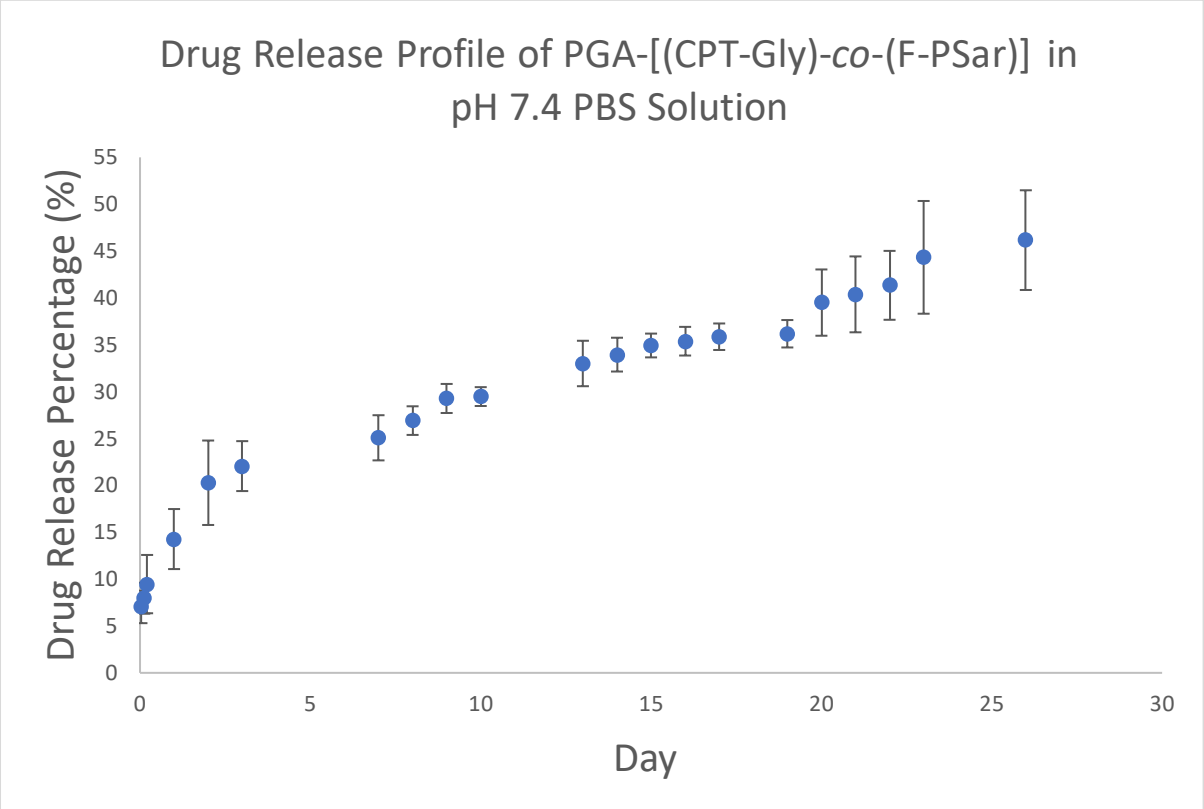

Figure 3.3-17. The drug release profile of PGA-[(CPT-Gly)-*co*-(F-PSar)] was evaluated in pH 7.4 PBS at 37°C over 26 days, three analyses were conducted on each of three independent samples.

In contrast, the drug release rate in the acidic condition at pH 5.0 proved unexpectedly slower than at pH 7.4. After the initial 5% burst release, only an additional 5% of the drug was gradually released over the 26 days (Figure 3.3-18) This observation stands in contrast to the anticipated hydrolysis rate of the ester bond in CPT-Gly under acidic conditions, as documented in the literature [132]. Several factors might account for this slower release in the acidic environment. Aggregation of NPs at pH 5.0 could reduce the surface area available for interaction with the surrounding solution (Table 3.3-5) [133]. Additionally, this aggregation might trigger precipitation of the drug conjugate as observed in DLS result that few micro large of particles present in the system (Table 3.3-5), leading to phase separation that limits contact with the solution and decelerates hydrolysis [133,134]. Furthermore, protonation of PGA at pH 5.0 may enhance its hydrophobicity, strengthening hydrophobic interactions with CPT and thereby further impeding hydrolysis and diffusion into the

aqueous phase [134].

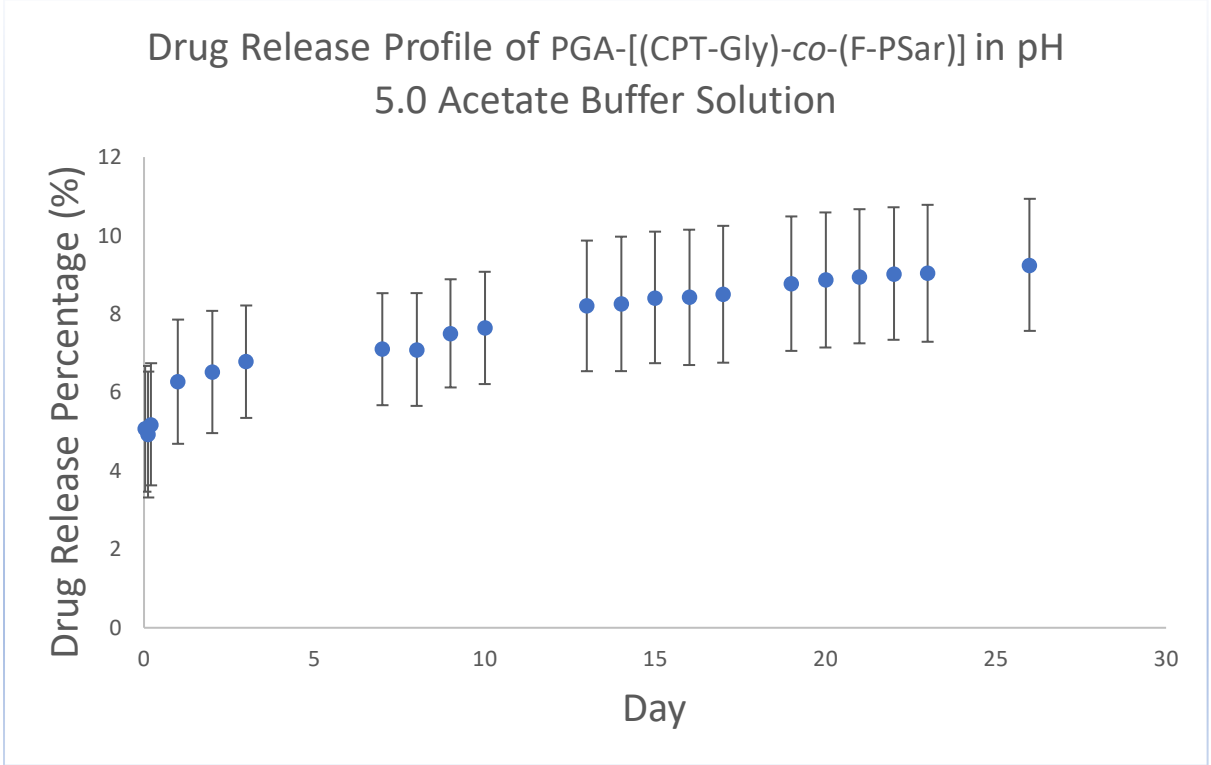

Figure 3.3-18. The drug release profile of PGA-[(CPT-Gly)-*co*-(F-PSar)] was evaluated in pH 5.0 acetate buffer solution at 37°C over 26 days, three replicate analyses were conducted on each of three independent samples.

Because of this unanticipated release profile, the slow and continuous release of CPT in acidic conditions, this drug conjugate is excluded from first-line pancreatic cancer treatment, which require rapid deposition of high quantity of therapeutic agent after endocytosis by the cancer cells [135,136]. However, given its slow drug releasing profile within acidic cancer cells, it offers potential advantages for targeting S-phase cancer cells and could be used in combination with other therapeutics in adjuvant treatments. CPT is a potent top-I inhibitor, primary affecting cells actively synthesising DNA during the S-phase [137,138,139]. However, cancer cells, including those in pancreatic tumours, often reside in the quiescent G0 phase for extended periods, potentially lasting 6 to 10 months based on cancer recurrence data [140,141]. Especially for pancreatic cancer, even after surgical resection and adjuvant therapy, patients still face significant morbidity and have almost inevitable recurrence with

median survival rate of approximate two years [13]. Moreover, CPT is not a substrate of Pgp [137,143,144], the most potent efflux pump contributed the most in drug resistance across many cancer cell lines [90,97], potentially allowing CPT to remain in cancer cells. And consequently, this prolonged G0 phase allows CPT to be released and accumulate gradually within these resting cells [137,143,144], increasing the likelihood that the drug will be present and effective when the cells eventually transition into the S-phase hoping to prevent recurrence, especially the S phase typically last for around 8 hours in normal pancreatic cells [142]. Given that less than a quarter of tumour cells are typically in this phase [132,145], a sustained release mechanism may selectively target these cells over an extended duration.

This characteristic of slow and sustained release in acidic conditions complements other features of the conjugate, placing it as a potential adjuvant therapeutic option for pancreatic cancer. In addition, the NPs demonstrate stability at physiological pH (Table 3.3-2,Table 3.3-3) likely to remain intact during circulation. Finally, fucose-mediated cell targeting facilitates specific uptake by pancreatic cancer cells to further enhance the potential of the disclosed polymeric drug delivery system. Together, these properties position PGA-[(CPT-Gly)-co-(F-PSar)] as a candidate for post-surgery adjuvant therapy for pancreatic cancer, capitalising on both its unique CPT release kinetics in acidic condition and its cell-targeting capabilities, with *in vitro* cell testing the next stage in product development.

As highlighted in the previous chapter, the release medium did not incorporate key biological interactions (such as enzymatic activity and protein binding), thereby limiting its physiological and in vivo relevance. Nevertheless, the present study offers a baseline for drug release under endosomal/lysosomal-like conditions. Future work incorporating biological components will be essential to generate a more representative and clinically relevant release profile.

3.4. Summary

To explore the impact of PSar modification, two conjugates, PGA-[(CPT-Gly)-*co*-(PSar)] and PGA-(CPT-Gly), were synthesised with comparable drug (CPT) content. DLS analysis revealed a key difference: while PGA-(CPT-Gly) produced NPs with a broad range of sizes, the PSar-modified PGA-[(CPT-Gly)-*co*-(PSar)] formed more uniform NPs, a critical factor for effective

drug delivery [146]. Furthermore, PSar enhanced NP stability in pH 7.4 PBS by preventing aggregation over time, a property observed in both PGA-(PSar-Gly-CPT) and the later-developed PGA-[(CPT-Gly)-*co*-(F-PSar)]. These results confirm the importance of including hydrophilic PSar in the polymer formulations to restrict polymer-polymer interactions and consequent NP aggregation.

Building on these advancements, a fucose incorporated drug conjugate, PGA-[(CPT-Gly)-*co*-(F-PSar)] was synthesised with a drug content of 39.8% (±4.4%) (w/w). The addition of PSar markedly improved water-solubility, enabling stable NP formation at concentrations up to 1.0 mg/mL, and the NPs maintaining their size in pH 7.4 PBS solution for over two weeks at room temperature, in the absence of aggregation. These NPs, ranging from 80nm to 160nm, are designed to benefit from the stealth effect imparted by PSar, which can reduce plasma protein binding, uptake by phagocytic cells and clearance by liver and kidney prolonging circulation time in the bloodstream [146,147,148].

CPT release from PGA-[(CPT-Gly)-*co*-(F-PSar)] revealed distinct release profiles under physiological (pH 7.4) and acidic (pH 5.0) conditions, mimicking healthy tissue and cancer cell endosomes/lysosomes, respectively. In both environments, an initial burst release of approximately 5% of CPT occurred within hours, then physically encapsulated non-conjugated CPT was gradually released over the first few days, followed by CPT release from slow hydrolysis of CPT- polymer conjugate. At pH 7.4, about 46% of the drug was released, demonstrating stability in physiological conditions. Unexpectedly, at pH 5.0, only an additional 5% was released, contradict to that anticipated. This result was probably because of NP aggregation reducing surface area and hydrolysis, and PGA protonation increasing hydrophobicity, further impeding drug diffusion. This slow, sustained release in acidic conditions could be beneficial when administered as part of the adjuvant therapy after surgery because the cancer cells can remain quiescent in G0 phase potentially lasting 6 to 10 months [140,141], given enough time for CPT cumulation, and activate once cancer cells entered S-phase, where CPT is most effective.

However, the overall yield of the synthesised polymeric drug conjugates was lower than expected, possibly due to two main factors. First, the hydrolysis of the ester bond in the CPT-Gly linker during dialysis may have degraded the conjugate [132]. Second, steric hindrance

from the bulky CPT moiety likely impeded the conjugation of PSar or the other way round, resulting in their loss during the reaction.

Interestingly, a comparison of different conjugate structures revealed insights into improving efficiency. The yield of PGA-(PSar-Gly-CPT), where CPT is positioned at the terminal end of the PSar, was higher than that of both PGA-[(CPT-Gly)-*co*-(PSar)] and PGA-[(CPT-Gly)-co-(F-PSar)]. This difference suggests that placing CPT at the terminal position enhances conjugation efficiency by allowing the amino group of PSar to react more effectively with PGA possibly by avoiding steric hindrance of bulky CPT. Additionally, PSar may offer steric protection to the ester bond, reducing its susceptibility to hydrolysis [132]. These findings highlight the importance of conjugate design in optimising synthesis outcomes.

To improve the yield and minimise the loss of the therapeutic agent, two modifications are recommended: (1) replacing glycine with an alternative amino acid linker featuring a bulkier side chain to better shield the ester bond [132]. and (2) increasing the distance between the carboxylate side chain and CPT by using a dimer or trimer instead of a single amino acid linker. The first change would enhance the preservation of the therapeutic agent, while the second would reduce steric hindrance from CPT, facilitating PSar conjugation and boosting overall reaction efficiency.

While the drug conjugate demonstrates promising properties—such as forming stable NPs in PBS and favourable size and uniformity for drug delivery systems [71,146,147,148], a significant challenge remains [115,116,117]. The uncontrolled conjugation of CPT-Gly and PSar introduces unpredictable physicochemical heterogeneity such as a range of NPs size were produced (80- 160nm), which may impede further study in clinical development [117]. Therefore, overcoming this variability is essential for advancing the conjugate toward practical applications. Specifically, the random attachment of CPT-Gly and PSar along the polymer chain can lead to inconsistent drug distribution and density, affecting the reproducibility of NP formation, drug release kinetics, and therapeutic efficacy. Addressing this issue will require future efforts focused on controlled conjugation strategies to ensure uniformity in drug distribution and NP behaviour. Also given the fact that the O-acetyl deprotection step result in loss of CPT or incomplete deprotection in some of the reaction trials, indicating the need for further optimisation.

3.5. Reference

1. Sarantis, P., Koustas, E., Papadimitropoulou, A., Papavassiliou, A. G., & Karamouzis, M. V. (2020). Pancreatic ductal adenocarcinoma: treatment hurdles, tumor microenvironment and immunotherapy. World Journal of Gastrointestinal Oncology, 12(2), 173-181. https://doi.org/10.4251/wjgo.v12.i2.173

2. Zhou, Q. and Melton, D. A. (2018). Pancreas regeneration. Nature, 557(7705), 351-358. https://doi.org/10.1038/s41586-018-0088-0

3. Hidalgo, M. (2010). Pancreatic cancer. New England Journal of Medicine, 362(17), 1605-1617. https://doi.org/10.1056/nejmra0901557

4. Maitra, A. and Hruban, R. H. (2008). Pancreatic cancer. Annual Review of Pathology: Mechanisms of Disease, 3(1), 157-188. https://doi.org/10.1146/annurev.pathmechdis.3.121806.154305

5. Pancreatric Section, British Society of Gastroenterology, Pancreatic Society of Great Britain and Ireland, Association of Upper Gastrointestinal Surgeons of Great Britain and Ireland, Royal College of Pathologists, & Special Interest Group for Gastro-Intestinal Radiology (2005). Guidelines for the management of patients with pancreatic cancer periampullary and ampullary carcinomas. Gut, 54 Suppl 5(Suppl 5), v1–v16. https://doi.org/10.1136/gut.2004.057059

6. Corbo, V., Tortora, G., & Scarpa, A. (2012). Molecular pathology of pancreatic cancer: from bench-to-bedside translation. Current Drug Targets, 13(6), 744-752. https://doi.org/10.2174/138945012800564103

7. Ghaneh, P., Costello, E., & Neoptolemos, J. P. (2008). Biology and management of pancreatic cancer. Postgraduate Medical Journal, 84(995), 478-497. https://doi.org/10.1136/gut.2006.103333

8. Lemmens, V., Bosscha, K., Schelling, G. v. d., Brenninkmeijer, S., Coebergh, J., & Hingh, I. H. J. T. d. (2011). Improving outcome for patients with pancreatic cancer through centralization. British Journal of Surgery, 98(10), 1455-1462. https://doi.org/10.1002/bjs.7581

9. Adamska, A., Domenichini, A., & Falasca, M. (2017). Pancreatic ductal adenocarcinoma: current and evolving therapies. International Journal of Molecular Sciences, 18(7), 1338. https://doi.org/10.3390/ijms18071338

10. Burris, H. A., Moore, M. J., Andersen, J. S., Green, M. R., Rothenberg, M. L., Modiano, M., … & Hoff, D. D. V. (1997). Improvements in survival and clinical benefit with gemcitabine as first-line therapy for patients with advanced pancreas cancer: a randomized trial.. Journal of Clinical Oncology, 15(6), 2403-2413. https://doi.org/10.1200/jco.1997.15.6.2403

11. Ansari, D., Gustafsson, A., & Andersson, R. (2015). Update on the management of pancreatic cancer: surgery is not enough. World Journal of Gastroenterology, 21(11), 3157-3165. https://doi.org/10.3748/wjg.v21.i11.3157

12. Pancreatic Cancer UK. (2022, July). Pancreatic ductal adenocarcinoma and other exocrine tumours. Pancreatic Cancer UK. https://www.pancreaticcancer.org.uk/information/just-diagnosed-with-pancreatic-cancer/pancreatic-ductal-adenocarcinoma-and-other-

exocrine-tumours/

13. Oberstein, P. E. and Olive, K. P. (2013). Pancreatic cancer: why is it so hard to treat?. Therapeutic Advances in Gastroenterology, 6(4), 321-337. https://doi.org/10.1177/1756283x13478680

14. Feig, C., Gopinathan, A., Neeße, A., Chan, D., Cook, N., & Tuveson, D. A. (2012). The pancreas cancer microenvironment. Clinical Cancer Research, 18(16), 4266-4276. https://doi.org/10.1158/1078-0432.ccr-11-3114

15. Yoshida, M., Takimoto, R., Murase, K., Sato, Y., Hirakawa, M., Tamura, F., … & Kato, J. (2012). Targeting anticancer drug delivery to pancreatic cancer cells using a fucose-bound nanoparticle approach. PLoS ONE, 7(7), e39545. https://doi.org/10.1371/journal.pone.0039545

16. Uzunparmak, B. and Şahin, İ. H. (2019). Pancreatic cancer microenvironment: a current dilemma. Clinical and Translational Medicine, 8(1). https://doi.org/10.1186/s40169-019-0221-1

17. Neeße, A., Gress, T. M., Tuveson, D. A., Michl, P., & Krug, S. (2013). Emerging concepts in pancreatic cancer medicine: targeting the tumor stroma. OncoTargets and Therapy, 33. https://doi.org/10.2147/ott.s38111

18. Peer, D., Karp, J. M., Hong, S., Farokhzad, O. C., Margalit, R., & Langer, R. (2007). Nanocarriers as an emerging platform for cancer therapy. Nature Nanotechnology, 2(12), 751-760. https://doi.org/10.1038/nnano.2007.387

19. Yang, L., Sajja, H. K., Cao, Z., Qian, W., Bender, L., Marcus, A. I., … & Wang, Y. A. (2014). Upar-targeted optical imaging contrasts as theranostic agents for tumor margin detection. Theranostics, 4(1), 106-118. https://doi.org/10.7150/thno.7409

20. Harvey, S. R., Hurd, T. C., Markus, G., Martinick, M. I., Penetrante, R. M., Tan, D., Venkataraman, P., DeSouza, N., Sait, S. N., Driscoll, D. L., & Gibbs, J. F. (2003). Evaluation of urinary plasminogen activator, its receptor, matrix metalloproteinase-9, and von Willebrand factor in pancreatic cancer. Clinical cancer research : an official journal of the American Association for Cancer Research, 9(13), 4935–4943.

21. Tan, X., Egami, H., Nozawa, F., Abe, M., & Baba, H. (2006). Analysis of the invasion-metastasis mechanism in pancreatic cancer: involvement of plasmin(ogen) cascade proteins in the invasion of pancreatic cancer cells. International Journal of Oncology. https://doi.org/10.3892/ijo.28.2.369

22. Samuel, N. and Hudson, T. J. (2011). The molecular and cellular heterogeneity of pancreatic ductal adenocarcinoma. Nature Reviews Gastroenterology &Amp; Hepatology, 9(2), 77-87. https://doi.org/10.1038/nrgastro.2011.215

23. Almoguera, C., Shibata, D., Forrester, K., Martin, J. J., Arnheim, N., & Perucho, M. (1988). Most human carcinomas of the exocrine pancreas contain mutant c-k-ras genes. Cell, 53(4), 549-554. https://doi.org/10.1016/0092-8674(88)90571-5

24. Rozenblum, E., Schutte, M., Goggins, M., Hahn, S. A., Panzer, S., Zahurak, M., Goodman, S. N., Sohn, T. A., Hruban, R. H., Yeo, C. J., & Kern, S. E. (1997). Tumor-suppressive pathways in pancreatic carcinoma. Cancer research, 57(9), 1731–1734.

25. Caldas, C., Hahn, S. A., Costa, L. T. d., Redston, M., Schutte, M., Seymour, A., … & Kern, S. E. (1994). Frequent somatic mutations and homozygous deletions of the p16 (mts1) gene in pancreatic adenocarcinoma. Nature Genetics, 8(1), 27-32. https://doi.org/10.1038/ng0994-27

26. Knudson A. G., Jr (1978). Retinoblastoma: a prototypic hereditary neoplasm. Seminars in oncology, 5(1), 57–60.

27. Zhao, R., Choi, B. Y., Lee, M., Bode, A. M., & Dong, Z. (2016). Implications of genetic and epigenetic alterations of cdkn2a (p16 ink4a) in cancer. EBioMedicine, 8, 30-39. https://doi.org/10.1016/j.ebiom.2016.04.017

28. Stefanoudakis, D., Frountzas, M., Schizas, D., Michalopoulos, N. V., Drakaki, A., & Toutouzas, K. G. (2024). Significance of tp53, cdkn2a, smad4 and kras in pancreatic cancer. Current Issues in Molecular Biology, 46(4), 2827-2844. https://doi.org/10.3390/cimb46040177

29. Kreuger, I. Z. M., Slieker, R. C., Groningen, T. v., & Doorn, R. v. (2023). Therapeutic strategies for targeting cdkn2a loss in melanoma. Journal of Investigative Dermatology, 143(1), 18-25.e1. https://doi.org/10.1016/j.jid.2022.07.016

30. Mizrahi, J. D., Surana, R., Valle, J. W., & Shroff, R. T. (2020). Pancreatic cancer. The Lancet, 395(10242), 2008-2020. https://doi.org/10.1016/s0140-6736(20)30974-0

31. Zhao, M., Mishra, L., & Deng, C. (2018). The role of tgf-β/smad4 signaling in cancer. International Journal of Biological Sciences, 14(2), 111-123. https://doi.org/10.7150/ijbs.23230

32. Du, X., Li, Q., Yang, L., Liu, L., Cao, Q., & Li, Q. (2020). Smad4 activates wnt signaling pathway to inhibit granulosa cell apoptosis. Cell Death &Amp; Disease, 11(5). https://doi.org/10.1038/s41419-020-2578-x

33. Yachida, S., & Iacobuzio-Donahue, C. A. (2013). Evolution and dynamics of pancreatic cancer progression. Oncogene, 32(45), 5253–5260. https://doi.org/10.1038/onc.2013.29

34. Kim, D. Y., Choi, Y. J., Seol, Y. M., & Kim, H. (2018). Adjuvant chemotherapy versus chemoradiation for patients with resected pancreatic adenocarcinoma: a single-center retrospective study. The Korean Journal of Pancreas and Biliary Tract, 23(3), 108-115. https://doi.org/10.15279/kpba.2018.23.3.108

35. Kaiser, M. H. (1985). Pancreatic cancer. Archives of Surgery, 120(8), 899. https://doi.org/10.1001/archsurg.1985.01390320023003

36. Klinkenbijl, J. H. G., Jeekel, J., Sahmoud, T., Pel, R. v., Couvreur, M., Veenhof, C., … & Wils, J. (1999). Adjuvant radiotherapy and 5-fluorouracil after curative resection of cancer of the pancreas and periampullary region. Annals of Surgery, 230(6), 776. https://doi.org/10.1097/00000658-199912000-00006

37. Jun, S., Oladeru, O. T., Miccio, J. A., Iovoli, A. J., Hermann, G. M., & Singh, A. K. (2019). Association of timing of adjuvant therapy with survival in patients with resected stage i to ii pancreatic cancer. JAMA Network Open, 2(8), e199126. https://doi.org/10.1001/jamanetworkopen.2019.9126

38. Neoptolemos, J. P., Stocken, D., Bassi, C., Ghaneh, P., Cunningham, D., Goldstein, D., … &

Cancer, f. t. E. S. G. f. P. (2010). Adjuvant chemotherapy with fluorouracil plus folinic acid vs gemcitabine following pancreatic cancer resection. Jama, 304(10), 1073. https://doi.org/10.1001/jama.2010.1275

39. Neoptolemos, J. P., Dunn, J., Stocken, D., Almond, J., Link, K. H., Beger, H. G., … & Büchler, M. (2001). Adjuvant chemoradiotherapy and chemotherapy in resectable pancreatic cancer: a randomised controlled trial. The Lancet, 358(9293), 1576-1585. https://doi.org/10.1016/s0140-6736(01)06651-x

40. Merkow, R. P., Bilimoria, K. Y., Tomlinson, J. S., Paruch, J. L., Fleming, J. B., Talamonti, M. S., … & Bentrem, D. J. (2014). Postoperative complications reduce adjuvant chemotherapy use in resectable pancreatic cancer. Annals of Surgery, 260(2), 372-377. https://doi.org/10.1097/sla.0000000000000378

41. Conroy, T., Desseigne, F., Ychou, M., Bouché, O., Guimbaud, R., Bécouarn, Y., … & Ducreux, M. (2011). Folfirinox versus gemcitabine for metastatic pancreatic cancer. New England Journal of Medicine, 364(19), 1817-1825. https://doi.org/10.1056/nejmoa1011923

42. Moore, M. J., Goldstein, D., Hamm, J., Figer, A., Hecht, J. R., Gallinger, S., … & Parulekar, W. R. (2007). Erlotinib plus gemcitabine compared with gemcitabine alone in patients with advanced pancreatic cancer: a phase iii trial of the national cancer institute of canada clinical trials group. Journal of Clinical Oncology, 25(15), 1960-1966. https://doi.org/10.1200/jco.2006.07.9525

43. Gupta, N., Jangid, A. K., Singh, M., Pooja, D., & Kulhari, H. (2018). Designing two-dimensional nanosheets for improving drug delivery to fucose-receptor-overexpressing cancer cells. ChemMedChem, 13(24), 2644-2652.

https://doi.org/10.1002/cmdc.201800575

44. Ling, D., Xia, H., Park, W., Hackett, M., Song, C., Na, K., … & Hyeon, T. (2014). Ph-sensitive nanoformulated triptolide as a targeted therapeutic strategy for hepatocellular carcinoma. ACS Nano, 8(8), 8027-8039. https://doi.org/10.1021/nn502074x

45. Arosio, D., Casagrande, C., & Manzoni, L. (2012). Integrin-mediated drug delivery in cancer and cardiovascular diseases with peptide-functionalized nanoparticles. Current Medicinal Chemistry, 19(19), 3128-3151. https://doi.org/10.2174/092986712800784748

46. Chen, X., Li, D., Wang, H., Jiao, Y., Wang, H., Yu, Y., … & Zhi, J. (2016). Fabrication of an egf modified nanodiamonds-based anti-cancer drug targeted delivery system and drug carrier uptake visualization by 3d raman microscopy. RSC Advances, 6(50), 44543-44551. https://doi.org/10.1039/c6ra04753j

47. Zhang, X., Guo, S., Fan, R., Yu, M., Li, F., Zhu, C., … & Gan, Y. (2012). Dual-functional liposome for tumor targeting and overcoming multidrug resistance in hepatocellular carcinoma cells. Biomaterials, 33(29), 7103-7114. https://doi.org/10.1016/j.biomaterials.2012.06.048

48. Kulhari, H., Pooja, D., Shrivastava, S., Kuncha, M., Naidu, V., Bansal, V., … & Adams, D. J. (2016). Trastuzumab-grafted pamam dendrimers for the selective delivery of anticancer drugs to her2-positive breast cancer. Scientific Reports, 6(1). https://doi.org/10.1038/srep23179

49. Pooja, D., Kulhari, H., Kuncha, M., Rachamalla, S. S., Adams, D. J., Bansal, V., … & Sistla, R. (2016). Improving efficacy, oral bioavailability, and delivery of paclitaxel using protein-

grafted solid lipid nanoparticles. Molecular Pharmaceutics, 13(11), 3903-3912. https://doi.org/10.1021/acs.molpharmaceut.6b00691

50. Haltiwanger, R. S. (2009). Fucose is on the trail of colon cancer. Gastroenterology, 137(1), 36-39. https://doi.org/10.1053/j.gastro.2009.05.010

51. Yuan, K., Listinsky, C. M., Singh, R., Listinsky, J. J., & Siegal, G. P. (2008). Cell surface associated alpha-l-fucose moieties modulate human breast cancer neoplastic progression. Pathology &Amp; Oncology Research, 14(2), 145-156. https://doi.org/10.1007/s12253-008-9036-x

52. Liu, Y., Yen, H., Chen, C., Chen, C., Cheng, P., Juan, Y., … & Wong, C. (2011). Sialylation and fucosylation of epidermal growth factor receptor suppress its dimerization and activation in lung cancer cells. Proceedings of the National Academy of Sciences, 108(28), 11332-11337. https://doi.org/10.1073/pnas.1107385108

53. Mackinnon, W. B., Delbridge, L., Russell, P., Lean, C. L., May, G. L., Doran, S., … & Mountford, C. E. (1996). Two-dimensional proton magnetic resonance spectroscopy for tissue characterization of thyroid neoplasms. World Journal of Surgery, 20(7), 841-847. https://doi.org/10.1007/s002689900128

54. MacKinnon, W. B., Russell, P. J., May, G. L., & Mountford, C. E. (1995). Characterization of human ovarian epithelial tumors (ex vivo) by proton magnetic resonance spectroscopy. International Journal of Gynecological Cancer, 5(3), 211-221. https://doi.org/10.1046/j.1525-1438.1995.05030211.x

55. Hirakawa, M., Takimoto, R., Tamura, F., Yoshida, M., Ono, M., Murase, K., … & Kato, J.

(2013). Fucosylated tgf-β receptors transduces a signal for epithelial–mesenchymal transition in colorectal cancer cells. British Journal of Cancer, 110(1), 156-163. https://doi.org/10.1038/bjc.2013.699

56. Munkley, J. (2019). The glycosylation landscape of pancreatic cancer (review). Oncology Letters. https://doi.org/10.3892/ol.2019.9885

57. Sen-itiroh Hakomori, Reiji Kannagi, Glycosphingolipids as Tumor-Associated and Differentiation Markers, JNCI: Journal of the National Cancer Institute, Volume 71, Issue 2, August 1983, Pages 231–251, https://doi.org/10.1093/jnci/71.2.231

58. Sugano, K., Ohkura, H., Maruyama, T., Watanabe, M., Hirohashi, S., Shimosato, Y., … & Abe, O. (1988). Sandwich radioimmunometric assay with murine monoclonal antibody, ncc-st-439, for serological diagnosis of human cancers. Japanese Journal of Cancer Research, 79(5), 618-625. https://doi.org/10.1111/j.1349-7006.1988.tb00031.x

59. Hakomori, S. (1989). Aberrant glycosylation in tumors and tumor-associated carbohydrate antigens. Advances in Cancer Research, 257-331. https://doi.org/10.1016/s0065-230x(08)60215-8

60. Tajiri, M., Ohyama, C., & Wada, Y. (2007). Oligosaccharide profiles of the prostate specific antigen in free and complexed forms from the prostate cancer patient serum and in seminal plasma: a glycopeptide approach. Glycobiology, 18(1), 2-8. https://doi.org/10.1093/glycob/cwm117

61. Itzkowitz, S. H., Yuan, M., Ferrell, L. D., Ratcliffe, R. M., Chung, Y. S., Satake, K., Umeyama, K., Jones, R. T., & Kim, Y. S. (1987). Cancer-associated alterations of blood group antigen

expression in the human pancreas. Journal of the National Cancer Institute, 79(3), 425–434.

62. Luo, G., Guo, M., Jin, K., Liu, Z., Liu, C., He, C., … & Yu, X. (2016). Optimize ca19-9 in detecting pancreatic cancer by lewis and secretor genotyping. Pancreatology, 16(6), 1057-1062. https://doi.org/10.1016/j.pan.2016.09.013

63. Goonetilleke, K. and Siriwardena, A. K. (2007). Systematic review of carbohydrate antigen (ca 19-9) as a biochemical marker in the diagnosis of pancreatic cancer. European Journal of Surgical Oncology (EJSO), 33(3), 266-270. https://doi.org/10.1016/j.ejso.2006.10.004

64. Liang, C., Fukuda, T., Isaji, T., Duan, C., Song, W., Wang, Y., … & Gu, J. (2021). A1,6-fucosyltransferase contributes to cell migration and proliferation as well as to cancer stemness features in pancreatic carcinoma. Biochimica Et Biophysica Acta (BBA) - General Subjects, 1865(6), 129870. https://doi.org/10.1016/j.bbagen.2021.129870

65. Tonetti, M., Sturla, L., Bisso, A., Zanardi, D., Benatti, U., & Flora, A. D. (1998). The metabolism of 6-deoxyhexoses in bacterial and animal cells. Biochimie, 80(11), 923-931. https://doi.org/10.1016/s0300-9084(00)88889-6

66. Wiese, T. J., Dunlap, J. A., & Yorek, M. A. (1994). L-fucose is accumulated via a specific transport system in eukaryotic cells.. Journal of Biological Chemistry, 269(36), 22705-22711. https://doi.org/10.1016/s0021-9258(17)31703-9

67. Borbás, E., Sinkó, B., Tsinman, O., Tsinman, K., Kiserdei, É., Démuth, B., … & Nagy, Z. K. (2016). Investigation and mathematical description of the real driving force of passive transport of drug molecules from supersaturated solutions. Molecular Pharmaceutics,

13(11), 3816-3826. https://doi.org/10.1021/acs.molpharmaceut.6b00613

68. Manzanares, D. and Ceña, V. (2020). Endocytosis: the nanoparticle and submicron nanocompounds gateway into the cell. Pharmaceutics, 12(4), 371. https://doi.org/10.3390/pharmaceutics12040371

69. Hollenberg, M. D. (1985). Biochemical mechanisms of receptor regulation. Trends in Pharmacological Sciences, 6, 299-302. https://doi.org/10.1016/0165-6147(85)90137-3

70. Lai, W. H., Cameron, P., Wada, I., Doherty, J., Kay, D. G., Posner, B. I., … & Bergeron, J. (1989). Ligand-mediated internalization, recycling, and downregulation of the epidermal growth factor receptor in vivo.. The Journal of Cell Biology, 109(6), 2741-2749. https://doi.org/10.1083/jcb.109.6.2741

71. Foroozandeh, P. and Aziz, A. A. (2018). Insight into cellular uptake and intracellular trafficking of nanoparticles. Nanoscale Research Letters, 13(1). https://doi.org/10.1186/s11671-018-2728-6

72. Brown, V. I. and Greene, M. I. (1991). Molecular and cellular mechanisms of receptor-mediated endocytosis. DNA and Cell Biology, 10(6), 399-409. https://doi.org/10.1089/dna.1991.10.399

73. Popova, N. V., Deyev, I. E., & Petrenko, A. G. (2013). Clathrin-mediated endocytosis and adaptor proteins. Acta Naturae, 5(3), 62-73. https://doi.org/10.32607/20758251-2013-5-3-62-73

74. Geuze, H. J., Slot, J. W., Strous, G. J., Lodish, H. F., & Schwartz, A. L. (1983). Intracellular site of asialoglycoprotein receptor-ligand uncoupling: double-label immunoelectron microscopy during receptor-mediated endocytosis. Cell, 32(1), 277-287. https://doi.org/10.1016/0092-8674(83)90518-4

75. Brown, M. S., Anderson, R. G., & Goldstein, J. L. (1983). Recycling receptors: the round-trip itinerary of migrant membrane proteins. Cell, 32(3), 663-667. https://doi.org/10.1016/0092-8674(83)90052-1

76. Goldstein, J. L., Brown, M. S., Anderson, R. G., Russell, D. W., & Schneider, W. J. (1985). Receptor-mediated endocytosis: concepts emerging from the ldl receptor system. Annual Review of Cell Biology, 1(1), 1-39. https://doi.org/10.1146/annurev.cb.01.110185.000245

77. Mikhaĭlov V. I. (1989). Molekuliarnye mekhanizmy oposredovannogo retseptorami éndotsitoza i ikh ispol'zovanie dlia napravlennogo transport biologicheski aktivnykh soedineniĭ [Molecular mechanisms of receptor-mediated endocytosis and their use in directed transport of biologically active compounds]. Molekuliarnaia biologiia, 23(3), 639–651.

78. Shepherd, V. L. (1989). Intracellular pathways and mechanisms of sorting in receptor-mediated endocytosis. Trends in Pharmacological Sciences, 10(11), 458-462. https://doi.org/10.1016/s0165-6147(89)80011-2

79. Arkar, K., Sarkar, H. S., Kole, L., & Das, P. K. (1996). Receptor-mediated endocytosis of fucosylated neoglycoprotein by macrophages. Molecular and Cellular Biochemistry, 156(2), 109-116. https://doi.org/10.1007/bf00426332

80. Taylor, M. E., Conary, J. T., Lennartz, M. R., Stahl, P. D., & Drickamer, K. (1990). Primary structure of the mannose receptor contains multiple motifs resembling carbohydrate-recognition domains.. Journal of Biological Chemistry, 265(21), 12156-12162. https://doi.org/10.1016/s0021-9258(19)38325-5

81. Lobel, P., Fujimoto, K., Ye, R. D., Griffiths, G., & Kornfeld, S. (1989). Mutations in the cytoplasmic domain of the 275 kd mannose 6-phosphate receptor differentially alter lysosomal enzyme sorting and endocytosis. Cell, 57(5), 787-796. https://doi.org/10.1016/0092-8674(89)90793-9

82. Hertel, L. W., Boder, G. B., Kroin, J. S., Rinzel, S. M., Poore, G. A., Todd, G. C., & Grindey, G. B. (1990). Evaluation of the antitumor activity of gemcitabine (2',2'-difluoro-2'-deoxycytidine). Cancer research, 50(14), 4417–4422.

83. Huang, P., Chubb, S., Hertel, L. W., Grindey, G. B., & Plunkett, W. (1991). Action of 2',2'-difluorodeoxycytidine on DNA synthesis. Cancer research, 51(22), 6110–6117.

84. Berlin, J., Catalano, P. J., Thomas, J. P., Kugler, J. W., Haller, D. G., & Benson, A. B. (2002). Phase iii study of gemcitabine in combination with fluorouracil versus gemcitabine alone in patients with advanced pancreatic carcinoma: eastern cooperative oncology group trial e2297. Journal of Clinical Oncology, 20(15), 3270-3275. https://doi.org/10.1200/jco.2002.11.149

85. Lima, C. M. R., Green, M. R., Rotche, R., Miller, W. H., Jeffrey, G. M., Cisar, L. A., … & Miller, L. L. (2004). Irinotecan plus gemcitabine results in no survival advantage compared with gemcitabine monotherapy in patients with locally advanced or metastatic pancreatic cancer despite increased tumor response rate. Journal of Clinical Oncology, 22(18), 3776-3783. https://doi.org/10.1200/jco.2004.12.082

86. Louvet, C., Labianca, R., Hammel, P., Lledo, G., Braud, F. d., André, T., … & Gramont, A. d. (2004). Gemox (gemcitabine + oxaliplatin) versus gem (gemcitabine) in non resectable pancreatic adenocarcinoma : final results of the gercor /giscad intergroup phase iii. Journal of Clinical Oncology, 22(14_suppl), 4008-4008. https://doi.org/10.1200/jco.2004.22.90140.4008

87. Richards, D. A., Kindler, H. L., Oettle, H., Ramanathan, R., Laethem, J. V., Peeters, M., … & Hoff, D. V. (2004). A randomized phase iii study comparing gemcitabine + pemetrexed versus gemcitabine in patients with locally advanced and metastatic pancreas cancer. Journal of Clinical Oncology, 22(14_suppl), 4007-4007. https://doi.org/10.1200/jco.2004.22.90140.4007

88. Reilly, E. M. O., Abou-Alfa, G. K., Létourneau, R., Harker, W. G., Modiano, M., Hurwitz, H. I., … & Eckhardt, S. G. (2004). A randomized phase iii trial of dx-8951f (exatecan mesylate; dx) and gemcitabine (gem) vs. gemcitabine alone in advanced pancreatic cancer (apc). Journal of Clinical Oncology, 22(14_suppl), 4006-4006. https://doi.org/10.1200/jco.2004.22.90140.4006

89. Kim, M. P. and Gallick, G. E. (2008). Gemcitabine resistance in pancreatic cancer: picking the key players. Clinical Cancer Research, 14(5), 1284-1285. https://doi.org/10.1158/1078-0432.ccr-07-2247

90. Szakács, G., Paterson, J. K., Ludwig, J. A., Booth-Genthe, C., & Gottesman, M. M. (2006). Targeting multidrug resistance in cancer. Nature Reviews Drug Discovery, 5(3), 219-234. https://doi.org/10.1038/nrd1984

91. Spratlin, J. L., Sangha, R., Glubrecht, D., Dabbagh, L., Young, J., Dumontet, C., … & Mackey, J. R. (2004). The absence of human equilibrative nucleoside transporter 1 is associated with reduced survival in patients with gemcitabine-treated pancreas adenocarcinoma. Clinical Cancer Research, 10(20), 6956-6961. https://doi.org/10.1158/1078-0432.ccr-04-0224

92. Bhutia, Y. D., Hung, S. W., Patel, B., Lovin, D., & Govindarajan, R. (2011). Cnt1 expression influences proliferation and chemosensitivity in drug-resistant pancreatic cancer cells. Cancer Research, 71(5), 1825-1835. https://doi.org/10.1158/0008-5472.can-10-2736

93. Mackey, J. R., Yao, S. Y., Smith, K. M., Karpinski, E., Baldwin, S. A., Cass, C. E., … & Young, J. D. (1999). Gemcitabine transport in xenopus oocytes expressing recombinant plasma membrane mammalian nucleoside transporters. JNCI Journal of the National Cancer Institute, 91(21), 1876-1881. https://doi.org/10.1093/jnci/91.21.1876

94. Mini, E., Nobili, S., Caciagli, B., Landini, I., & Mazzei, T. (2006). Cellular pharmacology of gemcitabine. Annals of Oncology, 17, v7-v12. https://doi.org/10.1093/annonc/mdj941

95. Saiki, Y., Yoshino, Y., Fujimura, H., Manabe, T., Kudo, Y., Shimada, M., … & Horii, A. (2012). Dck is frequently inactivated in acquired gemcitabine-resistant human cancer cells. Biochemical and Biophysical Research Communications, 421(1), 98-104. https://doi.org/10.1016/j.bbrc.2012.03.122

96. Wang, C., Zhang, W., Fu, M., Yang, A., Huang, H., & Xie, J. (2014). Establishment of human pancreatic cancer gemcitabine-resistant cell line with ribonucleotide reductase overexpression. Oncology Reports, 33(1), 383-390. https://doi.org/10.3892/or.2014.3599

97. Ambudkar, S. V., Dey, S., Hrycyna, C. A., Ramachandra, M., Pastan, I., & Gottesman, M. M. (1999). Biochemical, cellular, and pharmacological aspects of the multidrug transporter. Annual Review of Pharmacology and Toxicology, 39(1), 361-398. https://doi.org/10.1146/annurev.pharmtox.39.1.361

98. Rudin, D., Li, L., Niu, N., Kalari, K. R., Gilbert, J. A., Ames, M. M., … & Wang, L. (2011). Gemcitabine cytotoxicity: interaction of efflux and deamination. Journal of Drug Metabolism &Amp; Toxicology, 02(01). https://doi.org/10.4172/2157-7609.1000107

99. Liu, D., Bu, H., Li, H., Chen, H., Guo, H., WANG, Z., … & Lin, S. (2011). Emodin reverses gemcitabine resistance in pancreatic cancer cells via the mitochondrial apoptosis pathway in vitro. International Journal of Oncology, 40(4), 1049-1057. https://doi.org/10.3892/ijo.2011.1285

100. Mullany, S. A., Svingen, P. A., Kaufmann, S. H., & Erlichman, C. (1998). Effect of adding the topoisomerase i poison 7-ethyl-10-hydroxycamptothecin (sn-38) to 5-fluorouracil and folinic acid in hct-8 cells: elevated dttp pools and enhanced cytotoxicity. Cancer Chemotherapy and Pharmacology, 42(5), 391-399. https://doi.org/10.1007/s002800050835

101. Li, J., Hou, N., Faried, A., Tsutsumi, S., Takeuchi, T., & Kuwano, H. (2008). Inhibition of autophagy by 3-ma enhances the effect of 5-fu-induced apoptosis in colon cancer cells. Annals of Surgical Oncology, 16(3), 761-771. https://doi.org/10.1245/s10434-008-0260-0

102. Pavillard, V., Formento, P., Rostagno, P., Formento, J., Fischel, J., Francoual, M., … & Milano, G. (1998). Combination of irinotecan (cpt11) and 5-fluorouracil with an analysis of cellular determinants of drug activity. Biochemical Pharmacology, 56(10), 1315-1322. https://doi.org/10.1016/s0006-2952(98)00205-6

103. Mans, D. R., Grivicich, I., Peters, G. J., & Schwartsmann, G. (1999). Sequence-dependent growth inhibition and dna damage formation by the irinotecan–5-fluorouracil combination in human colon carcinoma cell lines. European Journal of Cancer, 35(13), 1851-1861. https://doi.org/10.1016/s0959-8049(99)00222-1

104. Zeghari-Squalli, N., Raymond, E., Cvitkovic, E., & Goldwasser, F. (1999). Cellular pharmacology of the combination of the DNA topoisomerase I inhibitor SN-38 and the diaminocyclohexane platinum derivative oxaliplatin. Clinical cancer research : an official journal of the American Association for Cancer Research, 5(5), 1189–1196.

105. Ducreux, M., Mitry, E., Ould-Kaci, M., Boige, V., Seitz, J. F., Bugat, R., … & Rougier, P. (2004). Randomized phase ii study evaluating oxaliplatin alone, oxaliplatin combined with infusional 5-fu, and infusional 5-fu alone in advanced pancreatic carcinoma patients. Annals of Oncology, 15(3), 467-473. https://doi.org/10.1093/annonc/mdh098

106. Nishi, Y., Yamane, N., & Tanimoto, T. (2007). Preparation and characterization of 6I,6n-di-O-(l-fucopyranosyl)-β-cyclodextrin (n=II–IV) and investigation of their functions. Carbohydrate Research, 342(15), 2173–2181. https://doi.org/10.1016/j.carres.2007.06.016

107. Hattie, M., & Stubbs, K. A. (2020). Generalising a Simple Methodology for the Regioselective Anomeric Deacetylation of Carbohydrates. Chemistryselect, 5(2), 875–877. https://doi.org/10.1002/slct.201904343

108. Zou, J., Fan, J., He, X., Zhang, S., Wang, H., & Wooley, K. L. (2013). A facile glovebox-free strategy to significantly accelerate the syntheses of well-defined polypeptides by n-

carboxyanhydride (nca) ring-opening polymerizations. Macromolecules, 46(10), 4223-4226. https://doi.org/10.1021/ma4007939

109. Byrd, H., & McEwen, C. N. (2000). The Limitations of MALDI-TOF Mass Spectrometry in the Analysis of Wide Polydisperse Polymers. Analytical Chemistry, 72(19), 4568–4576. https://doi.org/10.1021/ac0002745

110. Montaudo, G., Montaudo, M. S., Puglisi, C., & Samperi, F. (1995). Characterization of polymers by matrix-assisted laser desorption/ionization time-of-flight mass spectrometry: Molecular weight estimates in samples of varying polydispersity. Rapid Communications in Mass Spectrometry, 9(5), 453–460. https://doi.org/10.1002/rcm.1290090514

111. Rashidzadeh, H., & Guo, B. (1998). Use of MALDI-TOF To Measure Molecular Weight Distributions of Polydisperse Poly(methyl methacrylate). Analytical Chemistry, 70(1), 131–135. https://doi.org/10.1021/ac970568z

112. pfizer. "DBLTMIRINOTECAN INJECTION CONCENTRATE." Pfizer, pfizer, Aug. 2001, labeling.pfizer.com/ShowLabeling.aspx?id=12202

113. "Choosing the Concentration Range for DLS Size Measurement." Www.horiba.com, www.horiba.com/int/scientific/technologies/dynamic-light-scattering-dls-particle-size-distribution-analysis/concentration-range-for-dls-size-measurement/.

114. Zürich, JKweb, Webdesign Basel &. "LS Instruments | Experimental Guidelines - DLS Sample Preparation." Lsinstruments.ch, lsinstruments.ch/en/theory/dynamic-light-scattering-dls/experimental-guidelines-dls-sample-preparation.

115. Etheridge, M. L., Campbell, S., Erdman, A. G., Haynes, C. L., Wolf, S. M., & McCullough, J. (2013). The big picture on nanomedicine: the state of investigational and approved nanomedicine products. Nanomedicine: Nanotechnology, Biology and Medicine, 9(1), 1-14. https://doi.org/10.1016/j.nano.2012.05.013

116. Bobo, D., Robinson, K. J., Islam, J., Thurecht, K. J., & Corrie, S. R. (2016). Nanoparticle-based medicines: a review of fda-approved materials and clinical trials to date. Pharmaceutical Research, 33(10), 2373-2387. https://doi.org/10.1007/s11095-016-1958-5

117. Ekladious, I., Colson, Y. L., & Grinstaff, M. W. (2018). Polymer–drug conjugate therapeutics: advances, insights and prospects. Nature Reviews Drug Discovery, 18(4), 273-294. https://doi.org/10.1038/s41573-018-0005-0

118. Choi, J., Kwak, S., Kang, S. G., Lee, S., Park, M., Lim, S. H., … & Hong, S. (2002). Synthesis of highly crosslinked monodisperse polymer particles: effect of reaction parameters on the size and size distribution. Journal of Polymer Science Part A: Polymer Chemistry, 40(23), 4368-4377. https://doi.org/10.1002/pola.10514

119. Weber, B., Seidl, C., Schwiertz, D., Scherer, M., Bleher, S., Süss, R., … & Barz, M. (2016). Polysarcosine-Based Lipids: From Lipopolypeptoid Micelles to Stealth-Like Lipids in Langmuir Blodgett Monolayers. Polymers, 8(12), 427. https://doi.org/10.3390/polym8120427

120. Maeda, H. (2001). The enhanced permeability and retention (epr) effect in tumor vasculature: the key role of tumor-selective macromolecular drug targeting. Advances in

Enzyme Regulation, 41(1), 189-207. https://doi.org/10.1016/s0065-2571(00)00013-3

121. Maeda, H., Wu, J., Sawa, T., Matsumura, Y., & Hori, K. (2000). Tumor vascular permeability and the epr effect in macromolecular therapeutics: a review. Journal of Controlled Release, 65(1-2), 271-284. https://doi.org/10.1016/s0168-3659(99)00248-5

122. Sherwood, L. M., Parris, E. E., & Folkman, J. (1971). Tumor angiogenesis: therapeutic implications. New England Journal of Medicine, 285(21), 1182-1186. https://doi.org/10.1056/nejm197111182852108

123. Yu, H., Rowley, J. V., Green, D. C., & Thornton, P. D. (2020). Fucose-modified thermoresponsive poly(2-hydroxypropyl methacrylate) nanoparticles for controlled doxorubicin release from an injectable depot. Materials Advances, 1(5), 1293-1300. https://doi.org/10.1039/d0ma00280a

124. Knysh, Alexander, et al. “Dynamic Light Scattering Analysis in Biomedical Research and Applications of Nanoparticles and Polymers.” Journal of Biomedical Photonics & Engineering, 30 May 2023, pp. 020203–020203, https://doi.org/10.18287/jbpe23.09.020203.

125. Zürich, JKweb, Webdesign Basel &. “LS Instruments | Experimental Guidelines - DLS Sample Preparation.” Lsinstruments.ch, lsinstruments.ch/en/theory/dynamic-light-scattering-dls/experimental-guidelines-dls-sample-preparation.

126. Dziendzikowska, K., Czerwińska, M., Grodzicki, W., Oczkowski, M., Królikowski, T., Gromadzka-Ostrowska, J., Męczyńska-Wielgosz, S., Sikorska, K., Kamola, D., Sapierzyński, R., & Kruszewski, M. (2026). Comparative impact of polystyrene, rice bag-derived high-

density polyethylene nanoparticles, and polystyrene–silver nanoparticle interactions in a 28-day in vivo study in male and female Wistar rats. Scientific Reports, 16(1). https://doi.org/10.1038/s41598-026-35219-9

127. Maherani, B., Arab-Tehrany, E., Mozafari, M. R., Gaïani, C., & Linder, M. (2011). Liposomes: a review of manufacturing techniques and targeting strategies. Current Nanoscience, 7(3), 436-452. https://doi.org/10.2174/157341311795542453

128. Niu, L. and Panyam, J. (2017). Freeze concentration-induced plga and polystyrene nanoparticle aggregation: imaging and rational design of lyoprotection. Journal of Controlled Release, 248, 125-132. https://doi.org/10.1016/j.jconrel.2017.01.019

129. Trenkenschuh, E. and Frieß, W. (2021). Freeze-drying of nanoparticles: how to overcome colloidal instability by formulation and process optimization. European Journal of Pharmaceutics and Biopharmaceutics, 165, 345-360. https://doi.org/10.1016/j.ejpb.2021.05.024

130. Breunig, M., Bauer, S. E., & Goepferich, A. (2008). Polymers and nanoparticles: intelligent tools for intracellular targeting?. European Journal of Pharmaceutics and Biopharmaceutics, 68(1), 112-128. https://doi.org/10.1016/j.ejpb.2007.06.010

131. Liu, X., Chen, Y., Li, H., Huang, N., Jin, Q., Ren, K., … & Ji, J. (2013). Enhanced retention and cellular uptake of nanoparticles in tumors by controlling their aggregation behavior. ACS Nano, 7(7), 6244-6257. https://doi.org/10.1021/nn402201w

132. Deshmukh, M., Chao, P., Kutscher, H. L., Gao, D., & Sinko, P. J. (2010). A series of α-amino acid ester prodrugs of camptothecin: in vitro hydrolysis and a549 human lung

carcinoma cell cytotoxicity. Journal of Medicinal Chemistry, 53(3), 1038-1047. https://doi.org/10.1021/jm901029n

133. Gref, R., Minamitake, Y., Peracchia, M. T., Trubetskoy, V. S., Torchilin, V. P., & Langer, R. (1994). Biodegradable long-circulating polymeric nanospheres. Science, 263(5153), 1600-1603. https://doi.org/10.1126/science.8128245

134. Jeong, Y., Cheon, J., Kim, S. H., Nah, J., Lee, Y. M., Sung, Y., … & Cho, C. (1998). Clonazepam release from core-shell type nanoparticles in vitro. Journal of Controlled Release, 51(2-3), 169-178. https://doi.org/10.1016/s0168-3659(97)00163-6

135. Dong, X., Hu, J., Zhu, J., Wang, S., Zhuo, R., & Zhang, X. (2016). A redox-responsive mesoporous silica nanoparticle with a therapeutic peptide shell for tumor targeting synergistic therapy. Nanoscale, 8(37), 16702-16709. https://doi.org/10.1039/c6nr04784j

136. Li, Y., Chen, M., Yao, B., Lu, X., Song, B., Vasilatos, S. N., ⋯ & Sun, L. (2020). Dual ph/ros-responsive nanoplatform with deep tumor penetration and self-amplified drug release for enhancing tumor chemotherapeutic efficacy. Small, 16(32). https://doi.org/10.1002/smll.202002188

137. Hatefi, A. and Amsden, B. G. (2002). Camptothecin delivery methods. Pharmaceutical Research, 19(10), 1389-1399. https://doi.org/10.1023/a:1020427227285

138. Drwal, M. N., Marinello, J., Manzo, S. G., Wakelin, L. P. G., Capranico, G., & Griffith, R. (2014). Novel dna topoisomerase iiα inhibitors from combined ligand- and structure-based virtual screening. PLoS ONE, 9(12), e114904. https://doi.org/10.1371/journal.pone.0114904

139. Pourquier, P. and Pommier, . (2001). Topoisomerase i-mediated dna damage. Advances in Cancer Research, 189-216. https://doi.org/10.1016/s0065-230x(01)80016-6

140. Suzuki, F., Fujiwara, Y., Hamura, R., Haruki, K., Sakamoto, T., Shiba, H., … & Yanaga, K. (2019). Combination of distance from superior mesenteric artery and serum ca19-9 as a novel prediction of local recurrence in patients with pancreatic cancer following resection. Anticancer Research, 39(3), 1469-1478. https://doi.org/10.21873/anticanres.13264

141. Ewton, D. Z., Hu, J., Vilenchik, M., Deng, X., Luk, K., Polonskaia, A., … & Friedman, E. (2011). Inactivation of mirk/dyrk1b kinase targets quiescent pancreatic cancer cells. Molecular Cancer Therapeutics, 10(11), 2104-2114. https://doi.org/10.1158/1535-7163.mct-11-0498

142. Hija, A., Salpeter, S. J., Klochendler, A., Grimsby, J., Brandeis, M., Gläser, B., … & Dor, Y. (2014). G0-g1 transition and the restriction point in pancreatic β-cells in vivo. Diabetes, 63(2), 578-584. https://doi.org/10.2337/db12-1035

143. Beretta, G. L., Gatti, L., Perego, P., & Zaffaroni, N. (2013). Camptothecin resistance in cancer: insights into the molecular mechanisms of a dna-damaging drug. Current Medicinal Chemistry, 20(12), 1541-1565. https://doi.org/10.2174/0929867311320120006

144. Potmesil M. (1994). Camptothecins: from bench research to hospital wards. Cancer research, 54(6), 1431–1439

145. Li, Y., Lin, B., Agadir, A., Liu, R., Dawson, M. I., Reed, J. C., … & Zhang, X. (1998). Molecular determinants of ahpn (cd437)-induced growth arrest and apoptosis in human lung cancer cell lines. Molecular and Cellular Biology, 18(8), 4719-4731. https://doi.org/10.1128/mcb.18.8.4719

146. Danaei, M., Dehghankhold, M., Ataei, S., Davarani, F. H., Javanmard, R., Dokhani, A., … & Mozafari, M. R. (2018). Impact of particle size and polydispersity index on the clinical applications of lipidic nanocarrier systems. Pharmaceutics, 10(2), 57. https://doi.org/10.3390/pharmaceutics10020057

147. Di, J., Gao, X., Du, Y., Zhang, H., Gao, J., & Zheng, A. (2021). Size, shape, charge and "stealthy" surface: carrier properties affect the drug circulation time in vivo. Asian Journal of Pharmaceutical Sciences, 16(4), 444-458. https://doi.org/10.1016/j.ajps.2020.07.005

148. Chen, S., Zhou, P., Yang, W., Hu, D., Chen, P., Sun, P., … & Fan, Q. (2023). Stealth-like polysarcosine-modified nanoparticles with low dye doses and long blood circulation for efficient breast cancer pulmonary metastasis imaging. Biomaterials Science, 11(13), 4644-4651. https://doi.org/10.1039/d3bm00200d

Chapter 4. Replacement of Amino Acid NCAs

4.1. Introduction

Triphosgene is widely employed in the synthesis of NCAs from amino acids [1], serving as a solid-phase alternative to phosgene, a highly toxic and volatile gas notorious for its historical use as a chemical weapon during warfare [2,3]. While triphosgene offers improved handling and stability, it decomposes into phosgene upon exposure to moisture or elevated temperatures [4]. This poses a significant safety concern, particularly when large-scale production is involved, where the risk of accidental phosgene release escalates dramatically. Given these hazards, there is a pressing need to develop safer synthetic routes for poly(amino acids). Moreover, reducing the use of pricy triphosgene in poly(amino acid) synthesis helps to bring down the economic cost to the product. Consequently, the ROP of amino acid 2,5-diketopiperazines (DKPs) and amino acid diketomorpholines (DKMs) or namely morpholine-2,5-dione were attempted. In all instance, the use of triphosgene in monomer synthesis is eliminated.

4.1.1. Amino Acid Diketopiperazines (DKPs)

Naturally occurring DKPs are head-to-tail cyclic dipeptide dimers formed through the condensation of two amino acids (Figure 4.1-1)[5]. They not only abound in nature fungi, bacteria, the plant kingdom, and mammals and are also frequently generated as unwanted byproducts or degradation products in the synthesis of polypeptides [5]. Their well-defined structure, ability to form multiple hydrogen bonds and binding to a wide range of receptors[5,6], and versatile functional groups make them valuable templates for enzyme inhibitors [7] and other biologically relevant applications [5].

Given the ring structure of amino acid DKPs could be a potential alternative to NCAs used in poly(amino acid) synthesis by ROP, also owing to their straightforward synthesis, lack of hazardous reagents, and reasonable yields. Unlike NCAs that rely on toxic or moisture-sensitive reactants, the DKP-based strategy provides a safer and more environmentally friendly route for the development of amino acid-derived polymer precursors. This makes DKPs an attractive candidate for further research in sustainable polymer synthesis. Despite

their potential as monomers for poly(amino acid) creation, ROP of amino acid DKPs remains largely unexplored, with only few reported studies in the literature published across more than half a century[8,9,10,11,12].

In this study, the feasibility of amino acid DKP ROP was assessed for their potential as an alternative to NCAs in poly(amino acid) synthesis, ultimately aiming to eliminate the need to use hazardous phosgenants in poly(amino acid).

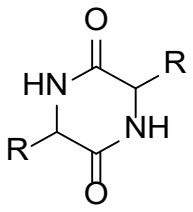

Figure 4.1-1. A representative structure of an amino acid DKP.

4.1.1.1. Synthesis of Amino Acid DKPs

Over the past century, numerous synthetic pathways have been developed for producing DKPs, which can be categorised into four primary methods: amide bond formation, N-alkylation, tandem cyclisation and C-acylation [5]. Among these, amide bond formation using dipeptides is the most widely adopted approach for DKP synthesis [5]. This method begins with the coupling of an N-protected α-amino acid and an α-amino acid ester to form a dipeptide, featuring an amine at one end and an ester at the other. Subsequent deprotection of the amino group triggers spontaneous cyclisation, substituting the ester group to form the DKP ring, while the reaction conditions depend on the protecting group and the ester group used (Scheme 4.1-1) [13,14,15].

In order to form DKPs, the amide bond must adopt a cis-orientation, which could be hindered by steric or electronic factors, leading to low cyclisation yields [5]. To overcome these challenges, techniques such as heating in acidic solution [13], or the use of base, which can cause racemisation of chiral material have been attempted [14]. Additionally, refluxing in high boiling solvents such as toluene or xylene for 24h [16] have been used to promote cyclisation.

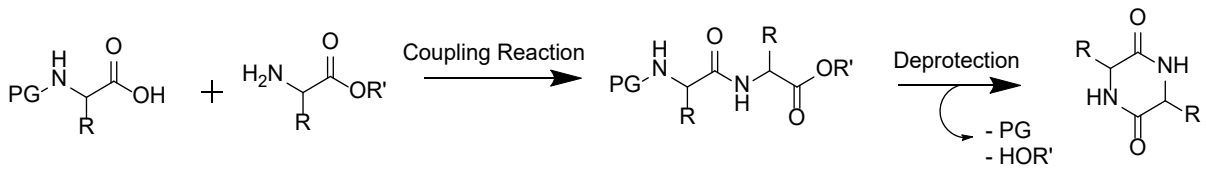

Scheme 4.1-1. General reaction scheme of DKPs via amide bond formation

However, owing to involvement of protection, esterification and deprotection steps prior or during the reaction, which reduce atom economy and require the inclusion of coupling agents such as DMAP, DCC, and EDC, reducing the process sustainability. These factors conflict with the goal of using DKPs for sustainable poly(amino acid) production. To address these concerns, this study employed thermal condensation of amino acid molecules in ethylene glycol or glycerol as a greener alternative for DKP synthesis [17].

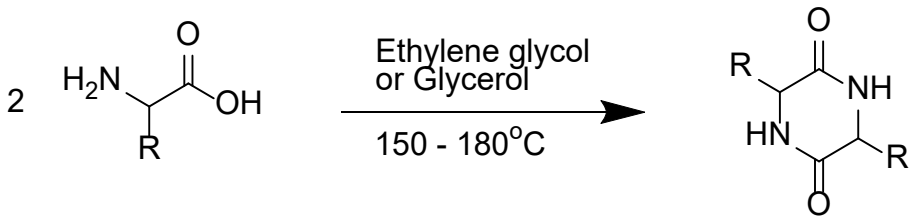

Scheme 4.1-2. Thermal condensation of amino acids

However, some DKPs cannot be synthesised via direct thermal condensation, particularly those containing protecting groups susceptible to thermolysis under high temperature[18]. For instance, Glu(OBzyl)-DKP synthesised in this study was produced via NHS/DCC coupling reaction [19]. In this approach, the carboxylate group is first activated through NHS-ester formation, followed by amine deprotection, which facilitates cyclisation by nucleophilic substitution at the NHS-ester [19].

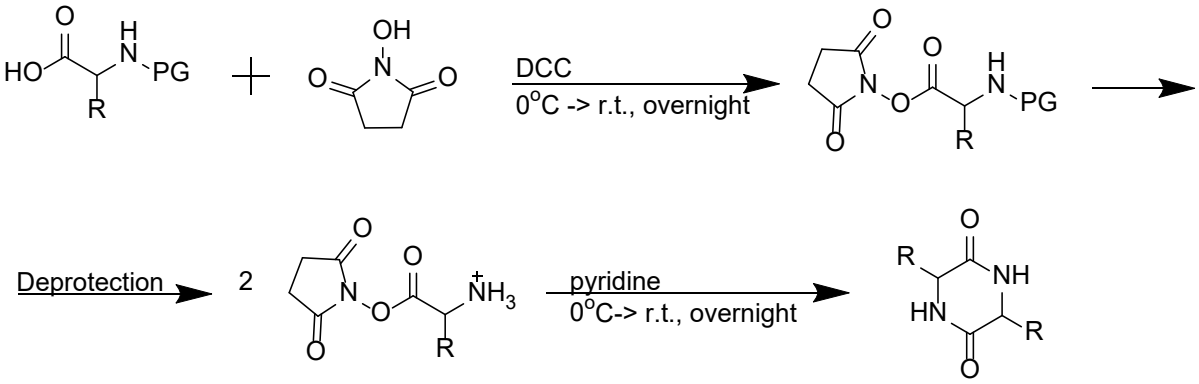

Scheme 4.1-3. NHS/DCC mediated DKP formation

4.1.1.2. Hypothesised Mechanism of ROP of Amino Acid DKPs

In 2022, a study demonstrated the successful oligomerisation of Ala-DKP using interfacial nano-pulsed discharge plasma [11,12], which generates highly reactive radical species or energetic photons that react with contacting materials [20,21,22]. Despite optimised conditions, this approach was limited to forming oligomers rather than longer polymer chains [12]. To address this limitation, this present research explored the use of various catalysts to facilitate the ROP of DKPs.

Given the structural similarities between DKPs, glycolides (or often referred as cyclic esters) and DKMs, catalysts designed for the ROP of these monomers may feasibly catalyse the ROP of DKPs (Figure 4.1-2). However, the application of these catalysts to break amide bonds in DKP ROP remains largely unexplored. Therefore, this study investigated the potential of catalysts originally developed for ester bond cleavage in the ROP of glycolides and DKMs to catalyse DKP ROP, aiming to achieve more effective polymerisation. Besides these, two additional catalysts, Ni(0)Cod_2:SIPr [23,24,25] and LiHMDS [26] that enable both transesterification and transamidation of amides species were also studied.

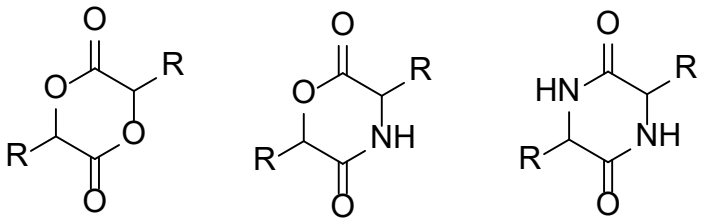

Figure 4.1-2. Glycolides (left), diketomorpholines (middle), amino acids DKPs (right)

4.1.1.2.1. MSA: DMAP Catalysed ROP Reaction

MSA: DMAP co- catalyst was reported for catalysing the ROP of cyclic ester at high temperature [27]. The usage of sole acid or base only result in their decomposition or evaporation at high temperatures, but the MSA:DMAP complex significantly enhances thermal stability, making it suitable for high temperature reactions such as ROP of cyclic ester and potentially DKPs [27].

There are two different mechanisms for the initiation of ROP lactide depending on the MSA: DMAP ratio. At a 1 : 1 ratio, conjugate acid of DMAP interacts with the carbonyl oxygen, while the conjugate base of MSA deprotonates the hydroxy initiator after nucleophilic addition (Scheme 4.1-4) [27]. The MSA:DMAP (1:1) demonstrated high catalytic efficiency in the ROP of L- lactide, achieving 99% of monomer conversion in just two hours [27].

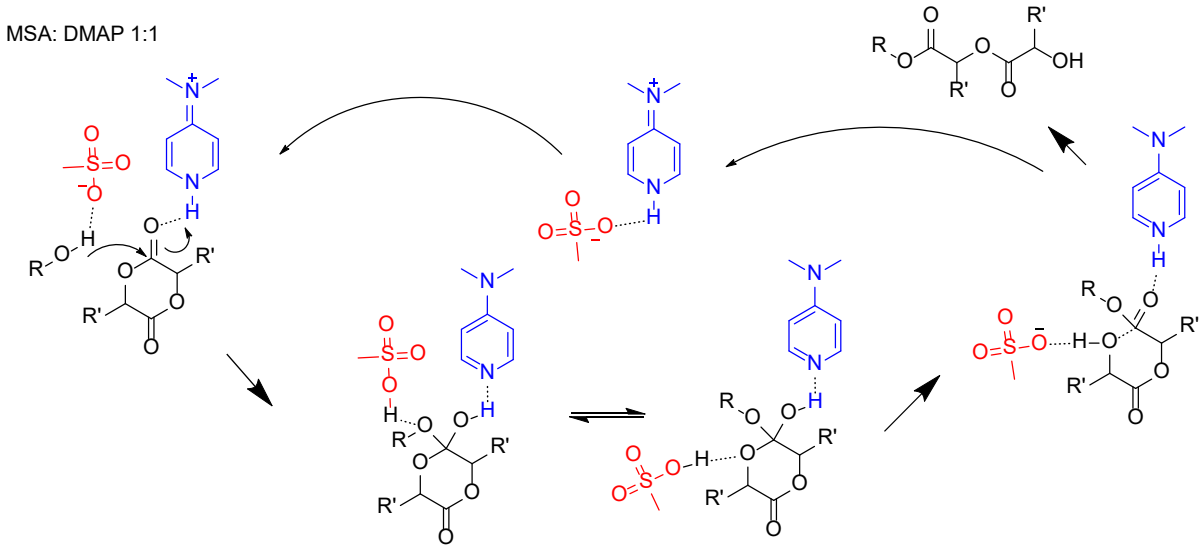

Scheme 4.1-4. Mechanism for the MSA: DMAP (1: 1) catalysed initiation of cyclic ester.

When the ratio is adjusted to 2:1 (MSA:DMAP), a more thermally stable catalyst complex forms, but the catalytic efficiency decreases, with L-lactide ROP reaching 97% monomer conversion only after 15 hours [27]. Although the catalytic mechanism remains similar to the 1:1 ratio (Scheme 4.1-5), their difference in reaction rate suggests MSA: DMAP (1:1) reduce the activation energy in initiation by a greater degree than that of MSA: DMAP [27]. However, a notable drawback of the 1:1 MSA: DMAP system is the high degree of

epimerisation observed during L-lactide ROP. To address this issue and explore their effectiveness, both 1:1 and 2:1 MSA: DMAP ratios were employed in this study to attempt the polymerisation of DKPs.

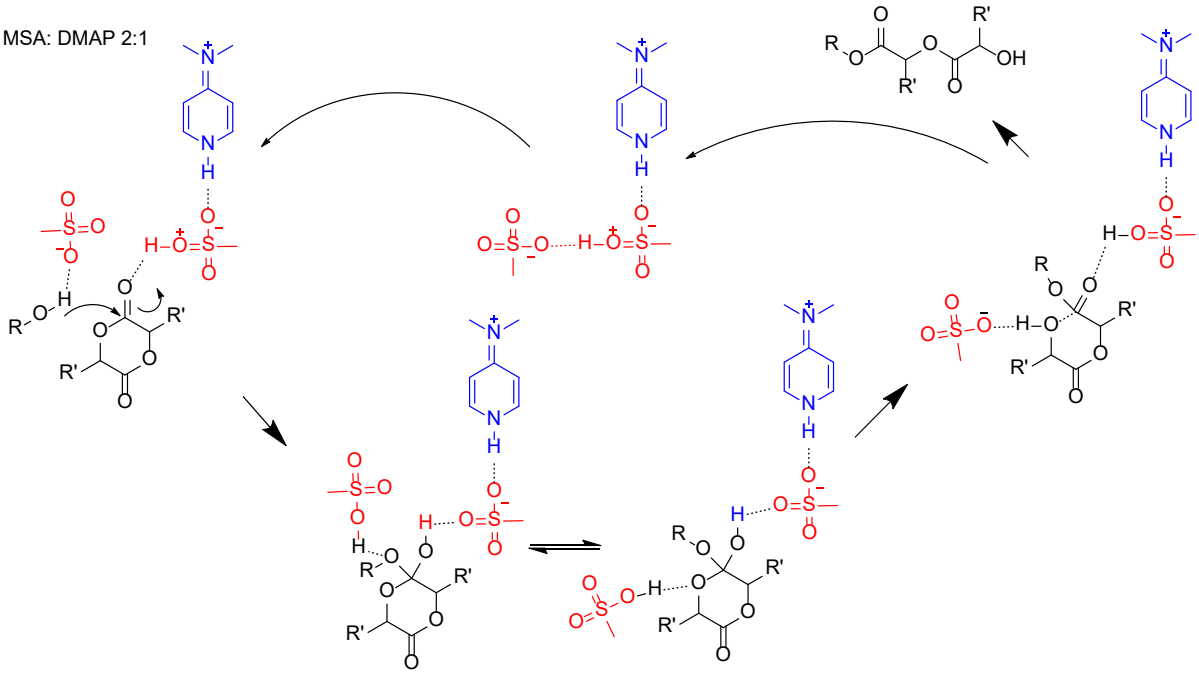

Scheme 4.1-5. Mechanism for the MSA: DMAP (2: 1) catalysed initiation of cyclic ester [27].

4.1.1.2.2. $Sn(Oct)_2$ Catalysed ROP Reaction

Organometallic catalysts are widely employed for efficient ROP to produce polymers with controlled molecular weights and narrow dispersity [28]. Among these, tin(II) 2-ethylhexanoate (Sn(Oct)2) (Figure 4.1-3), an FDA approved food grade catalyst, is frequently used to initiate the ROP of glycolides, yielding stereoregular polyesters with high molecular weights. [28,29].

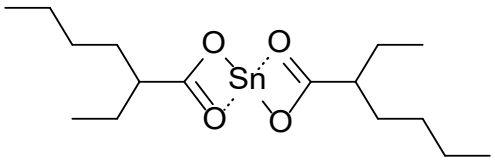

Figure 4.1-3. $Sn(Oct)_2$

$Sn(Oct)_2$ catalyse the ROP via coordination-insertion mechanism [30,31]. Prior to the actual ring-opening sequence, a stable complex was formed with alcohol coordinating to $Sn(Oct)_2$. The first step involved coordination of an alcohol to $Sn(Oct)_2$ forming **(1)** while simultaneously establishing a hydrogen bond with the carbonyl oxygen atom of the (Oct) ligand. A monomer then weakly complexes with this complex **(1)**, and the alcohol transforms into an alkoxy-type species via proton migration to the adjacent Oct ligand forming **(2)**. Followed by a nucleophilic attack by the hydroxy group on the monomer's carbonyl carbon, forming a new C-O bond, while the carbonyl oxygen coordinates to tin via an alkoxide bond through a four- centre transition state (**(3)** to **(4)**). The resulting carbonyl carbon adopts an sp^3 bonding geometry allowing for rotation around the C-O axis and positioning the endocyclic oxygen for ring opening. The ring-opening occurs via another four- centre transition state **(5)**, structurally similar to transition state **(3)**. And finally, a hydrogen transfer from the protonated (Oct)-H ligand to the ring opened monomer's end group, preserving its hydroxyl functionality and maintaining coordination with tin reaching a stable structure **(6)**, the analogue to species **(1)** (Scheme 4.1-6) [30].

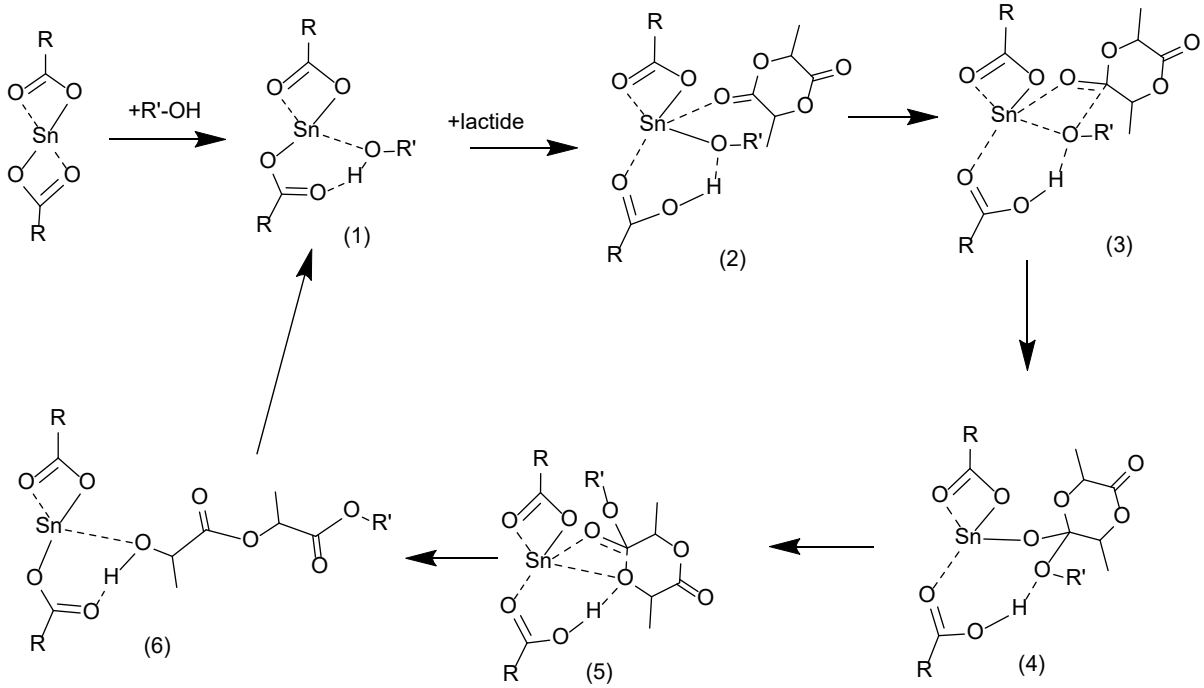

Scheme 4.1-6. Mechanism of $Sn(Oct)_2$ catalysed ROP of lactide [30].

However, applying $Sn(Oct)_2$ to the ROP of DKPs raises challenges, as the process involves amines as the sole nucleophiles for initiation and propagation, and the amide nitrogen in DKPs replaces the oxygen in cyclic esters. These differences cast doubt on whether the intermediates described in the $Sn(Oct)_2$ mechanism for cyclic esters apply to DKPs (Scheme 4.1-6). Consequently, this study experimentally investigated the applicability of $Sn(Oct)_2$ in catalysing DKP ROP.

4.1.1.2.3. DBU/ TBD Catalysed ROP Reaction

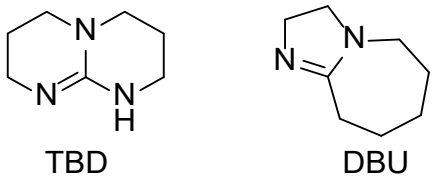

Figure 4.1-4. Chemical structure of TBD (left) and DBU (right)

Both 1,5,7-Triazabicyclo[4.4.0]dec-5-ene (TBD), and 1,8-diazabicyclo[5.4.0]- undec-7-ene (DBU) are effective organocatalysts for the ROP of cyclic esters such as lactide, valerolactone and caprolactone (Figure 4.1-4) [32]. Their catalytic effect in the ROP of cyclic esters was first reported in 2006 [32,33]. TBD can rapidly and controllably polymerise these monomers, while DBU polymerised lactide and with the addition of a thiourea catalyst extends its activity to the ROP of valerolactone and caprolactone [32]. Both catalysts yield polymers with high end-group fidelity, close agreement between theoretical and observed molecular weights, and a linear relationship between conversion and molecular weight [32]. The superior activity of TBD compared to DBU attributes to its bifunctionality, which allows simultaneous activation of the cyclic ester monomer and the alcohol group of the initiator/propagating species [32,34].

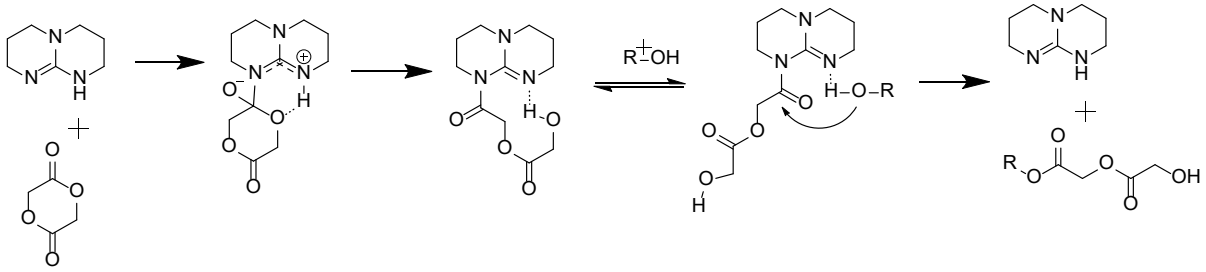

Scheme 4.1-7. Bifunctional nucleophilic mechanism of ROP of glycolide [34]

In TBD, the ROP of cyclic ester took place via a bifunctional nucleophilic mechanism [34]. The imine nitrogen of TBD nucleophilic attacks the carbonyl group of the monomer, forming an intermediate where the adjacent protonated nitrogen facilitates proton transfer to the resulting alkoxide, generating a TBD amide. Subsequently, hydrogen-bond activation of an incoming alcohol promotes esterification, releasing the ester and regenerating TBD [34]. This mechanism positions TBD as an efficient bifunctional transesterification catalyst, analogous to amino-thiourea systems below (Scheme 4.1-10)[32,34].

In contrast, DBU catalyses cyclic ester ROP through two competing pathways: the activated-alcohol pathway and the nucleophilic-attack pathway, which together provide a comprehensive understanding of the reaction network [33]. In the activated-alcohol pathway, DBU deprotonates the alcohol initiator, forming a hydrogen-bonded alkoxide that nucleophilic attacks the carbonyl carbon of the monomer, leading to ring opening (Scheme 4.1-8).

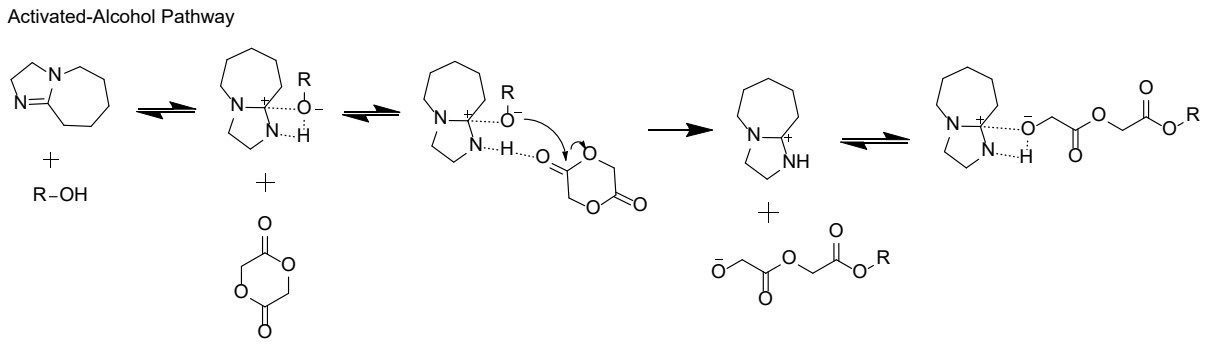

Scheme 4.1-8. DBU catalysed activated alcohol-initiated ROP glycolide by DBU [33]

The nucleophilic attack pathway was similar to that of TBD' s mechanism, where the imine nitrogen of DBU attacks the monomer's carbonyl, triggering ring-opening and forming an

alkoxide (Scheme 4.1-9). The chain propagation through nucleophilic attack by another ring opened monomer's alkoxide at the amide position, followed by intermolecular deprotonation, where a DBU hydrogen transfers to the alkoxide. The polymer chain was then cleaved from the DBU by an activated hydroxy group and regenerating DBU (Scheme 4.1-9).

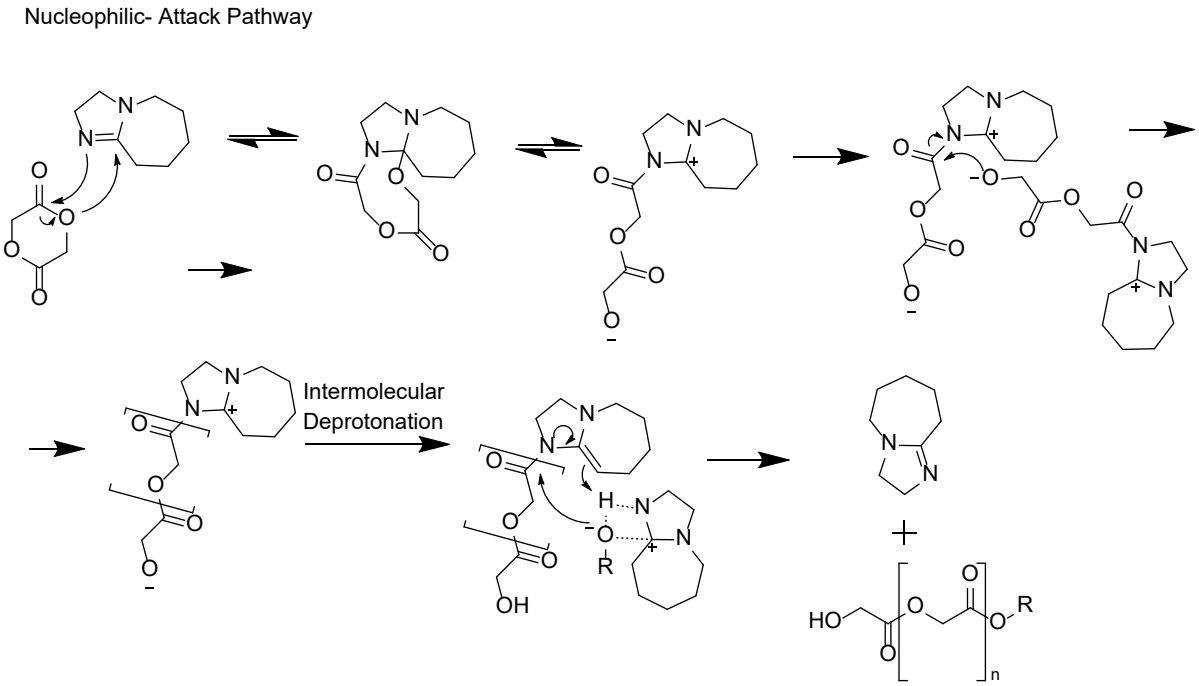

Scheme 4.1-9. DBU catalysed ROP of glycolide through nucleophilic attack pathway [33]

Compared to other catalysts, TBD and DBU possess greater possibility in catalysing the ROP of DKPs because their mechanisms involve both the formation and cleavage of amide bonds, whereas only ester bond cleavage was reported for other catalysts. Moreover, it has been reported that amine can serve as initiators in DBU catalysed ROP of cyclic esters[35], suggesting that the amine end group of ring-opened DKPs could participate in subsequent propagation steps. Consequently, this study explored the application of TBD and DBU in DKP polymerisation.

4.1.1.2.4. TBD: Thiourea Catalysed ROP Reaction

Thiourea derivatives have garnered significant attention in catalyst design in recent years [36]. They are known for displaying unique dual hydrogen-bond donor ability which plays a

pivotal role in catalysis [37,38]. This dual functionality enables thioureas to activate carbonyl and sulfoxide substrates, facilitating various stereoselective C-C bond forming reactions and other organic transformations [39,40,41]. Since the introduction of Takemoto's catalyst for the ROP of lactide in a well-controlled manner with high monomer conversion in 2005 [42]. Their ability to precisely control polymerisation and construct highly tailored polymers [43], has positioned thiourea catalysed ROP as a major catalytic method rivalling the efficiency and selectivity of traditional metal-based ROP [44,45].

The thiourea catalyse the ROP of cyclic ester through a hydrogen- bond activation mechanism. The two hydrogen- bond donors of the thiourea molecule activate the electrophilic carbonyl centre of the monomer via double hydrogen bonding (Scheme 4.1-10)[42,43]. While a H-bonding acceptor, a base, activates the initiator for a nucleophilic attack on the activated carbonyl [42,43]. This synergistic interplay between the thiourea and the base effectively activates both the monomer and initiator during ROP.

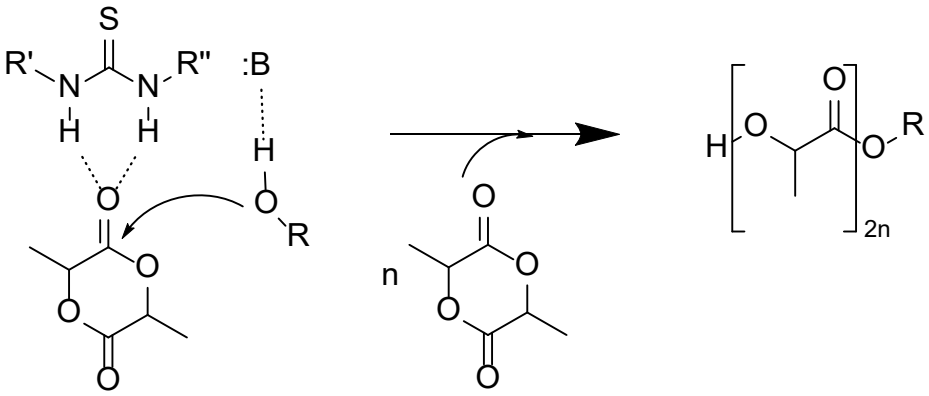

Scheme 4.1-10. Mechanism of thiourea catalysed ROP of lactide in the present of a base [42,43].

The catalytic effect of thiourea catalysts was further enhanced when paired with a strong base like TBD or DBU [46] or when alkoxides are used as initiators [47]. The strong base deprotonates the thiourea generating a thioimidate anion that activate both the alcohol initiator/chain end and the monomer. The nitrogen atom of the thioimidate forms a hydrogen bond with the alcohol, while the carbonyl of the monomer is activated through hydrogen bonding, resembling the bifunctional mechanism of TBD alone (Scheme 4.1-11) [32,46,47]. This activation enables an intramolecular nucleophilic attack that triggers ring-opening of the monomer [46,47].

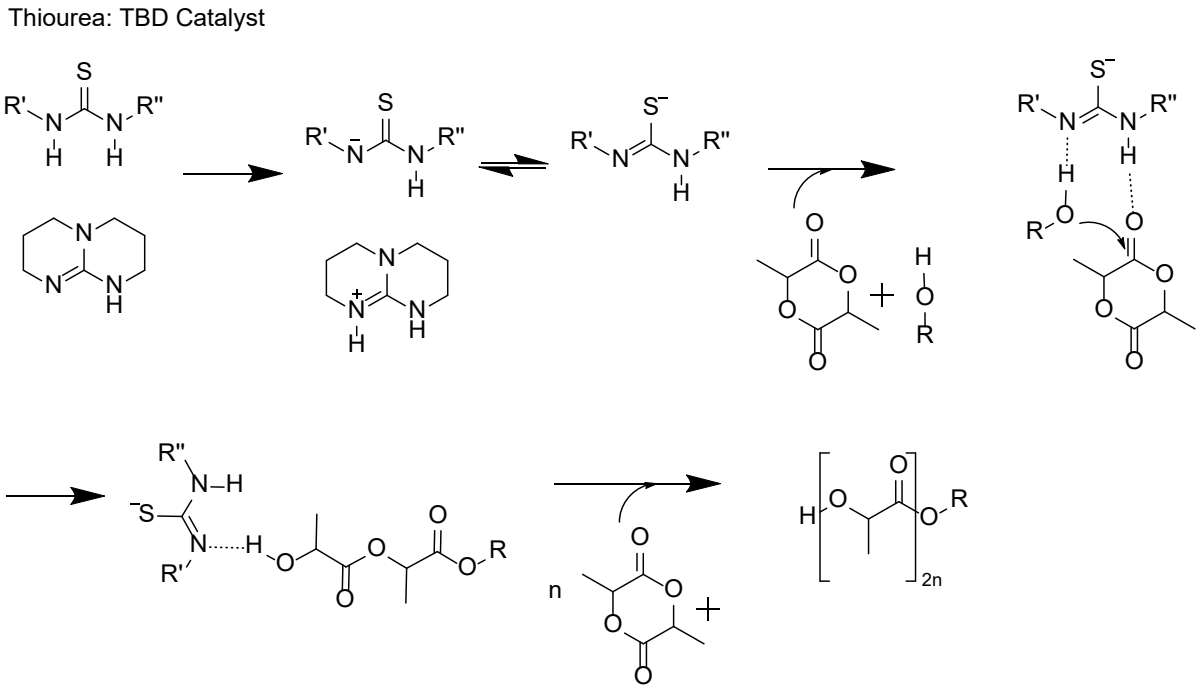

Scheme 4.1-11. Mechanism of TBD: thiourea catalysed ROP of lactide [32,46,47]

TBD: thiourea catalyst demonstrates exceptional efficiency, completing the ROP of lactide and different DKMs within hours with high monomer conversion and low dispersity at room temperature[46,47]. In contrast, other catalysts often require elevated temperatures and extended reaction times [27,28,29]. Therefore, due to its high catalytic effect in the ROP of cyclic ester, it is plausible to catalyse the ROP of DKPs if the amide nitrogen does not interfere with the catalytic system.

4.1.1.2.5. Ni(0)Cod_2 : SIPr Catalysed ROP Reaction

During initiation and propagation of ROP of DKPs, a secondary amide C-N bond needs to be cleaved followed by the formation of a new secondary amide C-N bond with an amine. However, the resonance stabilisation of amide creates a high activation energy barrier making C-N bond cleavage challenging (Figure 4.1-5)[48]. Thermodynamically, the conversion of a secondary amide to another amide is nearly thermoneutral and leading to equilibrium mixtures [48,49,50,51]. Consequently, secondary amide transamidation has remained largely underdeveloped for many years [23,24].

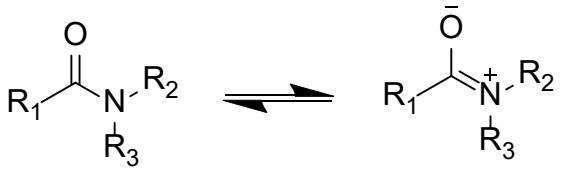

Figure 4.1-5. Amide resonance stabilisation [48]

In recent years, a two-step approach Ni-catalysed secondary amides transamidation was reported, surmounting both the kinetic and thermodynamic barriers of secondary amide transamidation (Scheme 4.1-12)[23,24,25]. In the first step, the secondary amide is N-functionalised with an electron-withdrawing group (Z), such as the Boc group [52], to weaken the acryl amide C-N bond [53,54,55,56,57]. In the second step, the N- activated amide **(2)** undergoes oxidative addition catalysed by Ni catalyst with the electron-rich SIPr ligand facilitating the formation of an intermediate **(3)** [24]. This intermediate is then intercepted by a primary or secondary amine to yield the desired product **(4)** [23,24,25]. The reaction is driven thermodynamically by the release of an amine bearing the electron-withdrawing group [25].

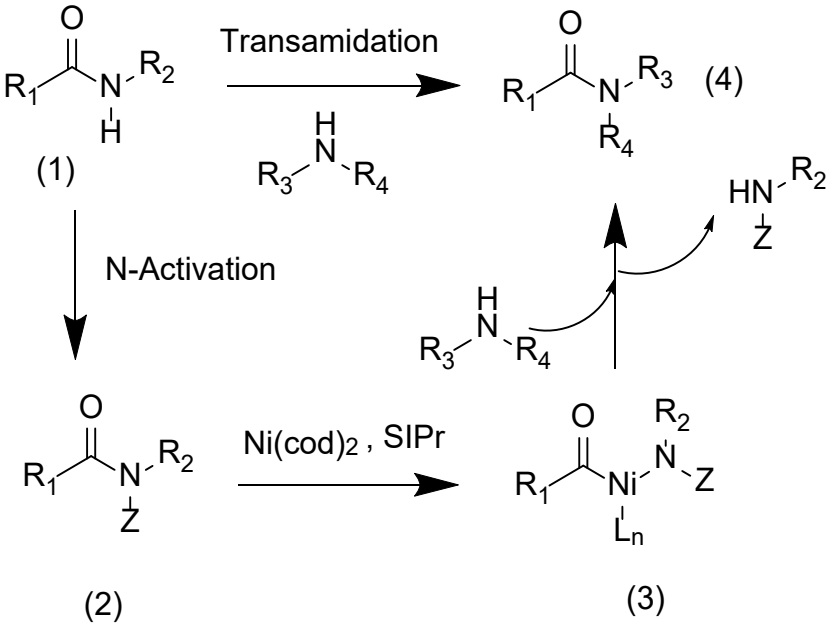

Scheme 4.1-12. Two-step approach to transamidation of secondary amides [23,24,25]

This Ni catalyst allows effective transamidation of various secondary amides without suffering from steric hindrance exerted by R_1 group [25], suggesting its potential applicability

to the ROP of DKPs with diverse side chains. This two- step Ni catalysed transamidation may allow the initiation/ propagation of DKPs, as a primary amine is used as initiator and propagate through the amine chain end. However, this approach requires prior activation of the amide with an electron-withdrawing group like Boc, as a result ROP of Sar-DKP is excluded from the methodology. However, given the reported Ni-SIPr catalysed transamidation reactions were carried out in mild conditions[23,24,25], intense heating may forcibly promote oxidative addition of the catalysed to the Sar-DKP's amide bond. Furthermore, Moreover, the presence of the electron-withdrawing Boc group on ring-opened DKPs prevents their participation in subsequent propagation steps, necessitating a simultaneous deprotection reaction in the same reaction mixture. This additional step complicating the reaction producing a mixture of poly(amino acid), and the DKP or the deprotection agents simply kill the catalyst.

Further challenges arise from the practical handling of the Ni catalyst. The $Ni(cod)_2$ requires glovebox handling and the ligand SIPr is unstable to benchtop conditions [25]. Although the more stable SIPr. HCl was used in this study, handling $Ni(cod)_2$ outside a glovebox introduces uncertainties that could affect the reliability of DKP ROP reactions.

4.1.1.2.6. LiHMDS Catalysed ROP Reaction

Lithium bis(trimethylsilyl)amide (LiHMDS) is a non-transition metal catalyst for the transamidation of amides and amidation of esters by highly selective acyl cleavage with non-nucleophilic amines at room temperature (Figure 4.1-6). Unlike the expensive, toxic and sensitive transition metal catalyst such the $Ni(cod)_2$: SIPr catalyst, LiHMDS offers a cost-effective, straightforward, safer, and robust alternative for amidation reactions [26]. This mild, transition-metal-free protocol demonstrates remarkable versatility, successfully transamidation of a wide range of non-nucleophilic amines and amides, including electronically diverse and sterically hindered anilines [26]. Notably, the reaction accommodates a wide range of challenging and sensitive substrates that are incompatible or problematic with metal-catalysed and high temperature protocols, including esters, halides, heterocycles, highly electron-deficient arenes as well as N,N-disubstituted anilines and deactivated aliphatic amines [26]. Additionally, LiHMDS effectively catalyse a broad spectrum

of amides, including aliphatic amides with linear, branched, or sterically hindered α-carbons, without the need for extensive ligand or reaction condition optimisation required by transition metal catalysed approaches, marking a significant advantage. [24,26].

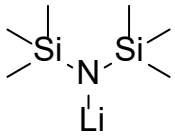

Figure 4.1-6. Chemistry structure of LiHMDS

However, applying LiHMDS to the ROP of DKPs still encounters similar challenges as the Ni catalyst. The reaction still follows the two- step transamidation pathway and require amide activation with an electron-withdrawing Boc group to weaken the amide bond. This inhibits subsequent propagation, necessitating a simultaneous deprotection of Boc group in the same reaction mixture and consequently resulted in a mixture of poly(amino acid) and DKP by this uncontrollable ROP reaction. Despite these challenges, LiHMDS offers a practical advantage over the $Ni(cod)_2$:SIPr catalyst due to its greater chemical stability, which simplifies handling and eliminates the need for stringent conditions like glovebox operations.

4.1.2. Amino acid Polydepsipeptides

Amino acid DKMs (Figure 4.1-7) derivatives have an ester group and an amide group in one 6-membered ring, are formally cyclic dimers of an α-hydroxyacid and an α-amino acid and are the simplest cyclic depsipeptides [58]. They are naturally occurring depsipeptides and could be found in flowers [59], mushrooms [60,61], sea cucumbers [62], bacteria [63], and algae [64] and in earth samples [65]. DKMs play a role as intermediates in the synthesis of optic active α-amino acids, also act as monomers for synthesis of polydepsipeptides also called as poly(ester amide) and their random copolymers or block copolymers with high molecular weight through ROP [18,43,46,58,66,67,68,69]. Polydepsipeptides consist of alternating copolymers of amino acids and hydroxy acids, integrating the properties of both amino acids and hydroxy acids[18,70,71]. Similar to poly(amino acids), polydepsipeptides yields versatile materials that combine desirable attributes such as biocompatibility, biodegradability, and favourable mechanical properties depends on the sidechain of the amino acid or the hydroxy acid used [71,72].

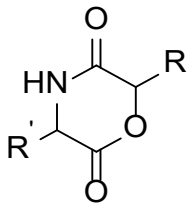

Figure 4.1-7. Amino acid DKM

One of the most critical attributes of polydepsipeptides is their exceptional biocompatibility, making them highly suitable for biomedical applications [72,73,74]. Studies have demonstrated that these polymers exhibit low toxicity and excellent tolerance in both *in vitro* and *in vivo* environments [72,73,74]. This inherent biocompatibility is a key advantage over other synthetic polymers with similar properties towards poly(amino acids), particularly in drug delivery[71,72,76,77,78,79] and tissue engineering[80,81,82,83]. A distinctive feature of polydepsipeptides is their unique degradation profile, which contributes to their improved biocompatibility. Unlike polyesters which produce acidic byproducts, polydepsipeptides degrade into both acidic and basic compounds, which naturally neutralise each other, preventing local acidosis and minimising tissue irritation[58,73,84,85].

Additionally, polydepsipeptides are designed to be biodegradable. The presence of ester linkages contributes to a controlled degradation process[86], which is crucial in medical applications where materials must gradually break down and be replaced by natural tissues[72]. Unlike traditional poly(amino acids), which often have limited degradation rate[7,18,70], polydepsipeptides possess hydrolysable ester and peptide bond in their main chain resulting relatively good thermal and mechanical properties with controllable degradation rate[71,86]. As a result, they present a significant advantage over many conventional synthetic polymers.

In summary, the biocompatibility, biodegradability, and favourable mechanical properties making polydepsipeptides as promising candidates for biomedical applications. Furthermore, they present a compelling alternative to poly(amino acids) and their precursors- amino acid NCAs. Thereby potentially eliminate the need for hazardous phosgene derivatives, offering a safer and more sustainable approach to polymer synthesis.

4.1.2.1. Synthesis of Amino Acid DKMs

DKM derivatives were generally synthesised by three major procedures (Scheme 4.1-13)[58,86]. **(A)** Cyclisation of N-(α-haloacyl)-α-amino acid salts, **(B)** Intramolecular transesterification of N-(α-hydroxyacyl)-α-amino acid esters and **(C)** Cyclisation of O-(α-aminoacyl)-α hydroxycarboxylic acids [74,58,86].

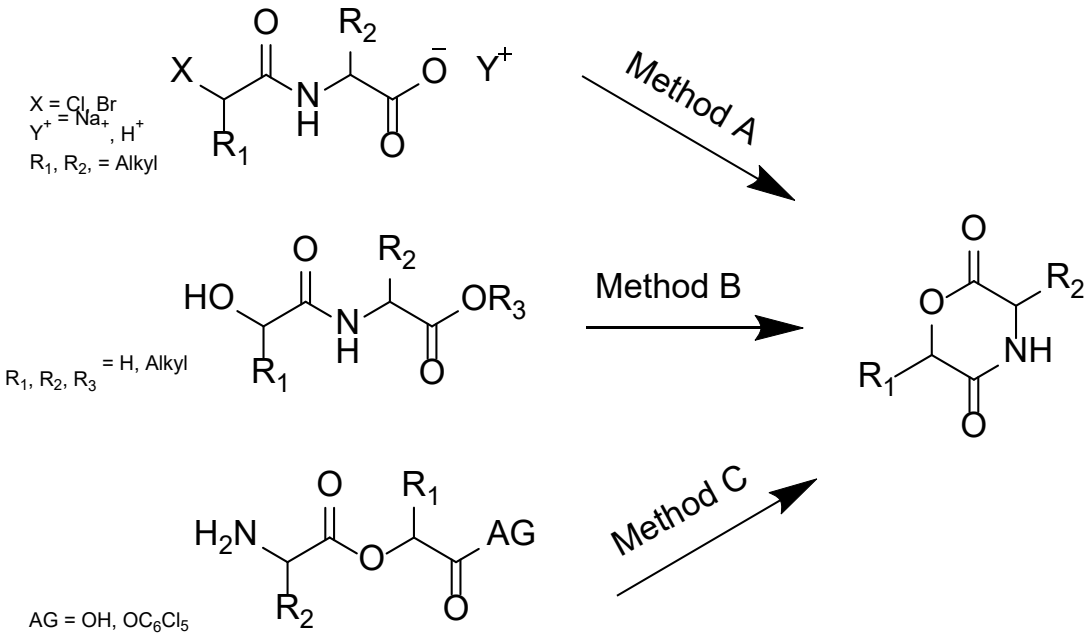

Scheme 4.1-13. Synthesis methods of DKM derivatives [58,86].

Method A: Cyclisation of N-(α-haloacyl)-α-amino acid salts

The starting materials N-(α-haloacyl)-α-amino acids and N-(α-halopropionyl)-α-amino acids were prepared in high yields by acylation of amino acids with bromopropionyl bromide or chloroacetyl chloride under Schotten Baumann reaction conditions [58,86]. Synthesis of 6-methylmorpholine-2,5-dione via heating of N-(2-bromopropionyl)-glycine sodium salt was first reported in 1943 [87]. And many DKMs have been synthesised by this method [88,89,90,91].

The cyclisation of N-(α-haloacyl)-α-amino acids and N-(α-halopropionyl)-α-amino acids was carried out in highly diluted DMF solution with triethylamine, NaOH, Na_2CO_3, or $NaHCO_3$ to neutralise the acid generated [87,88,89,91,92]. The cyclisation reaction goes through an

intramolecular S_N reaction mechanism which result in racemisation when optically active monomers were used [74,58,86]. Additionally, intermolecular reaction competes with cyclisation forming linear oligomers reducing the yield of DKMs. Despite these, this method still provides a higher yield compared to others [74]. However, synthesising DKMs with protected functional groups were via this method results in lower yields due to the thermolysis of the protecting groups [18,58].

Method B: Intramolecular transesterification of N-(α-hydroxyacyl)-α-amino acid esters

The synthesis of DKM via intramolecular transesterification in high yield in a highly diluted solution was first reported in 1982 by Hartwig and Schoellkopf [93]. The cyclisation reaction involves an intramolecular esterification mechanism that typically preserves stereochemistry at the C6 position of DKMs, as no nucleophilic attack occurs at this stereocentre [58]. But racemisation can occur under high-temperature conditions [94]. The cyclisation of N-(α-hydroxyacyl)-α-amino acid esters can be performed in four different ways. The acid catalysed esterification reaction using p-toluenesulfonic acid, MSA or trifluoromethanesulfonic acid [95]. Cyclisation by carbonyl diimidazole gave a quantitative yield yet the purification is tedious and results in large product losses [95]. Cyclisation Using Mitsunobu conditions with diethyl azodicarboxylate and triphenylphosphine [96]. While the simplest and the most effective cyclisation method was using reduced pressure and elevated temperature [95].

Method C: Cyclisation of O-(α-aminoacyl)-α-hydroxycarboxylic acids

The cyclisation of O-(α-aminoacyl)-α-hydroxycarboxylic acids relies on intramolecular amidation showed the lowest yields with racemisation observed at both C3 and C6 stereocentres [74,92]. However, significant improvements were made decades later by employing UV light irradiation (>290 nm) on O-(α-aminoacyl)-α-hydroxycarboxylic acids linked to a photolabile group [58,97]. The UV light triggers nucleophilic cleavage at the carboxyl site, forming an amide bond resulting in release of a DKM in high yield and purity, overcoming earlier limitations of this approach[97].

In this research, different methods were used to produce 4-methylmorpholine-2,5-dione (Sar-GA DKM), a DKM that consists of sarcosine and glycolic acid, which has not been

reported. Therefore, its synthesis was performed through different methods for optimisation. While benzyl 3-(2,5-dioxomorpholin-3-yl)propanoate (Glu(OBzyl)-GA DKM), a DKM that consist of Glu(OBzyl) and glycolic acid, was produced via method A as descript literature [18].

4.1.2.2. ROP of Amino Acid DKMs

The ROP of Amino acid DKMs is widely developed, and because DKMs contain a cyclic ester group, catalysts and methods for the ROP of cyclic esters also able to be used in DKMs' ROP including MSA: DMAP [27], $Sn(Oct)_2$ [30,31], DBU [32], TBD [32] and TBD: thiourea [46] those introduced above. But given the superior catalytic effect of TBD: thiourea, it was primarily tested in the ROP of Glu(OBzyl)-GA DKM and Sar-GA DKM.

4.2. Experimental

4.2.1. Diketopiperazine (DKP) Synthesis

4.2.1.1. Synthesis of Sar-DKP

Sarcosine (10.0 g, 0.112 mol) was added into an RB flask equipped with an air condenser. Ethylene glycol (100.0 mL) was added into the reaction flask followed by heating at 170 ^{o}C overnight under strong nitrogen flow into the system. The nitrogen flow can prevent the oxidisation of sarcosine and side reactions and drive the reaction to completion by removing the water steam generated during reaction. The solution was turned into clear yellow solution after the reaction. The solution was allowed to cool to room temperature before liquid- liquid extraction was performed. The crude product was extracted by DCM (25.0 mL x 4) and dried with anhydrous $MgSO_4$ and was later filtered followed by removal of DCM and yellow solid was obtained. The crude product was purified by hot recrystallisation in methanol then dried in vacuum overnight. The purified product was needle like white crystal. Yield: 80 %

^{1}H-NMR spectrum (400 MHz, $CDCl_3$) of Sar-DKP: 3.97 ppm (-CH_2-), 2.97 ppm (-CH_3) (Figure *4.3-3*)

4.2.1.2. Synthesis of Ala-DKP

Alanine (10.0 g, 0.112 mol) was added into an RB flask equipped with an air condenser. Ethylene glycol (100.0 mL) was added into the reaction flask followed by heating at 170 ^{o}C overnight under strong nitrogen flow into the system. The nitrogen flow can protect alanine from oxidisation and side reactions and drive the reaction to completion by blowing out the water vapour generated. The solution became a clear yellow solution after the reaction. Upon cooling to room temperature, and then in an ice bath, crystallisation of alanine DKP occurred. A small amount of 1,4-dioxane was added into the mixture to reduce the viscosity before suction filtration was done. The crude product was then washed with ice cold methanol and was later purified by hot recrystallisation in methanol then dried in vacuum overnight. The purified product were white crystals. Yield: 84%

^{1}H-NMR spectrum (400 MHz, DMSO-d_6) of Ala-DKP: 8.07 ppm (-NH-), 3.87 ppm (-N-CH-), 1.25 ppm (-CH_3) (Figure *4.3-6*)

^{13}C-NMR spectrum (100 MHz, DMSO-d_6) of Ala-DKP: 169.05 ppm (C1, C4), 49.76 ppm (C5,C2), 19.94 ppm (C9,C10) (Figure 4.3-7)

4.2.1.2.1. Boc activation of Ala-DKP

Ala-DKP (1.0 g, 7.03 mmol, 1.0 eqv) and DMAP (0.043 g, 0.352 mmol, 0.05 eqv) were added to an RB flask. The reaction vessel was purged with nitrogen three times over 15 minutes. Subsequently, 100.0 mL of anhydrous DMF was added, and the mixture was heated to 50°C until the Ala-DKP completely dissolved. Then, Boc_2O (1.84 g, 8.44 mmol, 1.2 eqv) in 20.0 mL anhydrous DMF was added in one portion to the reaction mixture, and the reaction was stirred overnight at 50°C under a nitrogen atmosphere. Following completion of the reaction, diethyl ether was added to the mixture to precipitate out unreacted Ala-DKP, which was removed by filtration. The filtrate was then evaporated under a nitrogen stream. The resulting crude product was purified by chromatography, eluent: ethyl acetate: hexane 3:7, Rf: 0.33. Finally, the product was dried under vacuum, yielding a purified white crystalline solid. Yield: 59%.

^{1}H-NMR spectrum (400 MHz, DMSO-d_6) of Boc modified Ala-DKP: 8.12 ppm (-NH-), 4.64 ppm (CH_3-C**H**-), 1.50-1.43 ppm (-O-C-(C**H$_3$**)$_3$) (Figure *4.3-9*)

4.2.1.3. Synthesis of Glu(OtBu)-DKP

L-Glutamic Acid 5-tert-butyl Ester (1.0 g, 4.9 mmol) was added into an RB flask connected with an air condenser. Exchange gas with nitrogen then DMF (10.0 mL) was added into the reaction flask followed by heating at 160 ^{o}C overnight. The solution was turned into clear yellow solution after the reaction. The solution was allowed to cool to room temperature then dried under nitrogen flow and yellow thick oily paste was obtained. Crystals formed after placing the crude product in open air at room temperature for two days. The crude product was collected by suction filtration and washed with cold acetone. And purified by hot recrystallisation in methanol and dried in vacuum overnight. The purified product was off white solid. Yield: trace amount.

^{1}H-NMR spectrum (400 MHz, DMSO-d_6, ppm) of Glu-DKP: 12.73 ppm (-COOH), 7.89 ppm (-NH-), 4.07 ppm (-N-CH-C=O), 2.31-1.96 ppm (-C**H$_2$**-C**H$_2$**-) (Figure *4.3-11*)

^{13}C-NMR spectrum (100 MHz, DMSO-d_6) of Glu-DKP: 176.98 ppm & 174.49 ppm (C13,C15 & C1, C4), 54.80 ppm (C2, C5), 29.08 ppm & 24.63 ppm (C9-C12) (Figure 4.3-12)

4.2.1.4. Synthesis of Glu(OBzyl)-DKP

Boc-Glu(OBzyl)-OH (5.0 g, 14.8 mmol, 1.0 eqv) and NHS (2.0 g, 17.8 mmol, 1.2 eqv) were placed in an RB flask and purged with nitrogen three times for 15 minutes each. The mixture was then dissolved in 100.0 mL of anhydrous acetonitrile. Meanwhile, DCC (3.7 g, 17.8 mmol, 1.2 eqv) was dissolved in 20.0 mL of anhydrous acetonitrile and added dropwise to the reaction mixture over 30 minutes at 0 °C under constant stirring. The reaction was gradually allowed to reach room temperature and stirred overnight. After completion, the solution was filtered by gravity to remove the by-product and concentrated by rotary evaporation. The crude product was dissolved in 20.0 mL of anhydrous ethyl acetate, cooled in an ice bath for 30 minutes, and filtered again. This process was repeated three times. Subsequently, 10.0 mL of TFA was added dropwise to the concentrated crude product in an ice bath over 30 minutes with constant stirring. After 2 hours, the reaction solution was evaporated under vacuum. The crude product was then dissolved in 5.0 mL of anhydrous

DMF, and 100.0 mL of pyridine was added dropwise at 0 °C, with the reaction left overnight. Afterward, the solution was evaporated under vacuum, and the crude product crystallised out upon the addition of a small amount of ethyl acetate, which was collected by filtration. The product was further purified by recrystallisation in methanol. Yield: 15%.

^{1}H-NMR spectrum (400 MHz, DMSO-d_6) of Glu(OBzyl)-DKP. 8.22 ppm (-NH-), 7.36 ppm (OBzyl), 5.08 ppm (-O-CH_2-), 3.90 ppm (-N-CH-C=O), 2.45-1.92 ppm (-C**H$_2$**-C**H$_2$**-) (Figure *4.3-14*)

4.2.1.5. Synthesis of Lys(Cbz)-DKP

The synthesis of Lys(Cbz)-DKP is the same as above but with Boc-Lys(Cbz)-OH. Yield: 40%

^{1}H-NMR spectrum (400 MHz, DMSO-d_6) of Lys(Cbz)-DKP: 8.09 ppm (-NH-), 7.34 ppm (phenyl ring), 5.0 ppm (-O-CH_2-), 3.79 ppm (-N-CH-C=O), 2.98 ppm (-C**H$_2$**-C**H$_2$**-NH-), 1.67-1.31 ppm (-CH-C**H$_2$**-C**H$_2$**-) (Figure 4.3-16)

DEPT-135 (100 MHz, DMSO-d_6) of Lys(Cbz)-DKP: 128.07 ppm & 127.46 ppm (aromatic carbons), 64.83 ppm (CH_2-Ph), 53.62 ppm (-N-CH-), 39.88 ppm, 32.39 ppm, 28.86 ppm & 21.30 ppm (-CH_2-CH_2-CH_2-CH_2-) (Figure 4.3-17)

4.2.2. Synthesis of Diketomorpholine DKM

4.2.2.1. Synthesis of Sarcosine-Glycolic acid Diketomorpholine (Sar-GA DKM)

Method 1

Synthesis of Sar-GA. TFA salt

Boc-Sarcosine-OH (3.0 g, 0.016 mol, 1.0 eqv), EDC.HCl (3.9 g, 0.019 mol, 1.2 eqv), and NHS (2.2 g, 0.019 mol, 1.2 eqv) were added to an RB flask, followed by purging with nitrogen three times for 15 minutes each. The mixture was dissolved in 100.0 mL of anhydrous acetonitrile. Meanwhile, t-butyl-2-hydroxyacetate (2.3 g, 0.017 mol, 1.1 eqv) and DMAP (0.6 g, 0.005 mol, 0.3 eqv) were dissolved in 20.0 mL of anhydrous acetonitrile and added to the reaction mixture in one portion after 30 minutes at room temperature. The reaction was

stirred overnight. The crude product was concentrated under vacuum and purified by column chromatography (DCM: Acetone, 9:1, Rf: 0.7). The fractions were concentrated, and the Boc protecting group was removed by 20.0 mL of DCM: TFA (1:1) mixture at room temperature for four hours. The Sarcosine-Glycolic acid TFA salt was precipitated and washed with diethyl ether four times and dried under vacuum overnight.

Cyclisation of Sar-GA. TFA salt

Sar-GA TFA salt (0.5 g, 0.002 mol, 1.0 eqv) was placed in an RB flask and purged with nitrogen three times for 15 minutes each. The compound was dissolved in 100.0 mL of anhydrous acetonitrile, followed by the addition of 2-Chloro-1-methylpyridinium iodide (0.98 g, 0.004 mol, 2.0 eqv) in a single portion. After 15 minutes, 3.0 mL of excess triethylamine was added dropwise to neutralize the generated acid. The reaction mixture was then stirred overnight under nitrogen at 60 °C. Upon completion, the mixture was concentrated under vacuum and purified by column chromatography (eluent: DCM: Acetone, 8:2, Rf: 0.6).). The final product appeared as a pale yellowish oil. Overall yield: 25%.

Method 2

Synthesis of N-(2-chloroacetyl)-N-sarcosine

Sarcosine (3.0 g, 0.034 mol, 1.0 eqv) was dissolved in 40 mL of 2N NaOH solution and cooled to 0 °C using an ice bath. A solution of chloroacetyl chloride (4.0 mL, 0.051 mol, 1.5 eq.) in 80.0 mL of a 1:1 (v/v) mixture of diethyl ether and dioxane was then added dropwise under vigorous stirring over 20 minutes. After the addition, stirring continued at room temperature, with additional NaOH solution added as needed to maintain the pH around 11. The reaction proceeded until no further pH changes were observed. Upon completion, the pH was adjusted to approximately 1 using 3N HCl. The crude product was extracted four times with ethyl acetate, and the organic layer was concentrated under reduced pressure. The residue was washed with diethyl ether and dried under vacuum. Yield: 58%.

Cyclization of N-(2-chloroacetyl)-N-sarcosine

$NaHCO_3$ (2.03 g, 0.024 mol, 4.0 eqv) was added in 70.0 mL of DMF and heated to 60°C. The previously obtained N-(2-chloroacetyl)-N-sarcosine crystals (1.0 g, 0.006 mol, 1.0 eqv) were dissolved in 30.0 mL of DMF and added dropwise under nitrogen protection. The reaction mixture was stirred overnight. After completion, the solution was cooled to 0°C in an ice bath for one hour and then filtered. The solvent was removed under a strong nitrogen stream. The crude product was purified using column chromatography (DCM: Acetone, 8:2, Rf: 0.6). The overall yield was 18%.

Method 3

Sarcosine (12.64 g, 0.14 mol, 1.2 eqv) and Glycolic acid (9.0 g, 0.12 mol, 1.0 eqv) were introduced into an RB flask and purged with nitrogen three times for 15 minutes. Subsequently, 120.0 mL of toluene was added, and the reaction mixture was refluxed at 150 °C overnight. After completion, toluene was removed by applying a strong nitrogen stream. The crude product was then purified by column chromatography (DCM: Acetone, 8:2, Rf: 0.6), yielding a pale yellowish oil. yield: 72%.

^{1}H-NMR spectrum (400MHs, $CDCl_3$) of Sar-GA DKM: 4.75 ppm (-O-CH_2-), 4.14 ppm (-N-CH_2-), 3.00 ppm (-N-CH_3) (Figure 4.3-22)

^{13}C-NMR (100 MHz, $CDCl_3$) of Sar-GA DKM: 164.11 ppm and 163.06 ppm (-C=O), 67.36 ppm (-O-CH_2-), 49.20 ppm (-N-CH_2-), 33.14 ppm (-CH_3) (Figure 4.3-23)

IR spectrum of Sar-GA DKM: 1755 cm^{-1} is the ester C=O stretch, 1686 cm^{-1} is the amide C=O stretch (Figure 4.3-24)

4.2.2.2. Synthesis of Glu (OBzyl)-Glycolic acid Diketomorpholine (Glu (OBzyl)-GA DKM)

Synthesis of Glu(OBzyl)-GA-Cl

H-Glu(OBzyl)-OH (3.0 g, 0.012 mol, 1.0 eqv) and Na_2CO_3 (5.36 g, 0.05 mol, 4.0 eqv) were

placed in an RB flask and purged with nitrogen three times for 15 minutes each. Anhydrous THF (50.0 mL) was then added, and the mixture was heated to 35°C. A solution of chloroacetate chloride (2.01 mL, 0.025 mol, 2.0 eqv) in 50.0 mL of anhydrous THF was added dropwise over the course of one hour. The reaction mixture was stirred continuously overnight. Upon completion, the mixture was filtered, and the solvent was removed under vacuum. The resulting yellowish oil was washed with petroleum ether (50.0 mL x 4)and Glu(OBzyl)-GA-Cl was allowed to crystallise under vacuum overnight. Yield: 95%

Cyclisation of Glu(OBzyl)-GA-Cl

In a separate RB flask, $NaHCO_3$ (1.07 g, 0.013 mol, 4.0 eqv) was added in 70.0 mL of DMF and heated to 60 °C. The previously obtained Glu (OBzyl)-GA-Cl crystals (1.0 g, 0.003 mol, 1.0 eqv) were dissolved in 30.0 mL of DMF and added dropwise under nitrogen protection. The reaction mixture was stirred overnight. After completion, the solution was cooled to 0 °C in an ice bath for one hour and then filtered. The solvent was removed under a strong nitrogen stream. The crude product was purified using column chromatography (eluent: ethyl acetate, Rf: 0.75). The overall yield was 24%.

^{1}H-NMR spectrum (400 MHz, $CDCl_3$) of Glu(OBzyl)-GA DKM: 7.36 ppm (OBzyl ring), 6.69 ppm (-NH-), 5.14 ppm (-O-CH_2-), 4.75 ppm(-O-CH_2-C=C), 4.25 ppm (-NH-C**H**-), 2.61-2.22 ppm (-C**H$_2$**-C**H$_2$**-) (Figure 4.3-26)

IR spectrum of Glu(OBzyl)-GA DKM: 3245cm^{-1} is C-H OBzyl stretching, 3155 cm^{-1} is N-H amide stretching, 2944 cm^{-1} is C-H sp^3 stretching, 1758 cm^{-1} is C=O ester stretching, 1684 cm^{-1} is C=O ester stretching, 1645 cm^{-1} is amide stretching (Figure 4.3-27).

4.2.3. Ring Opening Polymerisation of amino acid DKPs

Amino acid DKPs were placed in a Schlenk tube and purged with nitrogen three times for 15 minutes each. Initiator hexylamine or benzylamine was then added to the reaction flask, either alone or in combination with various solvents and catalysts, such as Tin(II) Octoate [100], MSA/ DMAP [27], DBU [32], TBD [34] etc. The reaction mixture was heated to

different temperatures under nitrogen and maintained for two weeks. ^{1}H-NMR analysis was performed daily to monitor the reaction progress. After two weeks, regardless of the extent of the reaction, the mixture was subjected to dialysis before further processing.

The reaction conditions were summaries into the table below (Table 4.2-1).

DKPs (50.0 eqv)	Initiator (1.0 eqv)	Solvent	Catalyst (0.1 eqv)	Temperature	Yield
Sar	Hexylamine, benzylamine	Acetonitrile DMF[1] DMSO Water	MSA: DMAP (1:1-2) [27]	80-180 ^{o}C [2]	N/A
			Tin(II)(Octoate)[100]		
			TBD[34]		
			DBU[32]		
			TBD: Schreiner's Thiourea Catalyst (1:3) [46]		
	Hexylamine, Benzylamine, Benzylalcohol	Acetonitrile, Toluene	Ni(0)Cod_2 : SIPr. HCl [25]	reflux	
Ala	Hexylamine, benzylamine	Acetonitrile DMF[1] DMSO Water	MSA: DMAP (1:1-2) [27]	80-180 ^{o}C [2]	N/A
			Tin(II)(Octoate) [100]		
			TBD [34]		
			DBU [32]		
			TBD: Schreiner's Thiourea Catalyst (1:3) [46]		

Glu(OBzyl)	Hexylamine, benzylamine	DMF[1]	N/A	120 -130°C	Trace
		toluene	Ni(0)Cod_2 : SIPr. HCl [25]	reflux	20%
Lys(Cbz)	Hexylamine, benzylamine	DMF[1]	MSA: DMAP (1:1-2) [27]	120 - 130C	N/A
			Tin(II)Octoate [100]		
			TBD [34]		
			DBU [32]		
			TBD: Schreiner's Thiourea Catalyst (1:3) [46]		

Table 4.2-1. summary of DKPs polymerisation reaction condition including the initiator, solvent, catalyst and reaction temperature. [1] : DMF decompose at temperature over 140 °C therefore for reaction using DMF, reaction temperature is limited to 130 °C. [2] : For reaction temperature that far exceed their solvent boiling point, heavy wall pressure round bottom vessel was used.

^{1}H-NMR spectrum (400 MHz, DMSO-d_6) of PGlu(OBzyl). 7.35 ppm (OBzyl ring), 5.10 ppm (-O-CH_2-), 4.53- 4.04 ppm (-C=O-C**H**-NH-), 2.28-1.99 ppm (-C**H_2**-C**H_2**-), 1.23- 0.87 ppm (initiator) (Figure *4.3-33*)

4.2.4. Ring Opening Polymerisation of N-Boc activated Ala-DKP

N-Boc-Ala-DKP (200 mg, 0.83 mmol, 50.0 eqv) and benzylamine (1.8 µL, 0.017 mmol, 1.0 eqv) and $FeCl_3$ (5.4 mg, 0.082 mmol, 2.0 eqv) were added into RB flask. The reaction vessel was then purged with nitrogen for 15 minutes (three times). Then LiHMDS (1.0 M) (165.1 µL, 0.17 mmol, 10.0 eqv) in 10.0 mL anhydrous DMF was added into the reaction flask then heated to reflux. The reaction mixture was then heated to 120 °C under the protection of nitrogen. The progress of the reaction was monitored daily using ^{1}H-NMR spectroscopy. And

the reaction was terminated after two weeks. The resulting solution was precipitated in and washed with diethyl ether four times and dried in vacuum overnight. Yield: 41%.

^{1}H-NMR spectrum (500 MHz, DMSO-d_6) of polyalanine from ROP of N-Boc-Ala-DKP: 7.15 ppm (-NH-), 4.55 ppm (-C**H**-CH_3), 1.45-1.23 ppm (-CH-C**H$_3$**) (Figure *4.3-18*)

4.2.5. Ring Opening Polymerisation of amino acid DKMs

Overall procedure

Amino acid DKM (100.0 eqv), benzyl alcohol (1.0 eqv), and a catalyst were added to the reaction flask, which was then purged with nitrogen three times for 15 minutes each. The solvent was subsequently added, and the reaction mixture was maintained under a nitrogen atmosphere at various temperatures for up to two weeks or until completion. The progress of the reaction was monitored daily using ^{1}H-NMR spectroscopy.

The reaction conditions were summaries into the table below (Table 4.2-2)

DKMs (100.0 eqv)	Initiator (1.0 eqv)	Solvent	Catalyst (0.1 eqv)	Temperature	Yield
Sar-GA	Benzylalcohol	Acetonitrile DMF[1] DMSO Water	MSA: DMAP (1:1-2)[27]	r.t.-160 °C [2]	N/A
			Tin (II)(Octoate) [100]		
			TBD [34]		
			DBU [32]		
			TBD: Schreiner's Thiourea Catalyst (1:3) [46]		
Glu(OBzyl)-GA	Benzylalcohol	Chloroform	TBD: Schreiner's Thiourea Catalyst (1:3) [46]	r.t.- reflux	39%

Table 4.2-2. summary of DKMs polymerisation reaction condition including the initiator, solvent, catalyst and reaction temperature. [1:] DMF decompose at temperature over 140 °C therefore for reaction using DMF, reaction temperature is limited to 130 °C. [2]: for reaction temperature that far exceed their solvent boiling point, heavy wall pressure round bottom vessel was used

^{1}H-NMR spectrum (400 MHz, DMSO-d_6) P(Glu(OBzyl)-GA): 8.65-8.51 ppm (-NH-), 7.33 ppm (Benzyl ring)), 5.08 ppm(-O-CH_2-C=C), 4.80- 4.45 ppm (-O-CH_2-C=O-, -C=O-C**H**-NH-), 2.32-1.84 ppm (-C**H$_2$**-C**H$_2$**-) (Figure *4.3-33*)

4.2.6. Synthesis of P(Sar-GA) Random Copolymer by Melt Condensation

Glycolic acid (1.0 g, 13.1 mmol, 1.0 eqv), sarcosine (1.17 g, 13.1 mmol, 1.0 eqv) and

$Sn(II)Oct_2$ (1.0% w/w) or zinc powder (1.0% w/w) combination with acetic anhydride (1.0% w/w) were loaded into a Schlenk tube, which was thrice purged with nitrogen for 15 minutes then reduced pressure to 30 mBar. Following this, the mixture was heated at 180 ^oC for 48 hours. A brown paste was obtained which was dissolved in 5.0 mL of DI water and dialysed against DI water for three days before being freeze dried. Yield: Trace

^{1}H-NMR spectrum (500 MHz, DMSO-d_6) of P(Sar-GA): 4.94-4.65 ppm (-C=O-CH_2-O-), 4.28-3.89 ppm (-C=O-C**H$_2$**-N(-CH_3)-) and 2.94-2.70 ppm (-N(-C**H$_3$**)-) (Figure *4.3-36*)

4.2.7. Synthesis of P(Glu-GA) Containing Drug Conjugate

4.2.7.1. Deprotection of P(Glu(OBzyl)-GA)

P(Glu(OBzyl)-GA) (0.2 g) was dissolved in 4.0 mL of TFA, and 1.2 mL of hydrobromic acid in acetic acid (33% HBr/AcOH) was added to the reaction flask dropwise. The reaction mixture was stirred at room temperature for 90 minutes and precipitated in cold diethyl ether and collected by centrifugation. The precipitate was dried under vacuum for two hours. The above process was repeated twice to fully deprotect the OBzyl protecting group. After deprotection, the polymer solution was precipitated and washed with diethyl ether until no acidic odour remained. Finally, the polymer was dried under vacuum overnight and used directly in subsequent reactions. Yield: 99%

4.2.7.2. Crosslinking of P(Glu-GA)

P(Glu-GA) (80 mg, 1.0 eqv), EDC.HCl (164 mg, 0.9 mmol, 2.0 eqv), and NHS (98 mg, 0.9 mmol, 2.0 eqv) were placed in an RB flask and purged with nitrogen three times for 15 minutes each. Anhydrous DMF (5.0 mL) was then added, and the mixture was stirred at room temperature for 30 minutes in ice bath to activate the carboxylate groups. Subsequently, ethylenediamine (5 µL, 0.07 mmol, 0.175 eqv) dissolved in 5.0 mL of anhydrous DMF was added dropwise. The reaction was stirred overnight and was allowed to slowly warm to room temperature. Upon completion, the mixture was dialysed against DI water for three days and then freeze dried. Yield: 93%

4.2.7.3. Synthesis of P(Glu-GA)-(PSar-Gly-CPT) Drug Conjugate

The above crosslinked P(Glu-GA) (10.0 mg, 1.0 eqv), EDC.HCl (20.5 mg, 0.11 mmol, 2.0 eqv) and NHS (12.3 mg, 0.11 mmol, 2.0 eqv) were placed in an RB flask and purged with nitrogen three times for 15 minutes each. Anhydrous DMF (1.0 mL) was then added, and the mixture was stirred for 30 minutes in ice bath to activate the carboxylate groups. Subsequently, PSar-Gly-CPT (43.5 mg, 0.04 mmol, 0.7 eqv) in 2 mL of anhydrous DMF was added dropwise. The reaction was allowed to warm to room temperature and was stirred overnight. Upon completion, the mixture was dialysed against DI water for three days and then freeze dried. Yield: 76%

^{1}H-NMR spectrum (500 MHz, DMSO-d_6) of P(Glu-GA)-(PSar-Gly-CPT): 8.71-7.18 ppm (-CH=C-(CPT), -COOH (P(Glu-GA)), -NH-), 5.50 ppm(-N-CH_2-C= (CPT)), 5.32-3.78 ppm (-O-CH_2-C=C-(CPT), -C**H_2**-NH- (CPT), -O-CH_2- (P(Glu-GA)), -C=O-C**H**-NH-(P(Glu-GA)), -C**H_2**-N(CH_3)- (PSar)), 2.95-2.73 ppm (-CH_2-N(C**H_3**)- (PSar)), 2.446-1.99 ppm (-C**H_2**-C**H_2**- (P(Glu-GA)), CH_3-C**H_2**-(CPT)) (Figure *4.3-38*)

4.2.7.4. Synthesis of P(Glu-GA)-[(CPT-Gly)-co-(F-PSar)] Drug Conjugate

The above crosslinked P(Glu-GA) (10.0 mg, 1.0 eqv), EDC.HCl (20.5 mg, 0.11 mmol, 2.0 eqv) and NHS (12.3 mg, 0.11 mmol, 2.0 eqv) were placed in a RB flask and purged with nitrogen three times for 15 minutes each. Anhydrous DMF (1.0 mL) was then added, and the mixture was stirred for 30 minutes in ice bath to activate the carboxylate groups. Subsequently, CPT-Gly (15.5 mg, 0.04 mmol, 0.7 eqv) and F-PSar (10.0 mg, 0.004 mmol, 0.07 eqv) in 5 mL of anhydrous DMF was added dropwise. The reaction was allowed to warm to room temperature while remain stirring overnight. Upon completion, the mixture was dialysed against deionised water for three days and then freeze-dried. Yield: 66%

^{1}H-NMR spectrum (500 MHz, DMSO-d_6) of P(Glu-GA)-[(CPT-Gly)-*co*-(F-PSar)]: 8.71-7.15 ppm (-CH=C-(CPT), -COOH (P(Glu-GA)), -NH-), 5.49 ppm(-N-CH_2-C= (CPT)), 5.32-3.91 ppm (-O-CH_2-C=C- (CPT), -C**H_2**-NH- (CPT), -O-CH_2- (P(Glu-GA)), -C=O-C**H**-NH-(P(Glu-GA)), -C**H_2**-N(CH_3)-(PSar)), 2.95-2.73 ppm (-CH_2-N(C**H_3**)- (PSar)), 2.16-1.86 ppm (-C**H_2**-C**H_2**- (P(Glu-GA)), CH_3-C**H_2**-

(CPT)), 2.13 ppm, 2.03 ppm, 1.93 ppm (-C=O-CH_3 (O-Acetyl of fucose)) (Figure *4.3-40*)

4.3. Result & Discussion

Triphosgene is used for the amino acid NCAs synthesis, which is solid substitute for the gaseous phosgene, a toxic, colourless gas that was used as a chemical weapon during warfare [1,3]. Despite its extra stability given by its solid form, phosgene is produced when in contact with moisture or in elevated temperature [4]. The safety risk skyrocketed when produced in massive scale. Therefore, there is a need to research on a safer monomer synthesis. And multiple amino acid DKPs and DKMs were produced as the alternate of their corresponding NCAs to examine their feasibility to undergo polymerisation.

4.3.2. Synthesis of DKPs

Sar-DKP, Ala-DKP, Boc activated Ala-DKP, Glu-DKP, Glu(OBzyl)-DKP and Lys(Cbz)-DKP were synthesised. Among them, Sar-DKP and Ala-DKP were synthesised through simple thermal condensation in ethylene glycol, while Glu-DKP was synthesised in an attempt to synthesise Glu(OtBu)-DKP through thermal condensation in ethylene glycol. Then Glu(OBzyl)-DKP and Lys(Cbz)-DKP were synthesised in a more sophisticated multi-steps reaction.

4.3.2.1. Synthesis of Sar-DKP

Sar-DKP (Figure 4.3-1) was synthesised via condensation at high temperature of sarcosine in ethylene glycol at 170 °C in the attempt to replace Sar-NCA to produce hydrophilic poly(amino acid)- PSar (Figure 4.3-2).

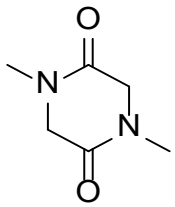

Figure 4.3-1. Sarcosine DKP

It also served as a prove of concept and study the possibility of its ROP reaction.

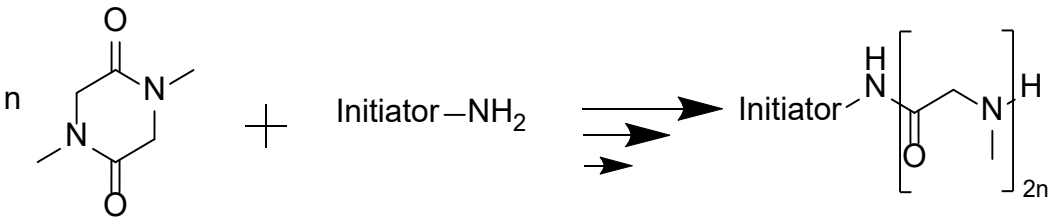

Figure 4.3-2. Ring opening polymerisation of Sar-DKP

The Sar-DKP synthesised was a white powder with 80 % yield, as confirmed by ^{1}H-NMR spectroscopy. Peak at 3.97 ppm represent the four protons of the Sar-DKP ring and peak at 2.97 ppm corresponds to the two methyl group of Sar-DKP (Figure 4.3-3) consistent with the literature[98].

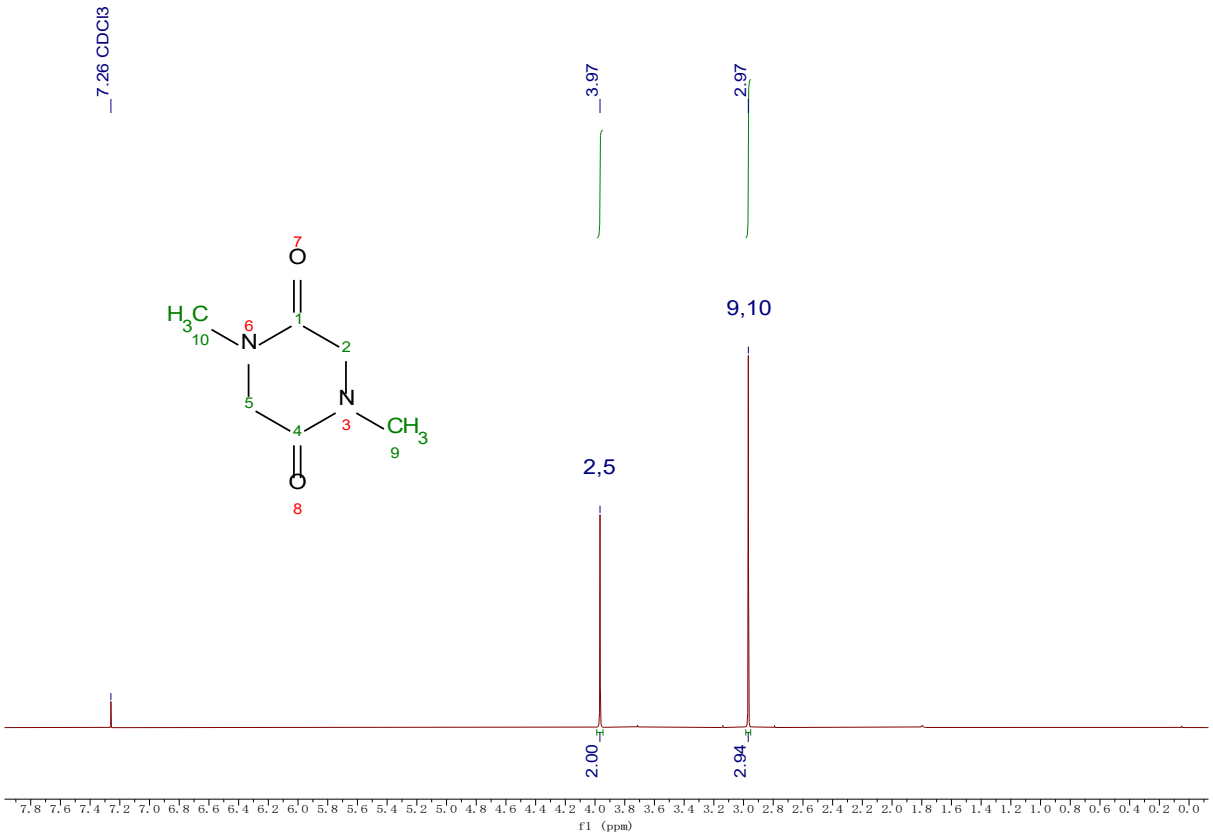

Figure 4.3-3. ^{1}H-NMR spectrum (400 MHz, $CDCl_3$) of Sar-DKP: 3.97 ppm (-CH_2-), 2.97 ppm (-CH_3) [98]

4.3.2.2. Synthesis of Ala-DKP

Ala-DKP(Figure 4.3-4) was chosen as the monomer to produce polyalanine (PAla) because of its structural simplicity which is served as a prove of concept and study the feasibility of its ROP reaction(Figure 4.3-5).

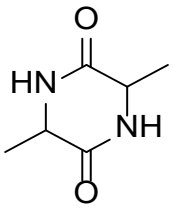

Figure 4.3-4. Ala-DKP

Ala-DKP was successfully synthesised through thermal condensation in ethylene glycol at 170 ^{o}C in attempt to substitute alanine NCA.

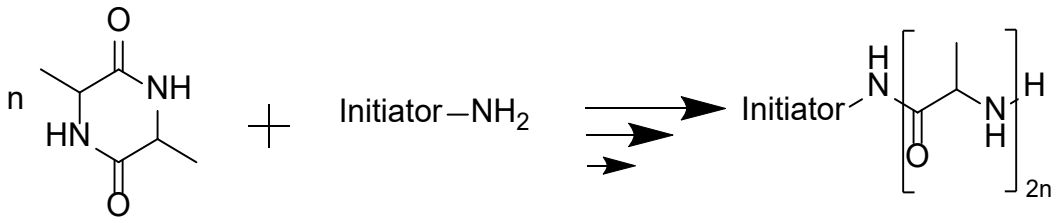

Figure 4.3-5. Ring opening polymerisation of Ala-DKP

The Ala-DKP synthesised was a white powder with high yield, as confirmed by ^{1}H-NMR spectroscopy. Peak at 8.07 represent the two amide protons of DKP, peak at 3.87 correspond to the two protons of DKP ring while peak at 1.25 ppm is for the two-methyl group of DKP .

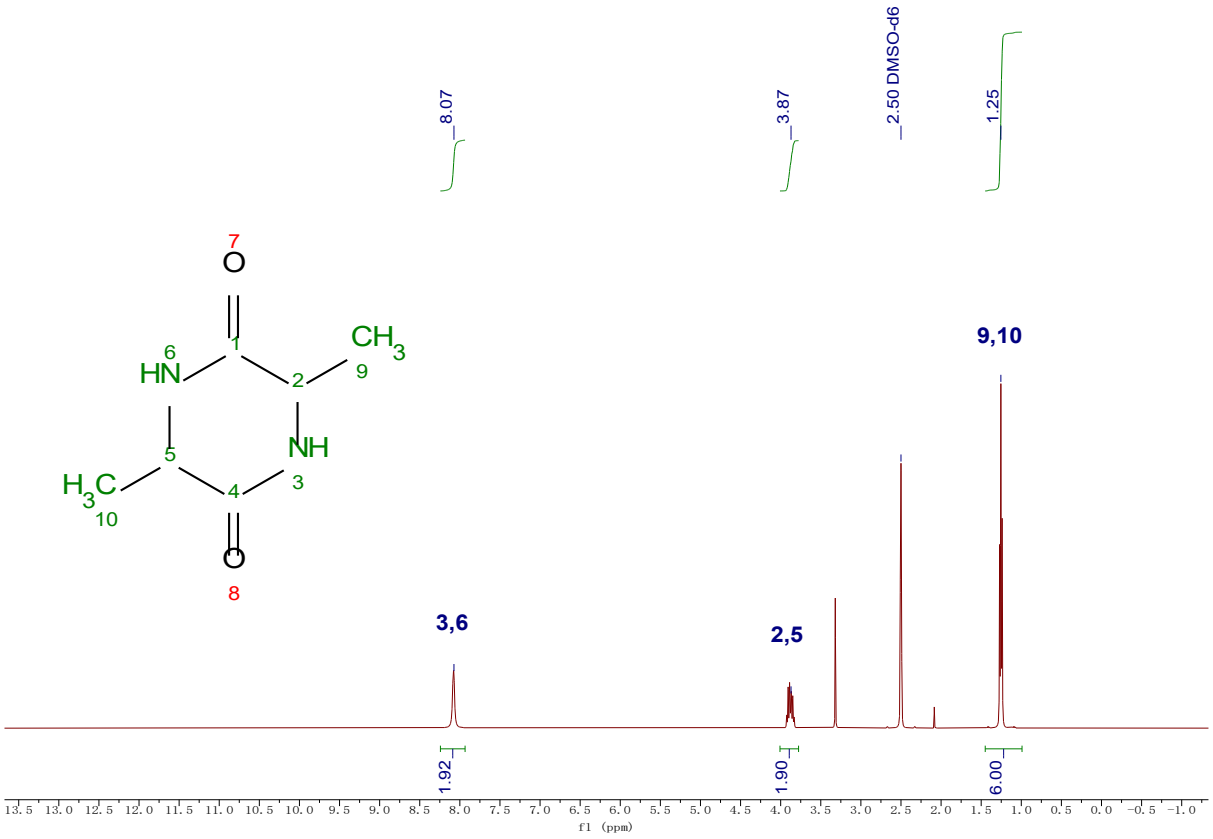

Figure 4.3-6. ^{1}H-NMR spectrum (400 MHz, DMSO-d_6) of Ala-DKP: 8.07 ppm (-NH-), 3.87 ppm (-N-CH-), 1.25 ppm (-CH_3)

The structure was further validated by ^{13}C NMR spectroscopy. The peak at 169.05 ppm was assigned to the two carbonyl quaternary carbons of the amino group, while the signal at 49.76 ppm corresponds to the two tertiary carbons of the DKP ring. The resonance at 19.94 ppm is attributed to the two methyl group carbons. (Figure 4.3-7). These signals are consistent with the expected structure of the monomer.

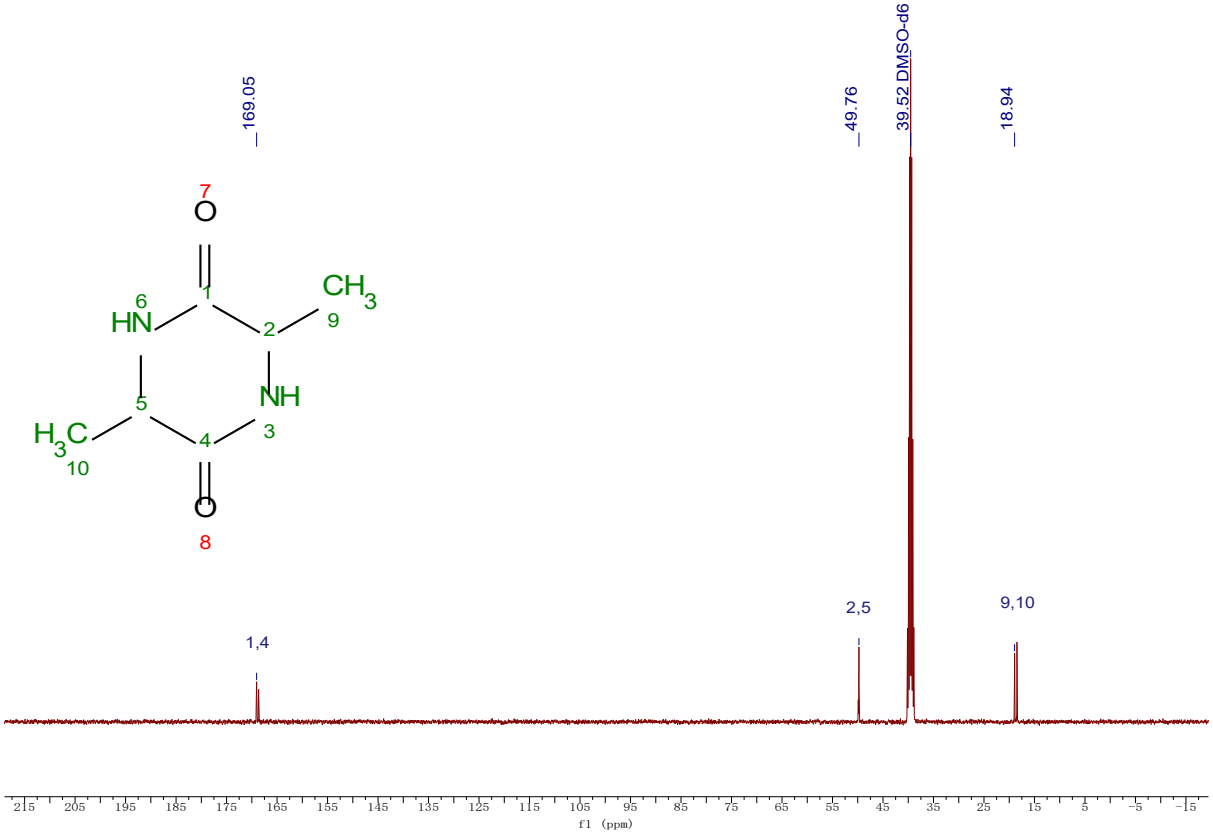

Figure 4.3-7. ^{13}C-NMR spectrum (100 MHz, DMSO-d_6) of Ala-DKP: 169.05 ppm (C1, C4), 49.76 ppm (C5,C2), 19.94 ppm (C9,C10)

4.3.2.2.1. Boc Activation of Ala-DKP

To facilitate the cleavage of the secondary amide bond in DKP, a Boc protecting group was introduced to one of the amide groups of Ala-DKP [25,26]. The electron-withdrawing nature of the Boc group increases the electrophilicity of the carbonyl carbon, thereby promoting catalytic amide bond cleavage [25,26]. For this study, Ala-DKP was chosen as a model compound due to its simplicity.

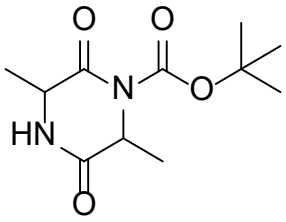

Figure 4.3-8. Boc activated amide of Ala-DKP (N-Boc-Ala-DKP)

The Boc activated Ala-DKP (Figure 4.3-8) was synthesised by heating Ala-DKP with Boc_2O in the presence of DMAP at 50 °C. Due to the temperature sensitivity of Boc_2O [109], the reaction was conducted at 50 °C. In addition, the low solubility of Ala-DKP required the use of a large amount of DMF to ensure complete dissolution. Product appears to be white powder, and its structure was confirmed by ^{1}H-NMR spectroscopy. Peak at 8.12 ppm is the amide proton, peak at 4.64 ppm belongs to the two protons of the DKP ring, peak at 1.50-1.43 ppm represent the Boc group and peak at 1.34 ppm are the methyl group of Ala-DKP (Figure 4.3-9) similar to that in the literature [99].

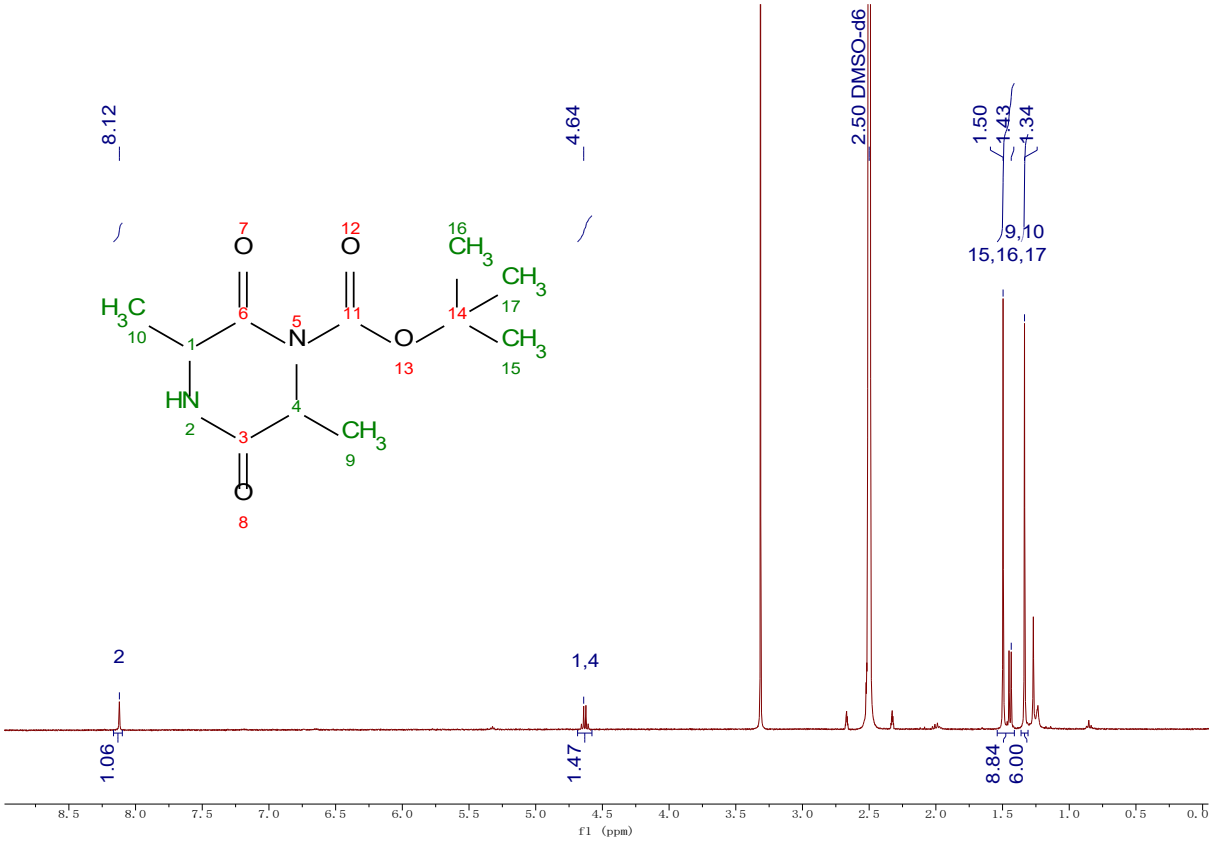

Figure 4.3-9. ^{1}H-NMR spectrum (400 MHz, DMSO-d_6) of Boc activated Ala-DKP: 8.12 ppm (-NH), 4.64

ppm (-CH-), 1.50-1.43 ppm (-C-CH_3), 1.34 ppm (-CH_3)

4.3.2.3. Synthesis of Glu(OtBu)-DKP

In order to produce PGA through NCA free polymerisation, the synthesis of its alternative monomer- DKP studied. The attempt to synthesise Glu(OBzyl)-DKP through hot condensation was unsuccessful. Therefore, Glu(OtBu)-OH was tested as an alternative. However, only trace amount of off-white solid was obtained after recrystallisation in acetone. The solid was characterised by ^{1}H-NMR spectroscopy, interestingly, the solid was not Glu(OtBu)-DKP(Figure 4.3-10) but Glu-DKP, which could result from the thermal deprotection of O-t-Butyl group.

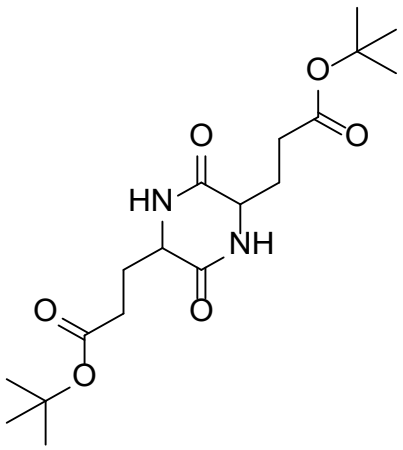

Figure 4.3-10. Glu (OtBu)-DKP

The tertiary butyl group was not observed in the ^{1}H-NMR spectra, and carboxylate proton at 12.7 ppm was observed instead (Figure 4.3-11), indicating the tertiary butyl group was cleaved during the reaction at high temperature [101]. Given by the harsh ROP of DKPs, the carboxylate group must remain protected, and therefore an alternative DKP synthesis was adopted.

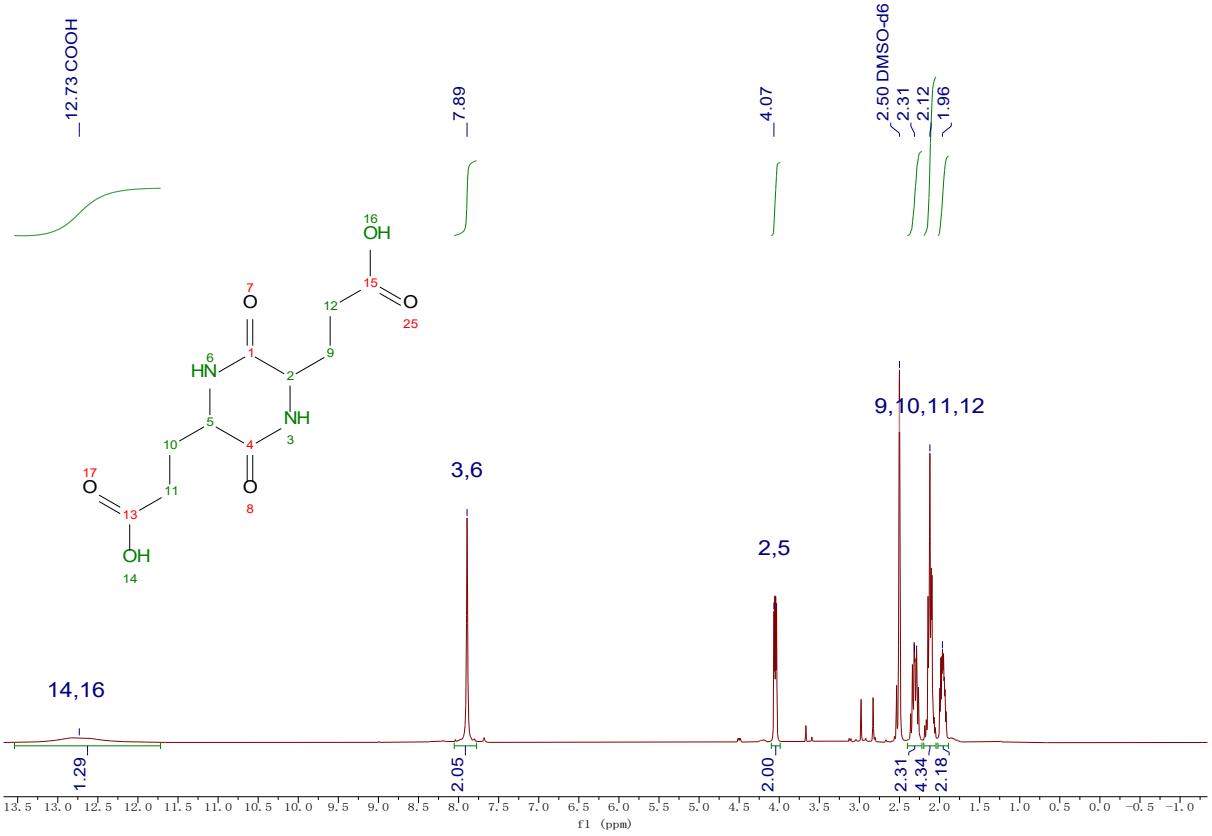

Figure 4.3-11. ^{1}H-NMR spectrum (400 MHz, DMSO-d_6) of Glu-DKP: 12.73 ppm (-COOH), 7.89 ppm (-NH-), 4.07 ppm (-N-CH-C=O), 2.31-1.96 ppm (-C**H**$_2$-C**H**$_2$-)

The structure was further confirmed by ^{13}C NMR spectroscopy. The signals at 176.98 ppm and 174.49 ppm were assigned to the carboxylate carbon and the two carbonyl carbons of the DKP ring. The peak at 54.80 ppm corresponds to the two carbons within the DKP ring, while the resonances at 29.08 ppm and 24.63 ppm are attributed to the four side-chain carbons (Figure 4.3-12).

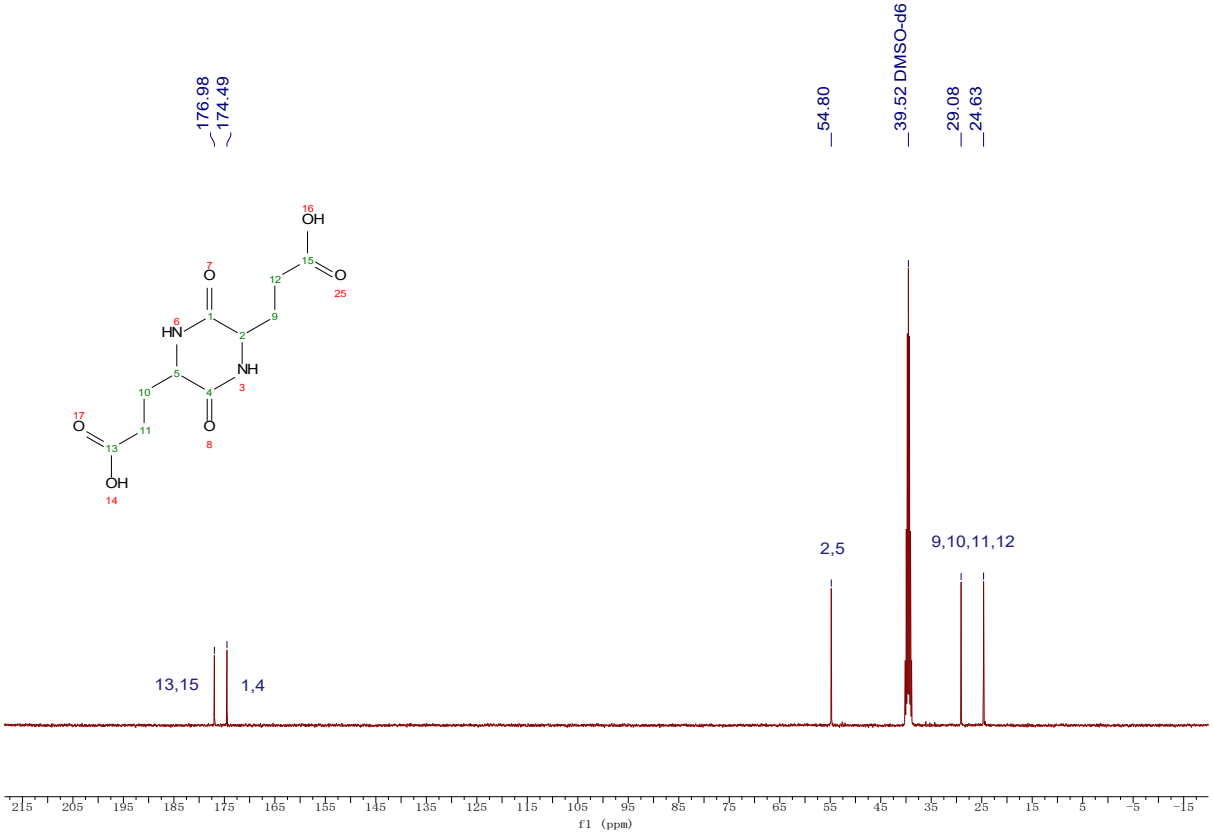

Figure 4.3-12. ^{13}C-NMR spectrum (100 MHz, DMSO-d_6) of Glu-DKP: 176.98 ppm & 174.49 ppm (C13,C15 & C1, C4), 54.80 ppm (C2, C5), 29.08 ppm & 24.63 ppm (C9-C12)

These NMR signals are consistent with the expected structure of Glu-DKP, and the absence of additional peaks indicates that a pure product was obtained.

4.3.2.4. Synthesis of Glu(OBzyl) -DKP

To replace Glu(OBzyl)-NCA in producing PGlu(OBzyl), Glu(OBzyl)-DKP (Figure 4.3-13) was synthesised. Unlike Sar-DKP and Ala-DKP, multiple attempts to synthesise Glu(OBzyl)-DKP by condensation at various temperature and solvents were not successful.

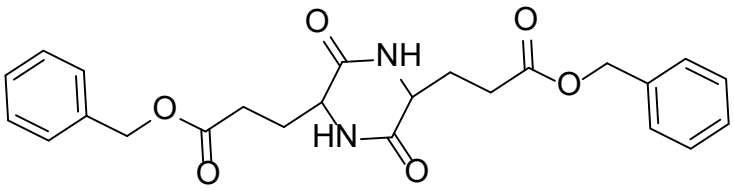

Figure 4.3-13. Glu(OBzyl)-DKP

Therefore, a more sophisticated synthesis of Glu(OBzyl)-DKP was adopted. An NHS-ester was first formed by DCC/NHS coupling reaction, the deprotection of Boc group releases the amino group which acted as a nucleophile to substitute the NHS- ester forming Glu(OBzyl)-DKP (Scheme 4.3-1) [19]. However, the reaction yield was still very low indicating there are still lot of room for improvement in the reaction scheme.

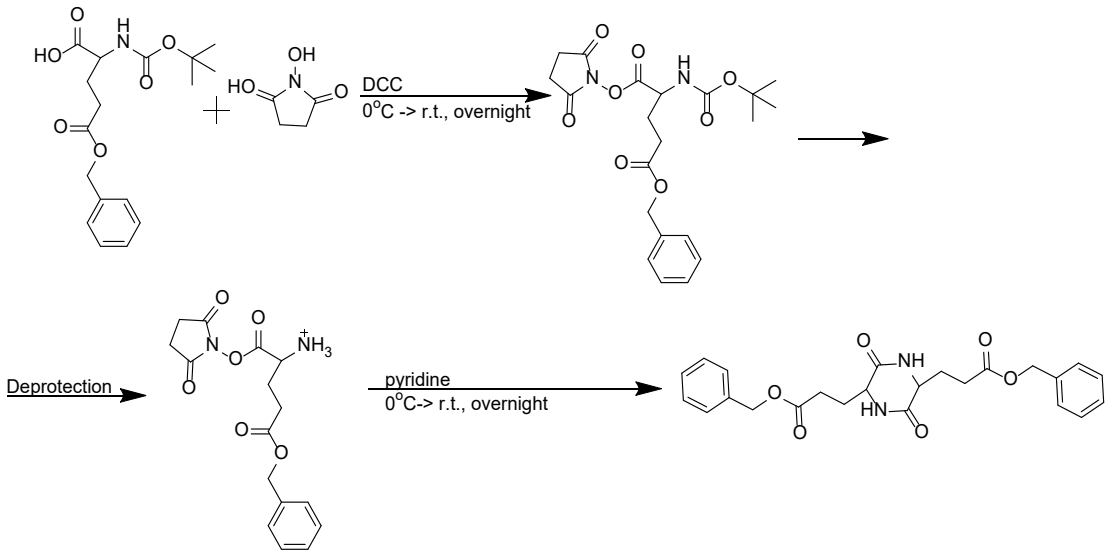

Scheme 4.3-1. Reaction scheme of Glu(OBzyl)-DKP synthesis.

The product was characterised with ^{1}H-NMR spectroscopy, the two OBzyl protecting groups was observed at 7.36 ppm and 5.08 ppm. peak at 8.22 ppm is the amide protons; peak at 3.90 ppm is the protons in the DKP ring, and peak from 2.45- 1.92 ppm represents the side chain protons (Figure 4.3-14) consistent to that in the literature [19].

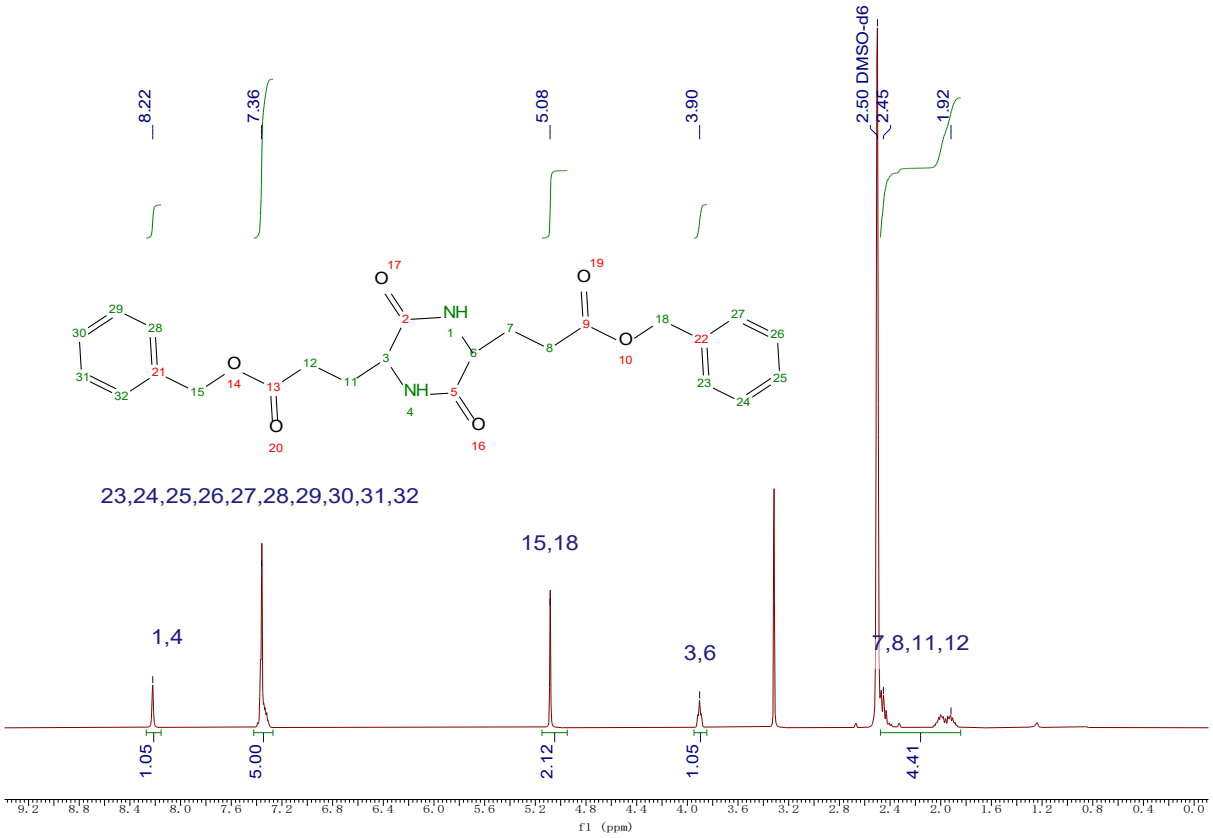

Figure 4.3-14. ^{1}H-NMR spectrum (400 MHz, DMSO-d_6) of Glu(OBzyl)-DKP: 8.22 ppm (-NH-), 7.36 ppm (OBzyl), 5.08 ppm (-O-CH_2-), 3.90 ppm (-N-CH-C=O), 2.45-1.92 ppm (-C**H**$_2$-C**H**$_2$-)

4.3.2.5. Synthesis of Lys(Cbz)-DKP

Polylysine has a functionalised primary amino group as the side- chain, which can undergo various modifications like coupling reaction [102] and cross-linkage [103]. But the common synthesis of polylysine, like other poly(amino acids), still rely on Lys-NCA [104,105]. Therefore, the potential of using DKP to synthesise polylysine was explored. The Lys(Cbz)-DKP (Figure 4.3-15) was first produced through the same method as the Glu(OBzyl)-DKP.

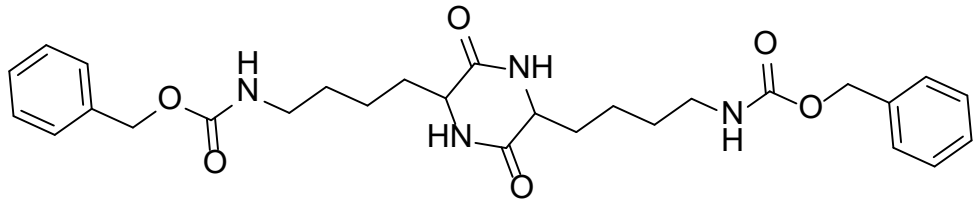

Figure 4.3-15. Lys(Cbz)-DKP

The product was characterised with ^{1}H-NMR spectroscopy, peak at 8.09 ppm is the amide proton of the DKP ring; peak at7.34 ppm and 5.00 ppm correspond to the protecting group protons; peak at7.21 ppm is the protected amine proton; peak at 3.79 ppm is the protons in ring DKP; peak at 2.98 ppm and from 1.67- 1.31 ppm represent the side chain protons (Figure 4.3-16).

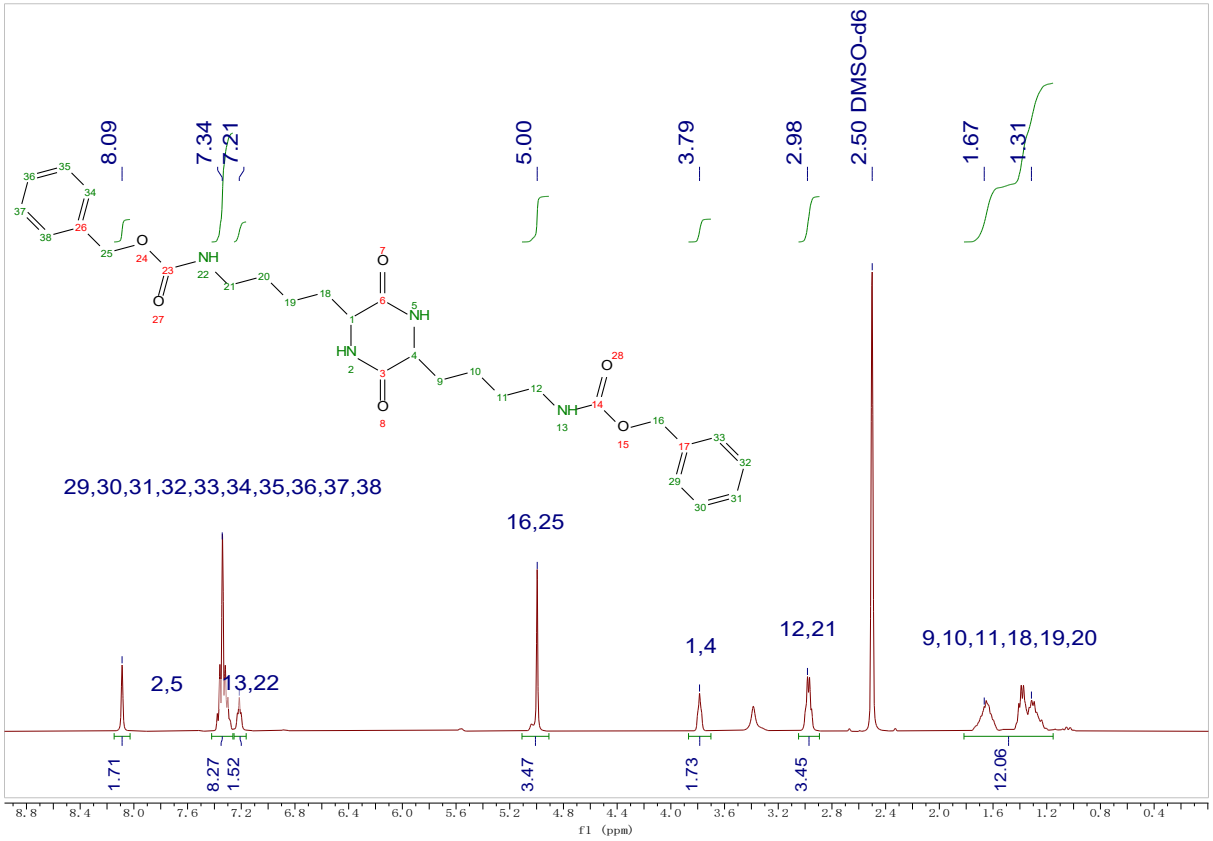

Figure 4.3-16. ^{1}H-NMR spectrum (400 MHz, DMSO-d_6) of Lys(Cbz)-DKP: 8.09 ppm (-NH-), 7.34 ppm (Cbz ring), 5.0 ppm (-O-CH_2-), 3.79 ppm (-N-CH-C=O), 2.98 ppm (-C**H**$_2$-C**H**$_2$-NH-), 1.67-1.31 ppm (-CH-C**H**$_2$-C**H**$_2$-)

The structure was further confirmed by DEPT-135 spectroscopy. The signals at 128.08 ppm and 127.46 ppm were assigned to the aromatic carbons. The peak at 64.83 ppm corresponds to the -**C**H_2-Ph of the Cbz protecting group. The signal at 54.80 ppm was attributed to the two tertiary carbons of the DKP ring, while the resonances at 39.88 ppm, 32.39 ppm, 28.86 ppm, and 21.30 ppm correspond to the eight secondary carbons (-**C**H_2)$_4$-) of the methylene chains (Figure 4.3-17). The spectra are consistent with the expected structure of the monomer and the absent of additional peaks indicates the purity of the sample.

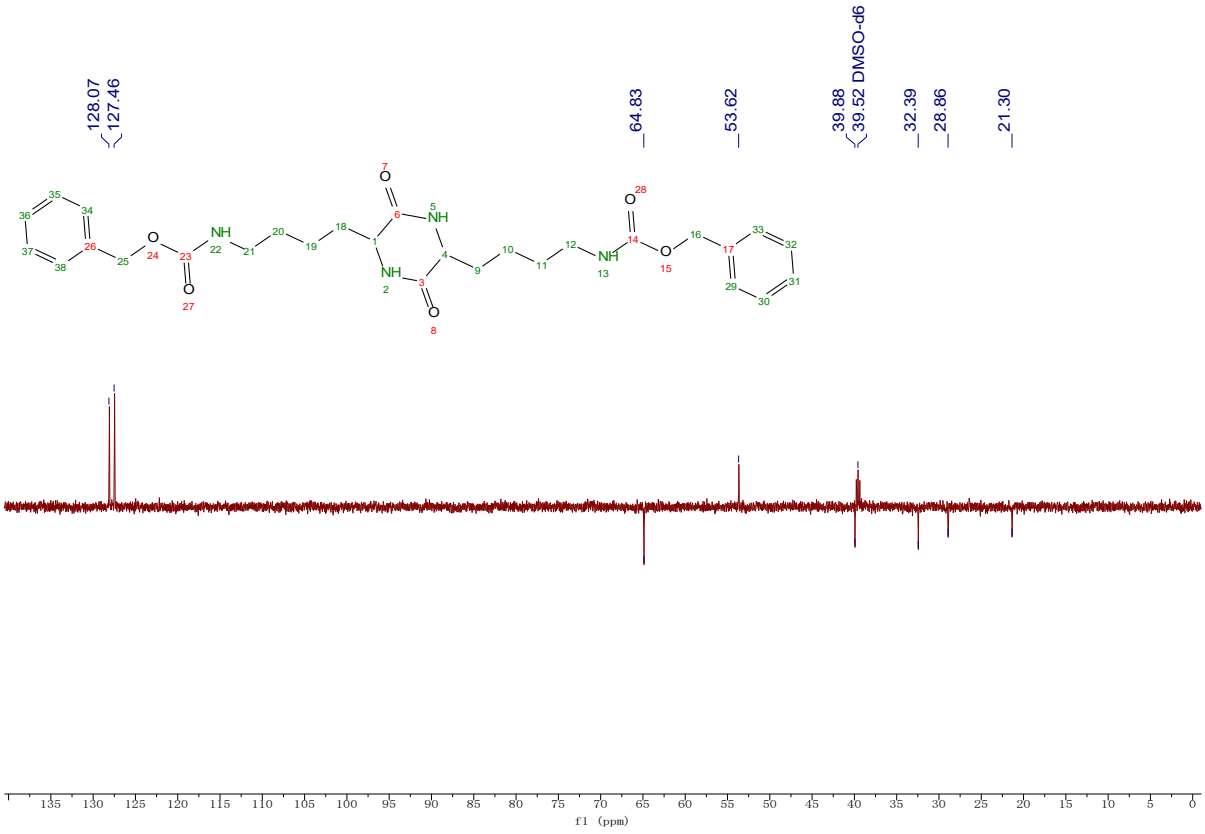

Figure 4.3-17. DEPT135 (100 MHz, DMSO-d_6) of Lys(Cbz)-DKP: 128.07 ppm & 127.46 ppm (aromatic carbons), 64.83 ppm (C25, C16), 53.62 ppm (C1, C4), 39.88 ppm, 32.39 ppm, 28.86 ppm & 21.30 ppm (C9- C12, C18- C21)

4.3.3. Summary on Amino Acid DKPs Synthesis

While amino acid DKPs hold potential as an alternative to NCAs for ROP, their synthesis

poses significant challenges. For some DKPs, such as Ala-DKP and Sar-DKP, production is straightforward, requiring only heating in ethylene glycol at high temperatures. However, others, like Glu(OBzyl)-DKP and Lys(Cbz)-DKP, demand complex, multi-step reactions that result in low yields and difficult purifications. As a result, even if DKPs can undergo ROP, the synthesis difficulties associated with certain type amino acids limit their practicality compared to NCAs. To address this, exploring new synthesis approaches, such as catalytic methods, is essential to improve the efficiency and the yield of DKP production across a broader range[106].

4.3.4. Ring Opening Polymerisation of DKPs

To minimise the reliance on the toxic and expensive triphosgene, amino acid DKPs were synthesised as potential alternatives for producing poly(amino acids). However, the feasibility of DKPs undergoing ROP remains largely unexplored, with scarce literature on the topic. The enhanced stability of DKPs' six-membered cyclic di-amide poses a significant challenge, making their ROP more difficult compared to NCAs and cyclic esters. Consequently, there is a need to develop an efficient method to polymerise DKPs, enabling the sustainable synthesis of poly(amino acids) and this chapter aims to make true of this via experimenting multiple catalysts among the commonly reported catalysts used in polymer chemistry.

4.3.4.1. ROP of Sar-DKP

To replace PSar created from NCAs, polymerisation of Sar-DKP was carried out using different catalysts, solvents at temperature range from 80 to 180 ^{o}C. However, polymerisation of Sar-DKP had not succeeded so far. Unlike other amino acid DKPs, Sar-DKP forms a secondary amino group rather than a primary amino group after initiation which is a weaker nucleophile and the methyl group on the amino group of both monomer and the initiated monomer also causes steric hindrance repelling the attack of the nucleophile, result in no initiation of propagation. Furthermore, the failed ROP of Sar-DKP with Ni(0)Cod_2: SIPr.HCl at elevated temperature indicating the activation of amide bond is necessary.

Consequently, alternative catalysts that do not require amide bond activation are needed in order to polymerise Sar-DKP.

4.3.4.2. ROP of Ala-DKP

To determine if the methyl group in Sar-DKP hindered the ROP reaction, attempt of ROP of Ala-DKP was employed in the same conditions. Ala-DKP as an isomer of Sar-DKP having a less hindered cyclic amide bond (-C=O-NH-) than that of Sar-DKP. However, its polymerisation failed so far, therefore, the ROP of Sar-DKP failed may not because of the reduced nucleophilicity of the initiated monomer but lies upon its stability of amide bond. Therefore, in order to polymerise DKPs, its amide bonds first need to be modified to increase its susceptibility in nucleophilic attack.

4.3.4.2.1. ROP of N-Boc Activated Ala-DKP

To polymerise N-Boc Ala-DKP, it was heated in DMF alone with amine initiator, LiHMDS catalyst and $FeCl_3$ at 120 ^oC. This was to explore a method for the ROP of DKPs, specifically Ala-DKP, by first activating the amide bond with an electron withdrawing Boc group, followed by LiHMDS catalysed ROP [26]. LiHMDS was selected for its well-documented ability to facilitate transamination at room temperature [26]. However, a significant challenge arose during the ROP process: according to the reaction mechanism (Scheme 4.1-12), Boc group remained attached to the ring-opened terminal amine, blocking further polymer chain propagation. To address this, $FeCl_3$ was introduced as a catalyst to deprotect the Boc group simultaneously [108].

This solution, however, presented a new complication. The deprotection process was not selective and affected all Boc groups in the reaction mixture including the Boc-activated DKP, making the $FeCl_3$ ratio critical. Too much $FeCl_3$ caused rapid deprotection, deactivating the Ala-DKP before ROP could occur, while too little $FeCl_3$ slowed the reaction, impeding propagation. Despite efforts to balance these factors, the method may not achieve high polymer yields due to the unavoidable deactivation of Ala-DKP.

Importantly, this approach was intended primarily as a proof of concept to establish a potential ROP method for DKPs. As a result, the optimal ratios between the monomer, initiator, and the two catalysts (LiHMDS and $FeCl_3$) were not determined.

After reaction, a brown solid obtained and was analysed by ^{1}H-NMR spectroscopy. Peak broadening at 7.15 ppm, 4.55 ppm and 1.45-1.23 ppm are observed, corresponding to the amide protons of the polymer chain, -C**H**(CH_3)- proton and the methyl group protons respectively (Figure 4.3-18). However, this peak broadening could also be caused by polymerisation or the paramagnetic residue of Fe ions in the sample after dialysis [107]

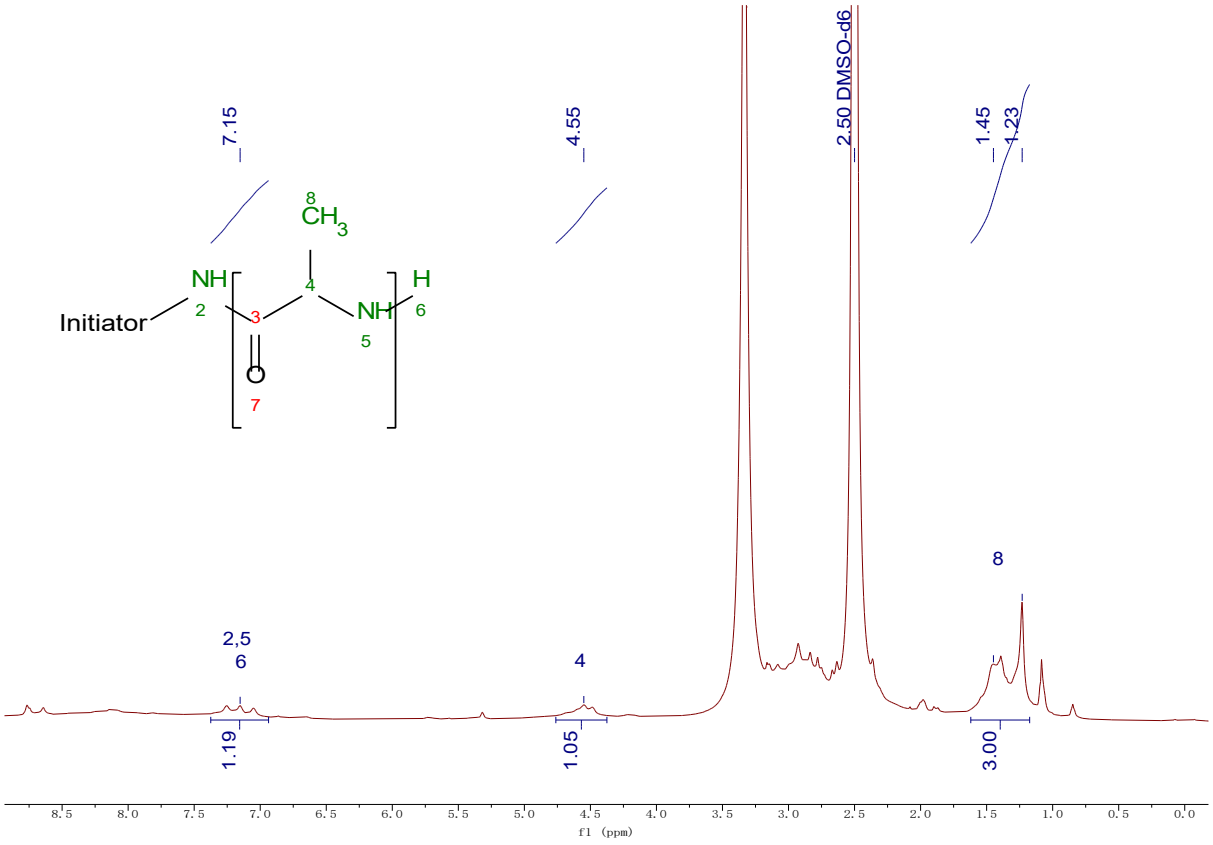

Figure 4.3-18. ^{1}H-NMR spectrum (500 MHz, DMSO-d_6) of polyalanine from ROP of N-Boc-Ala-DKP: 7.15 ppm (-NH-), 4.55 ppm (-C**H**-CH_3), 1.45-1.23 ppm (-CH-C**H$_3$**)

Because of the present of impurities such as Fe ions that can cause peak broadening in ^{1}H-NMR spectrum, MALDI-TOF mass spectrometry analysis was conducted to further characterise the product. The spectra show a broad bell-shaped peak from around 1800-4000 Da and peaked at around 2650 Da corresponds to approximately 36 repeating units

(Appendix 0-4).

However, it should be noted that MALDI-TOF analysis of higher molecular weight polymers often suffers from mass discrimination effects, where higher-mass species exhibit lower ionization efficiency [110,111]. In addition, detector saturation caused by intense signals from matrix ions and low-molecular-weight oligomers can further exacerbate this effect [112]. Consequently, the obtained molecular weights may be slightly underestimated compared to the actual values.

Therefore, in order to open the DKP ring, activation of the amide nitrogen is essential, yet this process further generate chemical wastes and currently there is not reported literature showing the control ROP of DKPs in this method, as a result ROP of DKPs not only cannot be classified as green chemistry and its replacement for NCAs still remain in question.

4.3.4.3. Synthesis of PGlu (OBzyl)

To replace PGA derived from Glu(OBzyl)-NCA in the drug conjugate synthesis, an alternative approach was explored by attempting to synthesise PGlu(OBzyl) from Glu(OBzyl)-DKP. This effort aimed to develop a more sustainable method for producing the polymer backbone of the drug conjugate. Among the amino acid DKP derivatives synthesised thus far, Glu(OBzyl)-DKP is the only one that has successfully undergone ROP to form PGlu(OBzyl) (Figure 4.3-19) by heating in DMF alone in the absence of any catalyst at 130 ^{o}C. However, the polymerisation was highly inefficient, yielding only trace amounts of polymer after dialysis. This low recovery could be attributed to the thermal degradation of the DKP monomer [18], a phenomenon also observed during the thermal condensation of Glu(OBzyl)-OH in ethylene glycol, suggesting that elevated temperatures may induce decomposition rather than polymerisation. Interestingly, when the reaction temperature was lowered slightly, the DKP monomer was fully recovered after dialysis, indicating temperature-dependent decomposition and ring-opening occur within a close temperature range.

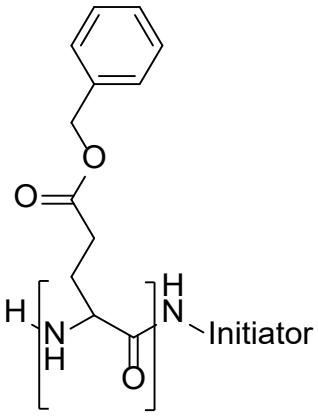

Figure 4.3-19. PGlu(OBzyl)

The structure of the product was confirmed with ^{1}H-NMR spectroscopy. The region from 7.6 to 7.0 ppm represents the benzyl group and amide protons, the peak at 5.10 ppm corresponds to the two protons of the benzyl protecting group, the range from 4.53 to 4.04 ppm is attributed to the proton on the polymer backbone, and the peaks between 2.28 and 1.99 ppm are assigned to the side chain protons (Figure 4.3-20) similar to that in the literature [113]

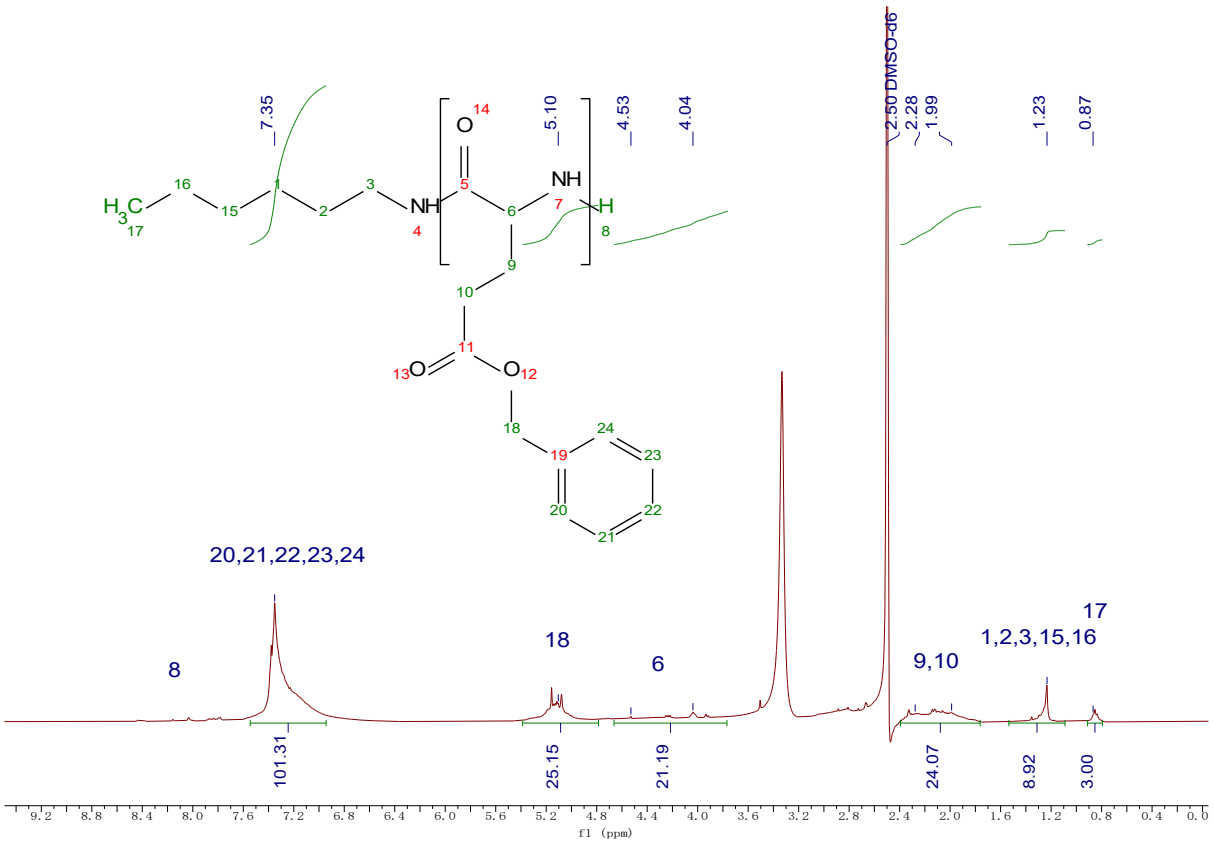

Figure 4.3-20. ^{1}H-NMR spectrum (400 MHz, DMSO-d_6) of PGlu(OBzyl) from Glu(OBzyl)-DKP. 7.35 ppm (OBzyl ring), 5.10 ppm (-O-CH_2-), 4.53- 4.04 ppm (-C=O-C**H**-NH-), 2.28-1.99 ppm (-C**H**$_2$-C**H**$_2$-), 1.23-0.87 ppm (initiator)

Molecular weight of PGlu(OBzyl) was assessed via MALDI-TOF mass spectrometry. Interestingly, spectra show three broad peaks across range 1500- 8000 Da and peaked at 2237 Da, 3246 Da and 6524 Da, each equivalent to approximately 10, 14 and 29 repeat units respectively (Appendix 0-5). This indicates the ROP of Glu(OBzyl)-DKP was highly un-controlled and need further optimisation. Moreover, as discussed previously, due to mass discrimination effects and detector saturation in MALDI-TOF analysis the measured molecular weights may be slightly underestimated relative to their true values[110,111,112].

Nevertheless, its successful polymerisation of Glu(OBzyl)-DKP in the absent of Boc activation indicates the carboxylate-OBzyl group at the side chain may act as an electro withdrawing group to weaken the amide bond and facilitating the transamidation/ propagation process. Therefore, Ni(0)cod_2: SIPr·HCl [25] was introduced to enhance the polymerisation process without prior amide bond activation, which successfully facilitated the ROP of Glu(OBzyl)-

DKP. Despite this improvement, the polymer yield remained low, at approximately 20% and contain impurities. The limited polymer recovery may be due to uncontrolled ring opening, leading to the formation of dimers and the thermal degradation of the monomer that were subsequently removed during dialysis.

Therefore, the catalysed ROP still need further optimisation such as using LiHMDS instead of $Ni(0)cod_2$: SIPr·HCl due to potential decomposition of catalyst during handling without glovebox [25]; lowering the reaction temperature to prevent thermal degradation of the DKP monomer. And Boc activation may not be needed to avoid further complication of the reaction system [25].

4.3.4.4. Synthesis of PLys(Cbz)

The ROP of Lys(Cbz) DKP failed that no ROP was detected during and after the reaction. And all the DKP used in each polymerisation reactions were recovered after dialysis and freeze drying. Because of its low solubility in many solvents at temperature below (≤60 ^{o}C), Lys(Cbz) DKP failed to perform amide activation with Boc group, due to thermal decomposition of the main reagent for Boc activation- Boc_2O above its melting point (63 ^{o}C) [109]. Hence catalysts that are used for transamidation, $Ni(0)Cod_2$: SIPr. HCl and LiHMDS were not tested. Therefore, its amide activation requires resorting to an alternative electron-withdrawing group in the future.

4.3.5. Synthesis of amino acid DKMs

Unlike the amino acid DKPs, amino acid DKMs are known for their ability to undergo controlled ROP [46,66,67,68]. This process enables the synthesis of well-defined polymers with precise molecular weights and architectures using suitable catalysts [46,47,69]. Unlike amino acid NCAs, phosgenants are not required for the synthesis of DKMs. Additionally, amino acid DKMs are significantly more stable than NCAs, though high temperatures are typically required for their ROP, even in the presence of catalysts such as tin(II) octoate [67]. However, a recently developed catalyst has been reported to facilitate ROP at room temperature [46,47,69]. Given these advantages, amino acid DKMs have the potential to

serve as an alternative to amino acid NCAs.

4.3.5.1. Synthesis of Sarcosine- Glycolic acid (Sar-GA) DKM

To produce poly(Sarcosine-Glycolic Acid) (P(Sar-GA)), Sar-GA DKM was synthesised first (Figure 4.3-21). In **Method 1**, Sar-GA DKM was synthesised using the cyclic agent 2-Chloro-1-methylpyridinium iodide as descripted in the literature (Scheme 4.3-2) [61, 114]. However, the purification was tedious and result in low yield with low purity.

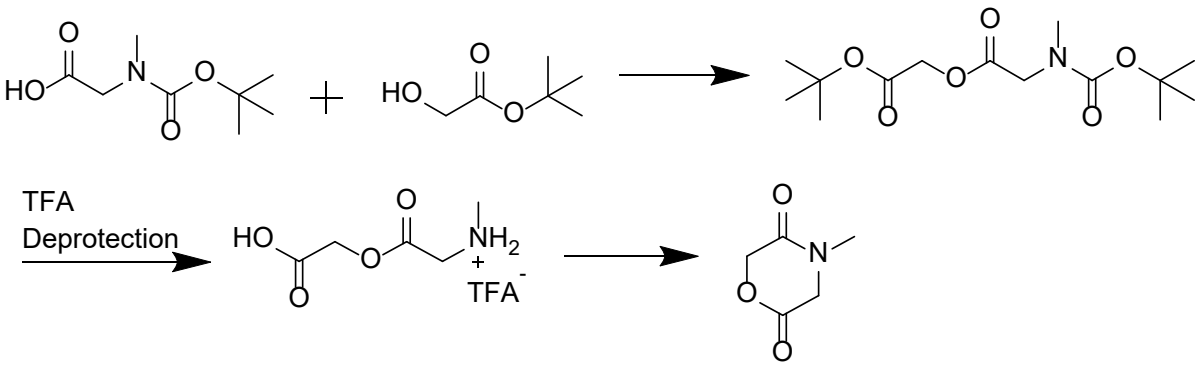

Scheme 4.3-2. Synthesis of Sar-GA DKM by method 1

In **Method 2**, sarcosine reacts with chloroacetyl chloride producing N-chloroacetyl-N-methylglycine then cyclisation was performed in DMF with $NaHCO_3$ under mild heating (Scheme 4.3-3) [18]. However, this method still only results in low product yield. Because both methods resulted in low overall yield. Therefore, the synthesis of Sar-GA DKM was resorted to **Method 3**, a new and more efficient approach in producing Sar-GA DKM.

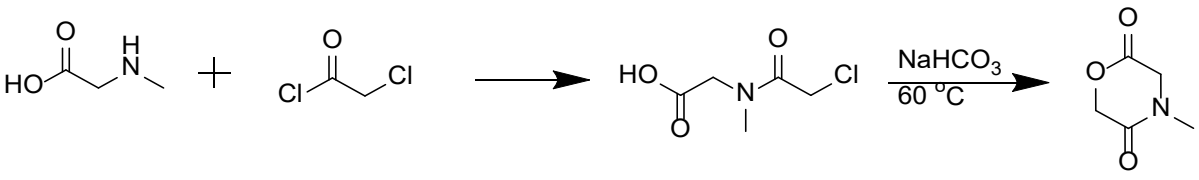

Scheme 4.3-3. Synthesis of Sar-GA DKM by Method 2

Method 3 is similar to that of Sar-DKP synthesis, both sarcosine and glycolic acid were refluxed in toluene at high temperatures to promote ester, amide condensation and cyclisation. This method provided a cleaner reaction with highest yield and minimal

impurities. However, its application was limited to sarcosine, as other amino acids, such as Glu(OBzyl)-OH, Lys(Cbz)-OH, and alanine only form clumps at the bottom of the reaction flask, preventing their reaction with glycolic acid. As a result, only Sar-GA was successfully synthesised using this approach.

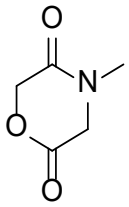

Figure 4.3-21. Sarcosine-Glycolic acid (Sar-GA) DKM

Distinct and sharp peaks of glycolic acid and sarcosine were observed in the ^{1}H-NMR spectrum. Peak at 4.76 ppm is the two glycolic acid proton, peak at 4.46 ppm is the two sarcosine protons and peak at 3.00 ppm is the methyl group protons of sarcosine(Figure 4.3-22).

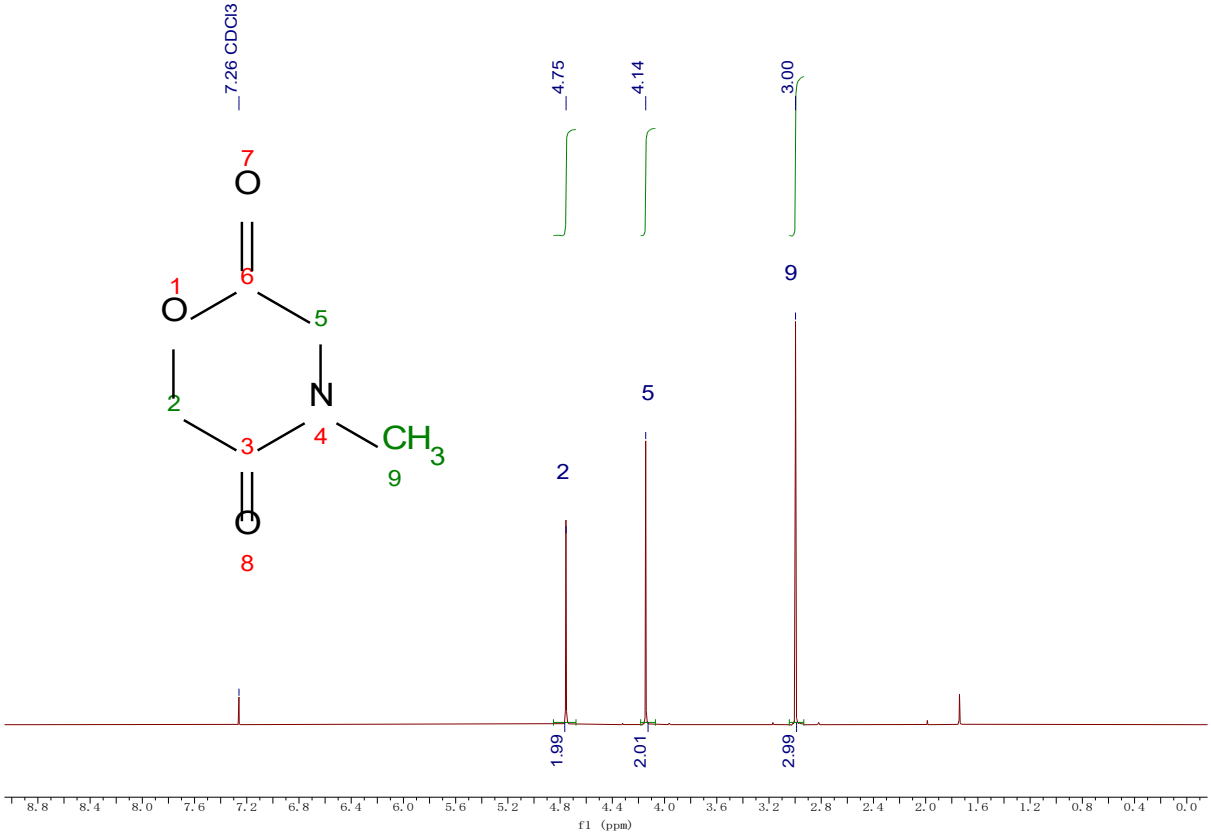

Figure 4.3-22. ^{1}H-NMR spectrum (400 MHz, $CDCl_3$) of Sar-GA DKM: 4.75 ppm (-O-CH_2-), 4.14 ppm (-N-

CH_2-), 3.00 ppm (-CH_3)

The structure was further validated by ^{13}C NMR spectroscopy. The peaks at 164.11 ppm and 163.06 ppm were assigned to the two quaternary carbonyl carbons of the cyclic ester, while the signal at 67.36 ppm corresponds to the secondary ester carbon of the DKM ring. The peak at 49.20 ppm is the secondary carbon of tertiary amide. The resonance at 33.14 ppm is attributed to the methyl group carbon. (Figure 4.3-23). These signals are consistent with the expected structure of the monomer.

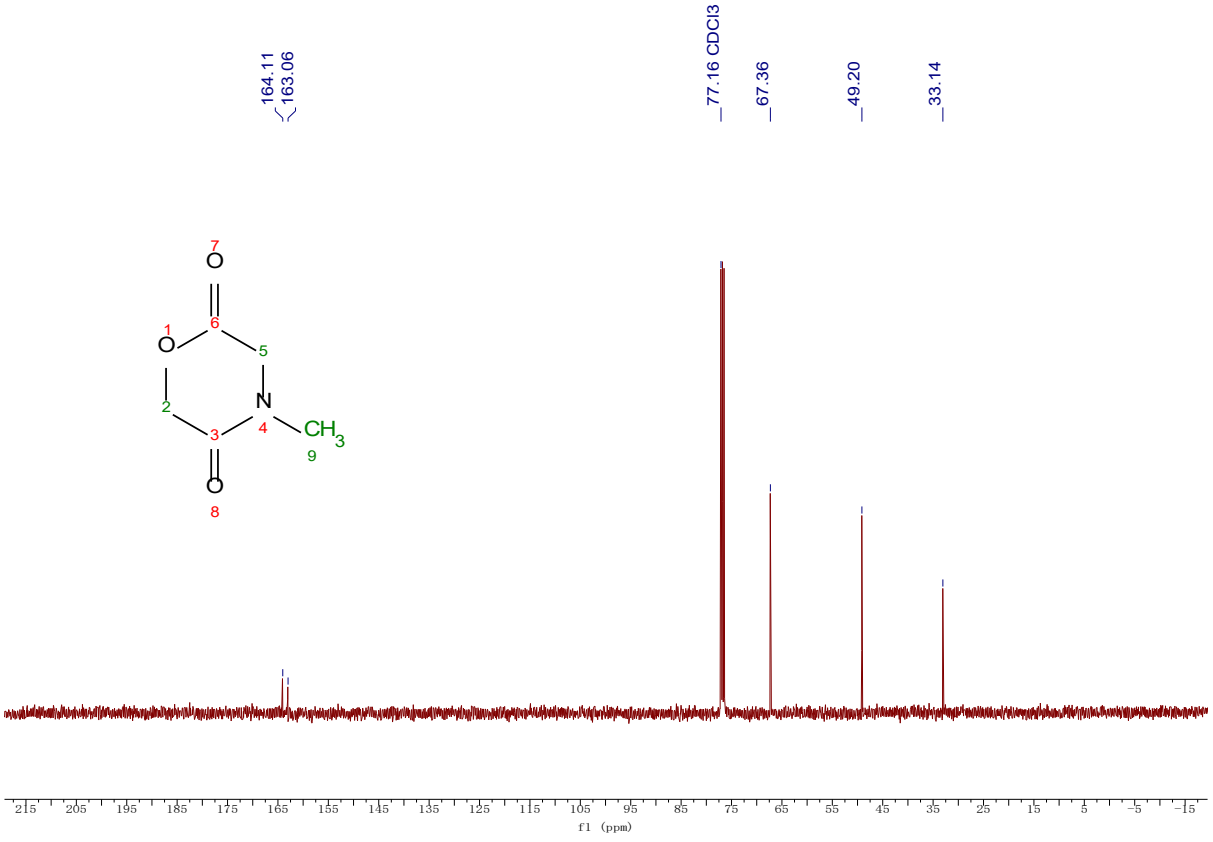

Figure 4.3-23. ^{13}C-NMR spectrum (100 MHz, $CDCl_3$) of Sar-GA DKM: 164.11 ppm and 163.06 ppm (C3, C6), 67.36 ppm (C2), 49.20 ppm (C5), 33.14 ppm (C9)

The disappearance of -OH and -NH peaks in the ^{1}H-NMR spectrum(Figure 4.3-22) and the disappearance of -COOH and -NH_2-$^{+}$ stretching at 3042cm^{-1} and 2977cm^{-1} (Figure 4.3-24)

confirmed the successful formation of Sar-GA DKM.

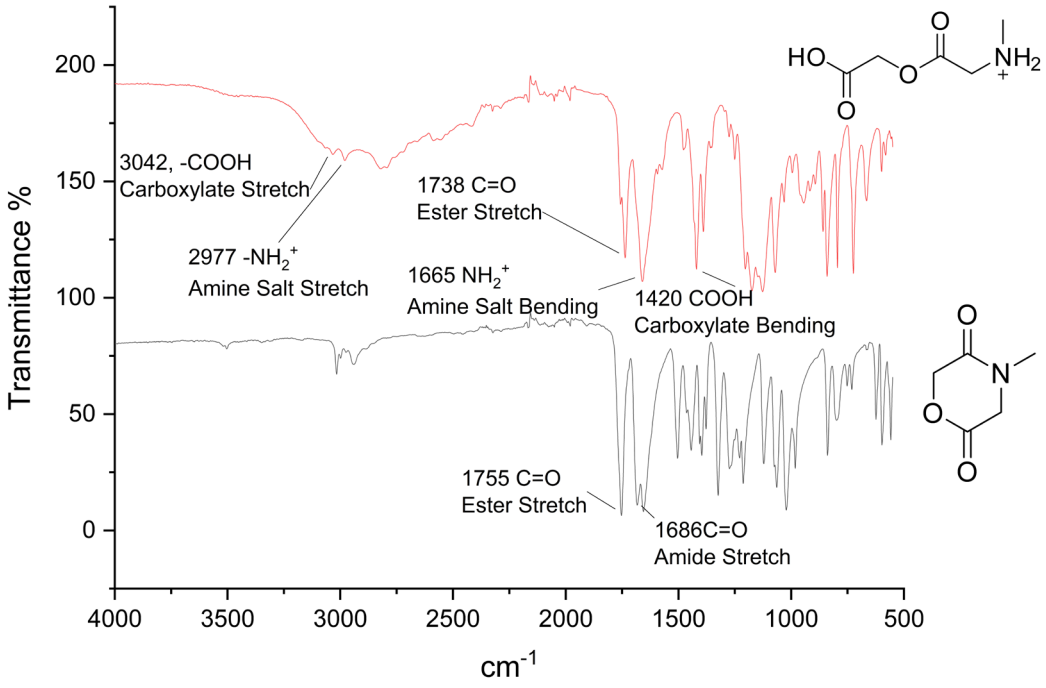

Figure 4.3-24. The FTIR spectrum of 2-(carboxymethoxy)-N-methyl-2-oxoethan-1-aminium (top) and Sar-GA DKM (bottom)

4.3.5.2. Synthesis of Glu (OBzyl)-GA DKM

Glu(OBzyl)-GA DKM (Figure 4.3-25) was successfully synthesised following the method in the literature[18]. H-Glu(OBzyl)-OH was first react with chloroacetate chloride to generate Glu(OBzyl)-GA-Cl. The resulted product was then heated to 60 °C in DMF with $NaHCO_3$ overnight to achieve cyclisation forming Glu(OBzyl)-GA DKM.

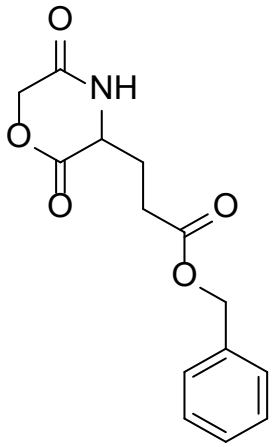

Figure 4.3-25. Glu (OBzyl)-glycolic acid DKM

The structure of the product was confirmed with ^{1}H-NMR spectroscopy (Figure 4.3-26). Peak at 7.36 ppm is the benzyl five protons of protecting group, peak at 6.69 ppm is the amide proton, peak at 5.14 ppm is the two proton from glycolic acid, peak at 4.75 ppm is the two proton from the benzyl protecting group, peak at 4.25 ppm is the proton from the amino acid backbone, peak at 2.61-2.22 ppm is the four protons of amino acid side chain, the NMR spectra is identical to that in the literature [71]. The absent of additional peaks indicate the purity of the monomer which is important for the later polymerisation.

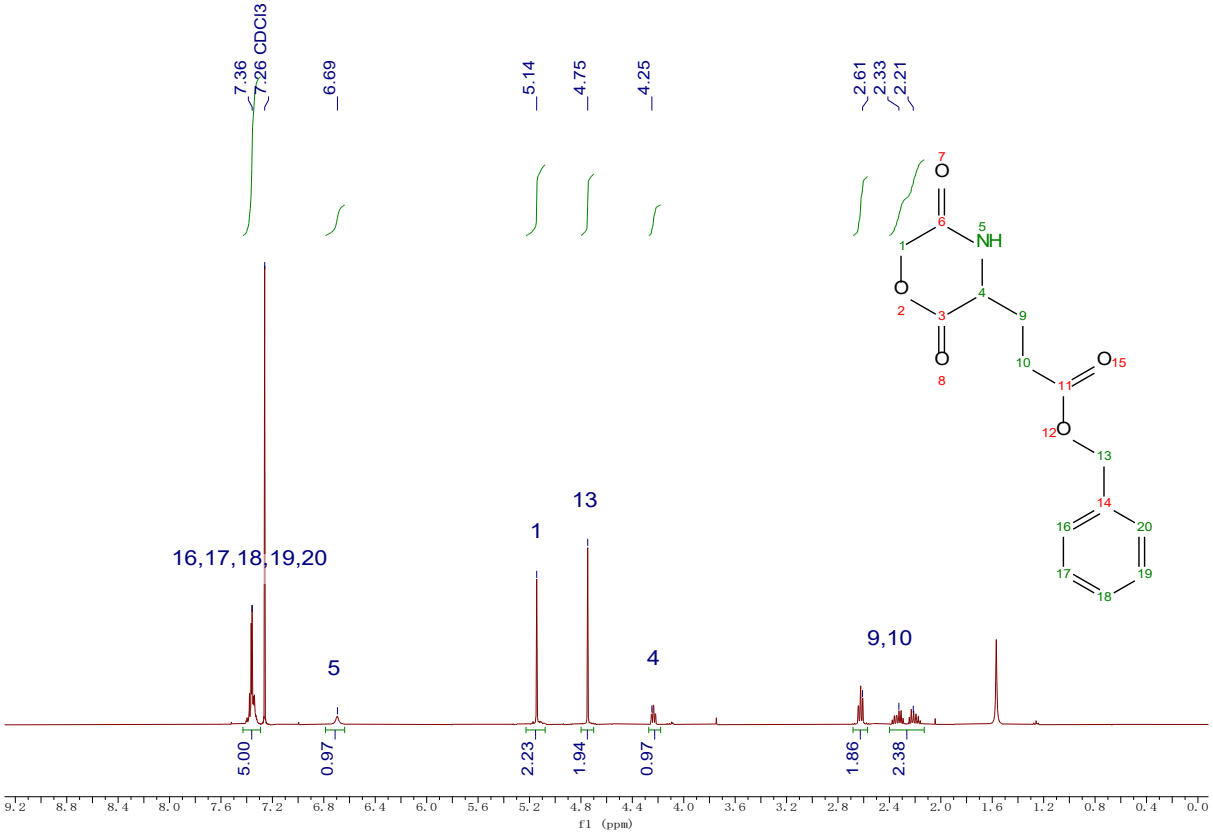

Figure 4.3-26. ^{1}H-NMR spectrum (400 MHz, $CDCl_3$) of Glu(OBzyl)-GA DKM: 7.36 ppm (Phenyl protons), 6.69 ppm (-NH-), 5.14 ppm (-O-CH_2-), 4.75 ppm(-O-CH_2-Ph), 4.25 ppm (-NH-C**H**-), 2.61-2.22 ppm (-C**H**$_2$-C**H**$_2$-)

The product was further characterised by FTIR spectroscopy. The band at 3245 cm^{-1} was assigned to C–H stretching of the OBzyl group, while the signal at 3155 cm^{-1} corresponds to N–H amide stretching. The peak at 2944 cm^{-1} is attributed to sp^3 C–H stretching. Absorptions at 1758 cm^{-1} and 1684 cm^{-1} were assigned to ester C=O stretching, and the band at 1645 cm^{-1} corresponds to amide carbonyl stretching (Figure 4.3-27).

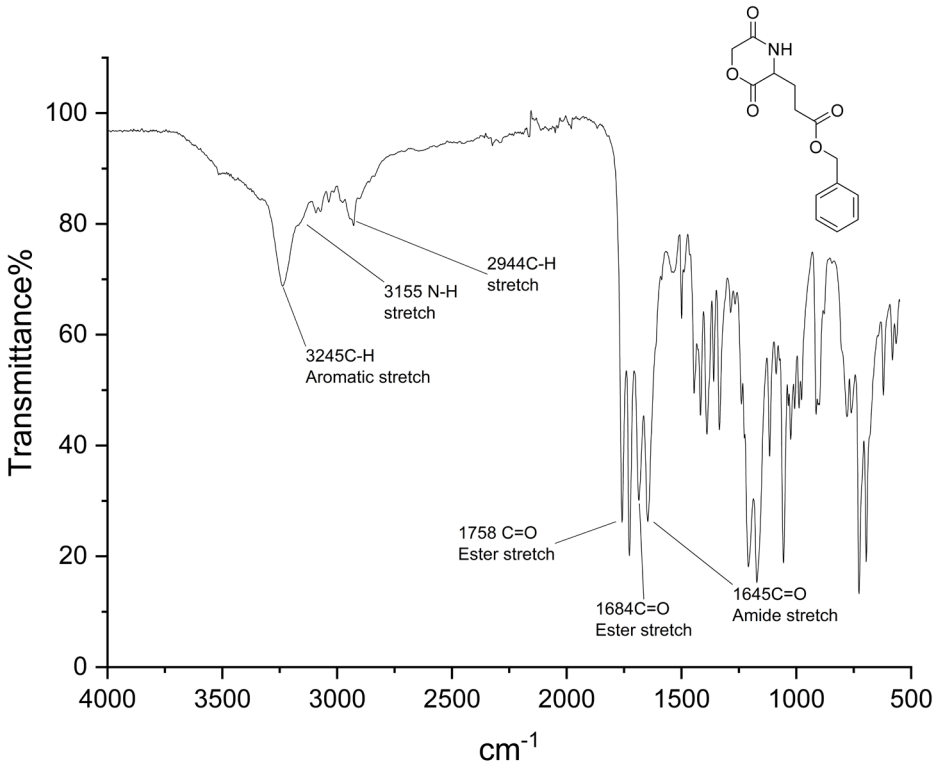

Figure 4.3-27. FTIR spectrum of Glu(OBzyl)-GA DKM: 3245cm^{-1} is C-H OBzyl stretching, 3155 cm^{-1} is N-H amide stretching, 2944 cm^{-1} is C-H sp^3 stretching, 1758 cm^{-1} is C=O ester stretching, 1684 cm^{-1} is C=O ester stretching, 1645 cm^{-1} is amide stretching

It was originally synthesised to replace Glu(OBzyl)-NCA. However, the yield was low with an overall yield of 24%. Consequently, there remains potential for optimisation in the reaction protocols to enhance product yield, such as minimising the reaction duration to mitigate the risk of self-ring opening that can occur with extended heating. Given the time and expense associated with producing the monomer, substituting Glu(OBzyl)-NCA with Glu(OBzyl)-GA DKM is currently deemed economically impractical.

4.3.6. Ring Opening Polymerisation of DKMs

4.3.6.1. Ring Opening Polymerisation of Sar-GA DKM

According to my knowledge, the production of P(Sar-GA) polydepsipeptide has not been reported before. Therefore, to produce a novel biodegradable, biocompatible and

hydrophilic polymer to replace PSar, ROP reactions of Sar-GA DKM were carried out. However, all attempts to polymerise Sar-GA DKM were unsuccessful. Despite the ROP of DKMs typically targeting ester bond cleavage, Sar-GA DKM remained stable, even under high heat and in the presence of strong basic catalysts such as TDB[34] and TBU[32], showing no signs of ring opening.

According to literature on catalytic mechanisms involving TBD [34,46] and TBU [32], as well as TBD: Schreiner's Thiourea co-Catalyst [46] and MeONa: Schreiner's Thiourea Catalyst [43], the presence of the N-methyl group of sarcosine is unlikely to hinder either the monomer-catalyst interaction or the nucleophilic attack of hydroxyl initiators. However, a white crystalline substance slowly formed in the reaction flask after contact with atmospheric air either after attempted ROP of Sar-GA DKM or in its pure form.

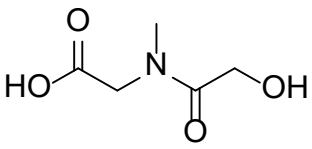

Figure 4.3-28. N-(2-hydroxyacetyl)-N-methylglycine.

Comprehensive analyses via ^{1}H-NMR, DEPT-135 and FTIR were conducted to characterise the white crystalline. Notably, the ^{1}H-NMR spectrum exhibited distinctive peaks at 12.75 ppm and 4.53 ppm, which correspond respectively to -COOH and -OH groups (Figure 4.3-29).

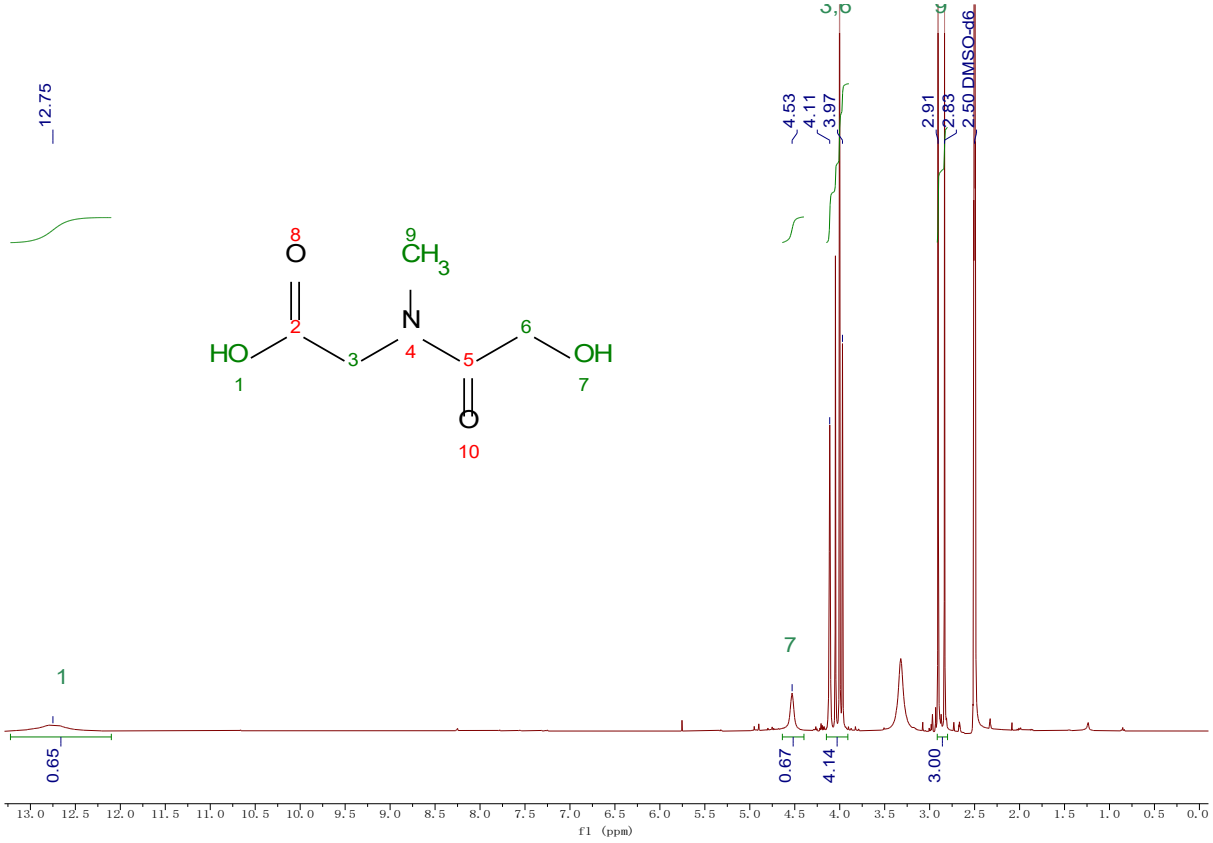

Figure 4.3-29. ^{1}H-NMR spectrum (400 MHz, DMSO-d_6) of N-(2-hydroxyacetyl)-N-methylglycine: 12.75 ppm(-COOH), 4.53 ppm (-OH), 4.11-3.97 ppm (-C**H**$_2$-N-, -C**H**$_2$-OH) 2.91-2.83 ppm (-N-CH_3)

The structure of the sample was further characterised with DEPT-135 spectroscopy. Peak at 59.46 ppm is the hydroxy carbon, while signal at 48.79 ppm correspond to the -**C**H_2- carbon in the sarcosine backbone. And the peak at 34.04 ppm is the methyl group carbon of the sarcosine (Figure 4.3-30).

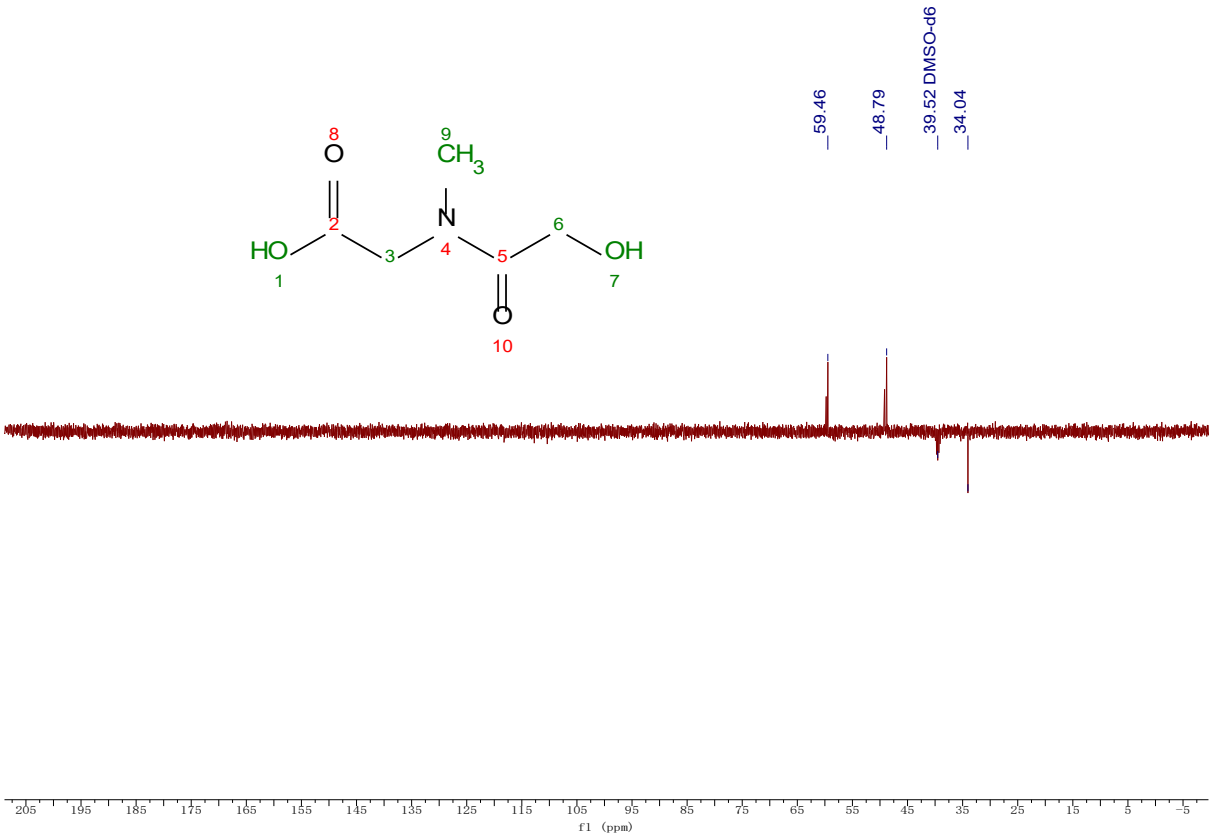

Figure 4.3-30. DEPT-135 (100 MHz, DMSO-d_6) of N-(2-hydroxyacetyl)-N-methylglycine: 59.46 ppm (C6), 48.79 ppm (C3), 34.04 ppm (C9)

Furthermore, the FTIR spectrum revealed absorption bands at 3326cm^{-1} and 2979cm^{-1} which are indicative of -OH stretching and -COOH stretching (Figure 4.3-31). These spectral features show that the obtained compound was probably N-(2-hydroxyacetyl)-N-methylglycine (Figure 4.3-28), ring opened form of Sar-Ga DKM, suggesting that ester bond hydrolysis occurred after contact with atmospheric air.

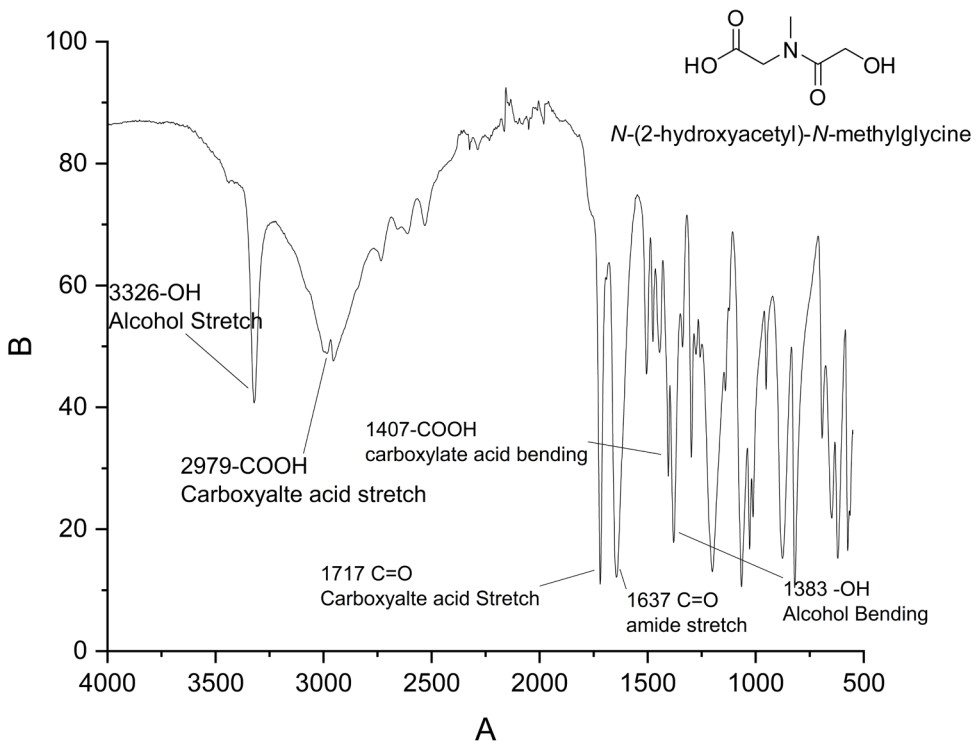

Figure 4.3-31. FTIR spectrum of N-(2-hydroxyacetyl)-N-methylglycine

Curiously, under the same reaction conditions, the hydroxyl initiator failed to initiate polymerisation of Sar-GA DKM. This result suggests that while Sar-GA DKM possesses the potential for ROP, it may require a more potent catalyst than those used in our study. For instance, the Schreiner's Thiourea Catalyst used in the ROP is approximately 2800 times less active than that of 1-(3,5-bis(trifluoromethyl)-phenyl-3-cyclohexyl-2-thiourea) (TU) [43], which may explain the lack of polymerisation.

Interestingly, Sar-GA DKM can also be synthesised via the thermal condensation of N-(2-hydroxyacetyl)-N-methylglycine (Figure 4.3-28). This alternative synthetic route suggests possible implications for its reactivity in future polymerisation studies, warranting further investigation.

4.3.6.2. Ring Opening Polymerisation of Glu(OBzyl)-GA DKM

To replace PGA, poly(Glutamic Acid-Glycolic Acid) polydepsipeptide (P(Glu-GA)) were

synthesised from the ROP of Glu(OBzyl)-GA DKM. P(Glu-GA) is a hydrophilic polymer that contains carboxylate groups in the side chain which can be subjected to modification such as conjugation to drug molecules or polymers. The structure of the synthesised product-P(Glu(Obzyl)-GA) was confirmed by ^{1}H-NMR spectroscopy(Figure 4.3-33). The ^{1}H-NMR spectrum revealed the region from 8.65 to 8.51 ppm is attributed to the amide proton, the peak at 7.33 ppm corresponds to the protons of the benzyl ring, the peak at 5.08 ppm represents the protons of the benzyl protecting group, the range from 4.80 to 4.45 ppm encompasses the protons from glycolic acid and the polymer backbone, and the region from 2.32 to 1.84 ppm accounts for the protons of the amino acid side chain.

Given the structural similarities between TU and Schreiner's Thiourea Catalyst, both have been successfully employed in the ROP of lactide and lactone, as documented in the literature [43]. However, the presence of strong electron-withdrawing groups such as -CF_3 in Schreiner's Thiourea Catalyst enhances its acidity compared to TU. This increased acidity diminishes the Lewis/Brønsted base interaction between the imidate ion and the initiator, resulting in an approximately 2800 times less effective catalytic performance than that exhibited by TU (Figure 4.3-32)[43].

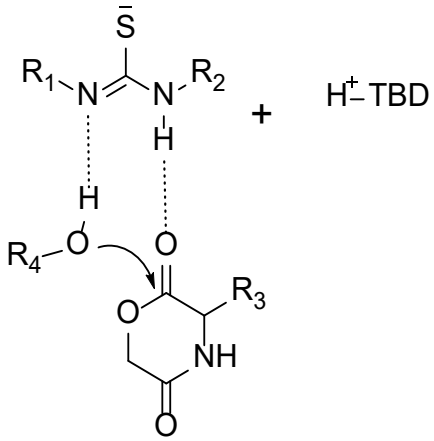

Figure 4.3-32. initiation mechanism of thiourea catalyst with TBD [43,46]

Despite this, the ROP reaction of Glu (OBzyl)-GA DKM with Schreiner's Thiourea Catalyst: TBD (3:1) proved unsuccessful at room temperature, with only minimal peak broadening detected in the ^{1}H-NMR spectrum after a week of reflux. Consequently, additional TBD was introduced during the reflux phase of the reaction to enhance the ROP rate.

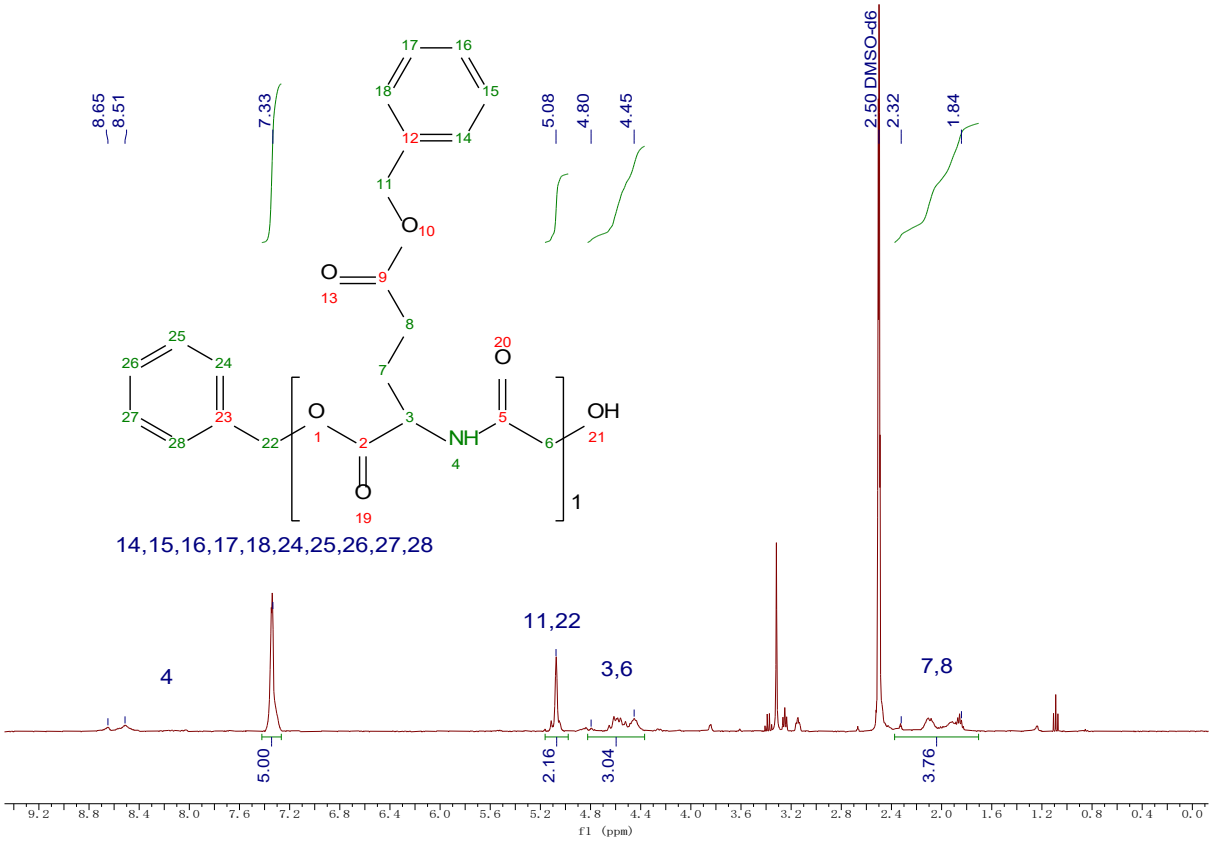

Figure 4.3-33. ^{1}H-NMR spectrum (400 MHz, DMSO-d_6) P(Glu(OBzyl)-GA): 8.65-8.51 ppm (-NH), 7.33 ppm (Phenyl ring), 5.08 ppm(-CH_2-Ph), 5.80-4.45 ppm (-CH_2-O-, -CH-), 2.32-1.84 ppm (-C**H**$_2$-C**H**$_2$-)

Its M_n and M_w were calculated through the below equations

$$Mn = \frac{\sum Ni*Mi}{\sum Ni} = \; Mn = \frac{32*1714.6974+16*1763.5653+\cdots+20*3338.2915+16*3295.1821}{32+16+\cdots+20+16} = 2285.00$$

Where *Ni* is the number of molecules or the intensity of percentage with molecular weight *Mi*.

$$Mw = \frac{\sum Ni*Mi^2}{\sum Ni*Mi} = \; Mw = \frac{32*1714.6974^2+16*1763.5653^2+\cdots+20*3338.2915^2+16*3295.1821^2}{32*1714.6974+16*1763.5653+\cdots+20*3338.2915+16*3295.1821} = 2383.60$$

Yielding a number average molecular weight (M_n) of 2285.0 Da, a weight average molecular weight (M_w) of 2383.6 Da, and a dispersity of 1.043 $Đ_M$, as determined by MALDI-TOF mass spectrometry (Figure 4.3-34). However, due to the mass discrimination and detector saturation in MALDI-TOF analysis, the measured molecular weights may be slightly lower than the true values [110,111,112]. Furthermore, signal resolution decreases with increasing

m/z, typically producing a broad bell-shaped distribution in the range of 2000–4000 Da, which complicates the accurate determination of M_w and M_n.

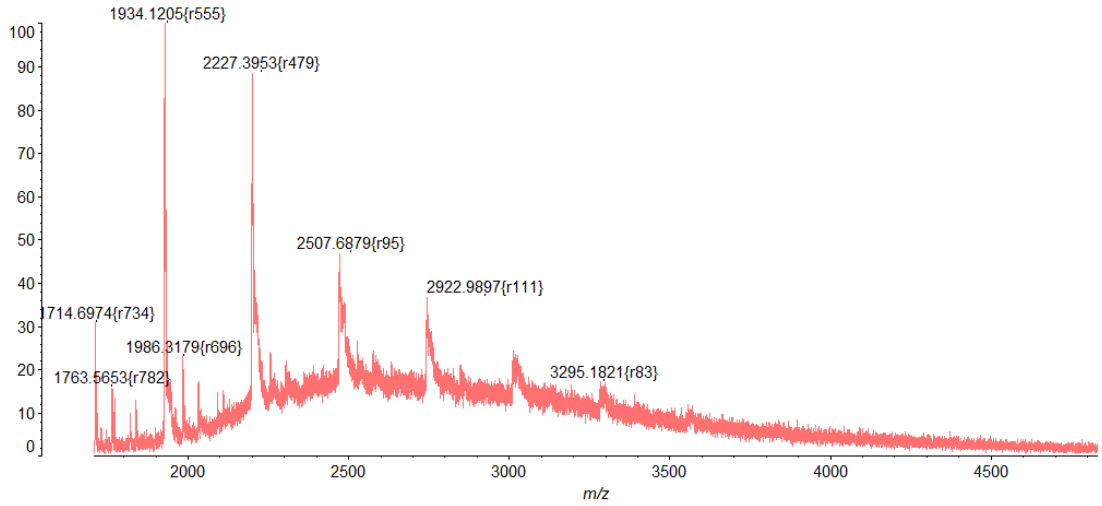

Figure 4.3-34. MALDI-TOF mass spectrometry analysis result of P(Glu(OBzyl)-GA)

This polymer was characterised as oligomer with approximately 8 repeating units. This resulted from the excessive addition of the superbase TBD, leading to self-initiation and the formation of cyclic polydepsipeptide, ultimately resulting in oligomer [46]. Therefore, to achieve a well-controlled P(Glu(OBzyl)-GA), it is recommended that TU be utilised [32,34,46].

4.3.7. Melt Polycondensation of Glycolic Acid and Sarcosine

Due to the unsuccessful ROP of Sar-GA DKM, I shifted the approach to melt polycondensation of glycolic acid and sarcosine as an alternative method for synthesising polydepsipeptides.

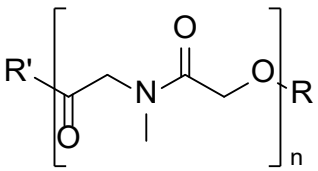

Figure 4.3-35. P(Sar-GA), R≠R'

It has proven effective in synthesising high molecular weight polydepsipeptides using glycolic acid, lactic acid, glycine[115,116] and alanine[116], as well as other functionalised amino acids such as glutamic acid [117] and aspartic acid[118,119]. These reactions typically require metallic catalysts such as $SnCl_2$, SnO, $ZnCl_2$, Zn, and Al [115,116,118]. Sn(II)Oct_2 was preferably selected as a substitute due to its well-documented efficacy in esterification and transesterification reactions [116,120,121].

Melt polycondensation presents a simple and straightforward approach to synthesising polydepsipeptides without the need for DKMs. However, this method comes with several challenges, including undesirable side reactions such as racemisation and backbiting, which can occur due to the high reaction temperatures [74], while the use of toxic metal catalysts poses safety concerns [122]. Moreover, compared to ROP, melt polycondensation affords limited control over molecular weight distribution, rendering it less suitable for applications demanding precise polymer structures.

The polymerisation was confirmed with ^{1}H-NMR spectroscopy, which revealed three characteristic broad peaks at 4.94-4.65 ppm (2H, glycolic acid), 4.28-3.89 ppm (2H, sarcosine), and 2.94-2.70 ppm (3H, sarcosine) (Figure 4.3-36).

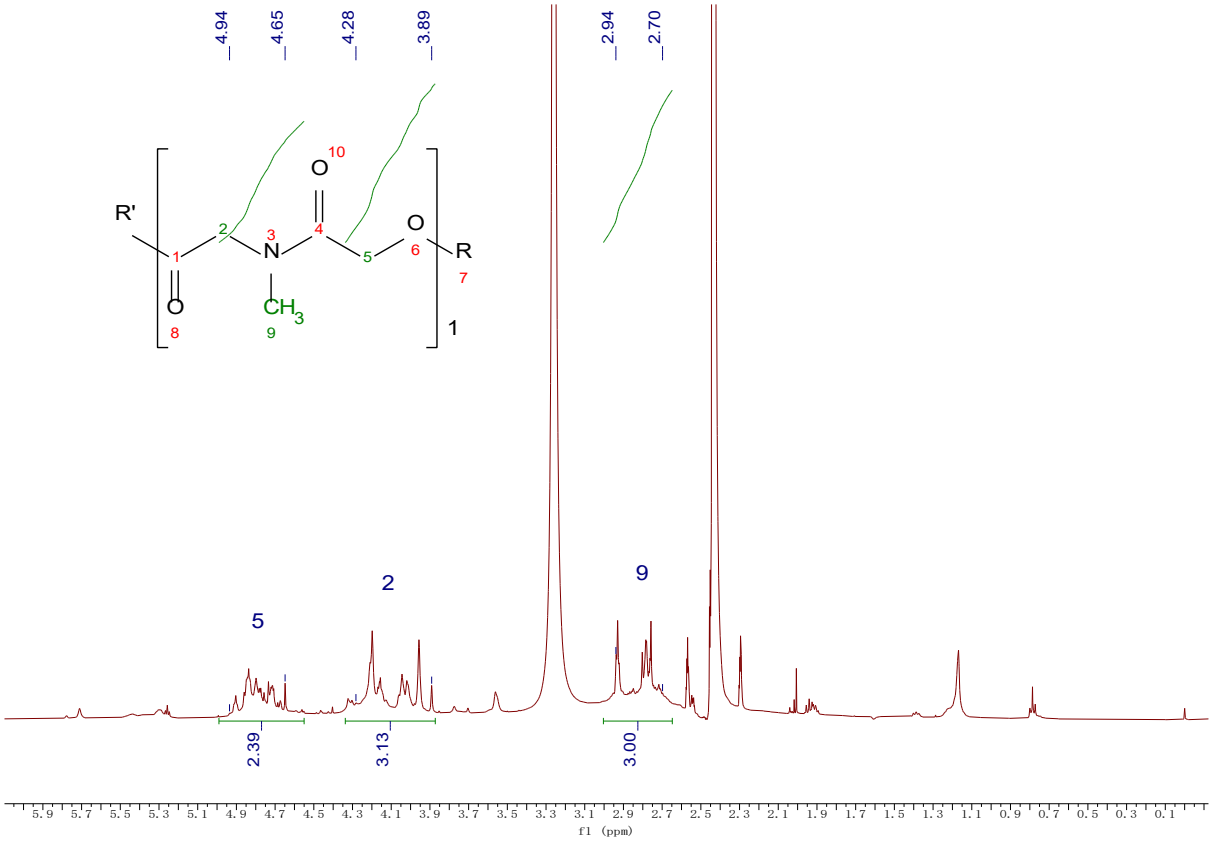

Figure 4.3-36. ^{1}H-NMR spectrum (500 MHz, DMSO-d_6) of P(Sar-GA): 4.94-4.65 ppm (2H (GA)), 4.28-3.89 ppm (2H (Sar)) and 2.94-2.70 ppm (3H (Sar))

Despite this confirmation, trace amount polymer yielded following dialysis, with ^{1}H-NMR spectra indicating persistent impurities that resisted removal. MALDI-TOF analysis further determined a molecular weight range of 1800-3200 Da (Appendix 0-6). However, mass discrimination and detector saturation effects may lead to underestimation of the true molecular weights [110,111,112]. As a result, the measure molecular weights may be slightly lower than the true values. Furthermore, signal resolution limitation producing a broad bell-shaped distribution complicating the accurate determination of M_w and M_n.

Initially, the low yield was hypothesised to result from an unclear catalytic interaction between Sn(II)Oct_2 and acetic anhydride. That the generation of water during melt condensation may cause the decomposition of Sn(II)Oct_2 to Sn(IV) deactivating the catalyst. Further study and analysis are needed to justify this claim such as the replacement of Sn(II)Oct_2 with $SnCl_2$, and to produce P(Sar-GA) through melt condensation polymerisation effectively.

4.3.8. Synthesis of P(Glu-GA)-(PSar-Gly-CPT) Drug Conjugate

To study how does changing the PGA into P(Glu-GA) will affect the properties of the drug conjugate, P(Glu-GA)-(PSar-Gly-CPT) was synthesised as a comparison of PGA-(PSar-Gly-CPT). But in order to mitigate the potential issue caused by oligomer in drug carrying system such as the NPs disintegration due to in vivo dilution after injection [126,132,133,134,135], the P(Glu-GA) oligomer produced was crosslinking procedure with 0.175 mol equivalent of ethylenediamine prior to its conjugation with CPT-Gly and F-PSar to increase its repeating unit as a initial prove of concept study. Then crosslinked P(Glu-GA) is subjugated to drug conjugate synthesis.

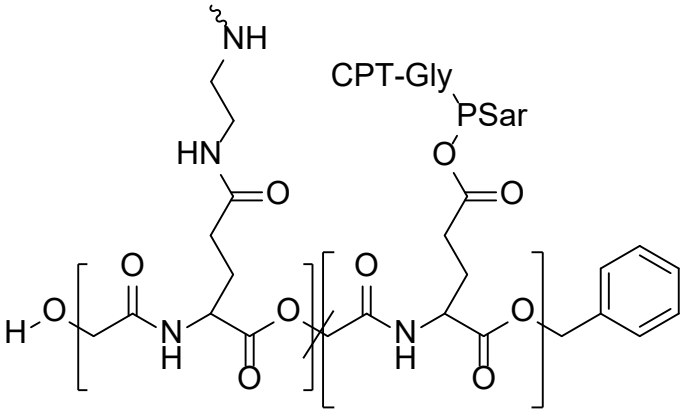

Figure 4.3-37. P(Glu-GA)-(PSar-Gly-CPT). /: indication of the random position of cross-linked side chain and CPT-Gly-PSar in P(Glu-GA) backbone.

P(Glu-GA)-(PSar-Gly-CPT) (Figure 4.3-37) was synthesised with drug content yield of 20.3% (w/w) calculated from ^{1}H-NMR integration (Figure 4.3-38). The drug content was estimated through proton integration in the ^{1}H-NMR spectrum through equation: $=$

$$\frac{(5.40-5.60\ ppm)/2*347.3}{\frac{\left((3.78-5.32\ ppm)-(5.40-5.60\ ppm*2)-\left(\frac{2.73-2.95\ ppm}{3}*2\right)\right)}{3}*187.2+\left(\frac{2.73-2.95\ ppm}{3}*71\right)+\left(\frac{5.40-5.60\ ppm}{2}*(404.4-17)\right)}$$

$$=\frac{\frac{0.08}{2}*347.3}{\frac{\left(1.29-0.08*2-\frac{0.91}{3}*2\right)}{3}*187.2+\frac{0.91}{3}*71+\frac{0.08}{2}*(404.4-17)}=0.203$$

Where 5.40-5.60 ppm correspond to the two protons of CPT, 3.78-5.32 ppm contains three proton from P(Glu-GA), four protons from CPT-Gly and two protons from PSar, 2.73-2.95 ppm represent the three protons from methyl group; 347.3 is the MW of CPT, 187.2 is the MW of P(Glu-GA) repeating unit, 71 is the MW of PSar repeating unit, 387.4 represent the MW of CPT-Gly after losing a -OH group during conjugation. The drug content was estimated purely by integration of characteristic signals in the ^{1}H NMR spectra, making the result sensitive to spectral resolution and integration accuracy. Therefore, orthogonal techniques should be used to further validate its drug content in the future.

Peaks from 8.71 to 7.18 ppm correspond to the five protons of CPT protons and the amide protons of the P(Glu-GA). While peaks at 5.50 ppm represent the two protons of CPT, and peaks from 5.32-3.78 ppm result from four protons from CPT, three protons from P(Glu-GA) and two protons from PSar. The broad peak from 2.95 to 2.73 ppm is three protons from PSar. Peaks from 2.45-1.99 ppm correspond to four protons of P(Glu-GA) side chain and two protons from CPT. Characteristic peaks in the spectra confirmed the presence of CPT, PSar, and P(Glu-GA) backbone structures. Therefore, the sample was used in the following analysis.

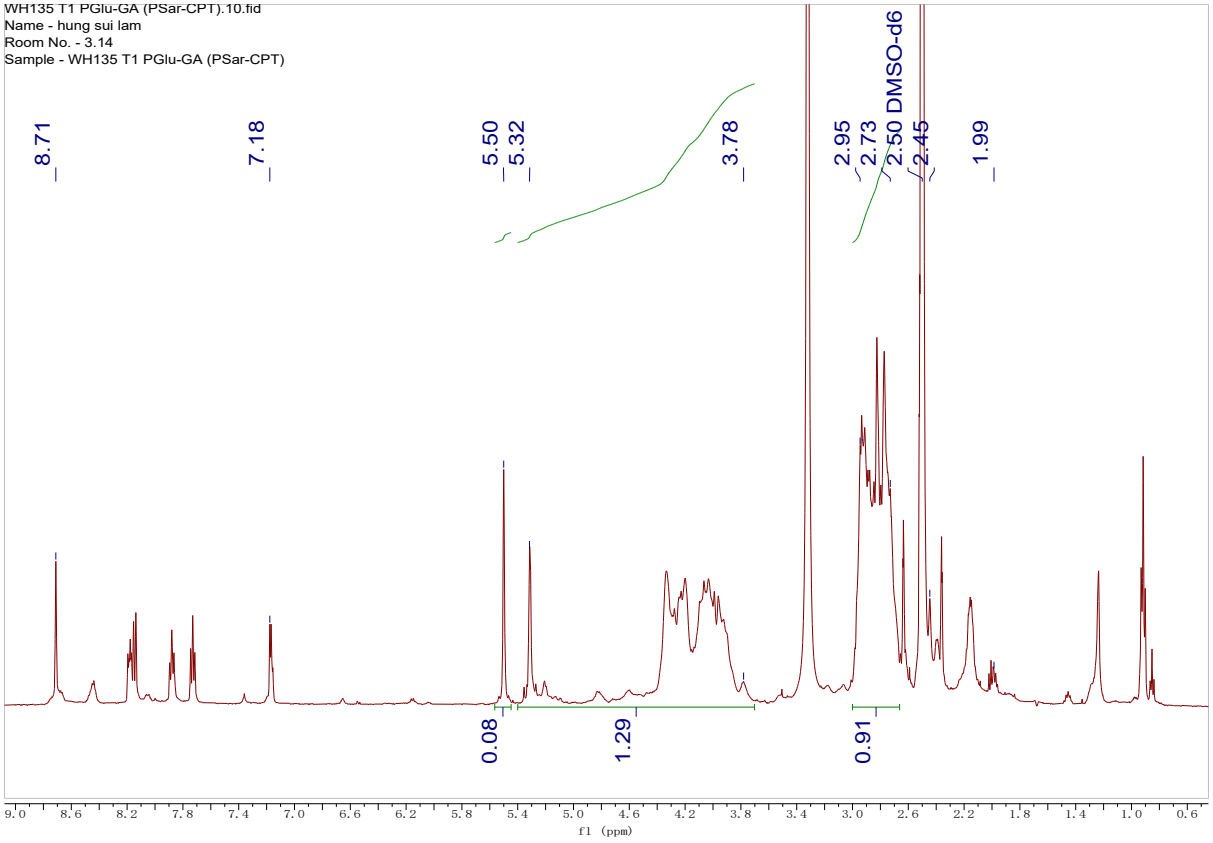

Figure 4.3-38. ^{1}H-NMR spectrum (500 MHz, DMSO-d_6) of P(Glu-GA) (PSar-Gly-CPT): 8.71-7.18 ppm (-CH=C-(CPT), -COOH (P(Glu-GA)), -NH-), 5.50 ppm(-N-CH_2-C= (CPT)), 5.32-3.78 ppm (-O-CH_2-C=C-(CPT), -C**H$_2$**-NH- (CPT), -O-CH_2- (P(Glu-GA)), -C=O-C**H**-NH-(P(Glu-GA)), -C**H$_2$**-N(CH_3)- (PSar)), 2.95-2.73 ppm (-CH_2-N(C**H$_3$**)- (PSar)), 2.45-1.99 ppm (-C**H$_2$**-C**H$_2$**- (P(Glu-GA)), CH_3-C**H$_2$**-(CPT))

Subsequently, the capability of this conjugate to self-assembly into NPs were analysed by DLS three times. Despite the successful synthesis and drug incorporation, the conjugate exhibited pronounced water solubility, which precluded its ability to form nanoparticles. At a concentration of 1.0 mg/mL, the conjugate remained fully dissolved in the aqueous medium. This suggests that the hydrophobic contribution of CPT, at 20.3% (w/w) was insufficient to promote the nanoprecipitation of the drug conjugate indicating at this stage this drug conjugate is not suitable as a cancer therapeutic as its high possibility in NPs disintegration after administration due to *in vivo* dilution even if it forms NPs at higher concentrations [126,132,133,134,135]. One solution could be increasing the drug content, thus to increase the hydrophobic interactions to promote the formation of NPs. Consequently, further research is necessary to systematically investigate how variations in CPT content influence

the conjugate's behaviour in aqueous environments.

4.3.9. Synthesis of P(Glu-GA)-[(CPT-Gly)-*co*-(F-PSar)]

The polymer drug conjugate P(Glu-GA)-[(CPT-Gly)-*co*-(F-PSar)] (Figure 4.3-39) was synthesised to investigate the impact of different polymeric backbones on the physicochemical properties of the resulting NPs.

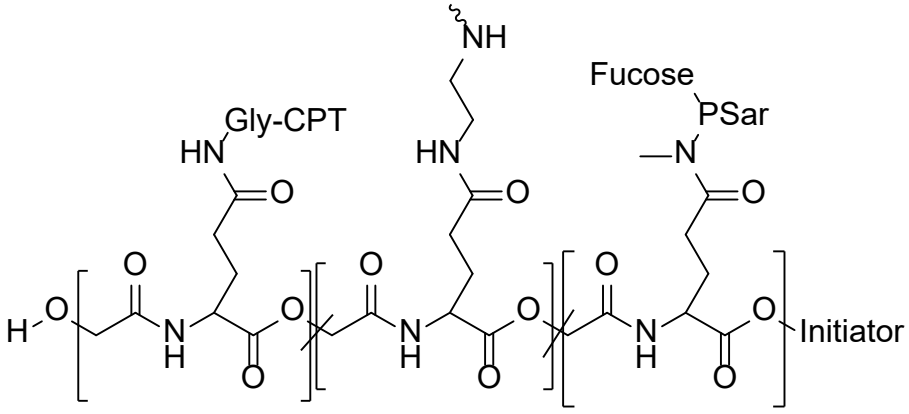

Figure 4.3-39. P(Glu-GA)-[(CPT-Gly)-*co*-(F-PSar)]. /: indication of the random position of cross-linked side chain, CPT-Gly and F-PSar in P(Glu-GA) backbone.

The drug content was estimated through ^{1}H-NMR integration, yielding a value of 28.8% (w/w). The drug content was estimated through proton integration in the ^{1}H-NMR spectrum through equation:

$$= \frac{(5.40-5.60\ ppm)/2*347.3}{\frac{\left((3.91-5.32\ ppm)-(5.40-5.60\ ppm*2)-\left(\frac{2.73-2.95\ ppm}{3}*2\right)\right)}{3}*187.2+\left(\frac{2.73-2.95\ ppm}{3}*71\right)+\left(\frac{5.40-5.60\ ppm}{2}*(404.4-17)\right)}$$

$$= \frac{\frac{0.15}{2}*347.3}{\frac{\left(1.47-0.15*2-\frac{0.55}{3}*2\right)}{3}*187.2+\frac{0.55}{3}*71+\frac{0.15}{2}*387.4} = 0.288$$

Where 5.4-5.6 ppm correspond to the two protons of CPT, 3.91-5.32 ppm contains three proton from P(Glu-GA), four protons from CPT-Gly and two protons from PSar, 2.73-2.95 ppm represent the three protons from methyl group; 347.3 is the MW of CPT, 187.2 is the MW of P(Glu-GA) repeating unit, 71 is the MW of PSar repeating unit, 387.4 represent the MW of CPT-Gly after losing a -OH group during conjugation. The drug content was estimated

only by integration of characteristic signals in the ^{1}H NMR spectra, making the result sensitive to spectral resolution and integration accuracy. Therefore, a wider range of techniques should be used to further validate its drug content in the future.

Additionally, the presence of distinct peaks corresponding to the O-acetyl groups of fucose at 2.13 ppm, 2.03 ppm, and 1.93 ppm in the ^{1}H-NMR spectrum provides strong evidence of the presence of F-PSar in the system(Figure 2.3-4).

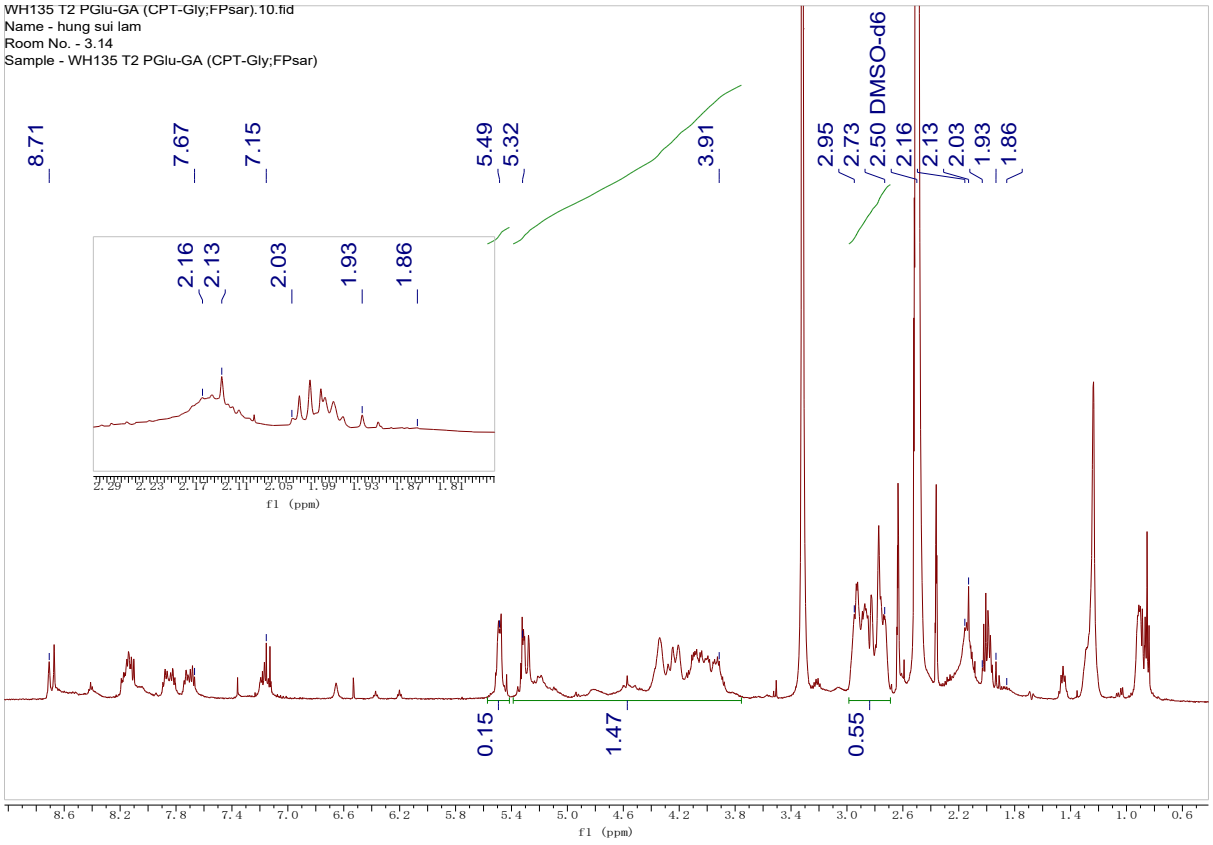

Figure 4.3-40. ^{1}H-NMR spectrum (500 MHz, DMSO-d_6) of P(Glu-GA)-[(CPT-Gly)-*co*-(F-PSar)]: 8.71-7.15 ppm (-CH=C-(CPT), -COOH (P(Glu-GA)), -NH-), 5.49 ppm(-N-CH_2-C= (CPT)), 5.32-3.91 ppm (-O-CH_2-C=C- (CPT), -C**H$_2$**-NH- (CPT), -O-CH_2- (P(Glu-GA)), -C=O-C**H**-NH-(P(Glu-GA)), -C**H$_2$**-N(CH_3)- (PSar)), 2.95-2.73 ppm (-CH_2-N(C**H$_3$**)- (PSar)), 2.16-1.86 ppm (-C**H$_2$**-C**H$_2$**- (P(Glu-GA)), CH_3-C**H$_2$**-(CPT)), 2.13 ppm, 2.03 ppm, 1.93 ppm (-C=O-CH_3 (O-Acetyl of fucose))

Subsequently, the ability of this conjugate to self-assembly into NPs was investigated by DLS three times each. The NPs were prepared via 'dropping- in' method in physiological simulating pH 7.4 PBS solution with two different concentrations- 500 µg/mL and 1.0 mg/mL

to evaluate the influence of concentration on particle formation, also as a comparison to that NPs concentration prepared from PGA-[(CPT-Gly)-*co*-(F-PSar)]. The results revealed a notable reduction in average NP size, from 1105 d.nm at 500 µg/mL to 562.5 d.nm at 1.0 mg/mL, as the concentration increased twofold (Table 4.3-1). Which may indicate that premicellar aggregation was observed at concentrations 500 µg/mL and these metastable large aggregates reorganise into smaller, more stable micelles as the concentration increases and approaches the CMC [123,124,125]. Also, the NPs size produced are much greater than that of PGA-[(CPT-Gly)-*co*-(F-PSar)], surpassing the maximum size threshold of cancer cell endocytosis [136] and in-vivo dilution [126,132,133,134,135] may further exacerbate this issue further preventing its application in endocytosis- mediated drug delivery at current stage. This phenomenon may be contributed by the improved solubility of the drug conjugate that the hydrophobic contribution of CPT at 28.8% (w/w) is not enough to promote formation of stable NPs at low concentration [124,126,127]. Therefore, a significant advantage of P(Glu-GA)-[(CPT-Gly)-*co*-(F-PSar)] lies in its improved water solubility compared to conjugates with PGA.

P(Glu-GA)-[(CPT-Gly)-*co*-(F-PSar)]	Z-Average (d.nm)	PDI Value
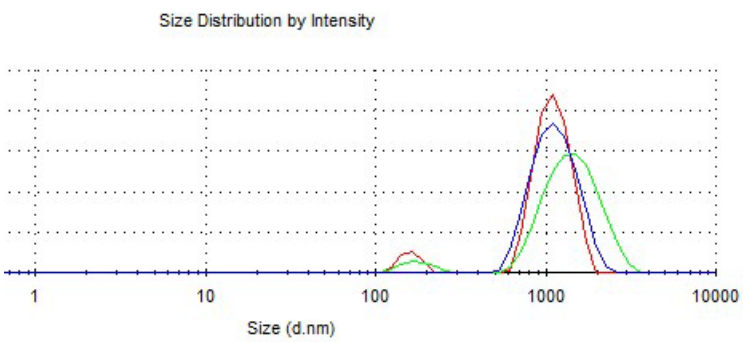 500 µg/mL	1105 (±37.63)	0.345 (±0.121)
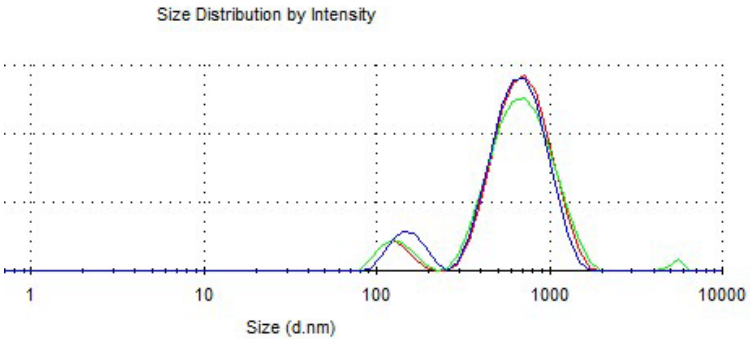 1.0 mg/mL	562.5 (±7.959)	0.313 (±0.004)

Table 4.3-1. DLS result (size distribution by intensity) of P(Glu-GA)-[(CPT-Gly)-*co*-(F-PSar)] in pH 7.4 PBS solution at concentration of 500 µg/mL and 1.0 mg/mL

This solubility advantage positions P(Glu-GA) as a promising alternative to PGA in drug conjugate synthesis. By potentially supporting elevated drug content without compromising NP stability improving the efficiency and efficacy of drug delivery platforms, warranting its consideration for further development due to its increased solubility. Also owing to its reduced ratio of carboxylate groups, aggregation or precipitation induced by protonation at low pH environment could be avoided or reduced.

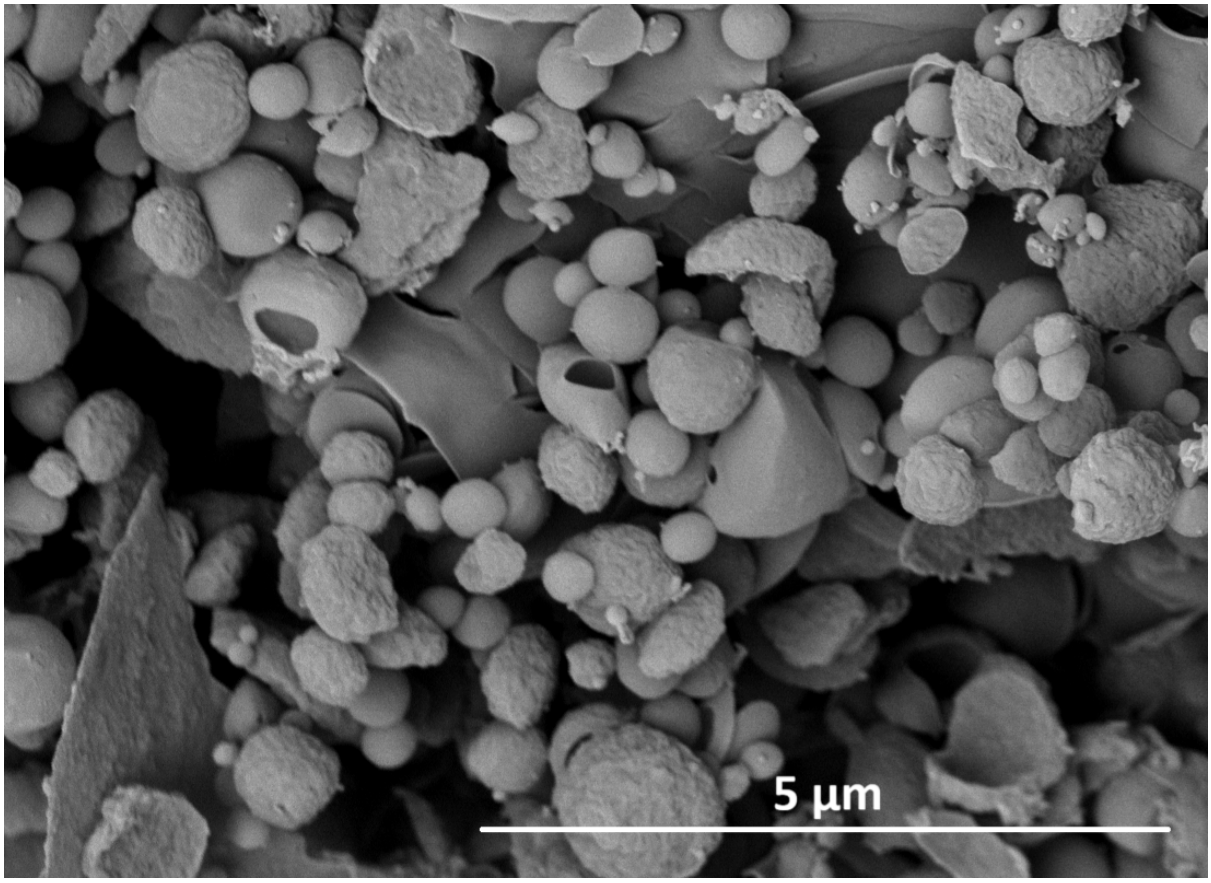

Figure 4.3-41. SEM result of P(Glu-GA)-[(CPT-Gly)-co-(F-PSar)] at concentration of 1.0 mg/mL

The morphology of the NPs was examined using SEM, which revealed spherical structures for the P(Glu-GA)-[(CPT-Gly)-*co*-(F-PSar)] NPs supporting the spherical assumption used to carry out the DLS analysis (Figure 4.3-41). The primary particles observed by SEM were generally around 500 nm, showing reasonable agreement with the size distribution obtained from DLS. Although DLS typically reports larger particle sizes due to the presence of hydration shell [137,138], whereas SEM reflects the dry core size under vacuum and is therefore generally expected to yield smaller values [139].

However, noticeable heterogeneity in particle size was evident, likely arising from uneven conjugation efficiency of the CPT-Gly and F-PSar during conjugate synthesis. Such size variation can affect colloidal stability and overall behaviour of the NPs in aqueous environments [140]. The discrepancy between SEM and DLS measurements may also be attributed to external forces during SEM sample preparation, leading to partial deformation or spreading of the particles. Furthermore, some particles appeared collapsed or ruptured,

likely due to rapid water sublimation during the freeze-drying process [141]. Also, large particles were observed, which can be attributed to mechanical stress put on the NPs during freeze drying process causing aggregation or fusion of the NPs [142,143]. Moreover, only small part of the NPs in the sample are observe in SEM, while DLS provides an ensemble-averaged size distribution of particles in suspension.

Despite these, future research should systematically examine the minimum drug content necessary to achieve effective self-assembly at low concentration. Such investigations would provide deeper insights into the relationship between drug content, self-assembly dynamics, and NP performance, guiding the optimisation of P(Glu-GA) based drug conjugate systems for clinical use.

4.4. Summary

Efforts to polymerise amino acid DKPs have encountered significant obstacles, largely due to the inherent stability of their amide bonds and the limitations of the catalysts employed. The amide bonds in DKPs, stabilised by resonance, present a high activation barrier to cleavage, impeding its ROP[25,128,129]. Moreover, the catalysts initially used were tailored for cyclic esters rather than cyclic amides, rendering them ineffective at breaking the amide bonds to form linear polymers. While catalysts for transamidation require for prior activation with an electron- withdrawing group Sar-DKP and Lys(Cbz)-DKP were exclude from this reaction due to N-methyl substitution and low solubility in the reaction temperature range, respectively.

Experimental results reveal distinct differences in the stability of various DKPs. For example, Sar-DKP, Ala-DKP, and Lys(Cbz)-DKP remain intact after polymerisation attempts, as they can be recovered through solvent evaporation and precipitation in solvents like diethyl ether or dialysis. In contrast, Glu(OBzyl)-DKP shows limited recovery, suggesting a less stable structure. This instability is likely due to its electron-withdrawing side chain, which increases the electrophilicity of the amide bond, making it more susceptible to nucleophilic attack [25,128]. Notably, Glu(OBzyl)-DKP stands out as the only DKP capable of polymerisation, albeit producing only trace amounts of polymer, without a catalyst. Other DKPs, such as Ala-DKP and Sar-DKP, lack such electron-withdrawing groups, making them more stable and less reactive.

Because the difficulty in polymerising DKPs stems from the stability of amides because of their resonance-stabilised bonds. To address this, two key strategies were proposed: (1) New catalysts, specifically designed for cyclic amides, are essential to effectively cleave the stable amide bonds in DKPs [25,26,128]; (2) Enhancing the electrophilicity of DKPs, such as by introducing electron-withdrawing groups like Boc group to the amide nitrogen, could make them more reactive to nucleophilic attack, facilitating polymerisation [25,26,128].

However, even specialised catalysts, such as the Ni(0)Cod_2: SIPr. HCl or LiHMDS known for their ability for transamidation, face practical limitations. The hydrochloric acid form of SIPr exhibits poor solubility in many solvents, and the low solubility of amino acid DKPs further restricts solvent options and the harsh handling conditions of Ni(0)Cod_2, as a result, only Sar-DKP and Glu(OBzyl)-DKP were tested with Ni(0)Cod_2: SIPr. HCl, limiting the scope of evaluation. And as the structure suggest, Sar-DKP could not be activated by Boc group and failed to force ring opening by increasing temperature. While Ni(0)Cod_2: SIPr. HCl increases the yield of ROP of Glu(OBzyl)-DKP, yet it accompanied with lower purity and require further optimisation.

While in case of DKMs, although Sar-GA DKM and Glu(OBzyl)-GA DKM were successfully synthesised, only Glu(OBzyl)-GA DKM was polymerised producing P(Glu-GA). Its un-expected slow reaction rate with TBD: Schreiner's Thiourea Catalyst proof the mistake in catalyst choosing, a more reactive thiourea like TU should be used instead [42,43]. And the addition of extra TBD increased the reaction rate but resulted in oligomerisation due to self-ring opening [46] further showcase the necessity in replacing Schreiner's Thiourea Catalyst used in this research. While in case of Sar-GA DKM, its ability to underwent self-ring-opening after exposed to atmospheric air shows its potential to ROP, yet further study is needed to understand its reaction mechanisms as no reaction taken place under various conditions with different catalysts, and reaction optimisation is also needed. To bypass the un-expected difficulty in polymerising Sar-GA DKM, P(Sar-GA) random polymer was synthesised via melt polycondensation. However, both $Sn(Oct)_2$ and zinc failed to effectively polymerising sarcosine and glycolic acid resulting in trace amount after dialysis.

After the production of P(Glu-GA), two drug conjugates, P(Glu-GA)-(PSar-Gly-CPT) and P(Glu-GA)-[(CPT-Gly)-*co*-(F-PSar)] with drug content of 20.3% and 28.8% respectively were

synthesised. Because of the increased water solubility and low drug content of P(Glu-GA)-(PSar-Gly-CPT), it remain soluble in aqueous solution while P(Glu-GA)-[(CPT-Gly)-*co*-(F-PSar)] formed NPs, their size shrink significantly by near 50% when its concentration increased two-fold (500 µg/mL ->1.0 mg/mL) which may suggest formation of large premicellar aggregates at lower concentration and reorganise into smaller, more stable micelles as the concentration increases [123,124,125]. Therefore, increase the drug content in both drug conjugate may promote their nanoprecipitation by improving their hydrophobic interactions in aqueous conditions [126,130,131]. However, a deeper study of these two drug conjugates such as will they respond to pH change the way PGA-[(CPT-Gly)-*co*-(F-PSar)] does given they have less carboxylate group available in the polymer backbone; what is the drug content required for the formation of stable NPs and their drug releasing profile etc., need to be answered in the future.

4.5. References

1. Otake, Y., Nakamura, H., & Fuse, S. (2018). Rapid and Mild Synthesis of Amino Acid N-Carboxy Anhydrides: Basic-to-Acidic Flash Switching in a Microflow Reactor. Angewandte Chemie International Edition, 57(35), 11389-11393. https://doi.org/10.1002/anie.201803549

2. Eckert, H. and Forster, B. (1987). Triphosgene, a crystalline phosgene substitute. Angewandte Chemie International Edition in English, 26(9), 894-895. https://doi.org/10.1002/anie.198708941

3. cruzvinchristopher. (2008, September 9). Chemical Warfare Left Its Legacy. Scribd. https://www.scribd.com/document/896681928/Chemical-Warfare-Left-Its-Legacy

4. Material Safety Data Sheet - University of Nevada, Reno,ehslegacy.unr.edu/msdsfiles/26588.pdf. Accessed 05 Aug. 2023.

5. Borthwick, Alan D. “2,5-Diketopiperazines: Synthesis, Reactions, Medicinal Chemistry, and Bioactive Natural Products.” Chemical Reviews, vol. 112, no. 7, 11 May 2012, pp. 3641–3716, https://doi.org/10.1021/cr200398y

6. Weng, J. H., Bado, A., Garbay, C., & Roques, B. P. (1996). Novel cck-b receptor agonists: diketopiperazine analogues derived from cck4 bioactive conformation. Regulatory Peptides, 65(1), 3-9. https://doi.org/10.1016/0167-0115(96)00065-1

7. Gomez-Monterrey, Isabel, et al. “Design, Synthesis, and Cytotoxic Evaluation of a New Series of 3-Substituted Spiro[(Dihydropyrazine-2,5-Dione)-6,3‘-(2‘,3‘-Dihydrothieno[2,3-b]Naphtho-4‘,9‘-Dione)] Derivatives.” Journal of Medicinal Chemistry, vol. 50, no. 8, Apr. 2007, pp. 1787–1798, https://doi.org/10.1021/jm0612158

8. Meggy, A. B. (1953). 175. glycine peptides. part i. the polymerization of piperazine-2 : 5-dione at 180°. J. Chem. Soc., 0(0), 851-855. https://doi.org/10.1039/jr9530000851

9. Meggy, A. B. (1956). 293. glycine peptides. part ii. the heat and entropy of formation of the peptide bond in polyglycine. Journal of the Chemical Society (Resumed), 1444. https://doi.org/10.1039/jr9560001444

10. Nagayama, M., Takaoka, O., INOMATA, K., & Yamagata, Y. (1990). Diketopiperazine-mediated peptide formation in aqueous solution. Origins of Life and Evolution of the Biosphere, 20(3-4), 249-257. https://doi.org/10.1007/bf01808107

11. Sasaki, M., Miyagawa, Y., Nonaka, K., Miyanomae, R., Quitain, A. T., Kida, T., … & Kawamura, K. (2022). Nano-pulsed discharge plasma-induced abiotic oligopeptide

formation from diketopiperazine. The Science of Nature, 109(4). https://doi.org/10.1007/s00114-022-01803-y

12. Sasaki, M., Nonaka, K., Yuka, S., Honma, T., Furusato, T., & Kawamura, K. (2025). Linear oligopeptide formation from alanine-diketopiperazine in acidic aqueous solutions using interfacial nano-pulsed discharge plasma. New Journal of Chemistry, 49(2), 514-520. https://doi.org/10.1039/d3nj05664c

13. Suzuki, K., Sasaki, Y., ENDO, N., & Mihara, Y. (1981). Acetic acid-catalyzed diketopiperazine synthesis.. Chemical and Pharmaceutical Bulletin, 29(1), 233-237. https://doi.org/10.1248/cpb.29.233

14. Depew, K. M., Marsden, S. P., Zatorska, D., Zatorski, A., Bornmann, W. G., & Danishefsky, S. J. (1999). Total synthesis of 5-n-acetylardeemin and amauromine: practical routes to potential mdr reversal agents. Journal of the American Chemical Society, 121(51), 11953-11963. https://doi.org/10.1021/ja991558d

15. Couladouros, E. A. and Magos, A. D. (2005). Total asymmetric synthesis of (?)-phenylhistine, (?)-aurantiamine and related compounds. part i. Molecular Diversity, 9(1-3), 99-109. https://doi.org/10.1007/s11030-005-1294-x

16. Bull, S. D., Davies, S. G., & Moss, W. O. (1998). Practical synthesis of schöllkopf's bis-lactim ether chiral auxiliary: (3s)-3,6-dihydro-2,5-dimethoxy-3-isopropyl-pyrazine. Tetrahedron: Asymmetry, 9(2), 321-327. https://doi.org/10.1016/s0957-4166(97)00623-x

17. Schott, H. F., LARKIN, J. B., Rockland, L. B., & Dunn, M. S. (1947). The synthesis of l(—)-leucylglycylglycine1. The Journal of Organic Chemistry, 12(3), 490-495.

https://doi.org/10.1021/jo01167a020

18. Burton, T. F., Garisoain, Z., Chaix, C., Aassine, J., Virapin, E., Voronova, A., Pinaud, J., & Giani, O. (2024). An Optimized and Universal Protocol for the Synthesis of Morpholine-2,5-Diones from Natural Hydrophobic Amino Acids and Their Mixture. ACS Omega, 9(26), 28583–28593. https://doi.org/10.1021/acsomega.4c02670

19. Bergeron, R. J., Phanstiel, O., Yao, G. W., Milstein, S., & Weimar, W. R. (1994). Macromolecular self-assembly of diketopiperazine tetrapeptides. Journal of the American Chemical Society, 116(19), 8479-8484. https://doi.org/10.1021/ja00098a007

20. Kim, H. (2004). Nonthermal plasma processing for air-pollution control: a historical review, current issues, and future prospects. Plasma Processes and Polymers, 1(2), 91-110. https://doi.org/10.1002/ppap.200400028

21. Fridman, A., Chirokov, A. V., & Gutsol, A. (2005). Non-thermal atmospheric pressure discharges. Journal of Physics D: Applied Physics, 38(2), R1-R24. https://doi.org/10.1088/0022-3727/38/2/r01

22. Shao, T., Wang, R., Zhang, C., & Yan, P. (2018). Atmospheric-pressure pulsed discharges and plasmas: mechanism, characteristics and applications. High Voltage, 3(1), 14-20. https://doi.org/10.1049/hve.2016.0014

23. Baker, E. L., Yamano, M. M., Zhou, Y., Anthony, S. M., & Garg, N. K. (2016). A two-step approach to achieve secondary amide transamidation enabled by nickel catalysis. Nature Communications, 7(1). https://doi.org/10.1038/ncomms11554

24. Dander, J. E., Baker, E. L., & Garg, N. K. (2017). Nickel-catalyzed transamidation of aliphatic amide derivatives. Chemical Science, 8(9), 6433-6438. https://doi.org/10.1039/c7sc01980g

25. Dander, J. E., & Garg, N. K. (2017). Breaking Amides using Nickel Catalysis. ACS Catalysis, 7(2), 1413–1423. https://doi.org/10.1021/acscatal.6b03277

26. Li, G. and Szostak, M. (2018). Highly selective transition-metal-free transamidation of amides and amidation of esters at room temperature. Nature Communications, 9(1). https://doi.org/10.1038/s41467-018-06623-1

27. Andere Basterretxea, Gabirondo, E., Jehanno, C., Zhu, H., Olivier Coulembier, Mecerreyes, D., & Sardon, H. (2021). Stereoretention in the Bulk ROP of l-Lactide Guided by a Thermally Stable Organocatalyst. Macromolecules, 54(13), 6214–6225. https://doi.org/10.1021/acs.macromol.1c01060

28. Schäfer, P. M. and Herres-Pawlis, S. (2020). Robust guanidine metal catalysts for the ring-opening polymerization of lactide under industrially relevant conditions. ChemPlusChem, 85(5), 1044-1052. https://doi.org/10.1002/cplu.202000252

29. Leenslag, J. W. and Pennings, A. J. (1987). Synthesis of high-molecular-weight poly(l-lactide) initiated with tin 2-ethylhexanoate. Die Makromolekulare Chemie, 188(8), 1809-1814. https://doi.org/10.1002/macp.1987.021880804

30. Ryner, M., Stridsberg, K., Albertsson, A., Schenck, H. v., & Svensson, M. (2001). Mechanism of ring-opening polymerization of 1,5-dioxepan-2-one and l-lactide with stannous 2-ethylhexanoate. a theoretical study. Macromolecules, 34(12), 3877-3881.

https://doi.org/10.1021/ma002096n

31. Kowalski, A., Duda, A., & Penczek, S. (2000). Mechanism of cyclic ester polymerization initiated with tin(ii) octoate. 2. macromolecules fitted with tin(ii) alkoxide species observed directly in maldi−tof spectra. Macromolecules, 33(3), 689-695. https://doi.org/10.1021/ma9906940

32. Lohmeijer, B. G. G., Pratt, R. C., Leibfarth, F., Logan, J. W., Long, D. A., Dove, A. P., Nederberg, F., Choi, J., Wade, C., Waymouth, R. M., & Hedrick, J. L. (2006). Guanidine and Amidine Organocatalysts for Ring-Opening Polymerisation of Cyclic Esters. Macromolecules, 39(25), 8574–8583. https://doi.org/10.1021/ma0619381

33. Sherck, N., Kim, H. C., & Won, Y. (2016). Elucidating a unified mechanistic scheme for the dbu-catalyzed ring-opening polymerization of lactide to poly(lactic acid). Macromolecules, 49(13), 4699-4713. https://doi.org/10.1021/acs.macromol.6b00621

34. Pratt, R. C., Lohmeijer, B. G. G., Long, D. A., Waymouth, R. M., & Hedrick, J. L. (2006). Triazabicyclodecene: a simple bifunctional organocatalyst for acyl transfer and ring-opening polymerisation of cyclic esters. Journal of the American Chemical Society, 128(14), 4556–4557. https://doi.org/10.1021/ja060662+

35. Alba, A., Boullay, O. T. d., Martín-Vaca, B., & Bourissou, D. (2015). Direct ring-opening of lactide with amines: application to the organo-catalyzed preparation of amide end-capped pla and to the removal of residual lactide from pla samples. Polymer Chemistry, 6(6), 989-997. https://doi.org/10.1039/c4py00973h

36. Doyle, A. G. and Jacobsen, E. N. (2007). Small-molecule h-bond donors in asymmetric

catalysis. Chemical Reviews, 107(12), 5713-5743. https://doi.org/10.1021/cr068373r

37. Serdyuk, O. V., Heckel, C. M., & Tsogoeva, S. B. (2013). Bifunctional primary amine-thioureas in asymmetric organocatalysis. Organic & Biomolecular Chemistry, 11(41), 7051. https://doi.org/10.1039/c3ob41403e

38. Fang, X. and Wang, C. (2015). Recent advances in asymmetric organocatalysis mediated by bifunctional amine–thioureas bearing multiple hydrogen-bonding donors. Chemical Communications, 51(7), 1185-1197. https://doi.org/10.1039/c4cc07909d

39. Sigman, M. S. and Jacobsen, E. N. (1998). Schiff base catalysts for the asymmetric strecker reaction identified and optimized from parallel synthetic libraries. Journal of the American Chemical Society, 120(19), 4901-4902. https://doi.org/10.1021/ja980139y

40. Schreiner, P. R. and Wittkopp, A. (2002). H-bonding additives act like lewis acid catalysts. Organic Letters, 4(2), 217-220. https://doi.org/10.1021/ol017117s

41. Okino, T., Hoashi, Y., & Takemoto, Y. (2003). Enantioselective michael reaction of malonates to nitroolefins catalyzed by bifunctional organocatalysts. Journal of the American Chemical Society, 125(42), 12672-12673. https://doi.org/10.1021/ja036972z

42. Dove, A. P., Pratt, R. C., Lohmeijer, B. G. G., Waymouth, R. M., & Hedrick, J. L. (2005). Thiourea-based bifunctional organocatalysis: supramolecular recognition for living polymerization. Journal of the American Chemical Society, 127(40), 13798-13799. https://doi.org/10.1021/ja0543346

43. Jain, I., & Malik, P. (2020). Advances in urea and thiourea catalyzed ring opening polymerisation: A brief overview. European Polymer Journal, 133, 109791. https://doi.org/10.1016/j.eurpolymj.2020.109791

44. Thomas, C. and Bibal, B. (2014). Hydrogen-bonding organocatalysts for ring-opening polymerization. Green Chem., 16(4), 1687-1699. https://doi.org/10.1039/c3gc41806e

45. Dharmaratne, N. U., Pothupitiya, J. U., & Kiesewetter, M. K. (2019). The mechanistic duality of (thio)urea organocatalysts for ring-opening polymerization. Organic & Biomolecular Chemistry, 17(13), 3305-3313. https://doi.org/10.1039/c8ob03174f

46. Shi, C., Guo, Y., Wu, Y.-H., Li, Z.-Y., Wang, Y.-Z., Du, F.-S., & Li, Z.-C. (2019). Synthesis and Controlled Organobase-Catalyzed Ring-Opening Polymerisation of Morpholine-2,5-Dione Derivatives and Monomer Recovery by Acid-Catalyzed Degradation of the Polymers. 52(11), 4260–4269. https://doi.org/10.1021/acs.macromol.8b02498

47. Zhang, X., Jones, G. O., Hedrick, J. L., & Waymouth, R. M. (2016). Fast and selective ring-opening polymerisations by alkoxides and thioureas. Nature Chemistry, 8(11), 1047–1053. https://doi.org/10.1038/nchem.2574

48. Pauling, L., Corey, R. B., & Branson, H. R. (1951). The structure of proteins: two hydrogen-bonded helical configurations of the polypeptide chain. Proceedings of the National Academy of Sciences, 37(4), 205-211. https://doi.org/10.1073/pnas.37.4.205

49. González-Rosende, M. E., Castillo, E., Lasri, J., & Sepúlveda-Arques, J. (2004). Intermolecular and intramolecular transamidation reactions. Progress in Reaction Kinetics and Mechanism, 29(4), 311-332. https://doi.org/10.3184/007967404775363426

50. Mucsi, Z., Chass, G. A., & Csizmadia, I. G. (2008). Amidicity change as a significant driving force and thermodynamic selection rule of transamidation reactions. a synergy between experiment and theory. The Journal of Physical Chemistry B, 112(26), 7885-7893. https://doi.org/10.1021/jp8023292

51. Eldred, S. E., Stone, D., Gellman, S. H., & Stahl, S. S. (2003). Catalytic transamidation under moderate conditions. Journal of the American Chemical Society, 125(12), 3422-3423. https://doi.org/10.1021/ja028242h

52. Ivanova, J., Štrumfs, B., & Žalubovskis, R. (2019). Access to nh-aziridine-2-carboxamides through davidsen acylimidodicarbonate activation. Comptes Rendus. Chimie, 22(4), 283-293. https://doi.org/10.1016/j.crci.2019.03.001

53. Greenberg, A. and Venanzi, C. A. (1993). Structures and energetics of two bridgehead lactams and their n- and o-protonated forms: an ab initio molecular orbital study. Journal of the American Chemical Society, 115(15), 6951-6957. https://doi.org/10.1021/ja00068a064

54. Greenberg, A., Moore, D. T., & Dubois, T. (1996). Small and medium-sized bridgehead bicyclic lactams: a systematic ab initio molecular orbital study. Journal of the American Chemical Society, 118(36), 8658-8668. https://doi.org/10.1021/ja960294h

55. Tani, K. and Stoltz, B. M. (2006). Synthesis and structural analysis of 2-quinuclidonium tetrafluoroborate. Nature, 441(7094), 731-734. https://doi.org/10.1038/nature04842

56. Szostak, R., Shi, S., Meng, G., Lalancette, R. A., & Szostak, M. (2016). Ground-state

distortion in n-acyl-tert-butyl-carbamates (boc) and n-acyl-tosylamides (ts): twisted amides of relevance to amide n–c cross-coupling. The Journal of Organic Chemistry, 81(17), 8091-8094. https://doi.org/10.1021/acs.joc.6b01560

57. Pace, V., Hölzer, W., Meng, G., Shi, S., Lalancette, R. A., Szostak, R., … & Szostak, M. (2016). Structures of highly twisted amides relevant to amide n−c cross-coupling: evidence for ground-state amide destabilization. Chemistry – A European Journal, 22(41), 14494-14498. https://doi.org/10.1002/chem.201603543

58. Feng, Y., & Guo, J. (2009). Biodegradable Polydepsipeptides. International Journal of Molecular Sciences, 10(2), 589–615. https://doi.org/10.3390/ijms10020589

59. Šmelcerović, A., Yancheva, D., Cherneva, E., Petronijević, Ž., Lamshoeft, M., & Herebıan, D. (2011). Identification and synthesis of three cyclodidepsipeptides as potential precursors of enniatin b in fusarium sporotrichioides. Journal of Molecular Structure, 985(2-3), 397-402. https://doi.org/10.1016/j.molstruc.2010.11.029

60. ABE, M., YAMANO, T., YAMATODANI, S., KOZU, Y., KUSUMOTO, M., Komatsu, H., … & YAMADA, S. (1959). On the new peptide-type ergot alkaloids, ergosecaline and ergosecalinine. Bulletin of the Agricultural Chemical Society of Japan, 23(3), 246-248. https://doi.org/10.1080/03758397.1959.10857567

61. M. Soledade C. Pedras, Chumala, P. B., & Quail, J. W. (2004). Chemical Mediators: The Remarkable Structure and Host-Selectivity of Depsilairdin, a Sesquiterpenic Depsipeptide Containing a New Amino Acid. Organic Letters, 6(24), 4615–4617. https://doi.org/10.1021/ol0478786

62. Suntornchashwej, S., Chaichit, N., Isobe, M., & Suwanborirux, K. (2005). Hectochlorin and morpholine derivatives from the thai sea hare, bursatella leachii. Journal of Natural Products, 68(6), 951-955. https://doi.org/10.1021/np0500124

63. Woolley, D. W., Schaffner, G., & Braun, A. (1955). Studies on the structure of the phytopathogenic toxin of pseudomonas tabaci. Journal of Biological Chemistry, 215(2), 485-493. https://doi.org/10.1016/s0021-9258(18)65970-8

64. Yang, S., Li, X., Li, X., Chi, L., & Wang, B. (2018). Two new diketomorpholine derivatives and a new highly conjugated ergostane-type steroid from the marine algal-derived endophytic fungus aspergillus alabamensis en-547. Marine Drugs, 16(4), 114. https://doi.org/10.3390/md16040114

65. Kagamizono, T., NISHINO, E., Matsumoto, K., Kawashima, A., Kishimoto, M., Sakai, N., … & Hanada, K. (1995). Bassiatin, a new platelet aggregation inhibitor produced by beauveria bassiana k-717. The Journal of Antibiotics, 48(12), 1407-1413. https://doi.org/10.7164/antibiotics.48.1407

66. Peng, X., Behl, M., Zhang, P., Mazurek-Budzyńska, M., Feng, Y., & Lendlein, A. (2018). Synthesis of Well-Defined Dihydroxy Telechelics by (Co)polymerisation of Morpholine-2,5-Diones Catalyzed by Sn(IV) Alkoxide. Macromolecular Bioscience, 18(12). https://doi.org/10.1002/mabi.201800257

67. Peng, X., Behl, M., Zhang, P., Mazurek-Budzyńska, M., Razzaq, M. Y., & Lendlein, A. (2016). Hexyl-modified morpholine-2,5-dione-based oligodepsipeptides with relatively low glass transition temperature. Polymer, 105, 318–326. https://doi.org/10.1016/j.polymer.2016.10.033

68. Tian, W., Chen, Q., Yu, C., & Shen, J. (2003). Amino-terminated poly(ethylene glycol) as the initiator for the ring-opening polymerisation of 3-methylmorpholine-2,5-dione. European Polymer Journal, 39(9), 1935–1938. https://doi.org/10.1016/s0014-3057(03)00091-0

69. Dirauf, M., Damiano Bandelli, Weber, C., Helmar Görls, Gottschaldt, M., & Schubert, U. S. (2018). TBD-Catalyzed Ring-Opening Polymerisation of Alkyl-Substituted Morpholine-2,5-Dione Derivatives. Macromolecular Rapid Communications, 39(23). https://doi.org/10.1002/marc.201800433

70. Ohya, Y., Toyohara, M., Sasakawa, M., Arimura, H., & Ouchi, T. (2005). Thermosensitive biodegradable polydepsipeptide. Macromolecular Bioscience, 5(4), 273-276. https://doi.org/10.1002/mabi.200400221

71. Ouchi, T., Nozaki, T., Okamoto, Y., Shiratani, M., & Ohya, Y. (1996). Synthesis and enzymatic hydrolysis of polydepsipeptides with functionalized pendant groups. Macromolecular Chemistry and Physics, 197(6), 1823–1833. https://doi.org/10.1002/macp.1996.021970604

72. Fonseca, A. C., Gil, M. H., & Simões, P. N. (2014). Biodegradable poly(ester amide)s – A remarkable opportunity for the biomedical area: Review on the synthesis, characterization and applications. Progress in Polymer Science, 39(7), 1291–1311. https://doi.org/10.1016/j.progpolymsci.2013.11.007

73. Winnacker, M., & Rieger, B. (2016). Poly(ester amide)s: recent insights into synthesis, stability and biomedical applications. Polymer Chemistry, 7(46), 7039–7046.

https://doi.org/10.1039/C6PY01783E

74. Rodriguez-Galan, A., Franco, L., & Puiggali, J. (2010). Degradable Poly(ester amide)s for Biomedical Applications. Polymers, 3(1), 65–99. https://doi.org/10.3390/polym3010065

75. Valle, L. J. d., Roca, D., Franco, L., Puiggalí, J., & Rodríguez-Galán, A. (2011). Preparation and release study of ibuprofen-loaded porous matrices of a biodegradable poly(ester amide) derived from l-alanine units. Journal of Applied Polymer Science, 122(3), 1953-1967. https://doi.org/10.1002/app.34017

76. Guo, K., & Chu, C. C. (2007). Controlled release of paclitaxel from biodegradable unsaturated poly(ester amide)s/poly(ethylene glycol) diacrylate hydrogels. Journal of Biomaterials Science, Polymer Edition, 18(5), 489–504. https://doi.org/10.1163/156856207780852569

77. Guo, K. and Chu, C. C. (2008). Biodegradable and injectable paclitaxel-loaded poly(ester amide)s microspheres: fabrication and characterization. Journal of Biomedical Materials Research Part B: Applied Biomaterials, 89B(2), 491-500. https://doi.org/10.1002/jbm.b.31239

78. Li, L., & Chu, C.-C. (2009). Nitroxyl Radical Incorporated Electrospun Biodegradable Poly(ester Amide) Nanofiber Membranes. Journal of Biomaterials Science, Polymer Edition, 20(3), 341–361. https://doi.org/10.1163/156856209x412209

79. Xie, Z., Guan, H., Chen, X., Lü, C., Chen, L., Hu, X., … & Jing, X. (2007). A novel polymer–paclitaxel conjugate based on amphiphilic triblock copolymer. Journal of Controlled Release, 117(2), 210-216. https://doi.org/10.1016/j.jconrel.2006.11.014

80. Karimi, P., Rizkalla, A. S., & Mequanint, K. (2010). Versatile biodegradable poly(ester amide)s derived from α-amino acids for vascular tissue engineering. Materials, 3(4), 2346-2368. https://doi.org/10.3390/ma3042346

81. DeFife, K. M., Grako, K., Cruz-Aranda, G., Price, S. J., Chantung, R., Macpherson, K., … & Turnell, W. G. (2009). Poly(ester amide) co-polymers promote blood and tissue compatibility. Journal of Biomaterials Science, Polymer Edition, 20(11), 1495-1511. https://doi.org/10.1163/092050609x12464344572881

82. Knight, D. K., Stutchbury, R., Imruck, D., Halfpap, C., Lin, S., Langbein, U., … & Mequanint, K. (2012). Focal contact formation of vascular smooth muscle cells on langmuir–blodgett and solvent-cast films of biodegradable poly(ester amide)s. ACS Applied Materials &Amp; Interfaces, 4(3), 1303-1312. https://doi.org/10.1021/am201582q

83. Ohya, Y., Matsunami, H., & Ouchi, T. (2004). Cell growth on the porous sponges prepared from poly(depsipeptide-co-lactide) having various functional groups. Journal of Biomaterials Science, Polymer Edition, 15(1), 111-123. https://doi.org/10.1163/156856204322752264

84. Feng, Y., Lu, J., Behl, M., & Lendlein, A. (2010). Progress in Depsipeptide-Based Biomaterials. Macromolecular Bioscience, 10(9), 1008–1021. https://doi.org/10.1002/mabi.201000076

85. Sung, H., Meredith, C., Johnson, C., & Galis, Z. S. (2004). The effect of scaffold degradation rate on three-dimensional cell growth and angiogenesis. Biomaterials, 25(26), 5735-5742. https://doi.org/10.1016/j.biomaterials.2004.01.066

86. Felton, G. P., Nova Science Publishers, Rodríguez-Galán, A., Franco, L., & Puiggalí, J. (2011). Biodegradable polymers : processing, degradation and applications (pp. 207–259). New York: Nova Science Publishers, Cop.

87. Chadwick, A. F. and Pacsu, E. (1943). The resolution and rates of hydrolysis of d,l-α-bromopropionic acid and its glycine derivatives1. Journal of the American Chemical Society, 65(3), 392-402. https://doi.org/10.1021/ja01243a025

88. Wang, D. and Feng, X. (1998). Copolymerization of ε-caprolactone with (3s)-3-[(benzyloxycarbonyl)methyl]morpholine-2,5-dione and the 13c nmr sequence analysis of the copolymer vol. 31, number 12, june 16, 1998, pp 3824−3831. Macromolecules, 31(19), 6740-6740. https://doi.org/10.1021/ma981987g

89. Zhang, G., Wang, D., & Feng, X. (1998). Preliminary study of hydrogen bonding in (3s)-3-[(benzyloxycarbonyl)methyl]- morpholine-2,5-dione and its effect on polymerization. Macromolecules, 31(18), 6390-6392. https://doi.org/10.1021/ma9803887

90. Veld, P. J. A. i., Ye, W., Klap, R., Dijkstra, P. J., & Feijén, J. (1992). Copolymerization of ε-caprolactone and morpholine-2,5-dione derivatives. Die Makromolekulare Chemie, 193(8), 1927-1942. https://doi.org/10.1002/macp.1992.021930813

91. Vinsova, J. (2001). Morpholine-2,5-diones - Their Preparation and Exploitation. Chemické Listy, 95(1). Retrieved from http://www.chemicke-listy.cz/ojs3/index.php/chemicke-listy/article/view/2453

92. Veld, P. J. A. i., Dijkstra, P. J., & Feijén, J. (1992). Synthesis of biodegradable

polyesteramides with pendant functional groups. Die Makromolekulare Chemie, 193(11), 2713-2730. https://doi.org/10.1002/macp.1992.021931101

93. Hartwig, W. and Schöllkopf, U. (1982). Asymmetrische synthesen über heterocyclische zwischenstufen, xvi. enantioselektive synthese von α-alkyl-α-phenylglycinen durch alkylieren von an c-6 chiral substituierten 3,6-dihydro-3-phenyl-2h-1,4-oxazin-2-onen. Liebigs Annalen Der Chemie, 1982(11), 1952-1970. https://doi.org/10.1002/jlac.198219821105

94. Charles E. Nakamura, Robert Di Cosimo, & John R. Moran. (1995). Process for the preparation of 3-, 6-substituted 2,5-morpholinediones (E.I. DU PONT DE NEMOURS AND COMPANY Patent). https://patents.google.com/patent/US5466801A/en

95. Kardassis, G., Brungs, P., NOTHHELFER, C., & Steckhan, E. (1998). Electrogenerated chiral cationic glycine equivalents — part 2: chiral 3-methoxy-2,5-morpholinediones from (s)-α-hydroxy acids and dimethyl aminomalonate. Tetrahedron, 54(14), 3479-3488. https://doi.org/10.1016/s0040-4020(98)00082-9

96. Mitsunobu, O. (1981). The use of diethyl azodicarboxylate and triphenylphosphine in synthesis and transformation of natural products. Synthesis, 1981(01), 1-28. https://doi.org/10.1055/s-1981-29317

97. Nicolaou, K., Safina, B. S., & Winssinger, N. (2001). A new photolabile linker for the photoactivation of carboxyl groups. Synlett, 2001(Special Issue), 0900-0903. https://doi.org/10.1055/s-2001-14661

98. Jainta, M., Nieger, M., & Bräse, S. (2008). Microwave-Assisted Stereoselective One-Pot

Synthesis of Symmetrical and Unsymmetrical 2,5-Diketopiperazines from Unprotected Amino Acids. European Journal of Organic Chemistry, 2008(32), 5418–5424. https://doi.org/10.1002/ejoc.200800605

99. Muramatsu, W., & Yamamoto, H. (2022). An economical approach for peptide synthesisviaregioselective C–N bond cleavage of lactams. Chemical Science, 13(21), 6309–6315. https://doi.org/10.1039/d2sc01466a

100. Kricheldorf, H. R., Kreiser-Saunders, I., & Stricker, A. (2000). Polylactones 48. snoct2-initiated polymerizations of lactide: a mechanistic study. Macromolecules, 33(3), 702-709. https://doi.org/10.1021/ma991181w

101. Cole, K. P., Ryan, S. J., Groh, J. M., & Miller, R. D. (2017). Reagent-free continuous thermal tert-butyl ester deprotection. Bioorganic & Medicinal Chemistry, 25(23), 6209-6217. https://doi.org/10.1016/j.bmc.2017.03.020

102. Vashist, S. K. (2012). Comparison of 1-Ethyl-3-(3-Dimethylaminopropyl) Carbodiimide Based Strategies to Crosslink Antibodies on Amine-Functionalized Platforms for Immunodiagnostic Applications. Diagnostics (Basel, Switzerland), 2(3), 23–33. https://doi.org/10.3390/diagnostics2030023

103. Wei, R., Chen, T., Wang, Y., Xu, Q., Feng, B., Weng, J., Peng, W., & Wang, J. (2021). By Endowing Polyglutamic Acid/Polylysine Composite Hydrogel with Super Intrinsic Characteristics to Enhance its Wound Repair Potential. Macromolecular Bioscience, 21(5). https://doi.org/10.1002/mabi.202000367

104. Deming, T. J. (2017). Functional Modification of Thioether Groups in Peptides,

Polypeptides, and Proteins. Bioconjugate Chemistry, 28(3), 691–700. https://doi.org/10.1021/acs.bioconjchem.6b00696

105. Deming, T. J. (2016). Synthesis of Side-Chain Modified Polypeptides. 116(3), 786–808. https://doi.org/10.1021/acs.chemrev.5b00292

106. Koshizuka, M., Shinoda, K., Makino, K., & Shimada, N. (2023). concise synthesis of 2,5-diketopiperazines via catalytic hydroxy-directed peptide bond formations. The Journal of Organic Chemistry, 88(11), 6901-6910. https://doi.org/10.1021/acs.joc.3c00195

107. Febrian, R., Roddy, J. P., Chang, C., Devall, C. T., & Bracher, P. J. (2021). Removal of Paramagnetic Ions Prior to Analysis of Organic Reactions in Aqueous Solutions by NMR Spectroscopy. Acs Omega, 6(23), 14727–14733. https://doi.org/10.1021/acsomega.9b02610

108. López-Soria, J., Pérez, S., Hernández, J., Ramírez, M., Martín, V., & Padrón, J. (2015). a practical, catalytic and selective deprotection of a boc group in n,n'-diprotected amines using iron(iii)-catalysis. RSC Advances, 5(9), 6647-6651. https://doi.org/10.1039/c4ra12143k

109. (1977). Di-tert-butyl dicarbonate. Organic Syntheses, 57, 45. https://doi.org/10.15227/orgsyn.057.0045

110. Byrd, H., & McEwen, C. N. (2000). The Limitations of MALDI-TOF Mass Spectrometry in the Analysis of Wide Polydisperse Polymers. Analytical Chemistry, 72(19), 4568–4576. https://doi.org/10.1021/ac0002745

111. Montaudo, G., Montaudo, M. S., Puglisi, C., & Samperi, F. (1995). Characterization of polymers by matrix-assisted laser desorption/ionization time-of-flight mass spectrometry: Molecular weight estimates in samples of varying polydispersity. Rapid Communications in Mass Spectrometry, 9(5), 453–460. https://doi.org/10.1002/rcm.1290090514

112. Rashidzadeh, H., & Guo, B. (1998). Use of MALDI-TOF To Measure Molecular Weight Distributions of Polydisperse Poly(methyl methacrylate). Analytical Chemistry, 70(1), 131–135. https://doi.org/10.1021/ac970568z

113. Han, J., Ding, J., Wang, Z., Yan, S., Zhuang, X., Chen, X., & Yin, J. (2013). The synthesis, deprotection and properties of poly(γ-benzyl-l-glutamate). Science China Chemistry, 56(6), 729–738. https://doi.org/10.1007/s11426-013-4839-3

114. Koch, C., Soňa Šimonyiová, Jörg Pabel, Annerose Kärtner, Polborn, K., & Wanner, K. (2003). Asymmetric Synthesis with 6-tert-Butyl-5-methoxy-6-methyl-3,6-dihydro-2H-1,4-oxazin-2-one as a New Chiral Glycine Equivalent: Preparation of Enantiomerically Pure α-Tertiary and α-Quaternary α-Amino Acids. European Journal of Organic Chemistry, 2003(7), 1244–1263. https://doi.org/10.1002/ejoc.200390179

115. Wang, Z., Hou, X., Mao, Z., Ye, R., & Finlow, D. E. (2008). Synthesis and Characterization of Biodegradable Poly(lactic acid-co-glycine) via Direct Melt Copolymerisation. Iranian Polymer Journal, 17(10), 791–798. Retrieved from https://www.researchgate.net/publication/228657529

116. Lu, D.-D., Yuan, J.-C., & Lei, Z.-Q. (2009). High molecular weight biodegraded poly(lactic acid-glycolic acid-ε-caprolactam) copolymer: direct polycondensation of lactic acid, glycolic acid andε-caprolactam using Sn(II)-organic anhydride as catalysts. Polymers for

Advanced Technologies, 20(6), 536–540. https://doi.org/10.1002/pat.1378

117. Lu, D., Ren, Z., Zhou, T., Wang, S., & Lei, Z. (2007). Synthesis and characterization of amphiphilic biodegradable poly(glutamic acid-co-lactic acid-co-glycolic acid) by direct polycondensation. Journal of Applied Polymer Science, 107(6), 3638–3643. https://doi.org/10.1002/app.27549

118. Ye, R., Wang, Z., Wang, Q., Yang, K., & Luo, S. (2011). Synthesis of biodegradable material poly(lactic acid-co-aspartic acid) via direct melt polycondensation and its characterization. Journal of Applied Polymer Science, 121(6), 3662-3668. https://doi.org/10.1002/app.34168

119. Shinoda, H., Asou, Y., Suetsugu, A., & Tanaka, K. (2003). Synthesis and characterization of amphiphilic biodegradable copolymer, poly(aspartic acid-co-lactic acid). Macromolecular Bioscience, 3(1), 34-43. https://doi.org/10.1002/mabi.200390007

120. Ferreira, A. B., Cardoso, A. L., & Silva, M. J. d. (2012). Tin-catalyzed esterification and transesterification reactions: a review. ISRN Renewable Energy, 2012, 1-13. https://doi.org/10.5402/2012/142857

121. Casas, A., Ramos, M. J., Rodríguez, J. F., & Pérez, Á. (2013). Tin compounds as lewis acid catalysts for esterification and transesterification of acid vegetable oils. Fuel Processing Technology, 106, 321-325. https://doi.org/10.1016/j.fuproc.2012.08.015

122. Albertsson, A.-C., & Varma, I. K. (2003). Recent Developments in Ring Opening Polymerisation of Lactones for Biomedical Applications. Biomacromolecules, 4(6), 1466–1486. https://doi.org/10.1021/bm034247a

123. Moraes, J. N. B. d. and Figueiredo, W. (2013). Formation of large micellar aggregates before equilibrium in diluted solutions. Physical Review E, 87(6). https://doi.org/10.1103/physreve.87.062315

124. Zhong, H., Yang, L., Zeng, G., Brusseau, M. L., Wang, Y., Li, Y., … & Tan, F. (2015). Aggregate-based sub-cmc solubilization of hexadecane by surfactants. RSC Advances, 5(95), 78142-78149. https://doi.org/10.1039/c5ra12388g

125. Hou, Y., Han, Y., Deng, M., Xiang, J., & Wang, Y. (2009). Aggregation behavior of a tetrameric cationic surfactant in aqueous solution. Langmuir, 26(1), 28-33. https://doi.org/10.1021/la903672r

126. Kim, S., Shi, Y., Kim, J. Y., Park, K., & Cheng, J.-X. (2009). Overcoming the barriers in micellar drug delivery: loading efficiency in vivo stability, and micelle–cell interaction. Expert Opinion on Drug Delivery, 7(1), 49–62. https://doi.org/10.1517/17425240903380446

127. Hadgiivanova, R. and Diamant, H. (2009). premicellar aggregation of amphiphilic molecules: aggregate lifetime and polydispersity. The Journal of Chemical Physics, 130(11). https://doi.org/10.1063/1.3088828

128. Hie, L., Nathel, N. F. F., Shah, T. K., Baker, E. L., Hong, X., Yang, Y., … & Garg, N. K. (2015). Conversion of amides to esters by the nickel-catalysed activation of amide c–n bonds. Nature, 524(7563), 79-83. https://doi.org/10.1038/nature14615

129. Greenberg, A., Breneman, C. M., & Liebman, J. F. (2003). The amide linkage: structural

significance in chemistry, biochemistry, and materials science. Wiley-Interscience.

130. Wang, Y., Xu, H., & Zhang, X. (2009). Tuning the Amphiphilicity of Building Blocks: Controlled Self-Assembly and Disassembly for Functional Supramolecular Materials. Advanced Materials, 21(28), 2849–2864. https://doi.org/10.1002/adma.200803276

131. Ali, A., Awang, M., Mat, R., Johari, A., Kamaruddin, M. J., & Sulaiman, W. R. W. (2014). Influence of hydrophilic polymer on pure water permeation, permeability coefficient, and porosity of polysulfone blend membranes. Advanced Materials Research, 931-932, 168-172. https://doi.org/10.4028/www.scientific.net/amr.931-932.168

132. Rösler, A., Vandermeulen, G. W. M., & Klok, H.-A. (2001). Advanced drug delivery devices via self-assembly of amphiphilic block copolymers. Advanced Drug Delivery Reviews, 53(1), 95–108. https://doi.org/10.1016/s0169-409x(01)00222-8

133. Talelli, M., Barz, M., Rijcken, C. J. F., Kiessling, F., Hennink, W. E., & Lammers, T. (2015). Core-crosslinked polymeric micelles: Principles, preparation, biomedical applications and clinical translation. Nano Today, 10(1), 93–117. https://doi.org/10.1016/j.nantod.2015.01.005.

134. Talelli, M., Rijcken, C. J. F., Hennink, W. E., & Lammers, T. (2012). Polymeric micelles for cancer therapy: 3 C's to enhance efficacy. Current Opinion in Solid State and Materials Science, 16(6), 302–309. https://doi.org/10.1016/j.cossms.2012.10.003

135. Sun, R., Luo, Q., Gao, C., & Wang, Y. (2014). Facile fabrication of reduction-responsive nanocarriers for controlled drug release. Polym. Chem., 5(17), 4879–4883. https://doi.org/10.1039/c4py00577e

136. Foroozandeh, P. and Aziz, A. A. (2018). Insight into cellular uptake and intracellular trafficking of nanoparticles. Nanoscale Research Letters, 13(1). https://doi.org/10.1186/s11671-018-2728-6

137. Knysh, Alexander, et al. “Dynamic Light Scattering Analysis in Biomedical Research and Applications of Nanoparticles and Polymers.” Journal of Biomedical Photonics & Engineering, 30 May 2023, pp. 020203–020203, https://doi.org/10.18287/jbpe23.09.020203.

138. Zürich, JKweb, Webdesign Basel &. “LS Instruments | Experimental Guidelines - DLS Sample Preparation.” Lsinstruments.ch, lsinstruments.ch/en/theory/dynamic-light-scattering-dls/experimental-guidelines-dls-sample-preparation.

139. Dziendzikowska, K., Czerwińska, M., Grodzicki, W., Oczkowski, M., Królikowski, T., Gromadzka-Ostrowska, J., Męczyńska-Wielgosz, S., Sikorska, K., Kamola, D., Sapierzyński, R., & Kruszewski, M. (2026). Comparative impact of polystyrene, rice bag-derived high-density polyethylene nanoparticles, and polystyrene–silver nanoparticle interactions in a 28-day in vivo study in male and female Wistar rats. Scientific Reports, 16(1). https://doi.org/10.1038/s41598-026-35219-9

140. Ekladious, I., Colson, Y. L., & Grinstaff, M. W. (2018). Polymer–drug conjugate therapeutics: advances, insights and prospects. Nature Reviews Drug Discovery, 18(4), 273-294. https://doi.org/10.1038/s41573-018-0005-0

141. Maherani, B., Arab-Tehrany, E., Mozafari, M. R., Gaïani, C., & Linder, M. (2011). Liposomes: a review of manufacturing techniques and targeting strategies. Current

Nanoscience, 7(3), 436-452. https://doi.org/10.2174/157341311795542453

142. Niu, L. and Panyam, J. (2017). Freeze concentration-induced plga and polystyrene nanoparticle aggregation: imaging and rational design of lyoprotection. Journal of Controlled Release, 248, 125-132. https://doi.org/10.1016/j.jconrel.2017.01.019

143. Trenkenschuh, E. and Frieß, W. (2021). Freeze-drying of nanoparticles: how to overcome colloidal instability by formulation and process optimization. European Journal of Pharmaceutics and Biopharmaceutics, 165, 345-360. https://doi.org/10.1016/j.ejpb.2021.05.024

Chapter 5. Metal Ion Complexation to Create a Platform for Chemodynamic Therapy

5.1. Introduction to Chemodynamic Therapy (CDT)

CDT is an innovative cancer treatment that that takes advantage of the unique biochemical environment of the tumour to generate ROS such as $O2^{\cdot -}$ and ·OH, leading to cancer cell death [1,2]. Unlike treatments such as photodynamic therapy, which relies on light, or thermotherapy, which uses heat, CDT operates without external stimuli [3]. Instead, it exploits the elevated H_2O_2 levels and overexpressed metal ions in tumours to produce highly reactive hydroxyl radicals (·OH) via Fenton and Fenton-like reactions [1,2] . This tumour-specific approach minimises damage to healthy tissues and reduces systemic toxicity compared to traditional chemotherapy and radiotherapy [4,5]. By inducing oxidative stress, CDT promotes apoptosis, necrosis, or autophagy in cancer cells, while sparing normal cells due to their lower H_2O_2 levels, neutral or slightly alkaline and stronger antioxidant defences[1,6,7,8,9,10,11,12]. Hence, CDT is highly selective and only activated by tumour endogenous stimulus. Compared with encapsulating chemotherapeutic drugs in polymeric nanoparticles, loading CDT metal ions offer a safer way of chemotherapy

5.1.1. The Mechanism of Chemodynamic Therapy

CDT's effectiveness rests on its ability to generate ROS, particularly ·OH, through Fenton and Fenton-like reactions[1,9,10,13]. In tumour cells, where H_2O_2 levels are elevated, metal ions such as Fe^{2+}, Cu^{2+}, or Mn^{2+} catalyse its conversion into ·OH under acidic conditions [14]. These radicals attack essential cellular components such as proteins, lipids, and DNA via oxidative damage leading to the destruction of cancer cells [1,5,9,10,15].

This process can be illustrated by the classical Fenton reaction:

$Fe^{2+} + H_2O_2 \rightarrow Fe^{3+} + OH^- + \cdot OH$

Due to the high oxidative stress and fast metabolism in cancer cells which struggle to neutralise this damage, unlike healthy cells, which are better equipped to manage ROS [5]. Additionally, the acidic nature of the TME (pH 6.0-7.0, dropping to 5.0-6.0 in late endosomes [16,17]) enhances the catalytic efficiency of these metal ions promoting ROS

generation[1,9].

While the classical Fenton reaction relies on Fe^{2+} as the catalyst, CDT also employs Fenton-like reactions, which utilise other transition metals, such as Cu^{2+}, Mn^{2+}, and Co^{2+}, expand CDT's versatility [1,9,10,15].

5.1.2. Advantages of Chemodynamic Therapy

CDT offers several compelling advantages for cancer treatment. It excels in precision targeting by exploiting the tumour's unique biochemical environment characterised by elevated H_2O_2 levels (up to 100 µM versus 20 nM in normal tissues [6,8,11]) and acidic pH to generate ROS primarily at the tumour site, thereby sparing surrounding healthy tissues [1,14]. This targeted approach proves particularly effective in hypoxic conditions, which are prevalent in solid tumours with poor blood supply and rapid growth [18,19,20,21]; unlike oxygen-dependent therapies such as photodynamic therapy [22], CDT requires no external stimulation, ensuring consistent performance in oxygen-deprived environments [3]. Additionally, CDT shows synergic effect when pairing with therapies like chemotherapy, radiotherapy, and PDT, where its catalytic metal ions sensitise cancer cells to improve overall efficacy [13,23,24]. Emerging research also highlighting its potential to boost anti-tumour immune responses when combined with immunotherapy [22,25,26,27]. Furthermore, the confinement of ROS production to the TME, CDT minimises widespread oxidative damage, reducing the side effects commonly associated with conventional therapies and supporting repeated administration [1,9,28].

5.1.3. Limitation of CDT

Despite its potential, CDT encounters several challenges. Tumours can develop resistance to ROS induced apoptosis by upregulating antioxidant defences, such as glutathione (GSH) and superoxide dismutase (SOD), which neutralise ROS[29,30,31]. The cell targeting effect of CDT also poses a challenge of overdosing the body with Fenton-type heavy metals may cause potential damage to healthy cells [32]. The concentration of H_2O_2 in cancer cells may not sufficient to accomplish satisfactory CDT [33,34]. The overall production of ·OH radical is

relatively low and their release is too rapid for effective, prolonged, CDT [35]. To address this, use of nanotechnology and combination therapies are employed in the chapter[10,36]. The use of PGA[(CPT-Gly)-*co*-(F-PSar)] drug conjugate to complex with Fenton metal ions, the fucose targeting group may selectively deliver both CPT and metal ions to the cancer cells where they accumulate and potentially excreting therapeutic effect synergistically.

5.1.4. Nanotechnology in CDT

Nanotechnology plays a crucial role in enhancing CDT by improving the delivery and stability of the catalytic metal ions. Metal encapsulated NPs have been developed to deliver these ions directly to the tumour site, where they can initiate the Fenton or Fenton-like reactions[8,9,13,18,24,32]. These NPs can be designed to release their metal ions in response to specific stimuli, such as the acidic pH of the TME, ensuring targeted ROS generation [37]. Beyond delivery, NPs sustain high metal ion concentrations at the tumour site via the EPR effect [38,39,40,41] and can carry additional therapeutic agents, facilitating multi-modal treatments integrating CDT with chemotherapy, immunotherapy, or photodynamic therapy [13,22,23,26,27,28,32,42].

5.1.5. Cu^{2+} ion Complexation with PGA

In this study, Cu^{2+} was chosen to be complexed with the drug conjugate produced- PGA-[(CPT-Gly)-*co*-(F-PSar)], due to its outstanding catalytic properties [9,36,42,44,43]. The copper-mediated Fenton-like reaction follows these pathways:

$$Cu^{2+} + GSH \rightarrow Cu^{+} + GSSG$$

$$Cu^{+} + H_2O_2 \rightarrow Cu^{2+} + \cdot OH + OH^{-}$$

First, the copper ion undergoes rapid redox cycling between Cu^{2+} and Cu^{+}, sustaining ROS production and depleting GSH, a key antioxidant that counteract with ROS generated, and greatly enhance ·OH generation (Figure 5.1-1)[9,15,43]. Also, Cu^{2+} can remains effective in less acidic tumour regions, broadening the scope of CDT in different tumour environments [9,36,42,44]. Moreover, the catalysed Fenton-like reaction rate of Cu^{2+} is ~160 times of that

Fe^{2+} significantly enhancing CDT's efficiency [9,15].

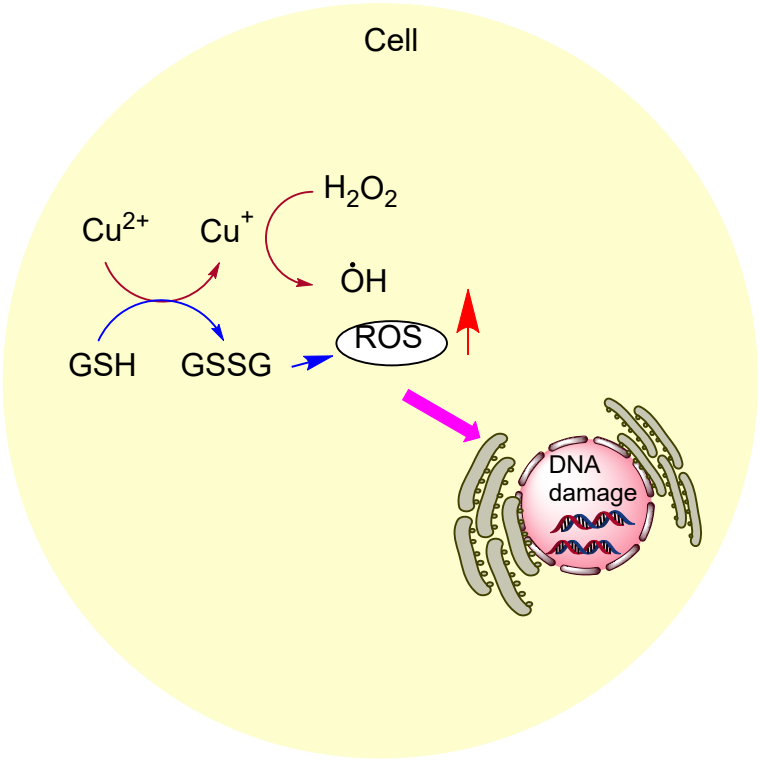

Figure 5.1-1. Illustration of Cu^{2+} ion mediated Fenton- like reaction pathways in cell.

The drug conjugate PGA-[(CPT-Gly)-*co*-(F-PSar)] may plausibly self-assemble into NPs in aqueous solution to transport Cu^{2+} to the tumour site by utilising the free carboxylate groups on the PGA backbone. At neutral pH, PGA forms two different complex structures with Cu^{2+} ion, first, the two carboxylate groups and an amide nitrogen of PGA bind with Cu^{2+} ion; second, the only two carboxylate groups of PGA bind with Cu^{2+} ion, forming Cu^{2+} -PGA complex that co-exist of both structures (Figure 5.1-2)[45,46]. Dissociation occurs in an acidic environment where the carboxylate group are protonated, releasing Cu^{2+} [45,46].

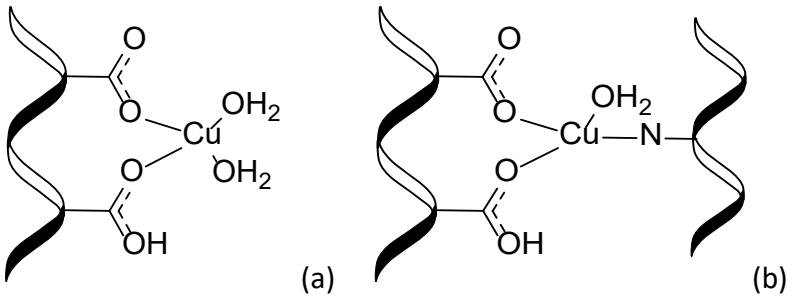

Figure 5.1-2. Structure of Cu^{2+}-PGA complex in aqueous solution at pH 7-8, a mixture of (a) & (b)

Because the drug conjugation process occupies most carboxylate groups, it is essential to select a metal ion capable of exerting its catalytic effect at low concentrations. Cu^{2+} emerged as the ideal choice due to their remarkable ability to sustain ROS production and deplete antioxidants[9,15], coupled with a catalytic rate for ROS generation that significantly surpasses that of Fe^{2+} [46,47]. This enhanced efficiency enables effective CDT at reduced metal concentrations, thereby minimising potential toxicity to healthy tissues. To further improve the precision of Cu^{2+} delivery, a fucose targeting group was incorporated into the conjugate, directing the therapy specifically toward pancreatic cancer cells. Additionally, co-administering Cu^{2+} with CPT introduces the potential for a synergistic therapeutic effect. CPT selectively disrupts DNA replication in S-phase cells [48]. While Cu^{2+} trigger widespread oxidative damage to cellular components, proteins, lipids, and DNA, through ROS generation [1,5,9,10,15]. Together, these complementary mechanisms may offer a more comprehensive and robust strategy for targeting and eliminating tumour cells.

5.2. Experimental

5.2.1. Encapsulation of Cu^{2+} ions

For simplicity, the MW of drug conjugate used for Cu^{2+} complexation was calculated as pure PGA. The obtained drug conjugate PGA-[(CPT-Gly)-*co*-(F-PSar)] was dissolved in anhydrous DMF at the concentration of 10.0 mg/mL. Next, 38.8 µL of 1.0 M $CuCl_2$ in anhydrous DMF was added per 10.0 mg of the drug conjugate. The resulting mixture was then stirred at room temperature for 30 minutes to allow complexation. Following this, the solution was dialysed in methanol prewashed dialysing bag (MWCO: 2000) against methanol for one day,

then against DI water for an additional two days to fully remove non-complexed Cu^{2+} ions. Finally, the purified solution was freeze dried to yield the Cu^{2+} complexed drug conjugate.

5.2.2. Release of Cu^{2+} ions

The Cu^{2+} complexed drug conjugate from above was dissolved in DMF at concentration of 10.0 mg/mL and added dropwise into pH 4.5 HCl solution under rapid stirring, then dialysed against pH 4.5 HCl solution for two days before being freeze dried.

5.3. Results & Discussion

To achieve combination of chemotherapeutic and chemodynamic therapy in cancer treatment, the ability of the drug conjugate to complex with Cu^{2+} was studied. The Cu^{2+} complexation was carried out by mixing the drug conjugate DMF solution with excessive $CuCl_2$ DMF solution. The use of anhydrous DMF was to prevent the generation of acid by $CuCl_2$ thus to circumvent the deprotonation of the carboxylate group. The weight ratio of inorganic material in the Cu^{2+} complexed drug conjugate was determined by thermogravimetric analysis (TGA) for three individual samples. As the temperature increased during TGA, the initial weight reduction stemmed primarily from the evaporation of moisture within the sample. This was followed by the decomposition of the drug conjugate's components, which begins with the decomposition of CPT occurring between 200°C and 300°C [49]. Then the complete decomposition of PSar and PGA was observed at around 500 ^{o}C (Figure 5.3-1) [50,51]. To ensure the complete removal of all organic materials, the temperature was further raised to 900°C. The analysis ultimately revealed an average inorganic residue weight of 2.93% (±0.39) compared to theoretical residue weight of 3.36% (assuming copper complex oxidised into CuO). Although close to theoretical number yet considering the extra carboxylate group for copper complexation given by the unsuccessful F-PSar and CPT-Gly coupling during reaction, its actual complexation efficiency may be lower.

Several factors likely contributed to affect the efficacy of Cu^{2+} ions complexation. During the preparation of the $CuCl_2$ DMF solution, exposure of $CuCl_{2(s)}$ to moisture in the air may have produced acid, which protonates the carboxylate groups of the drug conjugate, shifting the

equilibrium of Cu^{2+}- PGA complexation. Moreover, the dialysis bag, typically stored in DI water, was rinsed with methanol before use and might have retained trace amounts of water. This residual water could generate acid that protonates the copper-complexed carboxylate groups and again shift the equilibrium of Cu^{2+}- PGA complexation disrupting complexation. Furthermore, possibly after dialysis in methanol for a day, residual $CuCl_2$ persisted in sufficient quantities to acidify the water when the dialysis solution was switched to DI water, exacerbating the loss of complexed copper ions. Together, these issues account for the observed incomplete Cu^{2+} ion complexation.

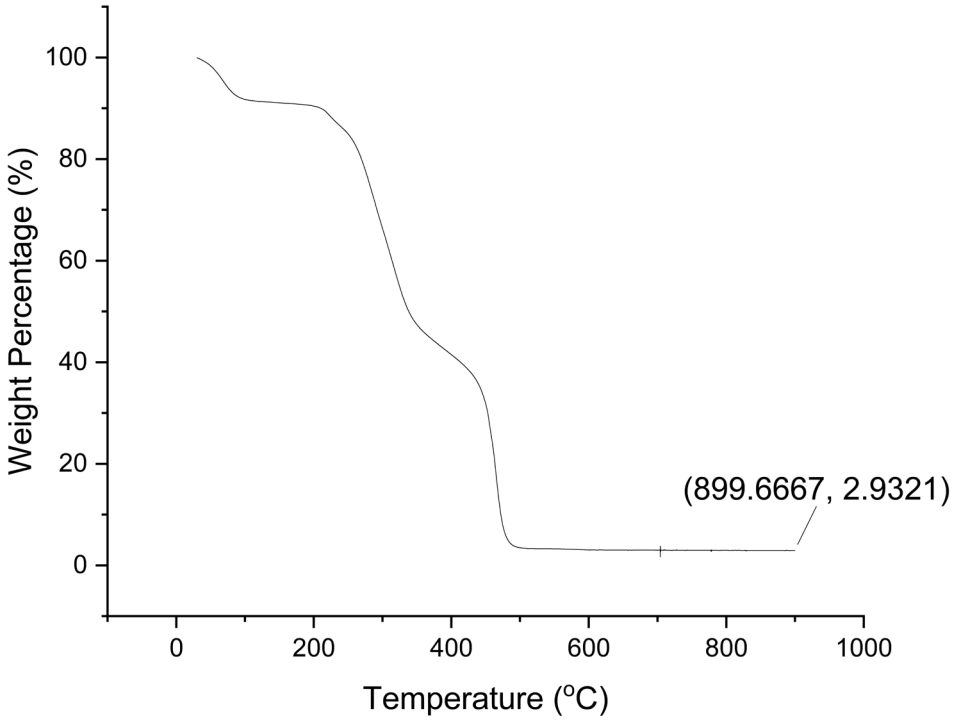

Figure 5.3-1. Average TGA result from three individual analysis on three samples of Cu^{2+} complexed drug conjugate.

Subsequently, the ash remaining after TGA was examined using energy dispersive X-ray (EDX) spectroscopy to identify the composition of the inorganic residue within the Cu^{2+} complexed drug conjugate. The EDX analysis indicated that the inorganic material consisted of copper oxide [52], confirming the copper- drug conjugate complexation (Figure 5.3-2).

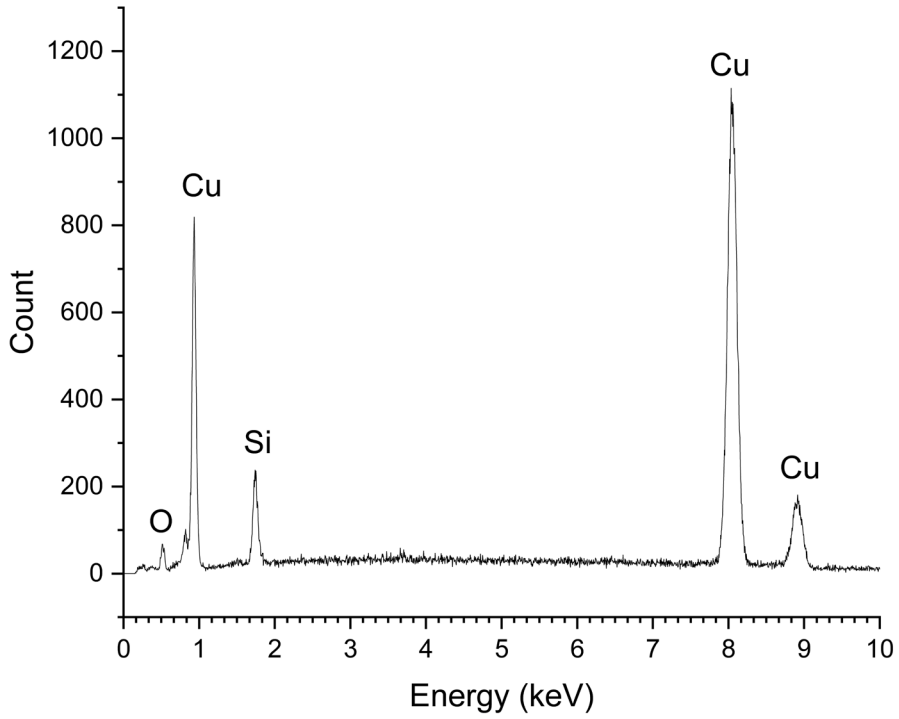

Figure 5.3-2. EDX Spectrum of sample residue after TGA

Although comprehensive copper ion release study was performed, analysis was not carried out due to no appropriate accessible equipment for this low Cu^{2+} concentration detection in the background of other ions present in PBS and acetate buffer solution. Nevertheless, to evaluate the conjugate's potential to release copper ions in the acidic pH of endosomes and lysosomes within cancer cells, the Cu^{2+} complexed drug conjugate was dialysed against a pH 4.5 HCl solution for two days before subjecting it to TGA. This analysis revealed that only 0.88% (±0.16%) residue remained, demonstrating that the drug conjugate can indeed release Cu^{2+} ions under acidic conditions (Figure 5.3-3). However, these findings have limitations and not fully represent the behaviour of the Cu^{2+} complexed drug conjugate in physiological conditions. Since TGA was the only method used to quantify Cu^{2+}, a pH 4.5 HCl solution was chosen over an acetate buffer solution, which is commonly employed to mimic physiological acidic environments, because metal ions in the buffer could interfere with TGA results. Similarly, the stability of the of Cu^{2+} complexed drug conjugate was not assessed in a pH 7.4 PBS solution due to metal ion interference. Additionally, testing in a slightly basic

solution was avoided, as Cu^{2+} forms more stable complex with PGA under basic conditions [45,46]. Yet without influence and interaction of other ions, the test of Cu^{2+} complexed drug conjugate in slight basic solution prepared with organic base would likely produce inaccurate and inconclusive outcomes.

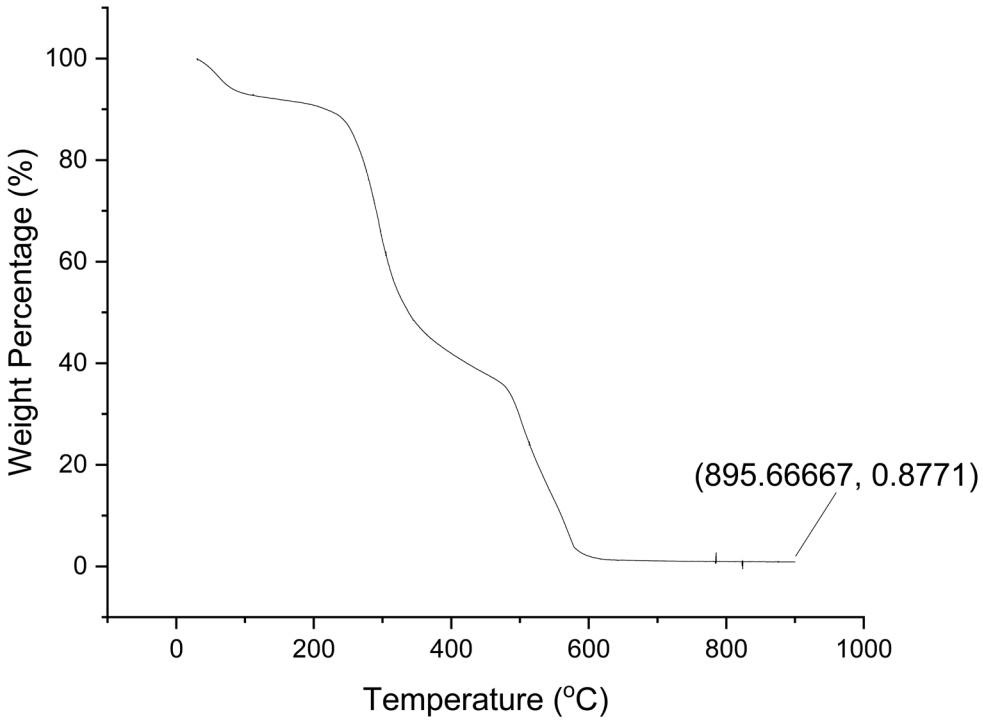

Figure 5.3-3. Average TGA from three individual analysis on three samples of Cu^{2+} complexed drug conjugate after dialysed against a pH 4.5 HCl solution for two days.

5.4. Summary

This study examined a Cu^{2+} ions complexed drug conjugate through TGA and EDX spectroscopy, revealing key insights into its composition and behaviour. TGA showed an initial weight loss from water evaporation, followed by the decomposition of the conjugate's components between 200°C and 300°C, with complete breakdown at round 500°C. After heating to 900°C to remove all organic material, the inorganic residue average of 2.93% (±0.39) close to theoretical residue weight of 3.36% (assuming copper complex oxidised into CuO). This incomplete complexation arose from multiple factors: acid production during $CuCl_2$ DMF solution preparation protonated these groups, residual water in the dialysis bag generated additional acid shifted the complexation equilibrium disrupting complexation. EDX analysis identified the inorganic residue as copper oxide, confirming the formation of copper- drug conjugate complex. The conjugate proved capable of releasing Cu^{2+} ions in acidic conditions, as demonstrated by dialysis against a pH 4.5 HCl solution, which left only 0.88% (±0.16%) residue after subsequent TGA, highlighting its potential for targeted release in acidic environments like cancer cell endosomes and lysosomes.

5.5. References

1. Tang, Z., Liu, Y., He, M., & Bu, W. (2018). Chemodynamic therapy: tumour microenvironment-mediated fenton and fenton-like reactions. Angewandte Chemie International Edition, 58(4), 946-956. https://doi.org/10.1002/anie.201805664

2. Hassannia, B., Vandenabeele, P., & Berghe, T. V. (2019). Targeting ferroptosis to iron out cancer. Cancer Cell, 35(6), 830-849. https://doi.org/10.1016/j.ccell.2019.04.002

3. Neufeld, M. J., Lutzke, A., Pratx, G., & Sun, C. (2020). High-z metal–organic frameworks for x-ray radiation-based cancer theranostics. Chemistry – A European Journal, 27(10), 3229-3237. https://doi.org/10.1002/chem.202003523

4. Yan, H., Zou, T., Tuo, Q., Xu, S., Li, H., Belaidi, A. A., … & Lei, P. (2021). Ferroptosis: mechanisms and links with diseases. Signal Transduction and Targeted Therapy, 6(1). https://doi.org/10.1038/s41392-020-00428-9

5. Liang, Q., Wang, Y., Li, Y., Wang, J., Liu, C., & Li, Y. (2024). Ferroptosis: emerging roles in lung cancer and potential implications in biological compounds. Frontiers in Pharmacology, 15. https://doi.org/10.3389/fphar.2024.1374182

6. Szatrowski, T. P., & Nathan, C. F. (1991). Production of large amounts of hydrogen peroxide by human tumor cells. Cancer research, 51(3), 794–798.

7. Murphy, M. P. (2008). How mitochondria produce reactive oxygen species. Biochemical Journal, 417(1), 1-13. https://doi.org/10.1042/bj20081386

8. Xu, X., Saw, P. E., Tao, W., Li, Y., Ji, X., Bhasin, S., … & Farokhzad, O. C. (2017). Ros-responsive polyprodrug nanoparticles for triggered drug delivery and effective cancer therapy. Advanced Materials, 29(33). https://doi.org/10.1002/adma.201700141

9. P Zhang, Q., Wang, J., Xu, L., Lu, S., Yang, H., Duan, Y., … & Liu, H. (2021). pegylated copper(ii)-chelated polydopamine nanocomposites for photothermal-enhanced chemodynamic therapy against tumor cells. Journal of Applied Polymer Science, 138(40). https://doi.org/10.1002/app.51172

10. Lin, L., Song, J., Song, L., Ke, K., Liu, Y., Zhou, Z., … & Chen, X. (2018). simultaneous fenton-like ion delivery and glutathione depletion by mno2-based nanoagent to enhance chemodynamic therapy. Angewandte Chemie, 130(18), 4996-5000. https://doi.org/10.1002/ange.201712027

11. Murphy, M. (2008). how mitochondria produce reactive oxygen species. Biochemical Journal, 417(1), 1-13. https://doi.org/10.1042/bj20081386

12. Vi Zhai, S., Hu, X., Hu, Y., Wu, B., & Xing, D. (2017). Visible light-induced crosslinking and physiological stabilization of diselenide-rich nanoparticles for redox-responsive drug release and combination chemotherapy. Biomaterials, 121, 41-54. https://doi.org/10.1016/j.biomaterials.2017.01.002

13. Ren, Z., Sun, S., Sun, R., Cui, G., Hong, L., Rao, B., … & Mao, Z. (2019). A metal–polyphenol-coordinated nanomedicine for synergistic cascade cancer chemotherapy and chemodynamic therapy. Advanced Materials, 32(6). https://doi.org/10.1002/adma.201906024

14. Kang, Y. W. and Hwang, K. (2000). Effects of reaction conditions on the oxidation efficiency in the fenton process. Water Research, 34(10), 2786-2790. https://doi.org/10.1016/s0043-1354(99)00388-7

15. McGivern, T., Afsharpour, S., & Marmion, C. J. (2018). Copper complexes as artificial dna metallonucleases: from sigman's reagent to next generation anti-cancer agent?. Inorganica Chimica Acta, 472, 12-39. https://doi.org/10.1016/j.ica.2017.08.043

16. Breunig, M., Bauer, S. E., & Goepferich, A. (2008). Polymers and nanoparticles: intelligent tools for intracellular targeting?. European Journal of Pharmaceutics and Biopharmaceutics, 68(1), 112-128. https://doi.org/10.1016/j.ejpb.2007.06.010

17. Liu, X., Chen, Y., Li, H., Huang, N., Jin, Q., Ren, K., … & Ji, J. (2013). Enhanced retention

and cellular uptake of nanoparticles in tumors by controlling their aggregation behavior. ACS Nano, 7(7), 6244-6257. https://doi.org/10.1021/nn402201w

18. Wang, J., Wang, X., Lu, S., Hu, J., Zhang, W., Xu, L., … & Liu, H. (2019). Integration of cascade delivery and tumor hypoxia modulating capacities in core-releasable satellite nanovehicles to enhance tumor chemotherapy. Biomaterials, 223, 119465. https://doi.org/10.1016/j.biomaterials.2019.119465

19. Zhang, T., Xu, C., Zhao, W., Gu, Y., Li, X., Xu, J., … & Chen, H. (2018). A redox-activated theranostic nanoagent: toward multi-mode imaging guided chemo-photothermal therapy. Chemical Science, 9(33), 6749-6757. https://doi.org/10.1039/c8sc02446d

20. Liu, J., Bu, W., & Shi, J. (2017). Chemical design and synthesis of functionalized probes for imaging and treating tumor hypoxia. Chemical Reviews, 117(9), 6160-6224. https://doi.org/10.1021/acs.chemrev.6b00525

21. Feng, L., Dong, Z., Wang, L., Liang, C., Chen, J., Ma, Q., … & Liu, Z. (2018). Glucose & oxygen exhausting liposomes for combined cancer starvation and hypoxia-activated therapy. Biomaterials, 162, 123-131. https://doi.org/10.1016/j.biomaterials.2018.02.004

22. Wang, X., Zhong, X., Liu, Z., & Cheng, L. (2020). Recent progress of chemodynamic therapy-induced combination cancer therapy. Nano Today, 35, 100946. https://doi.org/10.1016/j.nantod.2020.100946

23. Xue, T., Xu, C., Wang, Y., Wang, Y., Tian, H., & Zhang, Y. (2019). Doxorubicin-loaded nanoscale metal–organic framework for tumor-targeting combined chemotherapy and chemodynamic therapy. Biomaterials Science, 7(11), 4615-4623.

https://doi.org/10.1039/c9bm01044k

24. Chen, G., Yang, Y., Xu, Q., Ling, M., Lin, H., Ma, W., … & Yu, M. (2020). Self-amplification of tumor oxidative stress with degradable metallic complexes for synergistic cascade tumor therapy. Nano Letters, 20(11), 8141-8150. https://doi.org/10.1021/acs.nanolett.0c03127

25. Zhou, Q., Wang, Y., Li, X., Lu, N., & Ge, Z. (2021). Polymersome nanoreactor-mediated combination chemodynamic-immunotherapy via ros production and enhanced sting activation. Advanced Therapeutics, 4(11). https://doi.org/10.1002/adtp.202100130

26. Zhou, Y., Fan, S., Feng, L., Huang, X., & Chen, X. (2021). Manipulating intratumoral fenton chemistry for enhanced chemodynamic and chemodynamic-synergized multimodal therapy. Advanced Materials, 33(48). https://doi.org/10.1002/adma.202104223

27. Ahmad, W., Sajjad, W., Zhou, Q., & Ge, Z. (2024). Nanomedicine for combination of chemodynamic therapy and immunotherapy of cancers. Biomaterials Science, 12(18), 4607-4629. https://doi.org/10.1039/d3bm02133e

28. Li, S., Jiang, P., Jiang, F., & Liu, Y. (2021). Recent advances in nanomaterial-based nanoplatforms for chemodynamic cancer therapy. Advanced Functional Materials, 31(22). https://doi.org/10.1002/adfm.202100243

29. Balamurugan, M., Santharaman, P., Thangamuthu, M., Seenivasan, R., Sethy, N. K., Bhargava, K., … & Karunakaran, C. (2018). Recent trends in electrochemical biosensors of superoxide dismutases. Biosensors and Bioelectronics, 116, 89-99. https://doi.org/10.1016/j.bios.2018.05.040

30. Liu, T., Sun, L., Zhang, Y., Wang, Y., & Zheng, J. (2021). Imbalanced gsh/ros and sequential cell death. Journal of Biochemical and Molecular Toxicology, 36(1). https://doi.org/10.1002/jbt.22942

31. Yue, W., Li, G., Liu, J., Sun, J., Sun, H., Li, X., … & Miao, Y. (2007). Anti-oxidation and immune responses in mice upon exposure to manganese superoxide dismutase expressed in silkworm larvae, bombyx mori l. Cell Biology International, 31(9), 974-978. https://doi.org/10.1016/j.cellbi.2007.03.007

32. Dantas, K. C. F., Rosário, J. d. S., & Silva, P. P. (2022). Polymeric nanosystems applied for metal-based drugs and photosensitizers delivery: the state of the art and recent advancements. Pharmaceutics, 14(7), 1506. https://doi.org/10.3390/pharmaceutics14071506

33. Pan, Y., Zhu, Y., Xu, C., Pan, C., Shi, Y., Zou, J., … & Li, J. (2022). Biomimetic yolk–shell nanocatalysts for activatable dual-modal-image-guided triple-augmented chemodynamic therapy of cancer. ACS Nano, 16(11), 19038-19052. https://doi.org/10.1021/acsnano.2c08077

34. Xiao, Z., Zuo, W., Chen, L., Wu, L., Liu, N., Liu, J., … & Zhu, X. (2021). H2o2 self-supplying and gsh-depleting nanoplatform for chemodynamic therapy synergetic photothermal/chemotherapy. ACS Applied Materials &Amp; Interfaces, 13(37), 43925-43936. https://doi.org/10.1021/acsami.1c10341

35. Zhao, P., Li, H., & Bu, W. (2023). A forward vision for chemodynamic therapy: issues and opportunities. Angewandte Chemie International Edition, 62(7).

https://doi.org/10.1002/anie.202210415

36. Ma, B., Wang, S., Liu, F., Zhang, S., Duan, J., Zhao, L., … & Li, L. (2018). self-assembled copper–amino acid nanoparticles for in situ glutathione “and” h2o2 sequentially triggered chemodynamic therapy. Journal of the American Chemical Society, 141(2), 849-857. https://doi.org/10.1021/jacs.8b08714

37. Lin, L., Huang, T., Song, J., Ou, X., Wang, Z., Deng, H., … & Chen, X. (2019). Synthesis of copper peroxide nanodots for h2o2 self-supplying chemodynamic therapy. Journal of the American Chemical Society, 141(25), 9937-9945. https://doi.org/10.1021/jacs.9b03457

38. Maeda, H., Wu, J., Sawa, T., Matsumura, Y., & Hori, K. (2000). Tumor vascular permeability and the epr effect in macromolecular therapeutics: a review. Journal of Controlled Release, 65(1-2), 271-284. https://doi.org/10.1016/s0168-3659(99)00248-5

39. Skinner, S. A., Tutton, P. J., & O'Brien, P. E. (1990). Microvascular architecture of experimental colon tumors in the rat. Cancer research, 50(8), 2411–2417.

40. Matsumura, Y., & Maeda, H. (1986). A new concept for macromolecular therapeutics in cancer chemotherapy: mechanism of tumoritropic accumulation of proteins and the antitumor agent smancs. Cancer research, 46 12 Pt 1, 6387-92 .

41. Maeda, H. (2001). Smancs and polymer-conjugated macromolecular drugs: advantages in cancer chemotherapy. Advanced Drug Delivery Reviews, 46(1-3), 169-185. https://doi.org/10.1016/s0169-409x(00)00134-4

42. Brillas, E., Baños, M., Camps, S., Arias, C., Cabot, P., Garrido, J., … & Rodríguez, R. (2004). catalytic effect of fe2+, cu2+and uva light on the electrochemical degradation of nitrobenzene using an oxygen-diffusion cathode. New Journal of Chemistry, 28(2), 314-322. https://doi.org/10.1039/b312445b

43. Tang, W., Gao, H., Ni, D., Wang, Q., Gu, B., He, X., … & Peng, W. (2019). Bovine serum albumin-templated nanoplatform for magnetic resonance imaging-guided chemodynamic therapy. Journal of Nanobiotechnology, 17(1). https://doi.org/10.1186/s12951-019-0501-3

44. Soltani, T. and Lee, B. (2017). Enhanced formation of sulfate radicals by metal-doped bifeo3 under visible light for improving photo-fenton catalytic degradation of 2-chlorophenol. Chemical Engineering Journal, 313, 1258-1268. https://doi.org/10.1016/j.cej.2016.11.016

45. Zhao, X., Wang, S., Younis, M. R., Xia, X., & Wang, C. (2017). Asymmetric nanochannel–ionchannel hybrid for ultrasensitive and label-free detection of copper ions in blood. Analytical Chemistry, 90(1), 896-902. https://doi.org/10.1021/acs.analchem.7b03818

46. Fu, L., Wan, Y., Qi, C., He, J., Li, C., Yang, C., … & Huang, P. (2021). Nanocatalytic theranostics with glutathione depletion and enhanced reactive oxygen species generation for efficient cancer therapy. Advanced Materials, 33(7). https://doi.org/10.1002/adma.202006892

47. Zhang, C., Yan, L., Wang, X., Dong, X., Zhou, R., Gu, Z., … & Zhao, Y. (2019). Tumor microenvironment-responsive cu2(oh)po4 nanocrystals for selective and controllable radiosentization via the x-ray-triggered fenton-like reaction. Nano Letters, 19(3), 1749-1757. https://doi.org/10.1021/acs.nanolett.8b04763

48. Li, L. H., Fraser, T. J., Olin, E. J., & Bhuyan, B. K. (1972). Action of camptothecin on mammalian cells in culture. Cancer research, 32(12), 2643–2650.

49. Wang, S., Lin, S., Hsieh, T., & Chan, S. (2007). Thermal behavior and thermal decarboxylation of 10-hydroxycamptothecin in the solid state. Journal of Pharmaceutical and Biomedical Analysis, 43(2), 457-463. https://doi.org/10.1016/j.jpba.2006.07.023

50. Fetsch, C. and Luxenhofer, R. (2013). Thermal properties of aliphatic polypeptoids. Polymers, 5(1), 112-127. https://doi.org/10.3390/polym5010112

51. Portilla-Arias, J., García-Alvarez, M., Ilarduya, A. M. d., & Muñoz-Guerra, S. (2007). Thermal decomposition of microbial poly(γ-glutamic acid) and poly(γ-glutamate)s. Polymer Degradation and Stability, 92(10), 1916-1924. https://doi.org/10.1016/j.polymdegradstab.2007.06.011

52. Kouti, M., & Matouri., L. (2010). FABRICATION OF NANOSIZED CUPROUS OXIDE USING FEHLING'S SOLUTION. Scientia Iranica, 17, 73-78.

Chapter 6. Summary and Future Plans

6.1. Summary

A polymeric system for the controlled delivery of the chemotherapeutic CPT was the first aim of this research. Initially, the drug conjugate PSar-Gly-CPT was synthesised with various CPT loading contents. However, stable NPs could not form, rendering polymer modification necessary. PGA-(PSar-Gly-CPT) was subsequently produced and stable NPs of moderate dispersity were produced at concentrations of 100 µg/mL and 1.0 mg/mL, indicating that PGA conjugation facilitates stable NP formation. A second aim of the research was to incorporate metal ions in the NPs as a second mode of chemotherapy. To facilitate this, CPT-Gly and PSar/F-PSar were conjugated to PGA to yield PGA-[(CPT-Gly)-*co*-(PSar)] and PGA-[(CPT-Gly)-*co*-(F-PSar)]. Smaller, more uniform NPs formed at much greater concentrations compared to PGA-(CPT-Gly) that lack PSar. Consequently, PSar-modified drug conjugates demonstratively have the potential to be effective drug delivery systems, with PSar, a viable alternative to PEG in such systems. PGA-[(CPT-Gly)-*co*-(PSar)] NPs remained stable at pH 6.0 but aggregated at pH 5.5, suggesting that the NPs have sufficient stability to pass through the acidic extracellular environment (pH 6.0- 7.0), undergoing endocytosis into the cells[1,2] . Furthermore, PGA-[(CPT-Gly)-*co*-(PSar)] NPs slowly released CPT in pH 7.4 PBS solution at 37^{o}C with approximately 40% of CPT (w/w) released over 21 days. Which greatly reduce the cytotoxicity brought by rapid deposition of toxic CPT during circulation.

PGA-[(CPT-Gly)-*co*-(F-PSar)] NPs performed comparably to PGA-[(CPT-Gly)-*co*-(PSar)] NPs in acidic conditions, with both remaining stable at pH 6.0 and aggregating at pH 5.5, likely caused by the protonation of the PGA backbone. CPT release from PGA-[(CPT-Gly)-*co*-(F-PSar)] NPs was comparable to release from PGA-[(CPT-Gly)-*co*-(PSar)] NPs, with approximately 46% of CPT (w/w) released after 26 days in pH 7.4 PBS solution at 37^{o}C. However, the CPT release rate reduced dramatically in pH 5.0 acetic buffer solution at 37^{o}C. Which was unexpected slow, possibly due to the aggregation and crystallisation of the drug conjugate in acidic aqueous solution as shown by DLS analysis in pH 5.5 acetate buffer solution. This phenomenon cause phase separation that limits contact with the solution and prohibiting hydrolysis of CPT.

DKPs were investigated as alternatives to NCAs as monomers for poly(amino acid) synthesis.

Sar-DKP, Ala-DKP, Glu-DKP, Glu(OBzyl)-DKP and Lys(Cbz)-DKP were produced, among these only Glu(OBzyl)-DKP can be polymerised without modifications and use of any catalysts. The addition of Ni(0)Cod_2:SIPr.HCl increased polymer yield but impurities persisted after dialysis. Both Glu(OBzyl)-DKP synthesis and ROP require further optimisation because of their low overall yield. Boc activated Ala-DKP was polymerised when catalysed with LiHMDS and other results also suggest that the activation of amide bond in DKPs and use of appropriate catalyst (e.g. LiHMDS) are necessary for effective DKP ROP. Whilst DKPs may offer a route to polymers for drug delivery creation, the required use of catalysts for their polymerisation is not ideal for *in vivo* use and so focus shifted to alternative routes of biocompatible polymer synthesis.

Both Glu(OByzl)-GA DKM and Sar-GA DKM were successfully synthesised but only Glu(OByzl)-GA DKM could be polymerised. Though further optimisation is needed, P(Glu-GA) was produced and later conjugated to F-PSar and CPT-Gly, producing P(Glu-GA)-[(CPT-Gly)-*co*-(F-PSar)], and with PSar-Gly-CPT to generate P(Glu-GA)-(PSar-Gly-CPT). P(Glu-GA)-(PSar-Gly-CPT) NPs (20% CPT content w/w%) remained soluble in pH 7.4 PBS solution at 1.0 mg/mL, while Z-average values of NPs produced from P(Glu-GA)-[(CPT-Gly)-*co*-(F-PSar)] (28% CPT content w/w%) decreased by nearly 50% as the concentration increased from 500 µg/mL to 1.0 mg/mL. This indicates the formation of premicellar aggregation at 500 µg/mL with large aggregates reorganising into smaller, more stable micelles as the concentration increases. Including P(Glu-GA) increased the overall water solubility of the drug conjugate. Although Sar-GA DKM failed to be polymerised under the reaction conditions in this research, its hydrolysis degradation in open air forms N-(2-hydroxyacetyl)-N-methylglycine indicating its susceptibility to ring opening and potential polymerisation.

Sn(II)Oct_2: acetic anhydride catalysed polycondensation of sarcosine and glycolic acid only yielded trace amount of polymer after dialysis. The unsuccessful polymerisation may result from multiple factors. First, the secondary amine of sarcosine reduces efficiency of its nucleophilic reaction. Second, the generation of water during melt condensation can cause the decomposition of Sn(II)Oct_2 to Sn(IV) killing the catalyst. Further study and analysis are needed justify this claim by replacing Sn(II)Oct_2 with $SnCl_2$ as reported in literature.

The Cu^{2+} ion complexation with PGA-[(CPT-Gly)-*co*-(F-PSar)] was slightly lower than that

theoretical yield (3.36%) with averaged inorganic residue 2.93% (±0.39) after heated in TGA to 900 ^{o}C . And EDX confirmed the ash remain to be copper oxide. Dialysis against pH 4.5 HCl solution before TGA test showed dramatic decrease in inorganic residue proving the Cu^{2+} complexed drug conjugate able to release of Cu^{2+} ion in acidic conditions. This indicates the Cu^{2+} complexed drug conjugate has the potential in co-delivery of metal ion and CPT for CDT and chemotherapy allowing synergistic or additive therapeutic outcomes.

Overall, polymeric drug conjugate PGA-[(CPT-Gly)-*co*-(F-PSar)] was successfully developed by integrating PGA and F-PSar with fucose as the cell targeting group and CPT-Gly as the chemotherapeutic agent. While Cu^{2+} complexation capability to enable combined organic chemotherapy and inorganic CDT for pancreatic cancer treatment. Future work will focus on comprehensive *in vitro* and/or *in vivo* study can be carried out to further examine its therapeutic efficacy in the future. Also, more experiments on drug conjugate produced by replacing PGA with P(Glu-GA) needs to be carried out to optimise its drug content for better NP formation properties prior to biological testing. Additionally, challenges in ROP of DKPs and Sar-GA DKM still require further studies and left to be tackled in the future.

6.2. Future Research

All the drug conjugates produced in this research mainly characterised through ^{1}H NMR especially the estimation of their drug content. But this evaluation heavily depends on the spectral resolution and integration accuracy. Alternatively, UV–vis spectroscopy can be employed, where the absorbance intensity of the drug conjugate is measured and correlated with a calibration curve. This allows the drug content per conjugate to be estimated in a straightforward and relatively accurate manner. Moreover, the drug conjugate can be hydrolysed under basic conditions to fully release CPT, followed by HPLC analysis of the solution to determine drug content. To ensure complete release, measurements may need to be repeated over several days until consistent results are obtained. However, CPT may degrade or undergo transformation in basic solution, potentially leading to inaccurate quantification.

The NPs samples prepared from the drug conjugate were characterised and stored at room temperature in either pH 7.4 PBS or mildly acidic acetate buffer (pH 5.0-6.0), conditions that

may not support optimal long-term stability. To maximise shelf life and ensure reliable performance, future studies should explore alternative storage protocols, such as preparing NPs in DI water followed by refrigeration, freezing, or lyophilisation, which have been shown to significantly enhance stability. [1,6].

The NPs produced from the drug conjugate exhibited batch-to-batch variation in Z-average, which can potentially compromise its consistent drug delivery performance and hinder scalability for commercial production. These inconsistencies likely stem from minor fluctuations in experimental parameters across trials aside from the inherent randomness of the coupling reaction, such as temperature, concentration or stirring rate during both conjugate synthesis and the subsequent nanoprecipitation process. To ensure reproducible NP sizes, strict monitoring and precise control of these conditions are essential in subsequent preparations. Also to further minimise the burst release and the aggregation caused by residual unconjugated CPT-Gly, the coupling agent can be divided into two portions: the first added on the initial day and the second on the following day. This staged addition may enhance overall coupling efficiency by allowing better reaction progression. Subsequently, dialysis against methanol for two days ensures thorough removal of any remaining unreacted CPT-Gly.

Also, to propel this research toward clinical translation and maximise its impact on pancreatic cancer therapy, a progressive, multistage approach is essential. The NPs formulated from the drug conjugates have only been characterised in pH 7.4 PBS solution or mildly acidic acetate buffer (pH 5.0-6.0) lacking biological relevance. To advance toward pharmacological validation, progressing to *in vitro* cell assays are a critical next step which simulating TME and cellular interactions bridging the gap between the current buffer-based NPs characterisations and realism. Thereby evaluating key performance aspects including cellular uptake, intracellular metabolism, cytotoxicity, and drug release kinetics.

To evaluate the cellular uptake and targeting efficiency, confocal laser scanning microscopy for spatial imaging and intracellular distribution [7] or flow cytometry for high throughput, single cell quantitative analysis [8] with fluorescently labelled NPs such as incorporating fluorescein isothiocyanate (green) or rhodamine (red) into the drug conjugate to quantify uptake in pancreatic cancer cell lines overexpressing fucose receptors compare with healthy

pancreatic cells to assess selectivity. Time-lapse microscopy can track real-time endocytosis pathways of the NPs [9], while addition of free fucose as an competitive inhibitor occupying the fucose-binding proteins on cancer cells to confirm targeting specificity [10].

In terms of drug release kinetics, enzymes like proteases, matrix metalloproteinases, cathepsins, phospholipase, oxidoreductases, and esterases [11,12] can be added into the medium to better mimic the lysosomal conditions in the drug release study rather than simple acetate buffer [13], combined with HPLC analysis to produce a more accurate drug release kinetic profile. While its off- target toxicity can be quantified via 50% Inhibitory Concentration (IC_{50}) values colorimetric via 3-(4,5-dimethylthiazol-2-yl)-2,5-diphenyltetrazolium bromide (MTT) or Alamar Blue assays [14,15] comparing conjugated versus free CPT to demonstrate reduced toxicity. Additionally, pulse-chase analysis with radiolabelled or fluorescent CPT can monitor intracellular persistence and clearance over time [16] informing dosing intervals for optimal adjuvant therapeutic effect giving the drug conjugates' slow CPT releasing kinetics in lysosomal pH.

Despite Cu^{2+} complexation yields approaching theoretical values, the overall copper content remains low (2-3% w/w relative to CPT). Their potential synergistic effects of co-delivery of Cu^{2+} mediated CDT and CPT chemotherapy can be evaluated *in vitro* by comparing cu^{2+} complexed drug conjugate with that without Cu^{2+} complexation using the Chou-Talalay method. It quantifies interactions via combination index (CI), definition for additive effect (CI= 1), synergism (CI< 1), and antagonism (CI> 1) in drug combinations [17]. This provides CI isobologram, enables comparison of two conjugates at any effect and dose level [17].

Following promising *in vitro* test result, *in vivo* evaluation in genetically engineered mouse models containing pancreatic cancer is crucial for assessing systemic behaviour, where buffer and *in vitro* studies and fall short. Intravenous administration of near-infrared fluorescent-labelled NPs and track continuously via *in vivo* imaging systems to observe biodistribution, measure circulation half-life and blood clearance of NPs [18]. While inductively coupled plasma- mass spectrometry can be used to quantify tumour accumulation of Cu^{2+} and HPLC for CPT content in excised tumorous tissues.

To further examine the therapeutic efficacy and targeting benefits of Cu^{2+} complexed PGA-[(CPT-Gly)-*co*-(F-PSar)], comparison across free CPT, fucose- free conjugate and Cu^{2+}-free

conjugate with tumour volume monitored by MRI [19] or ultrasound [20] and overall survival analysed. Fucose-mediated targeting is expected to demonstrate enhanced EPR plus active cell targeting, while Cu^{2+} complexed conjugate may amplify efficacy through oxidative stress, potentially yielding additive or synergistic survival improvements.

Collectively, comparative studies against free CPT and fucose free conjugate would address core questions such as whether conjugated CPT shows reduced toxicity relative to the free drug, the duration of NP or released CPT persistence before clearance, and the advantages of fucose targeting and Cu^{2+} synergy.

The successful ROP of Glu(OBzyl)-DKP may refer to its electro withdrawing carboxylate-OBzyl group side chain weakening the amide bond and facilitating the transamidation/ propagation process. Therefore, replacing glutamic acid with aspartic acid, featuring a shorter side chain, could enhance this electron withdrawing effect, potentially further accelerating and improving the ROP process.

Observed NP aggregation at pH<6.0 is likely caused by protonation of free carboxylate groups along the PGA backbone. Therefore, replacing PGA with P(Glu-GA) may effectively prevent its aggregation at slight acidic environments as it directly reduces the number of carboxylate group available for protonation for the same MW. Enabling the effective CPT release in acidic condition. Owing to limited sample availability, more comprehensive studies of drug conjugates P(Glu-GA)-[(CPT-Gly)-co-(F-PSar)] and P(Glu-GA)-(PSar-Gly-CPT) including respond to pH change, minimum drug content for stable NP formation, detailed release profiles, and long term stability are warranted in future work.

The Schreiner's Thiourea Catalyst: TBD catalyst failed to effectively ROP Glu(OBzyl)-GA DKM even at elevated temperature consistent with literature indications of its limited efficacy. Replacing Schreiner's thiourea with a more reactive thiourea derivative- TU is recommended to achieve more effective and controlled polymerisation of P(Glu-GA). Also, the ROP of Sar-GA DKM can be tested if the failed ROP was due to the inappropriate catalysts used. Success here would allow replacement of PSar with P(Sar-GA) in drug conjugate synthesis, ultimately eliminating the need for hazardous triphosgene across the entire process.

Moreover, the current synthesis of the fucose-targeted drug conjugate PGA-[(CPT-Gly)-*co*-(F-PSar)] involves multiple steps especially in the modification of fucose as a NCA initiator. Its

multi-step synthesis suffers from low overall yields, prolonged reaction times due to laborious purifications, substantial huge solvent consumption and complications arising from O-acetyl group deprotection. Consequently, the existing scheme exhibits poor atom economy and limited environmental sustainability. On reflection of these reasons, a new reaction scheme for the synthesis of fucose mediated cell targeting drug conjugate PGA-[(CPT-Gly)-*co*-(F-PSar)] is shown at below:

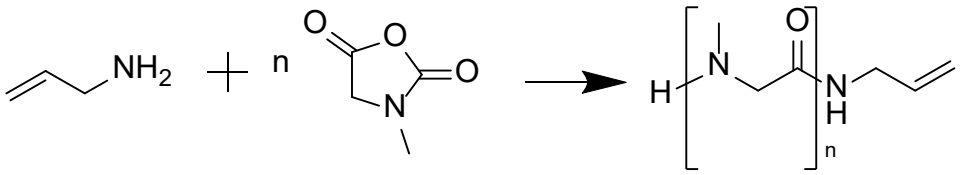

Scheme 6.2-1. ROP of Sar-NCA initiated by allylamine

Allylamine is used as the initiator of Sar-NCA (Scheme 6.2-1), then randomly coupled with PGA and CPT-Gly to produce drug conjugate PGA-[(CPT-Gly)-*co*-(Allyl-PSar)] (Scheme 6.2-2).

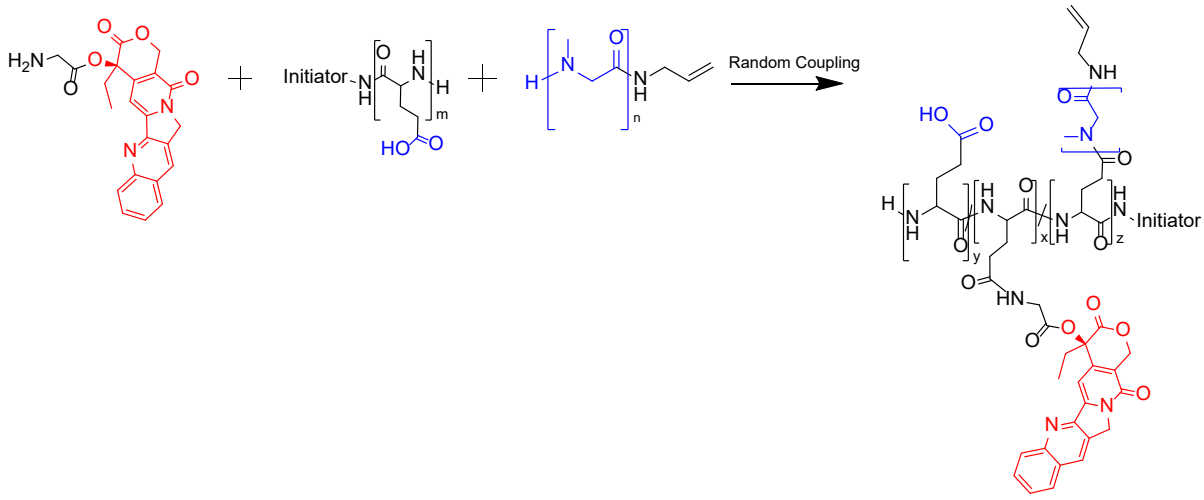

Scheme 6.2-2. Random coupling of CPT-Gly, PGA, and allyl-PSar to produce drug conjugate PGA-[(CPT-Gly)-*co*-(Allyl-PSar)]. /: indication of the random position of carboxylate side chain, CPT-Gly and allyl-PSar in PGA backbone.

Later unmodified fucose is added to the alkene at the terminal of PSar via a photocatalysed anti-Markovnikov hydration reaction. The transformation employs photocatalyst 9-Mesityl-10-methylacridinium as the photocatalyst in conjunction with a hydrogen-atom-transfer catalyst, phenyl disulfide and blue LED light irradiation at room temperature for a day to

produce PGA-[(CPT-Gly)-*co*-(F-PSar)] (Scheme 6.2-3)[21]. This method eliminates the need for prior fucose modification, significantly simplifying the process and reducing solvent consumption. Moreover, by carefully adjusting the fucose to alkene ratio and reaction concentration, undesired crosslinking to multiple alkenes can be minimised. The strategy also offers versatility, enabling the simultaneous attachment of multiple distinct cell targeting agents to the allyl-terminated PSar chain. This capability holds promise for overcoming the extensive genetic heterogeneity observed in PDAC, and potentially other cancers, thereby enhancing therapeutic specificity and efficacy.

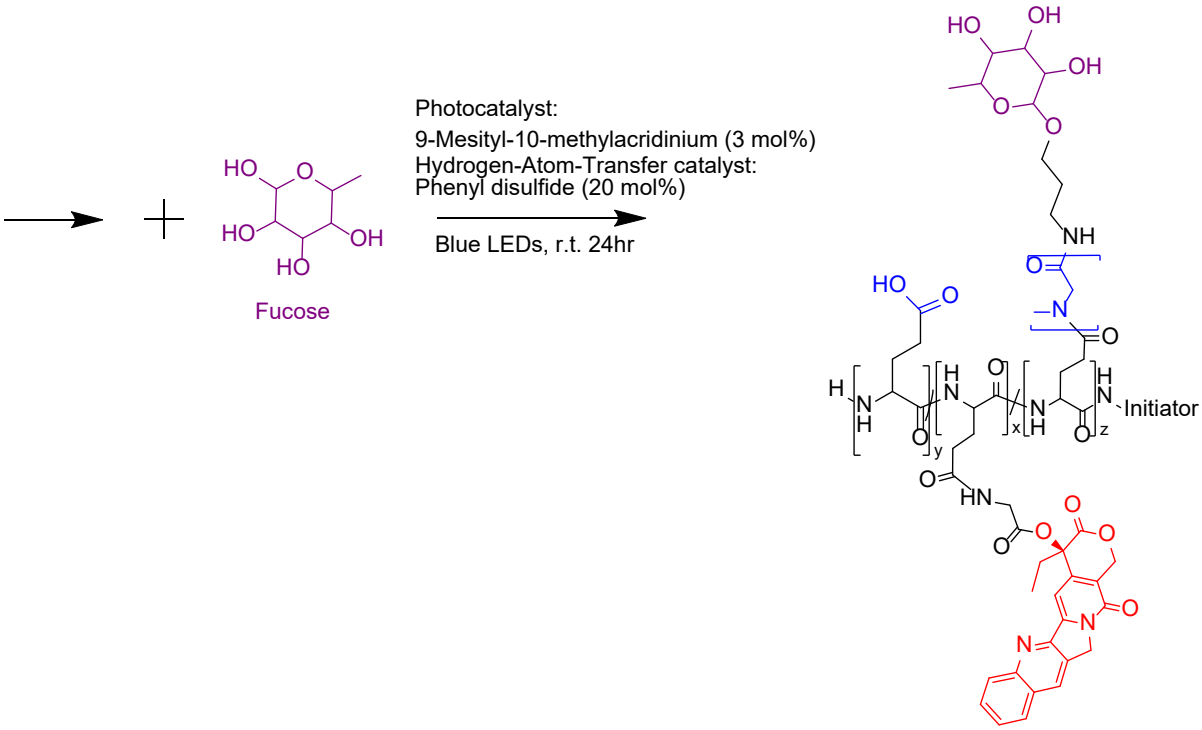

Scheme 6.2-3. anti-Markovnikov hydration reaction of drug conjugate PGA-[(CPT-Gly)-*co*-(Allyl-PSar)] with fucose with photocatalyst 9-Mesityl-10-methylacridinium in conjunction with a hydrogen-atom-transfer catalyst, phenyl disulfide under blue LED light at room temperature for a day to produce PGA-[(CPT-Gly)-co-(F-PSar)]. /: indication of the random position of carboxylate side chain, CPT-Gly and F-PSar in PGA backbone.

Furthermore, to mitigate the low reaction yields observed in the synthesis of PGA-[(CPT-Gly)-*co*-(PSar or F-PSar)], which are likely attributable to steric hindrance from the bulky CPT moiety. An alternative strategy involves conjugating CPT to a sarcosine dimer or trimer prior

to PGA coupling (Scheme 6.2-4). This modification increases the spatial separation between the PGA backbone and CPT unit, thereby reducing steric crowding and facilitating more efficient coupling of different components. Additionally, the extended linker enhances the overall hydrophilicity of the conjugate, improving aqueous solubility, and simplifies structural characterisation by minimising peak overlap in ^{1}H-NMR spectra. Preliminary optimisation trials will be required to determine the ideal oligomer length and reaction conditions for maximising yield.

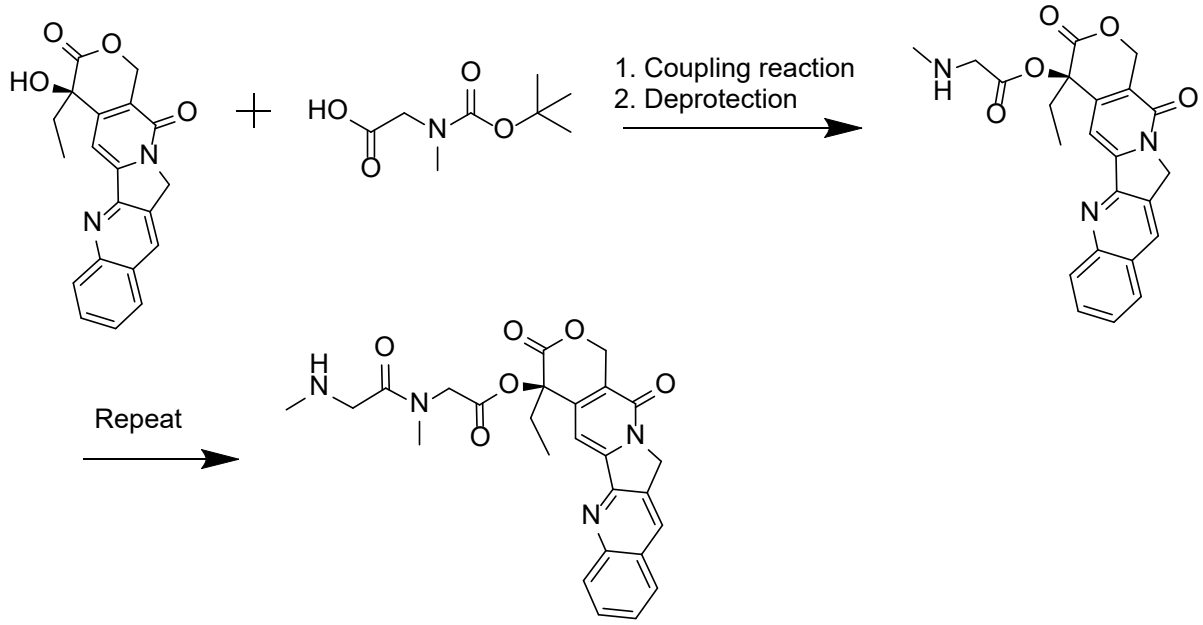

Scheme 6.2-4. Synthesis of camptothecin di-sarcosinate

6.3. References

1. Breunig, M., Bauer, S. E., & Goepferich, A. (2008). Polymers and nanoparticles: intelligent tools for intracellular targeting?. European Journal of Pharmaceutics and Biopharmaceutics, 68(1), 112-128. https://doi.org/10.1016/j.ejpb.2007.06.010

2. Liu, X., Chen, Y., Li, H., Huang, N., Jin, Q., Ren, K., … & Ji, J. (2013). Enhanced retention and cellular uptake of nanoparticles in tumors by controlling their aggregation behavior. ACS Nano, 7(7), 6244-6257. https://doi.org/10.1021/nn402201w

3. Gref, R., Minamitake, Y., Peracchia, M. T., Trubetskoy, V. S., Torchilin, V. P., & Langer, R. (1994). Biodegradable long-circulating polymeric nanospheres. Science, 263(5153), 1600-1603. https://doi.org/10.1126/science.8128245

4. Jeong, Y., Cheon, J., Kim, S. H., Nah, J., Lee, Y. M., Sung, Y., … & Cho, C. (1998). Clonazepam release from core-shell type nanoparticles in vitro. Journal of Controlled Release, 51(2-3), 169-178. https://doi.org/10.1016/s0168-3659(97)00163-6

5. Ball, R. L., Bajaj, P., & Whitehead, K. A. (2016). Achieving long-term stability of lipid nanoparticles: examining the effect of ph, temperature, and lyophilization. International Journal of Nanomedicine, Volume 12, 305-315. https://doi.org/10.2147/ijn.s123062

6. Ai, L., Li, Y., Zhou, L., Yao, W., Zhang, H., Hu, Z., … & Hu, Y. (2023). Lyophilized mrna-lipid nanoparticle vaccines with long-term stability and high antigenicity against sars-cov-2. Cell Discovery, 9(1). https://doi.org/10.1038/s41421-022-00517-9

7. Vukojević, V., Heidkamp, M., Yu, M., Johansson, B., Terenius, L., & Rigler, R. (2008). Quantitative single-molecule imaging by confocal laser scanning microscopy. Proceedings of the National Academy of Sciences, 105(47), 18176-18181. https://doi.org/10.1073/pnas.0809250105

8. Spangenberg, S. H., Zavareh, R. B., & Lairson, L. L. (2021). Protocol for high-throughput compound screening using flow cytometry in THP-1 cells. STAR Protocols, 2(2), 100400. https://doi.org/10.1016/j.xpro.2021.100400

9. Jiang, S., Qin, K., & Sun, L. (2023). Time-lapse live-cell imaging of pyroptosis by confocal

microscopy. STAR Protocols, 4(4), 102708. https://doi.org/10.1016/j.xpro.2023.102708

10. Palmer, T. and Bonner, P. (2011). Enzyme Inhibition. Enzymes, 126-152. https://doi.org/10.1533/9780857099921.2.126

11. Hu, Q., Katti, P. S., & Gu, Z. (2014). Enzyme-responsive nanomaterials for controlled drug delivery. Nanoscale, 6(21), 12273-12286. https://doi.org/10.1039/c4nr04249b

12. Wei, Y., Lv, J., Zhu, S., Wang, S., Su, J., & Xu, C. (2024). Enzyme-responsive liposomes for controlled drug release. Drug Discovery Today, 29(7), 104014. https://doi.org/10.1016/j.drudis.2024.104014

13. Joshi, N., Yan, J., Levy, S., Bhagchandani, S., Slaughter, K. V., Sherman, N. E., … & Karp, J. M. (2018). Towards an arthritis flare-responsive drug delivery system. Nature Communications, 9(1). https://doi.org/10.1038/s41467-018-03691-1

14. Damiani, E., Solorio, J. A., Doyle, A. P., & Wallace, H. (2019). How reliable are in vitro IC50 values? Values vary with cytotoxicity assays in human glioblastoma cells. Toxicology Letters, 302, 28-34. https://doi.org/10.1016/j.toxlet.2018.12.004

15. Hamid, R. A., Rotshteyn, Y., Rabadi, L., Parikh, R., & Bullock, P. L. (2004). Comparison of alamar blue and MTT assays for high through-put screening. Toxicology in Vitro, 18(5), 703-710. https://doi.org/10.1016/j.tiv.2004.03.012

16. Roboti, P., Witkos, T. M., & Lowe, M. (2013). Biochemical Analysis of Secretory Trafficking in Mammalian Cells. Methods for Analysis of Golgi Complex Function, 85-103.

https://doi.org/10.1016/b978-0-12-417164-0.00006-9

17. Chou, T. (2010). Drug Combination Studies and Their Synergy Quantification Using the Chou-Talalay Method. Cancer Research, 70(2), 440-446. https://doi.org/10.1158/0008-5472.can-09-1947

18. Peterson, N. C., Wilson, G. G., Huang, Q., Dimasi, N., & Sachsenmeier, K. F. (2016). Biodistribution Analyses of a Near-Infrared, Fluorescently Labeled, Bispecific Monoclonal Antibody Using Optical Imaging. Comparative medicine, 66(2), 90–99.

19. Partridge, S. C., Gibbs, J., Lü, Y., Esserman, L. J., Tripathy, D., Wolverton, D., … & Hylton, N. M. (2005). MRI Measurements of Breast Tumor Volume Predict Response to Neoadjuvant Chemotherapy and Recurrence-Free Survival. American Journal of Roentgenology, 184(6), 1774-1781. https://doi.org/10.2214/ajr.184.6.01841774

20. Varzaru, V. B., Moatar, A. E., Popescu, R., Puşcaşiu, D., Vlad, D. C., Vlad, C. S., … & Cobec, I. M. (2025). Assessing Ultrasound as a Tool for Monitoring Tumor Regression During Chemotherapy: Insights from a Cohort of Breast Cancer Patients. Cancers, 17(10), 1626. https://doi.org/10.3390/cancers17101626

21. Hu, X., Zhang, G., Bu, F., & Lei, A. (2017). Visible-light-mediated anti-markovnikov hydration of olefins. ACS Catalysis, 7(2), 1432-1437. https://doi.org/10.1021/acscatal.6b03388

6. Appendix

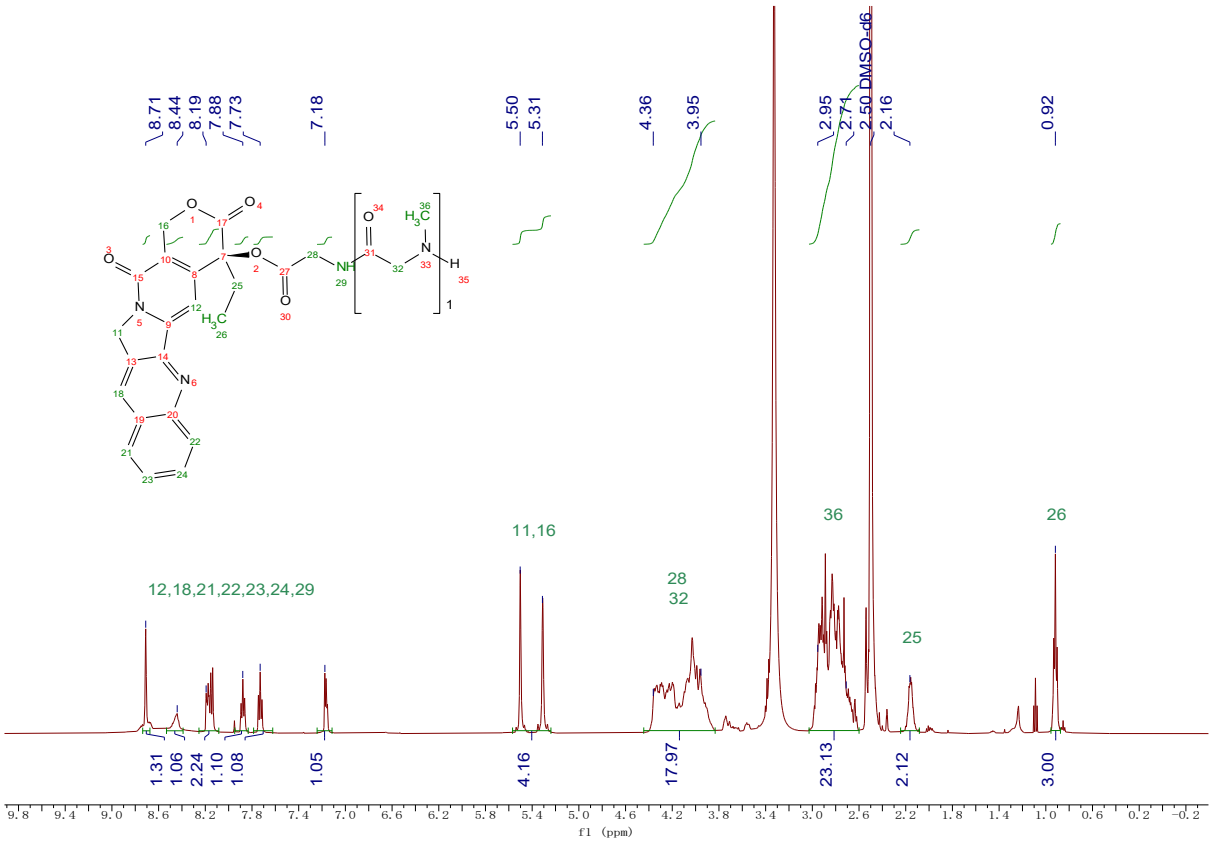

Appendix 0-1. ^{1}H-NMR spectroscopy (400 MHz, DMSO-d_6) of PSar-Gly-CPT (35% drug content): CPT-Gly: 8.71 ppm (=CH-), 8.44 ppm (- NH-), 8.19 ppm - 7.73 ppm (=CH-), 7.18 ppm (=CH-), 5.50- 5.31 ppm (-N-CH_2-, -OCH_2-), 4.36-3.95 ppm (-C=O-CH_2-N- (PSar)), 2.95-2.71 ppm (-N-CH_3), 2.16 ppm (CH3-C**H**$_2$-), 0.92 ppm (CH_3)

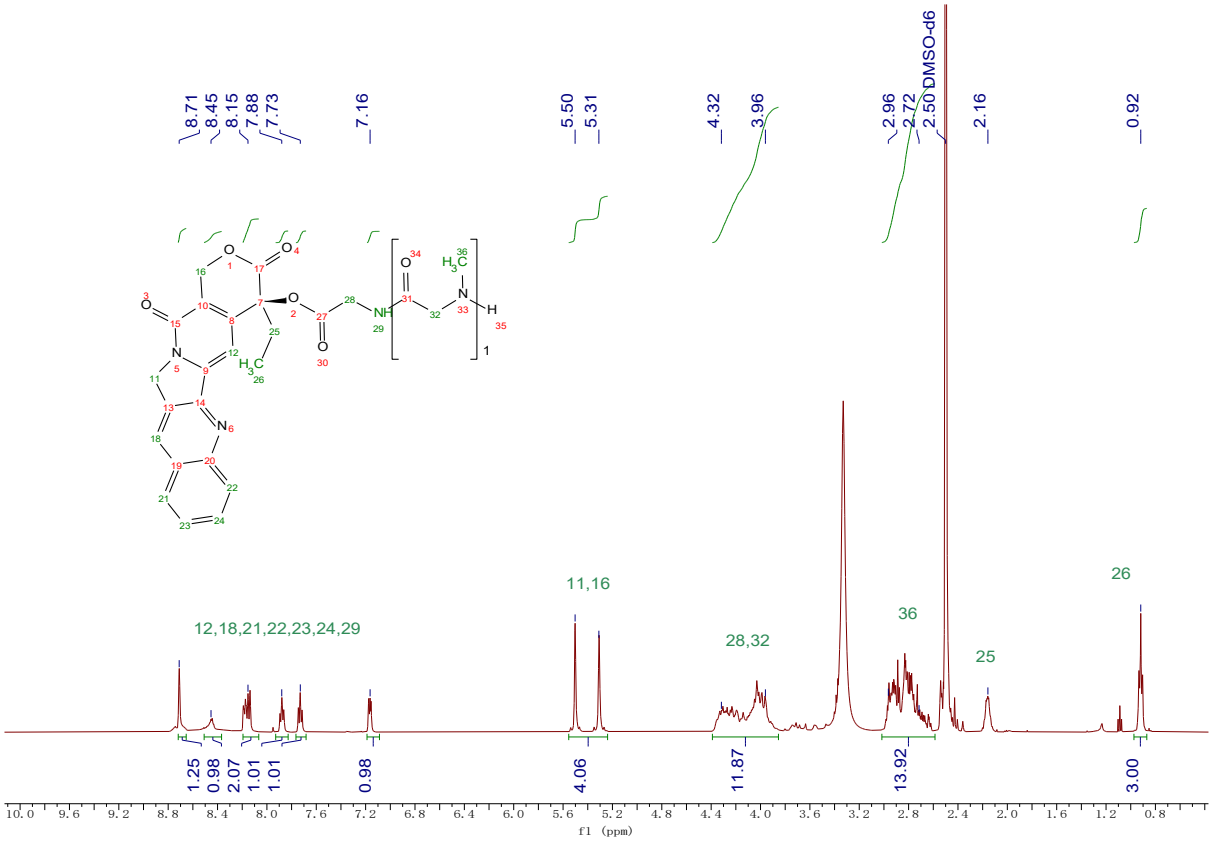

Appendix 0-2. ^{1}H-NMR spectroscopy (400 MHz, DMSO-d_6) of PSar-Gly-CPT: CPT-Gly (44% drug content): 8.71 ppm (=CH-), 8.45 ppm (-NH-), 8.15 ppm (=CH-), 7.88- 7.73 ppm (=CH-), 7.16 ppm (=CH-), 5.50- 5.31 ppm (-N-CH_2-, -OCH_2-), 4.32-3.96 ppm (-C=O-CH_2-N- (PSar)), 2.96-2.72 ppm (-N-CH_3), 2.16 ppm (CH3-C**H**$_2$-), 0.92 ppm (CH_3)

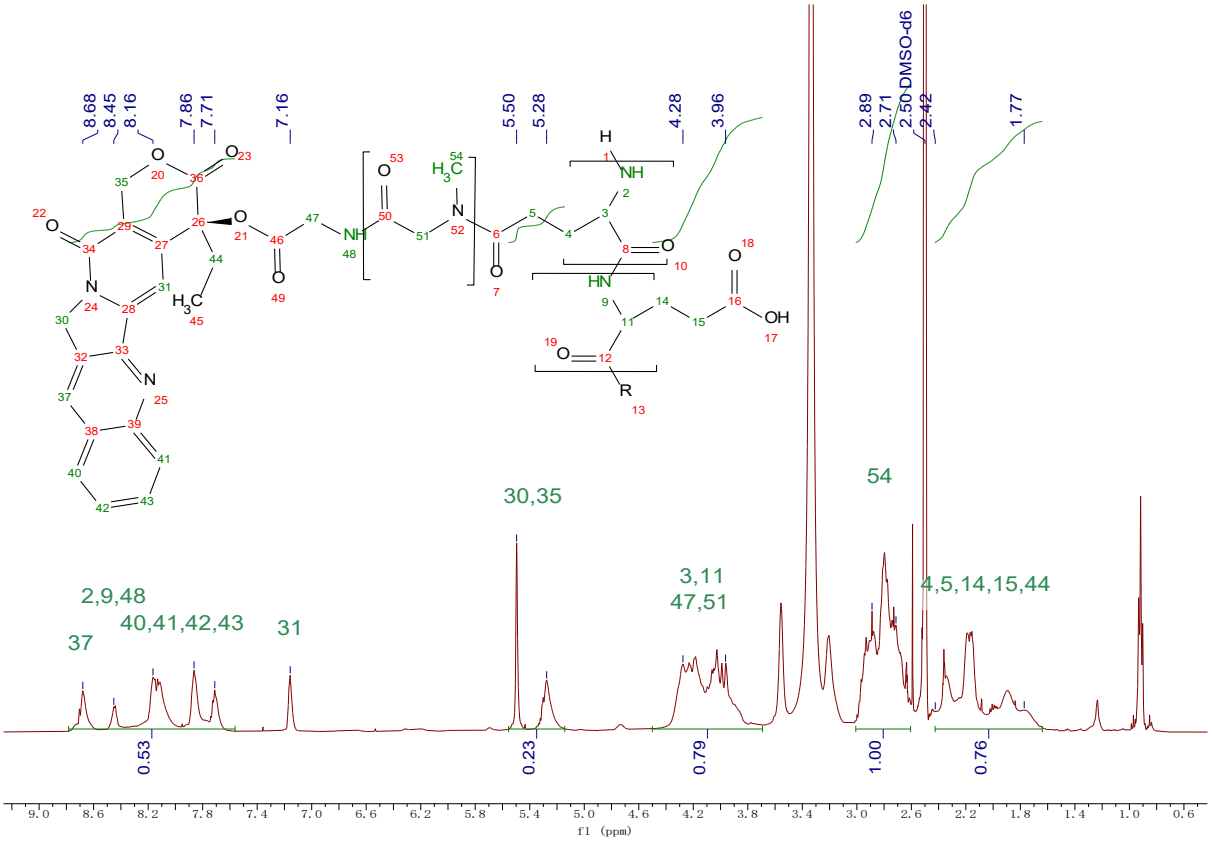

Appendix 0-3. ^{1}H-NMR spectrum (500 MHz, DMSO-d_6) of PGA-(PSar-Gly-CPT) (41.9% drug content): 8.68 ppm(=CH-), 8.45 ppm (-NH-), 8.17 ppm (=CH-), 7.86-7.71 ppm (=CH-), 7.16 ppm (=CH-), 5.50-5.28 ppm (-N-CH_2-, -O-CH_2-), 4.28-3.96 ppm (-NH-C**H**-C=O-,-NH-C$\mathbf{H_2}$-C=O-, -N(CH_3)-C$\mathbf{H_2}$-), 2.89-2.71 ppm (-N-CH_3), 2.43-1.78 ppm (-C$\mathbf{H_2}$-C$\mathbf{H_2}$-)

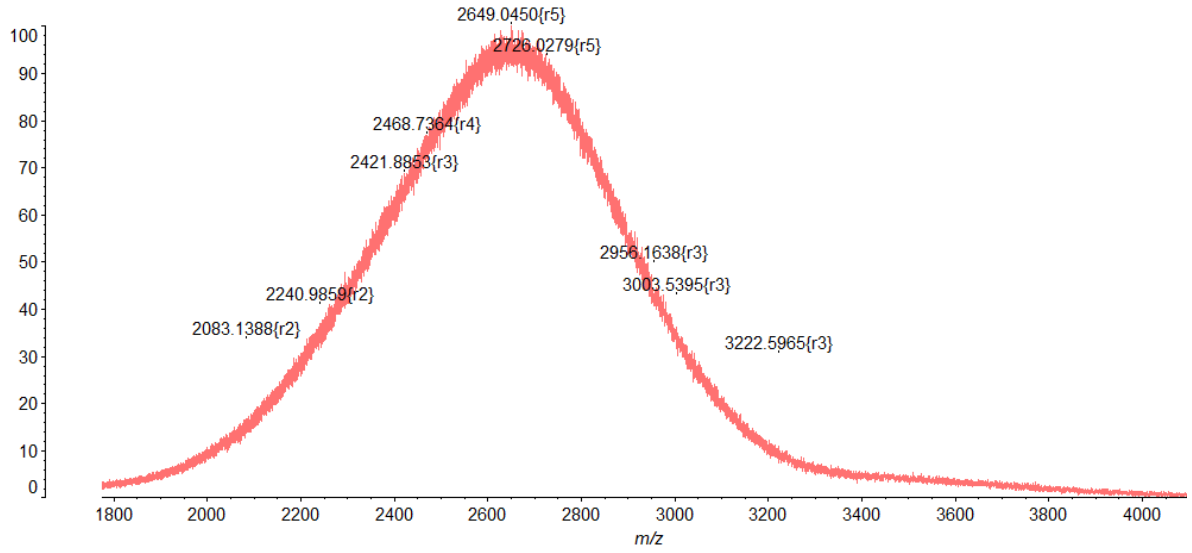

Appendix 0-4. MALDI-TOF mass spectrometry analysis result of ROP of amide-Boc activated Ala-DKP

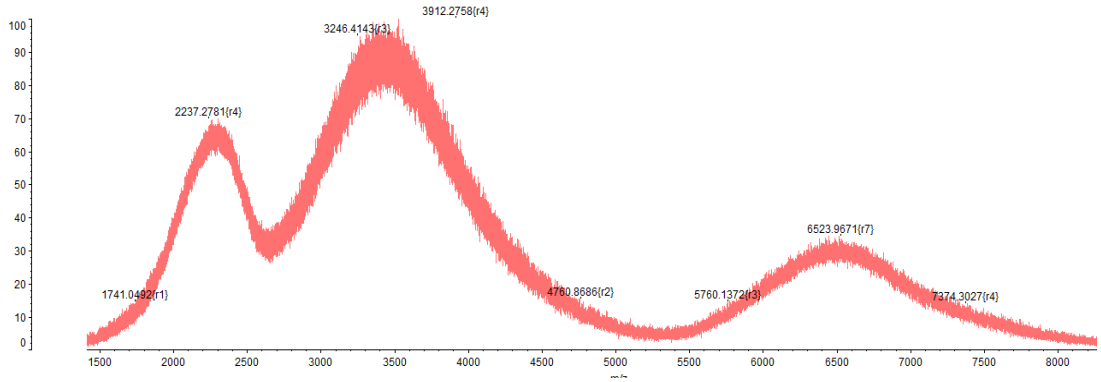

Appendix 0-5. MALDI-TOF mass spectrometry analysis result of PGlu (OBzyl) from DKP

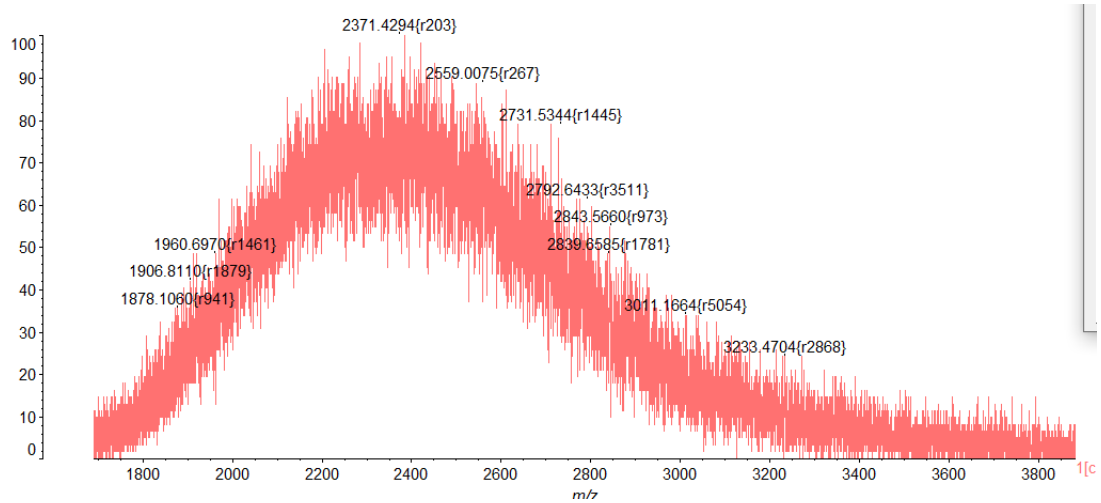

Appendix 0-6. MALDI-TOF mass spectrometry analysis result of P(Sar-GA)